Chemoproteomic Profiling of Anti-Cancer Natural Products for the Discovery of Druggable Nodes

By

Jessica N. Spradlin

A dissertation submitted in partial satisfaction of the

requirements for the degree of

Doctor of Philosophy

in

Chemistry

in the

Graduate Division

of the

University of California, Berkeley

Committee in charge:

Professor Daniel K. Nomura, Chair
Professor Matthew B. Francis
Associate Professor James A. Olzmann

Fall 2020

ABSTRACT

Chemoproteomic Profiling of Anti-Cancer Natural Products for the Discovery of Druggable Nodes

By

Jessica N. Spradlin

Doctor of Philosophy in Chemistry
University of California, Berkeley

Under Supervision of Professor Daniel K. Nomura, Chair

One of the foremost limitations of drug development efforts is that the majority of disease-driving proteins are considered to be "undruggable" by conventional definitions, which look for well-defined binding pockets. Broadly, the work outlined in this doctoral dissertation addresses the challenge of expanding the scope of druggability by applying chemoproteomic methods to map and profile reactive nucleophilic amino acids within proteins. Using this approach to map ligandable sites in the context of human disease we discover novel ligand binding sites that do not fall within the parameters for conventional drug targets, but still allow for functional modification of pharmacologically relevant proteins. One approach to discovering such sites is to map the protein targets of biologically active natural products. Natural products have long been known to be valuable therapeutic agents due to their variety of biological activity. There exists among these active compounds a subset of covalently acting molecules, which are well-suited for chemoproteomic profiling. Identifying the nucleophilic residues targeted by these covalently acting natural products not only yields better understanding of their mechanism of action but can also reveal unique reactive nodes which they access.

In one example of the utility of this approach I employed chemoproteomic profiling to discover that the anti-cancer natural product nimbolide, covalently reacts with a cysteine within an intrinsically disordered region of the E3 ubiquitin ligase RNF114. I demonstrated that covalent modification of RNF114 by nimbolide leads to impaired ubiquitination of the tumor suppressor p21 through a nimbolide-dependent destabilization of the RNF114-p21 interaction, causing the anti-cancer effects of this natural product through stabilization of p21. The discovery that nimbolide targets a substrate recognition domain within RNF114 also suggested that nimbolide could be used as a novel recruiter for the E3-activity of RNF114 in the design of proteolysis targeting chimeras (PROTACs). Consistent with this premise, I showed that a PROTAC linking nimbolide to the BRD4 inhibitor JQ1 led to degradation of BRD4 in breast cancer cells. Subsequent studies demonstrated the importance of identifying nimbolide as a novel E3 recruiter, as a nimbolide-dasatinib degrader led to preferential degradation of oncogenic BCR-ABL over c-ABL, a preference not seen with other known E3-recruiters. Finally, having identified

the reactive hotspot on RNF114 which is targeted by nimbolide, activity-based screening approaches have enabled us to identify a fully synthetic alternative to nimbolide, EN219, to recapitulate its anti-cancer effects and to ease development of further RNF114-recruiting PROTACs.

In a separate effort to pharmacologically recapitulate the effects of the natural product withaferin A, chemoproteomic profiling of this anti-cancer natural product identified a unique druggable hotspot, which sits at an interface within the protein phosphatase 2A (PP2A) tumor-suppressor complex. Interestingly, targeting this site on the regulatory subunit PPP2R1A, leads to activation of PP2A activity, inactivation of AKT signaling, and impaired breast cancer cell proliferation. Using activity-based screening I identified and optimized a more synthetically tractable cysteine-reactive covalent ligand, JNS 1-40, capable of recapitulating these effects and impairing *in vivo* tumor growth by selectively targeting this site. Discovery of this synthetically scalable PPP2R1A ligand has enabled its use as a PP2A activating tool compound in cancer studies and opens opportunities to recruit activated PP2A complex in heterobifunctional therapies in the future.

DEDICATION

Dedicated to the teachers, family, and friends that helped me feel capable and confident when I doubted myself in science and in life. I dedicate this dissertation and my future professional pursuits towards lifting others up in the ways I have been uplifted.

TABLE OF CONTENTS

ACKNOWLEDGEMENTS

Reflecting on the path, and the people along it, that led me to and through graduate school at Berkeley, my heart feels full. I'm so grateful for the support of my family, friends and scientific mentors.

To my little family, Stefano and Moose, I am grateful for the love and distractions that helped keep me sane during graduate school. Thank you, Stef, for listening to me complain when I needed it, but for also not letting me off the hook when I would try to make excuses to give up. You have always pushed me to work harder and think bigger than I would on my own. As much as you supported me through the big moments, some of my favorite memories of grad school are of the little things: time spent together binging TV, going on house-plant-buying sprees, making mini traditions out of tasting the monthly Salt&Straw flavors or having "sandwich Thursdays" in the park, and many more. Thank you, Moose, for being a dog, because that was enough. If anyone ever needed the unconditional love of a dog it is a burnt-out grad student, and my PhDog was a bit of sunshine on some of the harder days at Berkeley.

To my larger family, I feel so thankful to have had you close by over the last years. Mom and dad, I owe you not only the material support that allowed me to make it to graduate school, but also so many of the personal qualities that helped me thrive here. You always encouraged my independence and gave me the freedom to explore and learn on my own terms growing up. Mom, your creativity in all aspects of life, dedication to your work and compassion for others are an example I aspire to. Dad, you taught me that when it comes to doing a job right stubbornness can be a virtue, and your steadiness and encouragement have always been a reassuring presence in my life. I love you both so much and I try every day to make you proud. Rebecca, Priscilla and Isabella, thank you for reminding me not to take myself too seriously and for having my back in the times when it matters most. Thank you, Catalina and Benjamin, for giving me a home in Berkeley that is filled with so many happy memories and for welcoming me into your family. I always thought three siblings was enough, but Carolina, Vicente, and Eric proved that with family, more is more.

To all of the friends I've made at Berkeley, you will be what I remember when I think of my time in lab and you were the ones that made UC Berkeley and the Nomura lab special to me. Thanks Kim and Carl for letting me feel like one of the cool kids. Kim, I may never forgive you for leaving Berkeley early, but I am so happy grad school brought me such a fun, generous, grandma-chic friend. Please never stop sending me cow-print purchases to weigh in on and I will never stop entering you in Bryr giveaways. Carl, despite your occasionally prickly exterior you were always around when I needed help in lab, and you taught me so much about science (and a million other things I never knew I needed to know). I think some of your weird sense of humor rubbed off on me, but hopefully some of your endless scientific curiosity and adaptability did too. Lydia, thank you for being my boba buddy during the last years of grad school. When you joined the lab, I thought I was too jaded to be good lab mate, but your genuine spirit and positivity made me want to be a better friend and mentor in the group. Thank you, Cate and Jessica

for being such great friends and cycling companions during these last few months. Our rides have been a much-needed escape during a crazy phase of grad school and have been a welcome excuse to spend more time with two awesome women. Thank you to all Nomura lab members past and present who have helped keep lab work fun and to friends around Berkeley who reminded me there's more to life than grad school. There are too many of you to name, which is how I know I was truly blessed with a wealth of friends over the last four and a half years.

To my many mentors, thank you for giving me the opportunities that have shaped my scientific growth and thank you for showing me the best sides of science. Dan, your enthusiasm for scientific discovery helped keep me excited to be at the bench. Thank you for reminding me to see the promise in my data instead of only seeing the unanswered questions. Dr. C, you were the first person to trust me in a research position as a clueless Freshman and after you let me into the lab I never looked back (ok, maybe a few times). Your encouragement of me as a young scientist meant the world and you taught me how resourcefulness and perseverance are what makes a scientist successful. Dina, you taught me how to have fun at the bench, and more importantly showed me what it looks like for a woman to hold her own in the lab. Your confidence and leadership are still something I strive to emulate as a researcher. I hope that I'll have an opportunity someday to make the difference in a young scientist's career in the ways each of you has for me.

LIST OF FIGURES

LIST OF APPENDICES

LIST OF ABBREVIATIONS

A20	Tumor necrosis factor alpha-induced protein 3
ABL/c-ABL	Tyrosine kinase ABL1 (mammalian)
ABPP	Activity-Based Protein Profiling
ATP	Adenosine Triphosphate
ATP6V1A	V-type proton ATPase catalytic subunit A
BCA	Bicinchoninic acid assay
BCR	Breakpoint cluster region protein
BCR-ABL	BCR-ABL fusion gene
BET domain	Bromodomain and extra-terminal domain
BIRC2 (cIAP)	Baculoviral IAP repeat-containing protein 2
BRD4	Bromodomain containing protein 4
BTK	Bruton's tyrosine kinase
BTZ	Bortezomib
C377	Cysteine at position 377
C377A	Cysteine to alanine mutant at position 377
C8	Cysteine at position 8
C8A	Cysteine to alanine mutant at position
CASP14	Caspase 14
CDKN1A (P21)	Cyclin-dependent kinase inhibitor 1A
CDKN1C (P57)	Cyclin-dependent kinase inhibitor 1C
CHIP	E3 ubiquitin-protein ligase CHIP
CID	Collision-induced dissociation
CML	Chronic myeloid leukemia
CRBN	Protein cereblon
CTGF	Connective tissue growth factor
CuAAC	Copper(I) Azide-Alkyne Cycloaddition
DC50	50 % degradation concentration
DCAF16	DDB1- and CUL4-associated factor 16
DMEM	Dulbecco's modified eagle medium
DMSO	Dimethylsulfoxide
DSG1	Desmoglein-1
DTT	Dithiothreitol
E3	E3 ubiquitin ligase
EC50	50 % effective concentration
FBS	Fetal bovine serum
FKBP12	Peptidyl-prolyl cis-trans isomerase FKBP1B
FLAG Tag	DYKDDDDK polypeptide protein tag
FLG2	Filaggrin 2
FN1	Fibronectin
GAPDH	Glyceraldehyde-3-phosphate dehydrogenase
HPLC	High performance liquid chromatography
HSPD1	60 kDa heat shock protein, mitochondrial
IA	Iodoacetamide

IA-alkyne/IAyne	Iodoacetamide-alkyne conjugate (*N*-5-Hexyn-1-yl-2-iodoacetamide)
IC50	50 % inhibitory concentration
IDP	Intrinsically disordered protein
IMDM	Iscove's modified Dulbecco's medium
IMiD	Immunomodulatory imide drugs
isoTOP-ABPP	Isotopic tandem orthogonal proteolysis-enabled ABPP
ITMS	Ion-Trap Mass Spectrometer
KO	Knockout
KRas	GTPase KRas
$KRas^{G12C}$	Glycine 12 to Cysteine mutant GTPase KRas
L15	Leibovitz's L15 medium
LC-MS	Liquid chromatography–mass spectrometry
LyTAC	Lysosome-targeting chimera
MDM2	E3 ubiquitin-protein ligase Mdm2
mRNA	Messenger RNA
MS	Mass spectrometer
MS/MS	Tandem mass spectrometry
MS1	First MS for detection of initial ionization in MS/MS
MS2	Second MS for detection of fragment ionization in MS/MS
MudPIT	Multidimensional protein identification technology
MYC	Myc proto-oncogene
NF-kB	Nuclear factor kappa B
p53 (TP53)	Cellular tumor antigen p53
PBS	Phosphate-buffered saline
PEG	Polyethylene glycol
PEG10	Retrotransposon-derived protein PEG10
PhoRC	Phosphatase-Recruiting Chimera
POI	Protein of interest
PP2A	protein phosphatase 2A
PPP2CA	Serine/threonine-protein phosphatase 2A catalytic subunit alpha
PPP2R1A	Serine/threonine-protein phosphatase 2A regulatory subunit 1A
PROTAC	Proteolysis targeting chimera
PSM	Peptide spectral matches
qRT-PCR	Quantitative real-time polymerase chain reaction
RiboTAC	Ribonuclease targeting chimera
RING	Really interesting new gene protein family
RNA	Ribonucleic acid
RNAi	interfering RNA
RNF114	E3 ubiquitin-protein ligase RNF114
RNF4	E3 ubiquitin-protein ligase RNF4
RPMI	Roswell Park Memorial Institute Medium
SAR	Structure-activity relationship
SCFSKP2	S-phase kinase-associated protein 2
SDS	Sodium dodecyl sulphate
SDS-PAGE	Sodium dodecyl sulphate–polyacrylamide gel electrophoresis
siRNA	Short interfering RNA

TAB1	TGF-beta-activated kinase 1 and MAP3K7-binding protein 1
TBS	Tris-buffered saline
TBST	Tris-buffered saline with Tween
TCEP	Tris(2-carboxyethyl)phosphine
TEV	Tobacco etch virus
TMT	Tandem mass tag
TNBC	Triple negative breast cancer
TPD	Targeted protein degradation
TUBB1	Tubulin beta 1 chain
Ub	Ubiquitin
UBE1	Ubiquitin-like modifier-activating enzyme 1
UBE2D1	Ubiquitin-conjugating enzyme E2 D1
VHL	Von Hippel-Lindau disease tumor suppressor
WT	Wild-type

CHAPTER 1

Reimagining Druggability Using Chemoproteomic Platforms

This chapter is based on a manuscript in preparation “Reimagining Druggability Using Chemoproteomic Platforms” and has been adapted with permission from all co-authors.

1.1 The Undruggable Proteome

In the era of post-genomic research, we can better understand the genes and mutations that drive complex diseases like cancer [1]. But identifying a gene as a disease driver is just the first step; there must be strategies in place to create therapeutic interventions to counteract the malignant protein. Looking at existing pharmaceutical drug targets, it becomes clear that historically successful drugs have gone after well-defined binding pockets and active sites, where the drug competes against an endogenous small molecule binder [2]. Rational, structure-based drug design offers many advantages for efficient optimization of clinical leads and has played a significant role in drugging classes of disease drivers such as kinases, whose active sites are well suited to docking and modeling approaches [3]. Despite these successes, there are many more disease drivers that remain devoid of drugs and will require a different approach to develop small molecule drugs (**Fig. 1.1**). A "druggable" protein is traditionally defined as the convergence of disease relevance and the availability of drug-like small molecules that can selectively target the protein [4]. To expand the scope of druggability we must discover new ligandable sites within disease relevant targets. Discovery of protein binding ligands is more easily achievable if the protein has an evolved small molecule binding pocket, as would be the case for enzymes or receptors, however numerous key cancer drivers do not have these binding pockets and are considered undruggable.

Increased genomic and biochemical understanding of disease-related pathways has uncovered diverse classes of proteins including regulatory and scaffolding proteins that serve non-enzymatic functions, many of which remain undruggable. In the absence of a well-structured small molecule binding pocket, druggability can be difficult to predict and interfering with protein function may require a more nuanced intervention than an active-site inhibitor [5]. The list of undruggable targets includes some of the most fundamental drivers of disease including oncogenic and tumor suppressing transcription factors, such as c-Myc and p53 respectively, as well as the G-protein family, encompassing the Ras proteins [6]. Transcription factors are difficult to pharmacologically target due to their lack of deep binding pockets and in fact many are intrinsically disordered, lacking any defined structure to inform inhibitor design. Intrinsic disorder is commonly seen at surfaces which play roles in protein-protein interactions (PPIs) or protein-DNA interactions that mediate the function of these targets, meaning that targeting these sites is of significant interest. The non-enzymatic roles these proteins play introduces an additional complication for drugging them, as therapies must address the ability for these proteins to function through association of multi-component complexes and via downstream effectors [5]. While the RAS proteins and other related G-protein targets do contain an active site pocket, competing against a tightly-bound endogenous substrate makes active-site inhibitors difficult to develop [7]. Though the Shokat lab has taken advantage of the nucleophilic mutant residue in $KRas^{G12C}$, other KRas mutants as well as other Ras proteins are more challenging to address [8]. With these and many other hallmark cancer drivers remaining stubbornly intractable to conventional drug-discovery tactics, new unbiased approaches are needed not only to tackle these targets but also to identify novel druggable targets which modulate disease driving pathways.

To discover new druggable binding sites on proteins, chemoproteomic methods offer strategies to both identify and characterize nucleophilic amino acid hotspots on classically undruggable proteins or on new protein targets within undruggable pathways. Chemoproteomics takes advantage of chemical tools to understand the interactions of small molecules with proteins in the context of complex biological systems. The development of chemoproteomic probes and workflows to identify reactive sites in proteins offers new insight into a vast pool of untapped binding nodes which can be targeted for drug development [9]. Evaluating modern proteomic data sets reveals thousands of nucleophilic sites that can be modified by the array of small molecule probes discussed in this chapter. In theory, each of these sites can be targeted by a suitable electrophile, making chemoproteomic approaches a powerful entry point for discovery of new covalent drug binding sites. Discovery of new ligandable sites is especially significant in light of the new wave of bispecific therapies which can turn even non-inhibitory ligands into consequential binders by recruiting effector proteins [10]. Multi-specific, induced-proximity therapies such as bifunctional small molecule protein degraders also known as proteolysis targeting chimeras (PROTACs) are transforming modern drug discovery efforts and as I will discuss in this work, discovery and characterization of novel binding sites using chemoproteomics is one tactic which can rapidly advance induced-proximity therapies [11].

1.2 Chemoproteomic Methods in Drug Discovery

While covalently acting small molecules had historically fallen out of favor in drug discovery due to fears of non-specificity driven by their electrophilic groups, advances in design of selective irreversible drugs, proven by successes such as ibrutinib, have led to re-prioritization of covalent scaffolds [12]. Use of electrophilic, covalently-acting molecules takes advantage of the myriad of nucleophilic amino acid hotspots across the proteome to identify potential scaffolds for drug development against a protein of interest.

With renewed interest in utilizing covalent scaffolds in drug development, there is a need for comprehensive methods to identify, characterize and pharmacologically target nucleophilic and reactive amino acids across the proteome. Activity based protein profiling (ABPP) was identified by Cravatt as a method of probing proteins by employing either active-site directed or reactivity-based covalent probes to globally map protein functional sites in the proteome [13,14]. The ease of use and versatility make these methods particularly advantageous, and thus has led to a rapid expansion of chemoproteomic research [15]. Applications of ABPP include Tandem Orthogonal Proteolysis (TOP) as a form of competitive ABPP for the characterization of protein-protein interaction sites and the identification potent and selective small molecule inhibitor discovery [16]. More broadly, reactivity based covalent probes can be used for proteome-wide labeling of protein functional sites to identify active/druggable hotspots, thus providing an opportunity to expand our chemical arsenal.

1.2.1 isoTOP ABPP for Global Profiling of Amino Acid Hotspots

ABPP was first developed by Cravatt to profile hyperreactive serine hydrolases for the collective characterization of their catalytic activity [17]. They successfully used ABPP methodology to identify a fluorophosphonate inhibitor, which later served as an activity-based probe for serine hydrolases due to its broad reactivity across this class of enzymes. The selectivity and generalizability of this method to monitor proteome wide catalytic activity gave rise to the popularity of ABPP for its use on broader classes of reactive residues.

Perhaps the most well-established use of ABPP profiling is for proteins with reactive cysteine hotspots, due to the nucleophilic thiol group that makes them particularly favorable targets. In particular, a derivative of TOP strategy termed iso-TOP (isotopic tandem orthogonal proteolysis) ABPP was developed by Weerapana *et al.* to assess the extent of irreversible protein reactivity via cysteine specific iodoacetamide alkyne (IAyne) probes (**Fig. 1.2**) [18]. Beginning with separate control and treated proteome samples, pre-incubated with either vehicle or a covalently acting compound of interest, both samples are incubated with IAyne probe which will broadly label the reactive cysteines across the proteome. In the compound treated sample certain sites will no longer be accessible to the probe. Next, using copper(I)-catalyzed azide-alkyne cycloaddition (CuACC) an isotopically light TEV-cleavable biotin tag is clicked onto the probe-labeled sites in the control sample, while an isotopically heavy tag is used in the treated. This will allow peptides, which came from the control sample to be distinguished from those coming from the treated sample in the MS/MS readout downstream. After isotopic tagging, control and treated samples can be combined before avidin enriching for labeled proteins, tryptically digesting to leave behind only the peptide containing the modified site and finally cleaving the labeled peptides for LC-MS/MS analysis. Degree of small molecule site occupancy can be quantified using the ratio of light to heavy peptide, where a ratio of 1 indicates that the site was equally accessible to probe labeling in the control and treated sample, while an elevated indicates that the small molecule competed out the probe at that site. A key advantage of isoTOP lies with the probe, as its relatively small size enables the interrogation of previously inaccessible cysteines in proteins directly in complex proteome samples. This methodology was first used to quantify cysteine hyperreactivity, but has since been applied more generally to identify a wide variety of small molecule cysteine binding sites and to assess covalent molecule selectivity.

While large-scale compound screening is well established for assessing ligandability of a single protein *in vitro*, using covalent molecules which are readily amenable to isoTOP ABPP based target deconvolution, lead molecule screening can now be performed in complex proteome samples. This allows identification of new therapeutic targets through unbiased phenotypic screening and facilitates lead discovery against proteins that are not amenable to single protein *in vitro* screening. Overall, iso-TOP ABPP is particularly useful method to identify functional cysteines and determine cellular targets which is instrumental for drug discovery, and can be adapted for different protein classes by swapping out the reactive electrophilic warhead of the probe [19].

1.2.2. Chemoproteomic Profiling of Cysteine Reactivity for Drug Discovery

Extensive work across the chemoproteomics field has showcased the potential of pairing cysteine-reactive covalent fragment screening with chemoproteomics for rapid discovery of new druggable hotspots. Notably a 2016 paper by Backus *et al*. found that many simple cysteine reactive fragments, even when treated at high concentrations (500 μM) show remarkable specificity [20]. Some fragments labeled less that 0.1% of identified druggable cysteines, while more promiscuous compounds modified more than 15%. The majority of ligandable sites identified in this study were on proteins without reported ligands including classes of "undruggable" proteins like transcription factors and scaffolding proteins [20]. Using the same type of approach, Vinogradova *et al.* mapped the interactions of small molecule electrophiles with cysteines in human T cells [21]. Using chemoproteomic methods, this effort allowed exploration of cysteine reactivity changes upon T cell activation, deployed promiscuous scout fragments to broadly profile reactivity and identified electrophilic T cell modulators that show the promise of this approach to yield novel therapeutics [21].

Covalent fragment screening approaches can also be used on disease-relevant pathways to identify new therapeutic entry points. One example of this was in the screening of covalent fragments to identify novel activators of autophagy [22]. An acrylamide fragment was found to activate lysomal acidification and clearance of protein aggregates by modifying a reactive cysteine on the v-ATPase, ATP6V1A. While previous activators of autophagy are hampered by either incomplete activation of mTORC1 or non-specific inhibition of both mTORC1 and mTORC2, covalent targeting of ATP6V1A allows for selective activation of mTORC1 leading to promising cellular and in vivo activity [22]. This work highlights the ability of covalent fragment screening paired with target deconvolution to uncover new druggable sites as openings to alter disease-relevant pathways.

When a specific target protein is desired for a drug discovery project, covalent fragments can be used in functional screens allowing isoTOP ABPP to be applied downstream of the fragment screening campaign to better understand specificity of the lead compound. This type of work has allowed for covalent fragment screening to be applied to classically undruggable proteins such as Myc [23]. Though Myc is a major oncogenic transcription factor, like many disease relevant transcription factors it has remained intractable to traditional drug-discovery efforts due to its intrinsically disordered nature. By screening an electrophilic fragment library, a cysteine-reactive acrylamide was identified which could disrupt Myc-binding to its consensus DNA, impairing Myc transcriptional activity *in situ* [23]. By using this fragment screening approach a canonically undruggable site on an intrinsically disordered protein was identified giving traction for targeting such key disease drivers as Myc.

Finally, target identification for covalently-acting natural products is also a powerful approach to discover new druggable nodes. Covalently-acting natural products are amenable to rapid target identification through use of chemoproteomic strategies. Insights afforded by knowing specific sites of protein modifications of covalently acting natural

products can enable the pharmacological interrogation of the difficult to predict sites targeted by these natural products. The work discussed in this dissertation will showcase the ability of this approach to uncover unique druggable sites and will present examples of how the discovery of these sites can catalyze development of therapeutic interventions that take advantage of these nodes [24–27].

1.3 Chemoproteomics and Multi-specific Therapeutic Approaches

After decades of focus on inhibitor discovery in the pharmaceutical industry, in recent years considerable interest has arisen in the design of therapies which engage two or more protein targets simultaneously to enact their function. This therapeutic paradigm relies on recruitment of an effector protein into proximity of the disease-related target to exploit native systems of post-translational modification and cellular quality control machinery [10].

Targeted protein degradation (TPD) is a powerful therapeutic paradigm that uses small molecules to hijack the ubiquitin-mediated protein degradation system by inducing artificial proximity of an E3 ligase with a protein of interest (POI), leading to its poly-ubiquitination and degradation (**Fig. 1.3**) [11]. These degrader molecules can take the form of rationally constructed bifunctional degrader or proteolysis targeting chimera (PROTAC), linking an E3-recruiting ligand to a ligand against the POI (**Fig. 1.3a**), or can be molecular glue degraders, which are monovalent and more drug-like (**Fig. 1.3b**). This strategy offers a number of advantages over traditional inhibitor design. First, degradation of a protein more completely mitigates the full range of disease-causing effects of the POI than an inhibitor. Induced degradation of the protein will prevent the protein from fulfilling its scaffolding functions as well as any catalytic roles it plays [11]. This aspect makes TPD of many difficult drug-targets an attractive approach, due to the diverse roles these undruggable targets fulfill. Additionally, TPD is also not limited by the constraint of active site occupancy as degrader molecules have been shown to be capable of acting catalytically, with a single molecule degrading multiple equivalents of the targeted POI [11]. Other advantages rely on the added specificity conferred by the multivalency of the molecule. PROTACs can be targeted to specific protein isoforms and can turn a promiscuous protein ligand into a specific degrader [11].

The field of targeted protein degradation is rapidly advancing and promises to have profound impact on pharmaceutical drug development.[10] Largely due to concern over losing the catalytic efficacy, the question of whether covalency can be tolerated in small molecule degraders remains somewhat controversial. However, with continued focus on targeted protein degradation in academic and industry labs has allowed for the application of chemoproteomic methods to the advancement of targeted protein degradation as is highlighted by the work presented in this dissertation.

Use of covalent E3 recruiter ligands is perhaps the most obvious space for the use of covalent ligands, since prolonged occupancy of the E3 should ease assembly of the E3-degrader-POI tertiary complex and should still allow for covalency since the covalently modified E3 is not degraded like the POI. In the pursuit of drugging every protein, TPD

certainly shows great promise, however early indications as to the importance of E3-recruiter choice emphasize the necessity of optimizing every component of the bifunctional degrader. Extensive evidence exists for the E3-conferred selectivity of kinase recruiters with promiscuous ligands which degrade only a subset of the targeted kinases, depending on the E3 used [28,29]. Recently importance of E3 selection was also underscored work that collectively demonstrated that only VHL, but not CRBN was capable of degrading endogenous, untagged $KRas^{G12C}$ [30,31]. As evidence continues to emerge as to the importance of E3 selection for degradation profiles, it becomes apparent that the ability to recruit a wider variety of E3s would be advantageous for the utility of targeted protein degradation by bifunctional small molecules. There are over 600 E3 ligases in human cells, however small molecule recruiters have only been reported for 9 E3s with most published degraders using ligands for VHL and CRBN [32]. Due to the nature of this therapeutic modality, it is necessary to discover non-inhibitory E3-recruiters, requiring a discovery approach that does not focus on protein active sites. Due to its unbiased nature and deemphasizing of active site targeting, chemoproteomic E3-recruiter discovery has emerged as an attractive approach and has already yielded 3 covalent E3 recruiters through distinct approaches. The work in this dissertation will focus on the chemoproteomics-enabled target deconvolution for the anti-cancer natural product nimbolide, which unveiled a classically undruggable binding site within an intrinsically-disordered, substrate-binding region on the N-terminal region of the E3 ligase RNF114, which is targeted by the natural product [24]. Chemoproteomic target identification permitted biochemical exploration of the function of the natural product's binding site and subsequently enabled development of natural product-derived bifunctional degraders with distinct degradation profiles when compared to CRBN and VHL recruiters [24,25]. Uncovering this reactive site also allowed for activity-based fragment screening against the E3-binding site to discover a synthetic mimic for E3 recruitment [27].

While the scope of this work focuses on TPD, the potential of heterobifunctional molecules has been expanded to targeted lysosomal degradation, heterobifunctional recruitment of phosphatases and redirecting of ribonucleases to destroy malignant RNAs among others (**Fig. 1.4**) [33,34,35] The development of new bifunctional, induced-proximity approaches will require discovery of a wide array of ligandable sites across the proteome to recruit mediators of the desired function. Given the power of chemoproteomic strategies to uncover new reactive sites across a variety of functional space, chemoproteomics could be a boon to the development of new heterobifunctional modalities.

1.4 Figures

Figure 1.1

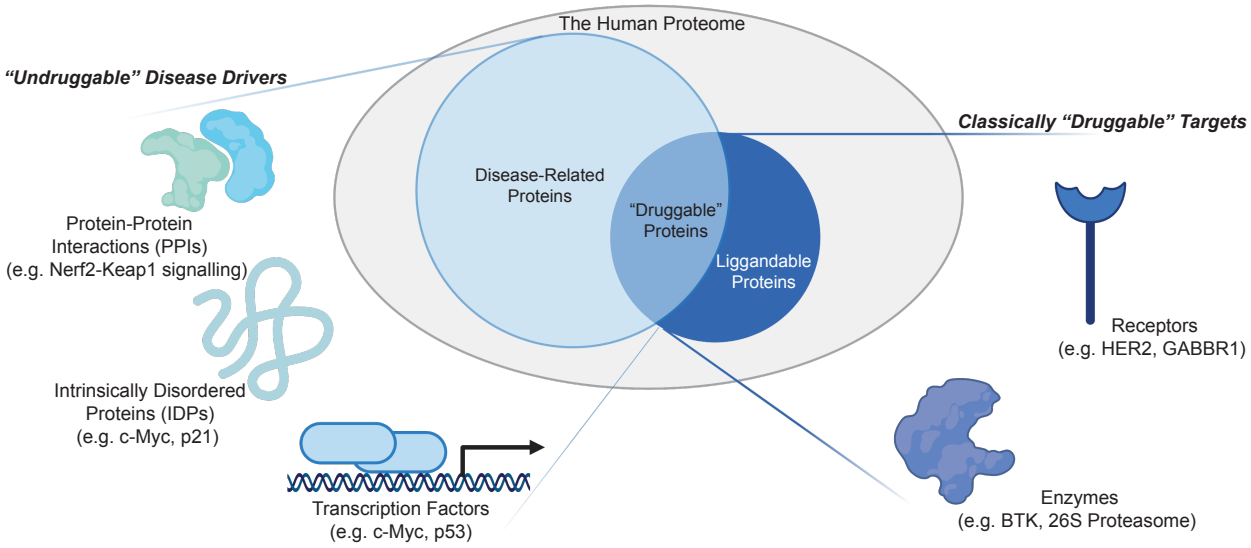

Figure 1.1. The Undruggable Proteome.
Druggable therapeutic targets require the convergence of disease relevance with the availability of drug-like small molecules capable of selectively binding to and modulating the function of the disease driver. While advances in genomic and biochemical interrogation of disease biology has yielded a better understanding of which genes drive complex diseases like cancer, availability of small molecule drugs is still largely limited to a small subset of therapeutic targets. Development of ligands for many of these "druggable" targets has been assisted by the presence of well-defined small-molecule binding sites. Many hallmark disease drivers remain intractable to conventional active site-centric drug discovery approaches due to a variety of reasons including non-enzymatic function and intrinsic disorder. These disease drivers make up what has been termed the "undruggable" proteome.

Figure 1.2

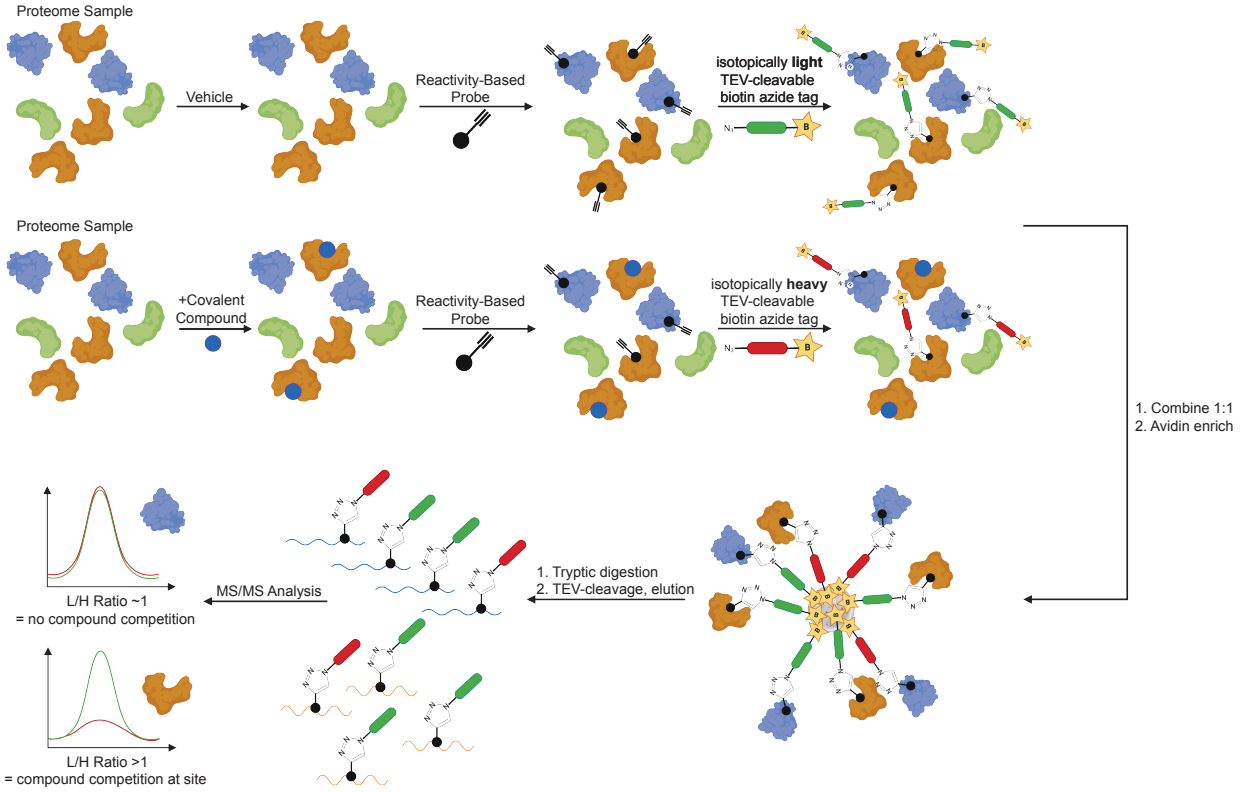

Figure 1.2. Isotopic Tandem Orthogonal Proteolysis-Enabled Activity-Based Protein Profiling (isoTOP-ABPP).
Control and treated proteome samples, pre-incubated with either vehicle or a covalently acting compound of interest, are incubated with IAyne probe which will broadly label the reactive cysteines across the proteome. Next, using copper(I)-catalyzed azide-alkyne cycloaddition (CuACC) an isotopically light TEV-cleavable biotin tag is clicked onto the probe-labeled sites in the control sample, while an isotopically heavy tag is used in the treated. After tagging, control and treated samples can be combined before avidin enriching for labeled proteins, tryptically digesting to leave behind only the peptide containing the modified site and finally cleaving the labeled peptides for LC-MS/MS analysis. Degree of small molecule site occupancy can be quantified using the ratio of light to heavy peptide, where a ratio of 1 indicates that the site was equally accessible to probe labeling in the control and treated sample, while an elevated indicates that the small molecule competed out the probe at that site.

Figure 1.3

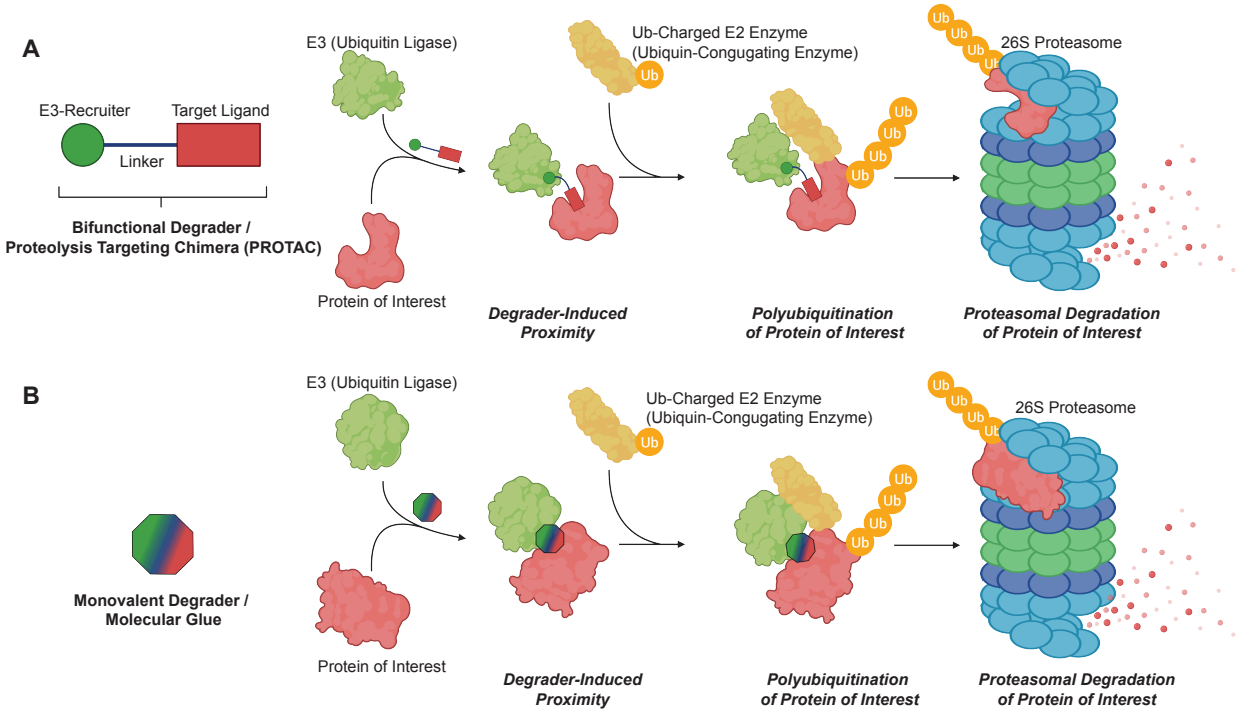

Figure 1.3. Targeted Protein Degradation (TPD) Strategies.
(**A**) Bifunctional degrader molecules, or proteolysis targeting chimeras (PROTACs), are designed by selecting a ligand for a protein of interest (POI), a recruiter for an E3 ubiquitin ligase, and linking these two small molecules together. With each side engaging with it's respective target, the bifunctional degrader induces proximity of the POI with the ubiquitin conjugating machinery, leading to polyubiquitination and eventually degradation of the POI by the proteasome. (**B**) Monovalent degraders, or molecular glues, have historically been discovered serendipitously and achieve the same end result as a PROTAC without use of individual ligands for the POI and E3. These small molecules tend to be smaller and more drug like and are thought to work by changing the exposed surface of the E3, leading to interactions with non-native neo-substrates.

Figure 1.4

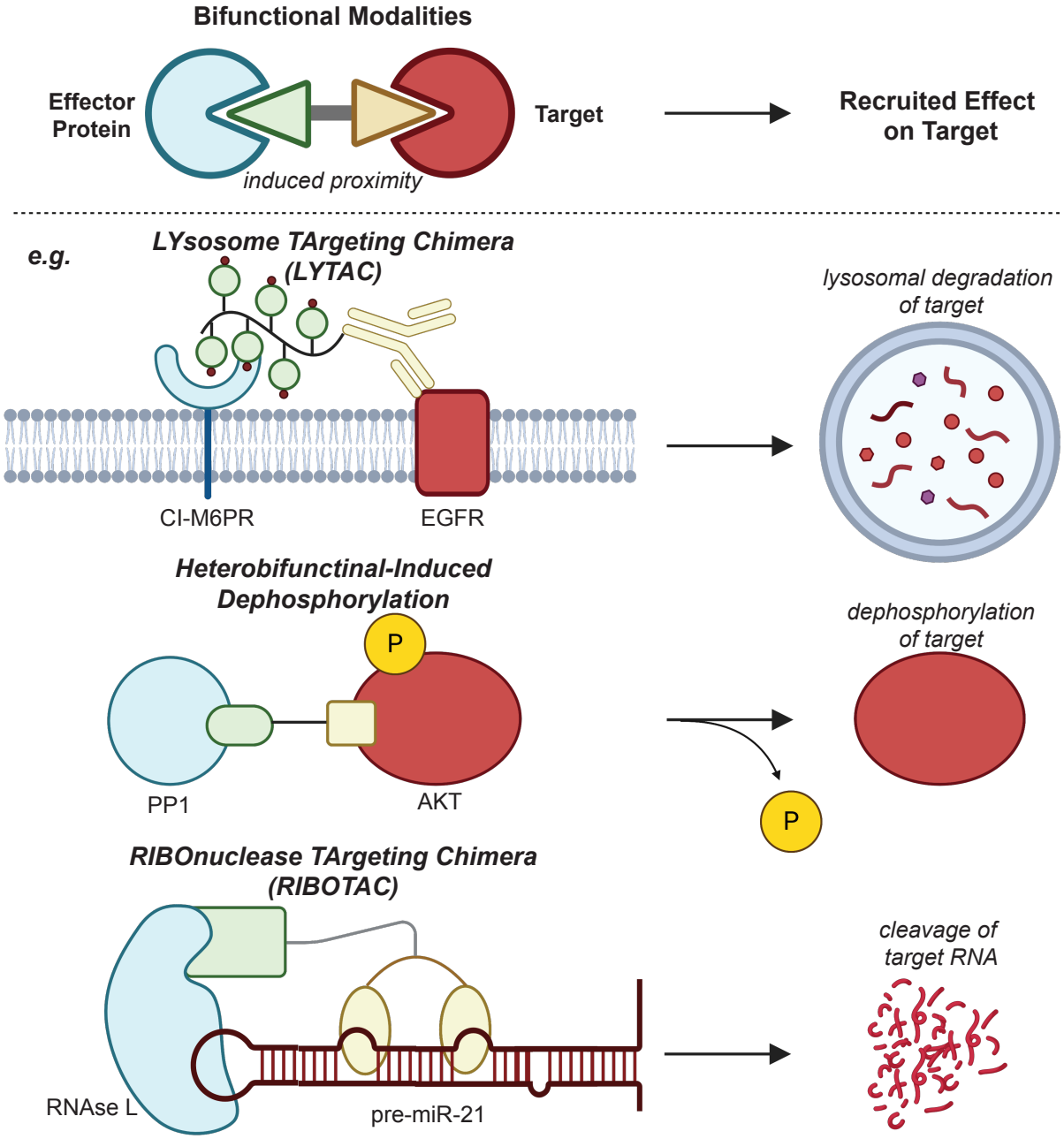

Figure 1.4. Heterobifunctional Modalities Beyond Targeted Protein Degradation. (**A**) Lysosome targeting chimeras (LyTACs) lead to lysosomal degradation of their targets by linking an antibody for the receptor or transmembrane protein of interest to the substrate of the lysomal receptor CI-M6PR, chains of the manose-6-phosphate. (**B**) Phosphatase recruiting chimeras (PhoRCs) are designed to recruit a protein phosphatase to a protein of interest, inducing dephosphorylation of the target. (**C**) Ribonuclease targeting chimeras (RiboTACs) are heterobifunctional molecules that induce targeted degradation of selected RNA sequences by recrtuing RNAse L.

CHAPTER 2

Chemoproteomic Profiling of the Anti-Cancer Natural Product Nimbolide Uncovers Druggable Site on the E3 Ligase RNF114

This chapter is based on the *Nature Chemical Biology* publication “Harnessing the anti-cancer natural product nimbolide for targeted protein degradation”[24] and has been adapted with permission from all co-authors.

2.1 Introduction

Natural products from organisms such as plants and microbes are a rich source of therapeutic lead compounds [36]. The characterization of their biological activities has resulted in myriad medications for a wide range of pathologies including cancer, bacterial and fungal infections, inflammation, and diabetes [36]. Among natural products there exists a subset of covalently acting molecules that bear electrophilic moieties capable of undergoing essentially irreversible reactions with nucleophilic amino acids within proteins to exert their therapeutic activity. Examples of these natural products include penicillin, which irreversibly inhibits serine transpeptidases inducing anti-bacterial activity, or wortmannin, which covalently modifies a functional lysine on PI3-kinase to inhibit its activity [36,37]. The covalent nature of the interaction between these natural products and their therapeutic targets makes them well-suited to the competitive chemoproteomic profiling methods introduced in the previous chapter of this dissertation, allowing for identification of novel druggable hotspots.

Discovering druggable hotspots targeted by anti-cancer and covalently-acting natural products can not only yield new cancer drugs and therapeutic targets but can also reveal unique insights into modalities accessed by natural products in protein targets that are often considered undruggable or difficult to tackle with standard drug discovery efforts. One example of a druggable modality that would be difficult to predict *a priori* is FK506 or Tacrolimus that inhibits peptidylprolyl isomerase activity by binding to FKBP12 thus creating a FKBP12-FK506 complex that modulates T cell signaling via inhibition of calcineurin [38]. Gaining insights into nature's strategies for engaging protein targets can thus provide access to new perspectives on what may be considered druggable.

In this study, we investigated the mechanism of action of the natural product nimbolide (**1**), a limonoid natural product derived from the Neem tree (*Azadirachta indica*) **(Fig. 2.1a)** [39]. Nimbolide has been shown to exert multiple therapeutic effects and possesses a cyclic enone capable of reacting with cysteines [40–42]. In the context of cancer, nimbolide has been shown to inhibit tumorigenesis and metastasis without causing any toxicity or unwanted side effects across a wide range of cancers [43]. While previous studies suggest that nimbolide impairs cancer pathogenicity through modulating signaling pathways and transcription factors linked to survival, growth, invasion, angiogenesis, inflammation, and oxidative stress the direct targets of nimbolide still remain poorly characterized [43].

Identifying direct protein targets of complex natural products remains challenging and often requires synthesizing analogs of these compounds bearing photoaffinity and enrichment handles, a task which is synthetically challenging and has the potential to alter the activity of the molecule[36]. Even with the generation of such probes, identifying the specific amino acid site targeted by natural products is challenging. In this study, we utilized activity-based protein profiling (ABPP) chemoproteomic approaches to map the proteome-wide targets of nimbolide in breast cancer cell proteomes. Using ABPP platforms, we reveal that one of the primary targets of nimbolide in breast cancer cells is cysteine-8 (C8) of the E3 ubiquitin ligase RNF114. Covalent modification of RNF114 by nimbolide leads to impaired ubiquitination and degradation of its substrate—the tumor

suppressor CDKN1A (p21)—leading to its rapid stabilization. Intriguingly, we show that this apparent inhibition of RNF114 activity is through impaired substrate recognition giving rise to the possibility that nimbolide could be used as an E3 ligase recruitment module for targeted protein degradation, as will be discussed in the subsequent chapter of this thesis.

2.2 Effects of Nimbolide on Breast Cancer Phenotypes

Though nimbolide has been shown to impair cancer pathogenicity across many different types of human cancers, we chose to focus on elucidating the role of nimbolide in triple-negative breast cancers (TNBC). TNBCs are devoid of estrogen, progesterone, and HER2 receptors and are amongst the most aggressive cancers with the worst clinical prognosis [44]. Very few targeted therapies currently exist for TNBC patients. Uncovering new therapeutic modalities in TNBCs would thus potentially contribute significantly to reducing breast cancer-associated mortalities. Consistent with previous reports showing anti-cancer activity in breast cancer cells, nimbolide impaired cell proliferation or serum-free cell survival in 231MFP and HCC38 TNBC cells **(Fig. 2.1b-2.1c, Supplementary Fig. 2.1a-2.1b)** [43]**.** We also show that these effects on 231MFP and HCC38 viability are due to a significant increase in apoptotic cells with nimbolide treatment, assessed by flow cytometry analysis **(Fig. 2.1d, Supplementary Fig. 2.1c-2.1e).**

2.3 ABPP to Map Nimbolide Targets in Breast Cancer Cells

To interrogate the mechanisms by which nimbolide impairs breast cancer pathogenicity, we applied the chemoproteomic platform outlined in the previous chapter, isoTOP-ABPP, to determine the specific protein targets of nimbolide. Pioneered by Cravatt and Weerapana, isoTOP-ABPP uses reactivity-based chemical probes to map reactive, functional, and ligandable hotspots directly in complex proteomes [45,46]. When used in a competitive manner, covalently-acting small-molecules can be competed against binding of broad reactivity-based probes to facilitate the rapid discovery of both proteins and ligandable sites targeted by the covalently-acting compound [47–49] **(Fig. 2.2a)**. In this study, we treated breast cancer cells *in situ* with vehicle or nimbolide followed by competitive labeling of proteomes with a cysteine-reactive alkyne-functionalized iodoacetamide probe **(IA-alkyne)** (**2**), after which isotopically light or heavy TEV-cleavable enrichment handles were appended to probe-labeled proteins for isoTOP-ABPP analysis. Probe-modified tryptic peptides were analyzed by liquid chromatography-mass spectrometry (LC-MS/MS) and light to heavy tryptic probe-modified peptide ratios, representing control versus treated IA-alkyne labeled sites, were quantified. IsoTOP-ABPP analysis of ligandable hotspots targeted by *in situ* nimbolide treatment in 231MFP TNBC cells showed one primary target showing an isotopic ratio >4 that was significantly engaged by nimbolide—the E3 ubiquitin ligase RNF114 **(Fig. 2b; Supplementary Dataset 1)**. Importantly, RNF114 knockdown using three independent small interfering RNA (siRNA) resembled the anti-proliferative effects of nimbolide in 231MFP cells **(Fig. 2c-2d, Supplementary Fig. 2a-2b)**. Further demonstrating that RNF114 contributes to the anti-proliferative effects of nimbolide, RNF114 knockdown led to significant resistance to nimbolide-mediated anti-proliferative effects **(Figure 2.2e, Supplementary Fig. 2.2c)**. While nimbolide likely possesses many additional targets beyond RNF114 that are not

accessible with isoTOP-ABPP approaches, our results suggested that RNF114 was a novel target of nimbolide and that RNF114 was in-part responsible for the anti-proliferative effects of this natural product. We thus chose to focus further characterization efforts on the interactions between nimbolide and RNF114.

2.4 Characterization of nimbolide interactions with RNF114

RNF114 is an E3 ubiquitin ligase of the RING family [50]. The site on RNF114 identified by isoTOP-ABPP as the target of nimbolide, C8, falls within the N-terminal region of the protein, predicted to be intrinsically disordered, and resides outside of the two annotated zinc finger domains **(Fig. 2.3a)**. Intrigued by the apparent targeting of an intrinsically disordered region of a protein by a natural product, we sought to investigate the interaction between nimbolide and RNF114.

Because isoTOP-ABPP is a competitive assay between the covalently-acting molecule and a broader reactive probe, it is an indirect read-out of potential nimbolide-targeting hotspots. To confirm that nimbolide directly targeted RNF114, we synthesized the alkyne-functionalized probe shown in three steps from nimbolide (**Fig. 2.3b**). Selective bromination at C2 of the furan moiety and subsequent Suzuki coupling with 4-Formylphenylboronic acid afforded the aryl-aldehyde (**3**), which was converted to its corresponding carboxylic acid (**4**) via Pinnick oxidation. Finally, coupling of (**4**) and propargyl amine (HATU, DIPEA) afforded the target **nimbolide-alkyne probe** (**5**). We confirmed that this nimbolide probe reacts with pure human RNF114 protein as shown by labeling of the protein on a denaturing SDS/PAGE gel. This labeling event was also competed by nimbolide and abrogated in the C8A RNF114 mutant **(Fig. 2.3c)**. As the nimbolide-alkyne probe is a synthetically laborious probe that requires the rather expensive nimbolide as a starting material, we also sought to develop a simpler probe that could label C8 of RNF114. In initial studies trying to validate RNF114 interactions with nimbolide, where we competed nimbolide against IA-alkyne labeling of RNF114, full inhibition of labeling was not observed, likely due to alkylation of multiple cysteines by IA-alkyne beyond C8 **(Fig. 2.3d)**. Thus, we synthesized a more tailored alkyne-functionalized cyclic enone probe **JNS27** (**6**), which showed selective labeling of C8 on RNF114 as evidenced by lack of labeling of C8A RNF114 mutant protein **(Fig. 2.3e)**. With JNS27, we were able to demonstrate full competition of JNS27 labeling with nimbolide with a 50 % inhibitory concentration (IC50) of 0.73 μM **(Fig. 2.3e)**. To demonstrate that nimbolide interactions with RNF114 are not completely driven by reactivity, but rather also through additional interactions with the protein, we show that nimbolide competes against labeling of RNF114 with a rhodamine-functionalized iodoacetamide probe (IA-rhodamine) at far lower concentrations compared to the simpler JNS27 probe or iodoacetamide with an IC50 of 0.55, 22, and >100 μM, respectively **(Supplementary Fig. 2.2d)**. Furthermore, a direct mass adduct of nimbolide was detected on the tryptic peptide containing C8 on RNF114 by LC-MS/MS after incubation of pure protein with the natural product **(Supplementary Fig. 2.2e)**. All of these experiments taken together provide evidence that nimbolide modifies an intrinsically disordered region of RNF114 at C8 through a covalent bond formation.

We next performed two complementary experiments to demonstrate that nimbolide directly engaged RNF114 in 231MFP breast cancer cells. First, we showed dose-responsive nimbolide-alkyne labeling of RNF114 *in situ* by treating Flag-tagged RNF114 expressing cells with the probe, followed by enrichment of Flag-tagged RNF114 and appending rhodamine-azide onto probe-labeled protein by CuAAC and visualizing by gel-based ABPP methods **(Fig. 2.3f, Supplementary Fig. 2.2f).** We observed robust *in situ* nimbolide-alkyne labeling with 10 μM of probe, but also observed lower but significant probe labeling even down to 100 nM **(Fig. 2.3f, Supplementary Fig. 2.2f)**. Second, we also showed *in situ* labeling of endogenous RNF114 with the nimbolide-alkyne probe by treating cells with the probe, followed by appending biotin-azide onto probe-labeled proteins by CuAAC and visualizing RNF114 pulldown by Western blotting **(Fig. 2.3g)**. In this case, significant pulldown was observed at 50 μM of the nimbolide-alkyne probe but not lower concentrations. In this experiment, we show that an unrelated protein such as GAPDH is not enriched by the nimbolide-alkyne probe **(Fig. 2.3g)**. Using these latter conditions, we also performed a complementary quantitative proteomic profiling study to identify any additional proteins that may be enriched from *in situ* labeling of 231MFP cells with the nimbolide-alkyne probe **(Supplementary Dataset 2)**. Due to acute cytotoxicity issues, we were not able perform *in situ* competition studies with higher concentrations of nimbolide itself. In this study, we showed that RNF114 was one of the proteins enriched by the nimbolide-alkyne probe by >10-fold compared to no-probe controls. We also identified 114 additional proteins that were enriched by the probe by >10-fold compared to no-probe controls. These proteins represent additional potential covalent or non-covalent targets that may contribute to the anti-proliferative effects of nimbolide. These enriched targets may also represent proteins with low to partial degrees of engagement with nimbolide, whereas isoTOP-ABPP experiments are meant to identify higher engagement targets. Additionally, these proteins may include probe-specific targets or proteins that may be enriched indirectly through interactions with direct nimbolide-labeled proteins **(Supplementary Dataset 2)**. Nonetheless, we show that RNF114 is engaged by the nimbolide-alkyne probe in breast cancer cells, even down to 100 nM, and that the anti-proliferative effects of nimbolide are at least in-part mediated by RNF114.

2.5 Effects of nimbolide on RNF114 function

RNF114 has been previously shown to ubiquitinate and mediate the degradation of the tumor suppressor p21, among other substrates [50–52]. In an *in vitro* reconstituted system, nimbolide inhibited both RNF114 autoubiquitination and p21 ubiquitination activity **(Fig. 2.4a-2.4b, Supplementary Fig. 2.3a-2.3b)**. The RNF114 C8A mutation did not affect basal RNF114 autoubiquitination activity, but attenuated the inhibition observed with nimbolide treatment **(Fig. 2.4c, Supplementary Fig. 2.3c)**. Previous characterization of RNF114 suggested that the N-terminus may be involved in substrate recognition [50]. Consistent with this premise, we found that the amount of p21 co-immunoprecipitated with RNF114 was reduced by nimbolide, suggesting that the apparent inhibition of RNF114 may be due to impaired substrate recognition, rather than inhibition of its catalytic activity **(Fig. 2.4d, Supplementary Fig. 2.3d)**. We further demonstrated that nimbolide treatment in 231MFP cells stabilized CDKN1A (p21) protein levels within 1 hour in a dose-responsive manner, with no significant changes to TP53

(p53) levels **(Fig. 2.4e, Supplementary Fig. 2.3e-2.3f)**. The elevated levels of CDKN1A observed were not due to transcriptional downregulation of mRNA levels, as p21 mRNA levels remained unchanged with nimbolide treatment **(Supplementary Fig. 2.3g)**. To identify other potential substrates of RNF114, we also performed a tandem mass tagging (TMT)-based quantitative proteomic experiment on 231MFP cells treated with nimbolide. Consistent with our Western blotting data, we observed CDKN1A (p21) as one of the proteins that were significantly elevated >2-fold with nimbolide treatment **(Fig. 2.4f, Supplementary Dataset 3).** We also observed the levels of several other targets that were heightened by nimbolide treatment, including CDKN1C (p57), PEG10, and CTGF. Beyond CDKN1A (p21) and CDKN1C (p57) which have previously been reported as potential RNF114 substrates [50], we conjectured that PEG10 and CTGF may also represent additional novel substrates of RNF114 **(Fig. 2.4f, Supplementary Dataset 3)**. Consistent with this premise, we demonstrated in an *in vitro* RNF114 ubiquitination assay that RNF114 ubiquitinates PEG10 and CTGF and that this ubiquitination is inhibited by nimbolide **(Fig. 2.4g)**. As both p21 and p57 are tumor suppressors that, when elevated, promote cell cycle arrest and apoptosis [53,54], we postulated that the stabilization of both of these tumor suppressors may be responsible for the anti-proliferative effect of nimbolide. We demonstrated that dual knockdown of CDKN1A (p21) and CDKN1C (p57) results in significant attenuation in nimbolide-mediated anti-proliferative effects in 231MFP breast cancer cells **(Fig. 2.4h-2.4i).** Collectively, these data suggest that nimbolide reacts with an intrinsically disordered C8 of RNF114 in breast cancer cells to disrupt RNF114-substrate recognition, leading to inhibition of ubiquitination of its substrates such as CDKN1A and CDKN1C, leading to their stabilization, and impaired cell proliferation in breast cancer cells.

2.6 Discussion

Collectively, this work shows compelling evidence that nimbolide impairs breast cancer pathogenicity in-part through targeting a substrate recognition domain at C8 within RNF114 to inhibit p21 ubiquitination and degradation, leading to its stabilization.

We demonstrate that nimbolide disrupts RNF114 interactions with one of its endogenous substrate p21 and we also show that p21 levels are rapidly stabilized in breast cancer cells in a p53-independent manner. Several other E3 ligases have also been reported to degrade p21, including SCF^{SKP2}, $CRL4^{CDT2}$, and CHIP under varying conditions during cell cycle or exogenous stress [55–57]. Previous studies have shown that RNF114 expression is elevated at late G1 phase to regulate p21 and p57 levels and is crucial for G1-to-S phase transition [50]. Other RNF114 substrates that have been reported include TAB1 involved in maternal-to-zygotic transition and A20 involved in NF-□B activity and T cell activation [58,59]. In cancer contexts or other cell and tissue types, nimbolide may thus have additional activities through regulating the levels of other RNF114 protein substrates. Intriguingly, we show CTGF and PEG10 may represent additional substrates of RNF114 as demonstrated by their nimbolide-induced stabilization *in situ* and polyubiquitination by RNF114 *in vitro*. Further studies are required to establish these additional proteins as direct and endogenous substrates of RNF114. Furthermore, while we show that RNF114 is one target of nimbolide that at least in-part mediates its

effects upon proliferation and targeted protein degradation, we also show with the nimbolide-alkyne probe that nimbolide likely possesses many additional protein targets. These additional targets may include other covalent interactions with cysteines that are not labeled by the IA-alkyne cysteine-reactive probe in isoTOP-ABPP experiments, may represent covalent interactions with other amino acids, may represent reversible interactions with additional protein targets, or may include proteins are indirectly enriched from interactions with direct nimbolide-labeled proteins. Despite nimbolide possessing multiple potential targets, we demonstrate that RNF114 is an important and functional target of nimbolide in breast cancer cells.

Our results also demonstrate that nimbolide functionally targets an intrinsically disordered region within RNF114. Intrinsically disordered regions and intrinsically disordered proteins (IDPs) represent an historically challenging area of drug development. Solving the structure of RNF114 covalently modified with nimbolide has thus far proven challenging, but future studies investigating whether nimbolide induces order in the N-terminus would provide insights into the ligandability of intrinsically disordered and undruggable protein targets and strategies for potentially targeting other E3 ligases.

Overall, our study further demonstrates the utility of using ABPP-based chemoproteomic platforms to identify unique druggable modalities exploited by natural products. Intriguingly, we show that a natural product can functionally access an E3 ligase protein-protein interaction site and remarkably does so in an intrinsically disordered region of the protein.

2.7 Figures

Figure 2.1

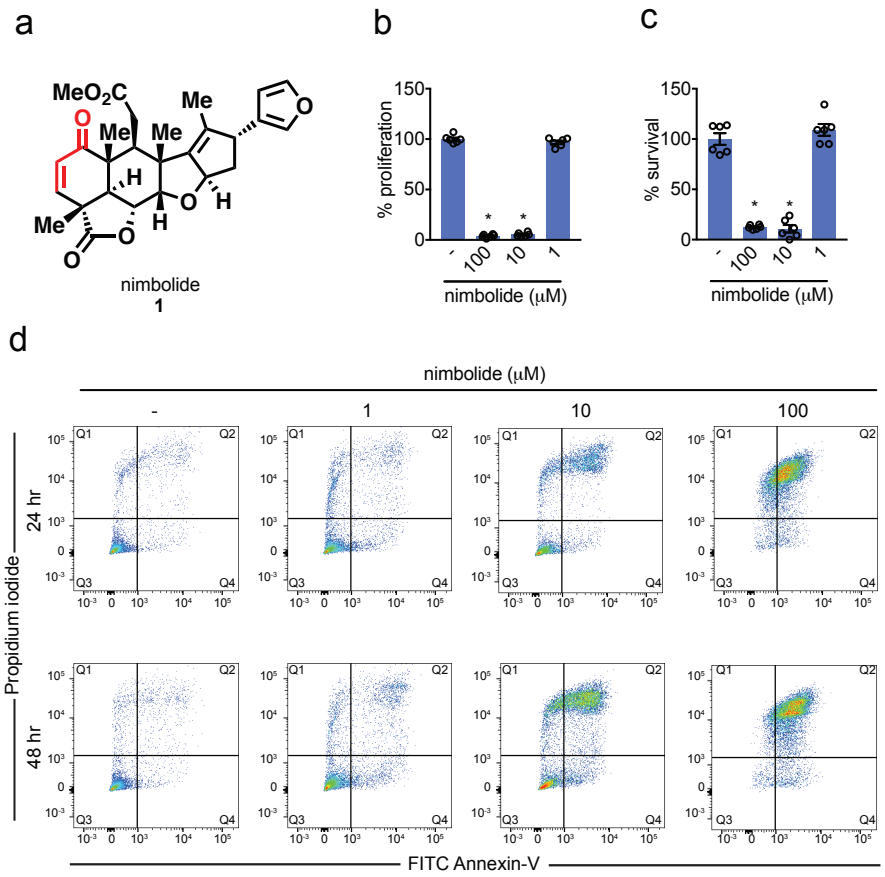

Figure 2.1. Nimbolide impairs breast cancer cell proliferation or survival.
(a) Structure of nimbolide. Nimbolide possesses a cyclic enone that is potentially cysteine-reactive. (b, c) 231MFP breast cancer cell proliferation in serum-containing media (b) and serum-free cell survival (c). Data shown in (b and c) are average ± sem, n=6 biologically independent samples/group. (d) Percent of propidium iodide and Annexin-V-positive (PI+/Annexin-V+) cells assessed by flow cytometry after treating 231MFP cells with DMSO vehicle or nimbolide for 24 or 48 h. Shown are representative FACS data from n=3 biologically independent samples/group. Quantitation of percentage of late-stage apoptotic cells defined as defined as FITC+/PI+ cells are shown in Supplementary Fig. 2.1d. Statistical significance was calculated with unpaired two-tailed Student's t-tests. Significance is expressed as *p=7.75x10-14 and 1.14x10-13 for 100 and 10 μM, respectively in (b) and *p=3.88x10-8 and 1.53x10-7 for 100 and 10 μM, respectively in (c) compared to vehicle-treated controls.

Figure 2.2

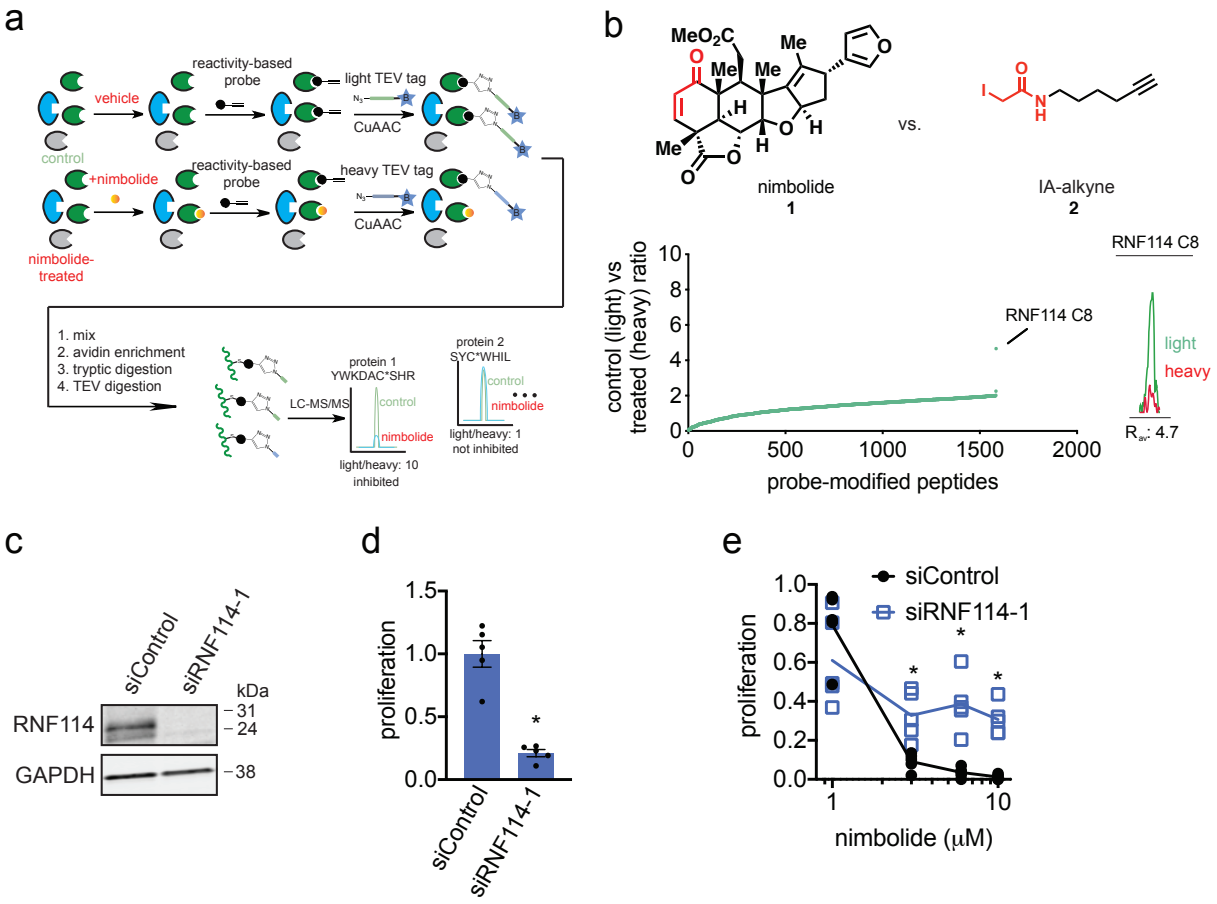

Figure 2.2. isoTOP-ABPP analysis of nimbolide in 231MFP breast cancer cell proteomes reveal RNF114 as a target.
(a) Schematic of isoTOP-ABPP in which 231MFP breast cancer cells were treated with DMSO or nimbolide (10 μM, 1.5 h *in situ*), after which cells were harvested and proteomes were labeled *ex situ* with IA-alkyne (100 μM, 1 h) followed by the isoTOP-ABPP procedure. **(b)** isoTOP-ABPP analysis of nimbolide (10 μM) in 231MFP breast cancer cells *in situ* analyzed as described in **(a).** Light vs heavy isotopic probe-modified peptide ratios are shown in the left plot where the primary target with the highest ratio was C8 of RNF114. Shown on the right is a representative MS1 light vs heavy peak for the probe-modified peptide bearing C8 of RNF114. **(c)** RNF114 knockdown by short interfering RNA (siRNA) targeting RNF114 validated by Western blotting of RNF114 compared to siControl 231MFP cells. GAPDH expression is shown as a loading control. Shown gel is a representative gel from n=3 biological replicates/group. **(d)** 231MFP cell proliferation after 24 h in siControl and siRNF114 cells. **(e)** Nimbolide effects on 231MFP siControl and siRNF114 231MFP breast cancer cells. Nimbolide effects on 231MFP siControl and siRNF114 231MFP breast cancer cells. Cells were treated with DMSO vehicle or nimbolide for 24 h after which proliferation was assessed. Data for siControl or siRNF114 group was normalized to the respective DMSO vehicle control in each group. Individual

biologically independent sample data is shown and the lines indicate mean values. Data shown in **(d)** is average ± sem. Data shown in **(b, c)** are from n=3, in **(d, e)** are from n=5 biologically independent samples/group. Statistical significance in **(d, e)** was calculated with unpaired two-tailed Student's t-tests. Significance in **(d)** is expressed as *$p=4.52x10^{-5}$ compared to siControl cells. Significance in **(e)** is expressed as *$p=1.90x10^{-5}$, $2.72x10^{-4}$, and 0.00101 for 10, 6, and 3 μM, respectively compared to the corresponding nimbolide treatment concentration from siControl groups.

Figure 2.3

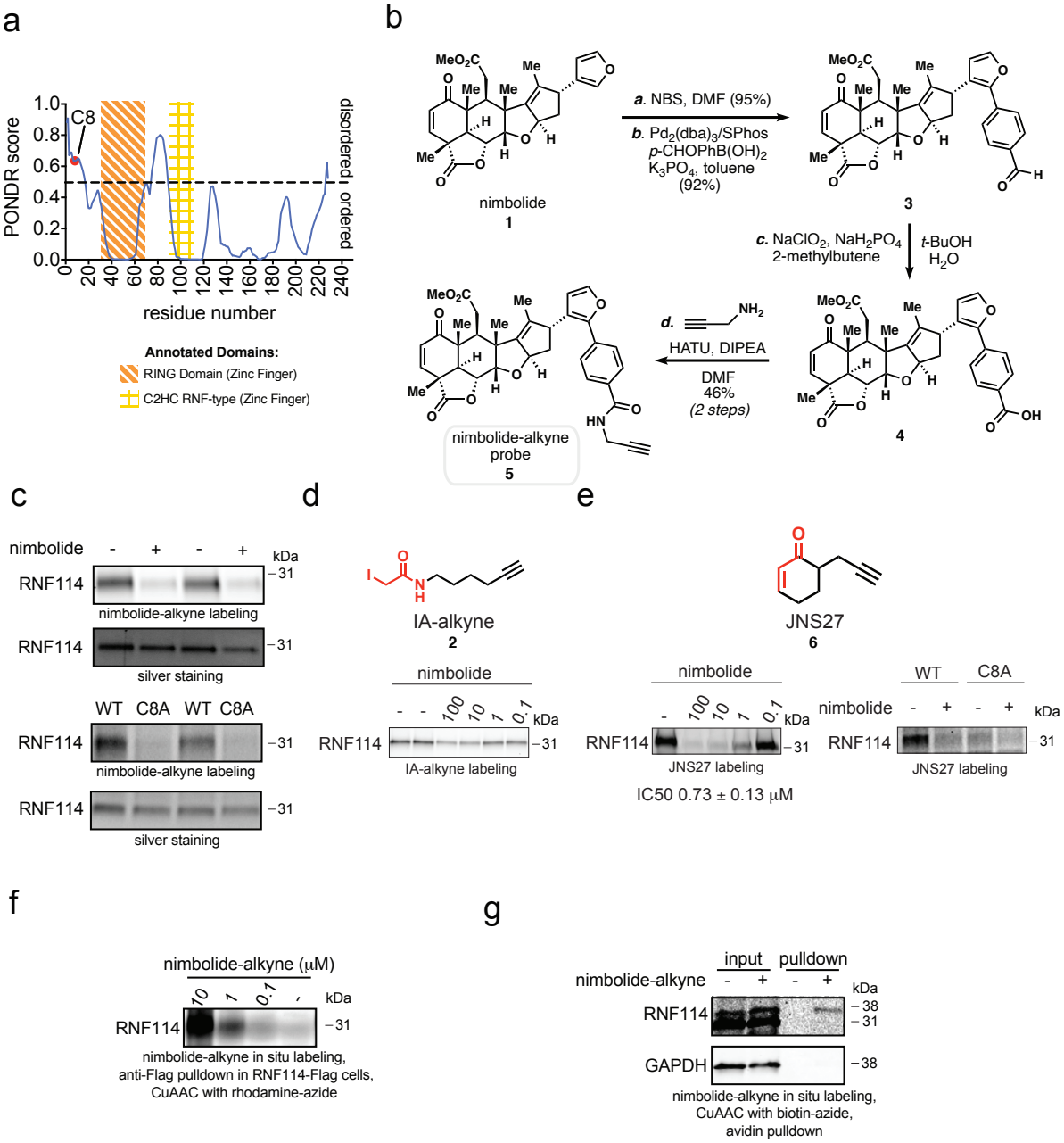

Figure 2.3. Nimbolide reacts covalently with C8 of RNF114.
(a) Nimbolide targets an intrinsically disordered region within RNF114 as assessed by PONDR. **(b)** Route for synthesis of the alkyne-functionalized nimbolide probe. **(c)** Gel-based ABPP analysis of pure human RNF114 protein labeled with nimbolide probe. In the upper two panels, pure RNF114 protein was pre-incubated with DMSO vehicle or nimbolide (100 μM, 30 min) prior to labeling with the nimbolide probe (10 μM, 1 h) in PBS. In the lower two panels, pure wild-type and C8A mutant RNF114 protein were labeled with the nimbolide probe (10 μM, 1 h) in PBS with 1 mg/ml BSA. **(d)** Gel-based ABPP

analysis of nimbolide competition against IA-alkyne (10 μM) or JNS27 (50 μM) labeling of pure RNF114 protein. Structures of IA-alkyne and JNS27 probes are shown with reactive moieties highlighted in red. Shown also is gel-based ABPP analysis of nimbolide (50 μM) competition against JNS27 labeling of wild-type and C8A mutant RNF114 protein. In these experiments, DMSO or nimbolide was pre-incubated for 30 min prior to probe labeling for 1 h. **(e)** Nimbolide-alkyne labeling of Flag-RNF114 in 231MFP cells. 231MFP cells stably expressing a Flag-tagged RNF114 were treated with DMSO vehicle or nimbolide-alkyne for 2 h. RNF114 was subsequently enriched from harvested cell lysates and then rhodamine-azide was appended onto probe-labeled proteins by CuAAC, after which nimbolide-alkyne labeling was visualized by SDS/PAGE and in-gel fluorescence. **(f)** Nimbolide-alkyne labeling of endogenous RNF114 in 231MFP cells. 231MFP cells were treated with DMSO vehicle or nimbolide-alkyne (50 μM) for 1.5 h. Biotin-azide was appended to probe-labeled proteins by CuAAC, and these proteins were subsequently avidin-enriched. Resulting pulled down proteins were analyzed by SDS/PAGE and Western blotting for RNF114. Gels shown in **(c-f)** are representative gels from n=3 biologically independent samples/group.

Figure 2.4

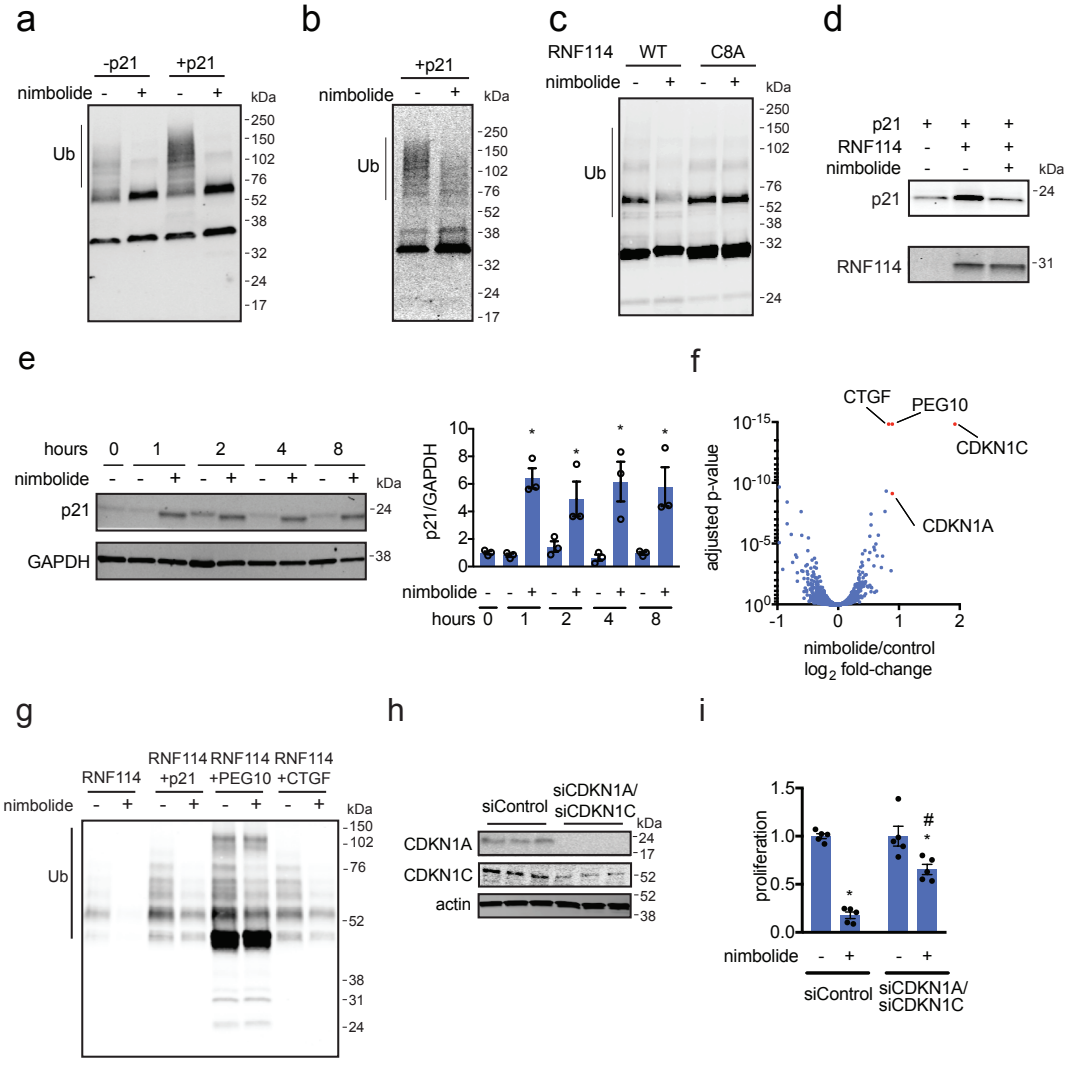

Figure 2.4. Nimbolide inhibits RNF114 activity through disrupting substrate recognition.

(a, b) RNF114 ubiquitination assay with pure GST-Ube1, GST-UBE2D1, and RNF114 protein, Flag-Ubiquitin and ATP with or without addition of p21 and blotting against Flag-ubiquitin (**a**) or p21 **(b). (c)** RNF114 autoubiquitination assay with DMSO or nimbolide (100 μM) treatment with wild-type or C8A mutant RNF114. **(d)** In an *in vitro* incubation of pure RNF114 and p21 protein, Flag-RNF114 pulldown and p21 enrichment were inhibited by nimbolide (100 μM). **(e)** 231MFP cells were treated with nimbolide (100 μM). Shown are p21 levels in DMSO control or nimbolide-treated cells. **(f)** Tandem mass tag (TMT)-based quantitative proteomic profiling of 231MFP breast cancer cells treated with DMSO vehicle or nimbolide (100 nM) for 12 h. Shown in red are proteins that are significantly heightened in levels >2-fold. Data shown in **(f)** are for 6397 proteins quantified with 2 or more unique peptides in n=3 biologically independent samples/group, see **Supplementary Dataset 3** for details. **(g)** RNF114 ubiquitination assay with pure GST-

Ube1, GST-UBE2D1, and RNF114 protein, Flag-Ubiquitin and ATP with the addition of p21 (CDKN1A), PEG10, or CTGF and blotting against Flag-ubiquitin. DMSO or Nimbolide (100 μM) was pre-incubated with RNF114, before the addition of the E1 and E2 enzymes, Flag-ubiquitin and ATP to start the reaction. **(h)** p21 (CDKN1A) and p57 (CDKN1C) expression in siControl and siCDKN1A/siCDKN1C 231MFP cells, assessed by Western blotting, alongside actin as a loading control. **(i)** 231MFP cell proliferation in siControl or siCDKN1A/siCDKN1C cells treated with DMSO vehicle or nimbolide (6 μM) for 24 h. Gels shown in **(a-e, g)** are representative images from n=3 biologically independent samples/group. Quantification for blots shown in **(a-d)** are in **Supplementary Fig. 2.3a-2.3d.** All three biologically independent samples/group are shown in **(h)**. Data shown in **(i)** are average ± sem, n=5 biologically independent samples/group. Statistical significance was calculated with unpaired two-tailed Student's t-tests in **(e, i)**. Significance is expressed as *p=000799, 0.0295, 0.00962, and 0.0135 for 1, 2, 4, and 8h, respectively compared to vehicle-treated control groups for each time point in **(e),** and $p=5.65x10^{-8}$ and 0.0173 compared to vehicle-treated siControl and siCDKN1A/siCDKN1C groups, respectively in **(i)**. Significance expressed as #$p=6.70x10^{-5}$ compared to nimbolide-treated siControl cells in **(i)**.

2.8 Acknowledgement of Co-Author Contributions

J.N. Spradlin, T.J. Maimone and D.K. Nomura conceived the project and wrote the paper. J.N. Spradlin, X. Hu, C.C. Ward, M.D. Jones, D.E. Bussiere, J.R. Thomas, J.A. Tallarico, J.M. McKenna, M. Schirle, T.J. Maimone and D.K. Nomura provided intellectual contributions and insights into project direction. J.N. Spradlin, X. Hu, S.M. Busby, M. To, J.A. Olzmann, M. Schirle, T.J. Maimone and D.K. Nomura designed the experiments and analyzed data. C.C. Ward, M.D. Jones developed bioinformatic methods and analyzed data for proteomics experiments. J.N. Spradlin, X. Hu, S.M. Busby, L. Ou, M.To, A. Proudfoot, E. Ornelas, M. Woldegiorgis, and D.K. Nomura performed experiments and analyzed data. A. Proudfoot, E. Ornelas, M. Woldegiorgis, and D.E. Bussiere provided pure RNF114 protein. J.N. Spradlin, X. Hu, and T.J. Maimone designed and synthesized compounds. J.N. Spradlin, S.M. Busby, M.D. Jones, J.A. Olzmann, D.E. Bussiere, J.R. Thomas, JAT, J.A. Tallarico, J.M. McKenna, M. Schirle, T.J. Maimone and D.K. Nomura edited the paper.

2.9 Methods

Cell Culture

The 231MFP cells were obtained from Prof. Benjamin Cravatt and were generated from explanted tumor xenografts of MDA-MB-231 cells as previously described [60]. HCC38 and HEK293T cells were obtained from the American Type Culture Collection. HEK293T cells were cultured in DMEM containing 10% (v/v) fetal bovine serum (FBS) and maintained at 37°C with 5% CO_2. 231MFP were cultured in L15 medium containing 10% FBS and maintained at 37°C with 0% CO_2. HCC38 cells were cultured in RPMI medium containing 10% FBS and maintained at 37°C with 5% CO_2. HAP1 RNF114 wild-type and knockout cell lines were purchased from Horizon Discovery. The RNF114 knockout cell line was generated by CRISPR/Cas9 to contain a frameshift mutation in a coding exon of RNF114. HAP1 cells were grown in Iscove's Modified Dulbecco's Medium (IMDM) in the presence of 10 % FBS and penicillin/streptomycin.

Survival and Proliferation Assays

Cell survival and proliferation assays were performed as previously described using Hoechst 33342 dye (Invitrogen) according to manufacturer's protocol and as previously described [47]. 231MFP cells were seeded into 96-well plates (40,000 for survival and 20,000 for proliferation) in a volume of 150 µL and allowed to adhere overnight. Cells were treated with an additional 50 µL of media containing 1:250 dilution of 1000 x compound stock in DMSO. After the appropriate incubation period, media was removed from each well and 100 µL of staining solution containing 10% formalin and Hoechst 33342 dye was added to each well and incubated for 15 min in the dark at room temperature. After incubation, staining solution was removed, and wells were washed with PBS before imaging. Studies with HCC38 cells were also performed as above but were seeded with 20,000 cells for survival and 10,000 cells for proliferation.

Assessing Apoptosis in Breast Cancer Cells

Apoptotic cells were analyzed in cells treated with DMSO vehicle or compound containing serum-free media for 24 or 48 h using flow cytometry. We measured the percentage of Annexin V-positive and propidium iodide-negative early apoptotic cells and Annexin V-positive and propidium iodide-positive late apoptotic cells as previously described [61]. Data analysis was performed using FlowJo software.

IsoTOP-ABPP Chemoproteomic Studies

IsoTOP-ABPP studies were done as previously reported [45,47,48]. Cells were lysed by probe sonication in PBS and protein concentrations were measured by BCA assay [62]. For *in situ* experiments, cells were treated for 90 min with either DMSO vehicle or covalently-acting small molecule (from 1000X DMSO stock) before cell collection and lysis. Proteomes were subsequently labeled with IA-alkyne labeling (100 μM) for 1 h at room temperature. CuAAC was used by sequential addition of tris(2-carboxyethyl)phosphine (1 mM, Sigma), tris[(1-benzyl-1H-1,2,3-triazol-4-yl)methyl]amine (34 μM, Sigma), copper (II) sulfate (1 mM, Sigma), and biotin-linker-azide—the linker functionalized with a TEV protease recognition sequence as well as an isotopically light or heavy valine for treatment of control or treated proteome, respectively. After CuAAC, proteomes were precipitated by centrifugation at 6500 x g, washed in ice-cold methanol, combined in a 1:1 control/treated ratio, washed again, then denatured and resolubilized by heating in 1.2 % SDS/PBS to 80°C for 5 minutes. Insoluble components were precipitated by centrifugation at 6500 x g and soluble proteome was diluted in 5 ml 0.2% SDS/PBS. Labeled proteins were bound to avidin-agarose beads (170 μl resuspended beads/sample, Thermo Pierce) while rotating overnight at 4°C. Bead-linked proteins were enriched by washing three times each in PBS and water, then resuspended in 6 M urea/PBS (Sigma) and reduced in TCEP (1 mM, Sigma), alkylated with iodoacetamide (IA) (18 mM, Sigma), then washed and resuspended in 2 M urea and trypsinized overnight with 0.5 μg/μl sequencing grade trypsin (Promega). Tryptic peptides were eluted off. Beads were washed three times each in PBS and water, washed in TEV buffer solution (water, TEV buffer, 100 μM dithiothreitol) and resuspended in buffer with Ac-TEV protease and incubated overnight. Peptides were diluted in water and acidified with formic acid (1.2 M, Spectrum) and prepared for analysis.

Mass Spectrometry Analysis

Peptides from all chemoproteomic experiments were pressure-loaded onto a 250 μm inner diameter fused silica capillary tubing packed with 4 cm of Aqua C18 reverse-phase resin (Phenomenex # 04A-4299) which was previously equilibrated on an Agilent 600 series HPLC using gradient from 100% buffer A to 100% buffer B over 10 min, followed by a 5 min wash with 100% buffer B and a 5 min wash with 100% buffer A. The samples were then attached using a MicroTee PEEK 360 μm fitting (Thermo Fisher Scientific #p-888) to a 13 cm laser pulled column packed with 10 cm Aqua C18 reverse-phase resin and 3 cm of strong-cation exchange resin for isoTOP-ABPP studies. Samples were analyzed using an Q Exactive Plus mass spectrometer (Thermo Fisher Scientific) using a 5-step Multidimensional Protein Identification Technology (MudPIT) program, using 0 %, 25 %, 50 %, 80 %, and 100 % salt bumps of 500 mM aqueous ammonium acetate and using a gradient of 5-55 % buffer B in buffer A (buffer A: 95:5

water:acetonitrile, 0.1 % formic acid; buffer B 80:20 acetonitrile:water, 0.1 % formic acid). Data was collected in data-dependent acquisition mode with dynamic exclusion enabled (60 s). One full MS (MS1) scan (400-1800 m/z) was followed by 15 MS2 scans (ITMS) of the nth most abundant ions. Heated capillary temperature was set to 200 °C and the nanospray voltage was set to 2.75 kV.

Data was extracted in the form of MS1 and MS2 files using Raw Extractor 1.9.9.2 (Scripps Research Institute) and searched against the Uniprot human database using ProLuCID search methodology in IP2 v.3 (Integrated Proteomics Applications, Inc) [63]. Cysteine residues were searched with a static modification for carboxyaminomethylation (+57.02146) and up to two differential modifications for methionine oxidation and either the light or heavy TEV tags (+464.28596 or +470.29977, respectively). Peptides were required to be fully tryptic peptides and to contain the TEV modification. ProLUCID data was filtered through DTASelect to achieve a peptide false-positive rate below 5%. Only those probe-modified peptides that were evident across two out of three biological replicates were interpreted for their isotopic light to heavy ratios. For those probe-modified peptides that showed ratios >2, we only interpreted those targets that were present across all three biological replicates, were statistically significant, and showed good quality MS1 peak shapes across all biological replicates. Light versus heavy isotopic probe-modified peptide ratios are calculated by taking the mean of the ratios of each replicate paired light vs. heavy precursor abundance for all peptide spectral matches (PSM) associated with a peptide. The paired abundances were also used to calculate a paired sample t-test p-value in an effort to estimate constancy within paired abundances and significance in change between treatment and control. P-values were corrected using the Benjamini/Hochberg method.

Knockdown of RNF114, CDKN1A (p21) and CDKN1C (p57) by RNA Interference (RNAi) in 231MFP Cells

RNAi was performed by using siRNA purchased from Dharmacon specific to RNF114 or p21 and p57 for dual knockdown. In brief, 231MFP cells were seeded at a density of $5x10^4$ cells per mL full media in a 96-well format. On day 0, 231MFP cells were transfected with corresponding small interfering RNA (siRNA) vs. non-targeting negative control (Dharmacon, ON-TARGETplus Non-targeting Pool D-001810-10-05) duplexes at 50 nM using Dharmafect 1 (Dharmacon) as a transfection reagent for 48 h. Thereafter (day 2), transfection media was supplemented with fresh DMSO or compound containing full L15 media and cultured for an additional 24 to 48 h before undergoing cell viability testing as described above. At the time of treatment (day 2), RNA was extracted for analysis by qRT-PCR and lysates were obtained for Western blotting confirmation of knockdown.

Targeting Sequences:
siRNF114-1: GUGUGAAGGCCACCAUUAA (Dharmacon J-007024-08-0002)
siRNF114-2: GCUUAGAGGUGUACGAGAA (Dharmacon J-007024-05-0002)
siRNF114-3: GCACGGAUACCAAAUCUGU (Dharmacon J-007024-06-0002)
siCDKN1A: AGACCAGCAUGACAGAUUU (Dharmacon J-003471-12-0002)
siCDKN1C: CUGAGAAGUCGUCGGGCGA (Dharmacon J-003244-13-0002)

Gene Expression by qPCR

Total RNA was extracted from cells using Trizol (Thermo Fisher Scientific). cDNA was synthesized using MaximaRT (Thermo Fisher Scientific) and gene expression was confirmed by qPCR using the manufacturer's protocol for Fisher Maxima SYBR Green (Thermo Fisher Scientific) on the CFX Connect Real-Time PCR Detection System (BioRad). Primer sequences for Fisher Maxima SYBR Green were derived from Primer Bank. Sequences of primers are as follows:
RNF114 Forward: AAT GTT CCA AAC CG
RNF114 Reverse: TTG CAG TGT TCC AC
CDKN1A Forward: TGT CCG TCA GAA CCC ATG C
CDKN1A Reverse: AAA GTC GAA GTT CCA TCG CTC
PPIA (Cyclophilin) Forward: CCC ACC GTG TTC TTC GAC ATT
PPIA (Cyclophilin) Reverse: GGA CCC GTA TGC TTT AGG ATG A

Gel-Based ABPP

Gel-based ABPP methods were performed as previously described [47]. Recombinant pure human proteins were purchased from Origene. Pure proteins (0.1 µg) were pre-treated with DMSO vehicle or covalently-acting small molecules for 30 min at room temperature in an incubation volume of 50 µL PBS, and were subsequently treated with JNS27 (50 µM final concentration) for 1 h at room temperature. CuAAC was performed to append rhodamine-azide (1 µM final concentration) onto alkyne probe-labeled proteins. Samples were then diluted with 20 µL of 4 x reducing Laemmli SDS sample loading buffer (Alfa Aesar) and heated at 90 °C for 5 min. The samples were separated on precast 4-20% TGX gels (Bio-Rad Laboratories, Inc.). Prior to scanning by ChemiDoc MP (Bio-Rad Laboratories, Inc), gels were fixed in a solution of 10% acetic acid, 30% ethanol for 2 hrs. Inhibition of target labeling was assessed by densitometry using ImageJ.

Synthesis and Characterization of the Nimbolide-Alkyne Probe and Degraders XH1 and XH2

See appendix "Chapter 2 Supplementary Information" for experimental details.

Synthesis and Characterization of JNS27

See appendix "Chapter 2 Supplementary Information" for experimental details.

Covalent Ligand Library

The synthesis and characterization of most of the covalent ligands screened against RNF114 have been previously reported [47,64–66]. Synthesis of TRH 1-156, TRH 1-160, TRH 1-167, YP 1-16, YP 1-22, YP 1-26, YP 1-31, YP 1-44 have been previously reported [67–74]. Compounds starting with "EN" were purchased from Enamine LLC. The synthesis and characterization of other covalent ligands not previously reported are described in appendix "Chapter 2 Supplementary Information"

Western Blotting

Antibodies to RNF114 (Millipore Sigma, HPA021184), p21 (Cell Signaling Technology, 12D1), GAPDH (Proteintech Group Inc., 60004-1-Ig), BRD4 (Abcam plc, Ab128874), DYKDDDDK Tag (Cell Signaling Technology, D6W5B) and beta-actin

(Proteintech Group Inc., 6609-1-Ig) were obtained from various commercial sources and dilutions were prepared per recommended manufacturers' procedures. Proteins were resolved by SDS/PAGE and transferred to nitrocellulose membranes using the iBlot system (Invitrogen). Blots were blocked with 5 % BSA in Tris-buffered saline containing Tween 20 (TBST) solution for 1 h at room temperature, washed in TBST, and probed with primary antibody diluted in recommended diluent per manufacturer overnight at 4 °C. Following washes with TBST, the blots were incubated in the dark with secondary antibodies purchased from Ly-Cor and used at 1:10,000 dilution in 5 % BSA in TBST at room temperature. Blots were visualized using an Odyssey Li-Cor scanner after additional washes. If additional primary antibody incubations were required the membrane was stripped using ReBlot Plus Strong Antibody Stripping Solution (EMD Millipore, 2504), washed and blocked again before being reincubated with primary antibody.

Expression and Purification of Wild-type and C8A Mutant RNF114 Protein

RNF114 was expressed and purified using several methods. In each case, RNF114 activity and sensitivity to nimbolide was confirmed. For the first method, we purchased wild-type mammalian expression plasmids with C-terminal FLAG tag were purchased from Origene (Origene Technologies Inc., RC209752). The RNF114 C8A mutant was generated with Q5 site-directed mutagenesis kit according to manufacturer's instructions (New England Biolabs, E0554S). Expression and purification conditions were optimized as reported previously [75]. HEK293T cells were grown to 60% confluency in DMEM (Corning) supplemented with 10 % FBS (Corning) and 2 mM L-glutamine (Life Technologies) and maintained at 37 °C with 5% CO_2. Immediately prior to transfection, media was replaced with DMEM containing 5 % FBS. Each plate was transfected with 20 µg of overexpression plasmid with 100 µg PEI (Sigma). After 48 h cells were collected in TBS, lysed by sonication, and batch bound with anti-DYKDDDDK resin (GenScript, L00432) for 90 min. Lysate and resin was loaded onto a gravity flow column and washed, followed by elution with 250 ng/µL 3 x FLAG peptide (ApexBio, A6001). Purity and concentration were verified by PAGE, UV/Spectroscopy, and BCA assay.

For the second method, DNA encoding the complete human isoform of RNF114 (Uniprot id: Q9Y508) was codon optimized for expression in *E. coli* and synthesized by Integrated DNA Technologies. Constructs containing the complete RNF114 sequence were amplified using primers containing 20 base pair homology to a pET24a plasmid (Novagen) that also contained a His_8-MBP-TEV sequence between Nde1 and BamH1 restriction sites. Products for PCR were assessed using 1% agarose gels (Invitrogen), and a QIAquick Gel Extraction kit (Qiagen) was used to purify PCR products of the correct length. Gibson Assembly (NEB Gibson Assembly 2x Master Mix) was used to assemble the purified PCR product into the linearized vector. This vector was then transformed into chemically competent *E. coli* 10G cells (Lucigen, Middleton, WI). Kanamycin (Kan)-resistant colonies were grown in LB media, and a Miniprep (Qiagen) kit was used to isolate the plasmid before sequence verification with appropriate primers.

pET24a His_8–MBP plasmid (100 ng) containing the desired RNF114 construct was transformed into chemically competent *E. coli* BL21(DE3) cells (NEB product # C2530H). The following day, a single transformed colony was used to inoculate 50 mL of nutrient rich LB medium containing kanamycin (50 µg/mL) and was incubated at 37 °C overnight, with agitation (250 rpm). The following morning, an overnight starter culture was

inoculated to a starting optical density at 500 nM (OD_{600}) of 0.1 in Terrific Broth (TB) (1 L) containing 50 mM 3-(N-morpholino)propanesulfonic acid (MOPS) pH 7.5, 1 mM zinc chloride, and Kan (50 µg/mL). Cells were grown until achieveing an OD_{600} of 0.8 at 37 °C with agitation at 250 rpm. At this stage, expression of the RNF114 fusion protein was induced with 1 mM isopropyl β-D-1-thiogalactopyranoside (IPTG), and the temperature of the incubator was reduced to 18 °C. Cells were harvested by centrifugation after growth for 18 h at 18 ˚C. Cells were subsequently washed with 1x phosphate buffered saline (PBS) buffer and stored at -20 ˚C.

E. coli cells (10 g) containing the overexpressed RNF114 fusion protein were re-suspended in 80 mL of lysis buffer (50 mM Tris, pH 7.5, 150 mM NaCl, 2 Roche protease inhibitor tablets [without EDTA], 200 mM $ZnCl_2$, 1 mM DTT) and sonicated on ice, with a cycling time of 60 seconds on, 60 seconds off, over a total sonication time of three minutes. The cell lysate was centrifuged at 18,000 rpm for 20 minutes and the soluble protein was incubated with agitation for four hours at 4 ℃ with 2 mL of Ni-NTA resin, which had been pre-equilibrated with wash buffer (50 mM Tris, pH 7.5, 150 mM NaCl, 200 mM $ZnCl_2$, 1 mM DTT, 25 mM imidazole). The cell lysate / Ni-NTA resin mixture was placed into a disposable column and all non-tagged soluble protein, which do not bind to the resin, was collected for a second round of purification. The resin was washed with 25 mL of wash buffer before the His-MBP-RNF114 protein was eluted from the Ni-NTA resin with 25 mL of elution buffer (50 mM tris, pH 7.5, 500 mM imidazole, 200 mM $ZnCl_2$, 150 mM NaCl, 1 mM DTT). This process was repeated incubating the collected flow thorough with an additional 2 mL of pre-equilibrated Ni-NTA resin.

His-MBP-RNF114 protein was simultaneously digested at 4 ℃ with TEV protease (100 units / mg MBP-RNF114), and dialyzed overnight against dialysis buffer (50 mM tris, pH 7.5, 150 mM NaCl, 200 mM $ZnCl_2$, 1 mM DTT). The following morning two 5 mL His Trap Excel columns assembled in tandem were placed on an Äkta Avant and equilibrated with five column volumes of wash buffer. The TEV cleaved sample was loaded onto the column at a rate of 2 mL/min and the resin was washed with an additional five column volumes of wash buffer. All fractions containing cleaved RNF114 were concentrated to a 5 ml volume. Samples were then loaded onto a pre-equilibrated HiLoad 16/60 Superdex 75 gel filtration column (GE Healthcare). Columns were pre-equilibrated with either 25 mM Tris, pH 7.5, 137 mM NaCl or 20 mM Sodium Phosphate pH 6.8, 150 mM NaCl. The gel filtration column was run using a flow rate of 0.25 mL/min and 2 mL fractions were collected. Fractions corresponding to peaks eluting from the gel filtration column were analyzed using SDS-PAGE and all fractions containing RNF114 were concentrated to a final concentration of 10 mg/mL, flash frozen in liquid nitrogen and stored at -80 ˚C until needed.

Generation of Stably Expressing FLAG-RNF114 231MFP Cell Lines by Lentiviral Transduction

Human RNF114 with C-terminal FLAG tag was inserted into pLenti vector by FastCloning [76]. FLAG-RNF114 lentivirus was generated by co-transfection of FLAG-RNF114, VSV.G and psPAX2 into HEK 293T cells using Lipfectamine 2000 transfection reagent (ThemoFischer). 24h after transfection media was exchanged for DMEM with 10% heat-inactivated serum (HIS) and after an additional 24hr virus-containing media was collected and filtered with 0.45 µM filter onto 231MFP cells with equal volume HIS

L15 media, in the presence of 10 µg/mL polybrene (Santa Cruz). 24h after transduction, puromycin (2 µg/mL) was added to cells and stably expressing FLAG-RNF114 were obtained after puromycin selection for 72hr. 231MFP cells stably expressing FLAG-eGFP were generated in parallel as control.

In situ Nimbolide-Alkyne Probe Labeling and FLAG-RNF114 Pulldown

231MFP cells stably expressing FLAG-RNF114 were treated with either vehicle (DMSO) or 100 nM to 10 µM nimbolide alkyne probe for 2-4hr. Cells were harvested in PBS and lysed by sonication. Total protein concentration of lysates were normalized by BCA assay and normalized lysates were incubated 1.5 hr at 4 °C with 50 µL or FLAG-agarose slurry. After incubation samples were transferred to spin columns and washed 3X with 500 µL PBS. Proteins were eluted using 2 50 µL washes of PBS supplemented with 250 ng/µL 3 x FLAG peptide (ApexBio A6001). CuAAC was performed to append rhodamine-azide onto alkyne probe-labeled proteins and after addition of loading buffer samples were separated on precast 4-20% TGX gels (Bio-Rad Laboratories, Inc.) and imaged on ChemiDoc MP (Bio-Rad Laboratories, Inc).

LC-MS/MS Analysis of RNF114

Purified RNF114 (10 µg) in 50 µL PBS were incubated 30 min at room temperature either with DMSO vehicle or covalently acting compound (100 µM). The DMSO control was then treated with light IA while the compound treated sample was incubated with heavy IA for 1 h each at room temperature (200 µM final concentration, Sigma-Aldrich, 721328). The samples were precipitated by additional of 12.5 µL of 100% (w/v) TCA and the treated and control groups were combined pairwise, before cooling to -80 °C for 1 h. The combined sample was then spun for at max speed for 10 min at 4 °C, supernatant is carefully removed and the sample is washed with ice cold 0.01 M HCl/90 % acetone solution. The pellet was resuspended in 4 M urea containing 0.1 % Protease Max (Promega Corp. V2071) and diluted in 40 mM ammonium bicarbonate buffer. The samples were reduced with 10 mM TCEP at 60 °C for 30 min. The sample was then diluted 50% with PBS before sequencing grade trypsin (1 µg per sample, Promega Corp, V5111) was added for an overnight incubation at 37 °C. The next day the sample was centrifuged at 13200 rpm for 30 min. The supernatant was transferred to a new tube and acidified to a final concentration of 5 % formic acid and stored at -80 °C until MS analysis.

RNF114 Ubiquitination Assay

Recombinant Myc-Flag-RNF114 proteins were either purified from HEK292T cells as described above or purchased from Origene (Origene Technologies Inc., TP309752). For *in vitro* auto-ubiquitination assay, 0.2 µg of RNF114 in 25 µL of TBS was pre-incubated with DMSO vehicle or the covalently-acting compound for 30 min at room temperature. Subsequently, 0.1 µg of UBE1 (Boston Biochem. Inc, E-305), 0.1 µg UBE2D1 (Boston Bichem. Inc, e2-615), 5 µg of Flag-ubiquitin (Boston Bichem. Inc, u-120) in a total volume of 25 µL Tris buffer containing 2 mM ATP, 10 mM DTT, and 10 mM $MgCl_2$ were added to achieve a final volume of 50 µL. For substrate-protein ubiquitination assays, 0.1ug of the appropriate substrate protein, purchased from commercial sources, was added at this stage (p21 and PEG10: Origene , CTGF: R&D Systems). The mixture

was incubated at 37 °C with agitation for 1.5 h. 20 µL of Laemmli's buffer was added to quench the reaction and proteins were analyzed by western blot assay.

RNF114/p21 Co-Immunoprecipitation

Recombinant Flag-tagged RNF114 was used as bait to precipitate pure recombinant p21 (Origene Technologies Inc., TP309752 and TP720567) using Anti-Flag agarose beads (GenScript Biotech Corp., L00432). One microgram of Flag-RNF114 was added to 50 µL of TBS, followed by the addition of nimbolide (100 µM final concentration, Cayman Chemical Co., 19230) or equivalent volume of DMSO. Samples were incubated at room temperature for 30 min. One microgram of pure p21 was added to each sample, and samples were incubated at room temperature 30 min with agitation. Ten microliters of Flag agarose beads were added to each sample, and samples were agitated at room temperature for 30 min. Washes (3 times, 1 mL TBS) were performed before proteins were eluted using 50 µL of TBS supplemented with 250 ng/µL 3 x FLAG peptide (ApexBio A6001). Supernatant (30 µL) were collected and after the addition of Laemmli's reducing agent (10 µL), samples were boiled at 95 °C for 5 min and allowed to cool. Samples were analyzed by Western blotting as described above.

***In situ* Nimbolide-Alkyne Probe Labeling and Biotin-Azide Pulldown**

Experiments were performed following an adaption of a previously described protocol [77]. 231MFP cells were treated with either vehicle (DMSO) or 50 µM nimbolide alkyne probe for 90 min. Cells were harvested in PBS and lysed by sonication. For preparation of Western blotting sample, 195 µL of lysate was aliquoted per sample to which 25 µL of 10% SDS, 5 µL of 5 mM biotin picolylazide (900912 Sigma-Aldrich) and 25 µL of click reaction mix (3 parts TBTA 5 mM TBTA in butanol:DMSO (4:1, v/v), 1 part 50 mM Cu(II)SO4 solution, and 1 part 50 mM TCEP). Samples were incubated for 2 h at 37 °C with gentle agitation after which 1.2 mL ice cold acetone were added. After overnight precipitation at -20 °C, samples were spun in a prechilled centrifuge at 1250 g for 10 min allowing for aspiration of excess acetone and subsequent reconstitution of protein pellet in 200 µL PBS containing 1% SDS by probe sonication. At this stage, total protein concentration was determined by BCA assay and samples were normalized to a total volume of 230 µL, with 30 µL reserved as input. 20 µL of prewashed 50% streptavidin agarose bead slurry was added to each sample and samples were incubated overnight at rt with gentle agitation. Supernatant was aspirated from each sample after spinning at 90 g for 2 min at rt. Beads were transferred to spin columns and washed 3X with PBS. To elute, beads were boiled 5 min in 50 µL LDS sample buffer. Eluents were collected by centrifugation and analyzed by immunoblotting.

The resulting samples were analyzed as described below in the TMT-based quantitative proteomic profiling section.

TMT-Based Quantitative Proteomic Profiling.

Cell Lysis, Proteolysis and Isobaric Labeling. Treated cell-pellets were lysed and digested using the commercially available Pierce™ Mass Spec Sample Prep Kit for Cultured Cells (Thermo Fisher Scientific, P/N 84840) following manufacturer's instructions. Briefly, 100 µg protein from each sample was reduced, alkylated, and digested overnight using a combination of Endoproteinase Lys-C and trypsin proteases.

Individual samples were then labeled with isobaric tags using commercially available Tandem Mass Tag™ 6-plex (TMTsixplex™) (Thermo Fisher Scientific, P/N 90061) or TMT11plex (TMT11plex™) isobaric labeling reagent (Thermo Fisher Scientific, P/N 23275) kits, in accordance with manufacturer's protocols.

High pH Reversed Phase Separation. Tandem mass tag labeled (TMT) samples were then consolidated, and separated using high-pH reversed phase chromatography (RP-10) with fraction collection as previously described [77]. Fractions were speed-vac dried, then reconstituted to produce 24 fractions for subsequent on-line nanoLC-MS/MS analysis.

Protein Identification and Quantitation by nanoLC-MS/MS. Reconstituted RP-10 fractions were analyzed on a Thermo Orbitrap Fusion Lumos Mass Spectrometer (Xcalibur 4.1, Tune Application 3.0.2041) coupled to an EasyLC 1200 HPLC system (Thermo Fisher Scientific). The EasyLC 1200 was equipped with a 20 µL loop, set-up for 96 well plates. A Kasil-fritted trapping column (75 µm ID) packed with ReproSil-Pur 120 C18-AQ, 5 µm material (15mm bed length) was utilized together with a 160mm length, 75 µm inner diameter spraying capillary pulled to a tip diameter of approximately 8-10 µm using a P-2000 capillary puller (Sutter Instruments, Novato, CA). The 160mm separation column was packed with ReproSil-Pur 120 C18-AQ, 3 µm material (Dr. Maisch GmbH, Ammerbuch-Entringen, Germany). Mobile phase consisted of A= 0.1% formic acid/2% acetonitrile (v/v), and Mobile phase B= 0.1% formic acid/98% acetonitrile (v/v). Samples (18 µL) were injected on to trapping column using Mobile Phase A at a flow rate of 2.5 µL/min. Peptides were then eluted using an 80 minute gradient (2% Mobile Phase B for 5 min, 2%-40% B from 5-65 min, followed by 70% B from 65-70 minutes, then returning to 2% B from 70-80 min) at a flowrate of 300 nL/min on the capillary separation column with direct spraying into the mass spectrometer. Data was acquired on Orbitrap Fusion Lumos Mass Spectrometer in data-dependent mode using synchronous precursor scanning MS^3 mode (SPS-MS3), with MS^2 triggered for the 12 most intense precursor ions within a mass-to-charge ratio *(m/z)* range of 300-1500 found in the full MS survey scan event. MS scans were acquired at 60,000 mass resolution (*R*) at *m/z* 400, using a target value of 4×10^5 ions, and a maximum fill time of 50 ms. MS^2 scans were acquired as CID ion trap (IT) rapid type scans using a target value of 1×10^4 ions, maximum fill time of 50 ms, and an isolation window of 2 Da. Data-dependent MS^3 spectra were acquired as Orbitrap (OT) scans, using Top 10 MS^2 daughter selection, automatic gain control (AGC) target of 5×10^4 ions, with scan range of *m/z* 100-500. The MS^3 maximum injection time was 86 ms, with HCD collision energy set to 65%. MS^3 mass resolution (*R*) was set to 15,000 at *m/z* 400 for TMT6plex experiments, and 50,000 at *m/z* 400 for TMT11-plex experiments. Dynamic exclusion was set to exclude selected precursors for 60 s with a repeat count of 1. Nanospray voltage was set to 2.2 kV, with heated capillary temperature set to 300 ºC, and an S-lens RF level equal to 30%. No sheath or auxiliary gas flow is applied.

Data Processing and Analysis. Acquired MS data was processed using Proteome Discoverer v. 2.2.0.388 software (Thermo) utilizing Mascot v 2.5.1 search engine (Matrix Science, London, UK) together with Percolator validation node for peptide-spectral match filtering [78]. Data was searched against Uniprot protein database

(canonical human and mouse sequences, EBI, Cambridge, UK) supplemented with sequences of common contaminants. Peptide search tolearances were set to 10 ppm for precursors, and 0.8 Da for fragments. Trypsin cleavage specificity (cleavage at K, R except if followed by P) allowed for up to 2 missed cleavages. Carbamidomethylation of cysteine was set as a fixed modification, methionine oxidation, and TMT-modification of N-termini and lysine residues were set as variable modifications. Data validation of peptide and protein identifications was done at the level of the complete dataset consisting of combined Mascot search results for all individual samples per experiment via the Percolator validation node in Proteome Discoverer. Reporter ion ratio calculations were performed using summed abundances with most confident centroid selected from 20 ppm window. Only peptide-to-spectrum matches that are unique assignments to a given identified protein within the total dataset are considered for protein quantitation. High confidence protein identifications were reported using a Percolator estimated <1% false discovery rate (FDR) cut-off. Differential abundance significance was estimated using a background-based ANOVA with Benjamini-Hochberg correction to determine adjusted p-values.

CHAPTER 3

Harnessing the Natural Product Nimbolide for Targeted Protein Degradation

This chapter is based on the *Nature Chemical Biology* publication “Harnessing the anti-cancer natural product nimbolide for targeted protein degradation”[79] and the *ACS Chemical Biology* publication “A Nimbolide-Based Kinase Degrader Preferentially Degrades Oncogenic BCR-ABL”,[25] and both have been adapted with permission from all co-authors.

3.1 Introduction

Targeted protein degradation (TPD) and proteolysis-targeting chimeras (PROTACs) are powerful therapeutic paradigms that employ heterobifunctional molecules to recruit an E3 ligase to a protein of interest for polyubiquitination and degradation by the proteasome[80,81]. While this technology is a very promising drug discovery paradigm for tackling so far intractable therapeutic targets, and small-molecule PROTACs have entered human clinical trials [82], a major challenge in the application of this technology is the small number of known E3 ligase recruiters. While there are ~600 different E3 ligases, many with different cellular localization, only a few E3 ligase recruiters have been identified and successfully employed, including small-molecule recruiters for cereblon (CRBN), VHL, MDM2, and cIAP [83–88]. Amongst these, most reported degraders have used either CRBN or VHL ligands. Additionally, recent reports also suggest resistance to degraders may occur through reprogramming of cellular machinery on the E3 ligase binding side, and that there are certain proteins that have been resistant to degradation by the commonly recruited E3s[89,90]. The discovery of new E3 ligase recruiters is thus necessary to expand the scope of TPD applications.

In the work outlined in the previous chapter I demonstrated using chemoproteomic profiling that the natural product nimbolide covalently modifies and inhibits the E3 ligase RNF114. Importantly, my work identified that inhibition of RNF114 activity by nimbolide is through impaired substrate recognition giving rise to the possibility that nimbolide could be used as an E3 ligase recruitment module for targeted protein degradation. In this chapter I demonstrate that nimbolide can be used to recruit RNF114 to non-native protein substrates for targeted protein degradation applications.

Recently, chemoproteomic platforms have been used to discover additional recruiters beyond nimbolide that act through covalent targeting of cysteines on E3 ligases. These covalent recruiters include CCW16 that targets RNF4 and SB002 that binds to DCAF16. To show proof-of-concept, these new recruiters were linked to JQ1 or to an SLF ligand to show proteasome-dependent degradation of BRD4 or FKBP12, respectively [79,91,92]. While these studies have effectively shown that E3 ligases can be targeted covalently for recruitment and degradation of their target proteins, both FKBP12 and BRD4 are among targets that are considered easily degradable, that is, many PROTACs have been developed that efficiently and robustly degrade these targets in a selective and proteasome-dependent manner.

In the first section of this work, employing nimbolide-JQ1 degraders, we observe selective degradation of BRD4 over related Bromodomain and extraterminal domain (BET) family members [79]. We further investigate the broader utility and selectivity of nimbolide-based PROTACs against protein targets that possess additional degradation selectivity challenges, namely human kinases. Among these targets, selective targeting of the oncogenic fusion protein BCR-ABL, a driver of chronic myelogenous leukemia (CML), over c-ABL, an important non-receptor tyrosine kinase involved in numerous cellular processes [93], have proven to be challenging with studied PROTACs exploiting CRBN or VHL recruitment. Pioneering studies by the Crews lab have shown that BCR-

ABL PROTACs, consisting of CRBN or VHL recruiters linked to BCR-ABL ATP binding pocket-targeting kinase inhibitors such as dasatinib and bosutinib or allosteric inhibitors such as GNF-2, showed preferential degradation of c-ABL over modest degradation of BCR-ABL [94,95]. Notably, this work has spurred development of various degradation strategies targeting BCR-ABL [96–100]. In this study, we aimed to determine whether our covalent RNF114 recruiter, nimbolide, could be used to target and degrade kinases, and if so, whether differential selectivity in degrading BCR-ABL, compared to similar BCR-ABL PROTACs employing VHL or CRBN could be attained.

3.2 Nimbolide as an RNF114 Recruiter for Degradation of BRD4

Given the evidence that nimbolide targets a potential substrate recognition site, we conjectured that nimbolide could be used to recruit RNF114 to non-native protein substrates to mediate their proteasomal degradation through the development of heterobifunctional degraders using nimbolide as an RNF114 recruiter. To demonstrate feasibility, two degraders formed by linking nimbolide to the Bromodomain and extra-terminal (BET) family inhibitor JQ1 were synthesized **(Fig. 3.1a; Supplementary Fig. 3.1a)**. Prior studies have demonstrated efficient proteasome-dependent degradation of BET family members and in particular BRD4 with JQ1-based degraders linked to either a CRBN (cereblon)-recruiter thalidomide or a VHL recruiter [83,101]. Previously prepared acid (**1**) was coupled to JQ1-functionalized amines containing both longer (PEG-based) (**2**) and shorter (alkyl-based) (**3**) spacer units, arriving at degraders **XH1** (**4**) and **XH2** (**5**) **(Fig. 3.1a; Supplementary Fig. 3.1a)**. We show that **XH2** still binds to RNF114 with an IC50 of 0.24 μM **(Fig. 3.1b)**. While **XH1** did not show appreciable BRD4 degradation, **XH2** treatment in 231MFP cells led to BRD4 degradation after a 12 h treatment **(Fig. 3.1c; Supplementary Fig. 3.1b)**.

Interestingly, **XH2** showed less degradation at 1 μM compared to 0.1 and 0.01 μM and the VHL-recruiting JQ1 control degrader, MZ1, showed less degradation at 20 μM compared to 10, 1, and 0.1 μM, which we attribute to the “hook effect” previously reported with other degraders including the previously reported JQ1-based degrader MZ1 [81,101] **(Fig. 3.1c-3.1d)**. We had hoped that by introducing covalency on one end of the PROTAC molecule we might remove the hook effect limitation on dosing in long treatment time points, however our results indicate that even with covalent molecules saturation of binding sites on the E3 and target protein can prevent tertiary complex formation.

To confirm proteasome-dependence of BRD4 degradation, we showed that the **XH2**-mediated degradation of BRD4 was attenuated by pre-treatment of cells with the proteasome inhibitor bortezomib (BTZ) **(Fig. 3.1e)**. **XH2**-mediated BRD4 degradation was also prevented by pre-treatment with an E1 ubiquitin-activating enzyme inhibitor (TAK-243) or pre-competing with the BRD4 inhibitor JQ1 **(Fig. 3.1f, Supplementary Fig. 3.1g)**. However, treatment with a translation inhibitor (emetine) had no effect of the observed degradation of BRD4 **(Supplementary Fig. 3.1h)**.

To further demonstrate that the degradation of BRD4 by **XH2** was through the specific recruitment of RNF114, we showed that degradation of BRD4 by **XH2**, but not

MZ1, was not observed in RNF114 knockout (KO) HAP1 cells compared to wild-type (WT) HAP1 cell counterparts **(Fig. 3.1g-5h, Supplementary Fig. 3.1i)**. We further showed that re-expression of wild-type RNF114 in HAP1 RNF114 knockout cells led to the restoration of BRD4 degradation by XH2 **(Supplementary Fig. 3.1j).**

The selectivity of **XH2**-mediated degradation of proteins was demonstrated using a TMT-based quantitative proteomic profiling experiment to assess changes in protein expression. We showed that **XH2** selectively degrades BRD4 in 231MFP breast cancer cells while sparing the other identified BET family members BRD2 and BRD3 **(Fig. 3.1i; Supplementary Dataset 3)**. Of note, we also observed several proteins that showed increased levels upon **XH2** treatment including CDKN1A, CDKN1C, PEG10, and CTGF, which were observed as elevated in levels with nimbolide treatment alone **(Fig. 3.1i; Supplementary Dataset 3)**. There were also additional proteins that were upregulated, such as DSG1, FN1, FLG2, and CASP14 **(Fig. 3.1i; Supplementary Dataset 3)**. These upregulated proteins may be potential substrates of RNF114 with stabilization stemming from the nimbolide portion of XH2, as is likely the case with CDKN1A, CDKN1C, PEG10 and CTGF. The other targets may be downstream transcriptional effects stemming from JQ1-mediated BRD4 inhibition and degradation. Our results indicate that nimbolide reactivity with RNF114 can be exploited to recruit this E3 ligase to other protein substrates, such as BRD4, to ubiquitinate and selectively degrade them opening up possibilities to investigate unique degradation profiles of nimbolide-based recruiters.

3.3 A Nimbolide-Based Kinase Degrader Preferentially Degrades Oncogenic BCR-ABL

The scope of targets amenable to nimbolide-based, RNF114-mediated protein degradation has without question been hampered by the extreme cost of nimbolide (2020 Sigma price = $77,000 USD/gram) making small-scale, multi-step synthetic manipulations of this acid-sensitive scaffold highly challenging. Commercial neem leaf powder (*Azadirachta Indica* extract), however, remains a popular and inexpensive health supplement containing varying amounts of nimbolide. Using a newly devised extraction protocol (see Chapter 3 Supporting Information), my collaborators were able to obtain gram quantities of analytically pure nimbolide from a single 1 lb. can of Organic Veda™ neem leaf extract (2020 price ~ $30 USD) without the need for HPLC purification **(Fig. 3.2)**. Importantly, this process opens the door to the synthetic and chemical biology communities to manipulate this complex triterpene scaffold for biological and especially TPD applications.

With access to significant quantities of nimbolide, we synthesized two nimbolide-based degraders linked to the tyrosine kinase inhibitor dasatinib employing both short alkyl (see **BT2**) and longer PEG-based (see **BT1**) linkers in analogy to previous work (**Fig. 3.2**, see Chapter 3 Supporting Information for synthetic details) [79]. Treatment of K562 leukemia cells expressing the fusion oncogene BCR-ABL for 24 h with **BT1** and **BT2** led to loss of both BCR-ABL and c-ABL, with a more pronounced effect observed with **BT1 (Fig. 3.3a)**. We were not able to determine whether higher concentrations of **BT1** or **BT2** led to impaired degradation due to “hook effects,” previously observed with

other PROTACs, including nimbolide-based degraders [79,84,85], because of acute K562 cytotoxicity encountered at higher degrader concentrations.

While our prior work on BRD4 degradation with Nimbolide/JQ-1-based PROTACS had found shorter linkers to be superior, we observed here that a longer linker between dasatinib and nimbolide showed better performance in degrading BCR-ABL and c-ABL, potentially due to improved positioning and formation of the ternary complex between RNF114 and the kinases, or because of increased accessibility of the degrader to the kinases in cells due to limitations of cell-permeability. Interestingly, both **BT1** and **BT2** showed more degradation of BCR-ABL than c-ABL, demonstrating opposite preference to Crews' findings **(Fig. 3.3a)**. We show that phosphorylated CRKL, downstream of c-ABL signaling was inhibited by both **BT1** and **BT2**, indicating that **BT1** and **BT2** sufficiently engaged ABL in cells **(Fig. 3.3a).** While performing rescue studies with proteasome inhibitors, NEDDylation inhibitors, or excess dasatinib or nimbolide was challenging due to the acute toxicity of these compounds in this cell line, the degradation of BCR-ABL or c-ABL with **BT1** treatment was not observed with nimbolide or dasatinib treatment, nor with co-treatment of both compounds **(Fig. 3.3b).** Furthermore, attempted rescue experiments with **BT1** in RNF114 knockout HAP1 cell lines, which we used previously in the context of BRD4 degradation,[9] were unsuccessful as these cells did not express detectable levels of BTK or c-ABL as judged by Western blotting. Nonetheless, our previous studies have convincingly demonstrated that nimbolide-JQ1 degraders reduced BRD4 levels in an RNF114- and proteasome-dependent manner [79].

We next performed a more detailed time-course analysis comparing our **BT1** degrader with previously reported CRBN and VHL-recruiting dasatinib degraders of related linker length and composition **(Fig. 3.4a-3.4c, Supplementary Fig. 3.2)**. Consistent with previous reports, the CRBN-dasatinib PROTAC showed preferential and faster degradation of c-ABL compared to BCR-ABL **(Fig. 3.4a)**. We also observed no significant degradation of BCR-ABL during the 24 h time-course with >50 % of degradation of c-ABL when employing the VHL-dasatinib degrader, consistent with Crews' findings **(Fig. 4.3b)**. In contrast, **BT1** showed faster and preferential degradation of BCR-ABL over c-ABL at every time-point tested **(Fig. 4.3c)**. We also noted that **BT1**, CRBN-dasatinib, and VHL-dasatinib did not fully degrade BCR-ABL or c-ABL under the conditions tested. This incomplete degradation may be due to the faster rate of re-synthesis of BCR-ABL and c-ABL in the cell compared to the rate of degradation by the degraders. Alternatively, longer treatment times may result in more complete degradation. Another possibility may be that these degraders may preferentially degrade certain pools of BCR-ABL and c-ABL in the cell, such as nuclear versus cytosolic pools of BCR-ABL and c-ABL [102]. Additionally, while CRBN-dasatinib potently ablates the known dasatinib target Bruton's tyrosine kinase (BTK), and VHL-dasatinib shows robust, but diminished degradation, substantially lower levels of degradation for these kinases is noted with **BT1** treatment **(Fig. 3.5a, 3.5b)**. We also attempted quantitative proteomic experiments on **BT1** to look at degradation selectivity, but these studies proved challenging because of the cytotoxicity induced by the time we observed robust BCR-ABL and c-ABL degradation necessary to detect total changes in ABL by proteomic methods (since we could not

observe the BCR-ABL fusion tryptic peptide of the BCR-ABL protein). These findings further highlight the emerging complexities inherent to kinase degradation [103–112].

3.4 Nimbolide-Based Degrader Elevates p21 Levels for Synergistic Anti-Proliferative Effect

In the preceding chapter I reported that nimbolide disrupts endogenous RNF114 substrate recognition through targeting an N-terminal cysteine (C8), leading to accumulation of endogenous RNF114 substrates such as the tumor suppressors CDKN1A (p21) and CDKN1C (p57) which in turn results in impaired breast cancer cell viability. Our previously described nimbolide-JQ1 BRD4 degrader showed selective degradation of BRD4, but also enhanced levels of p21 and p57 in breast cancer cells. We demonstrate here that **BT1** treatment also led to greatly elevated levels of CDKN1A (p21) levels in K562 cells—an effect that was not observed with dasatinib, CRBN-dasatinib, or VHL-dasatinib treatments **(Fig. 3.5a, 3.5b).** These results indicate that a nimbolide-based BCR-ABL degrader may possess additional therapeutic properties beyond dasatinib alone. While dasatinib impaired K562 cell proliferation at much lower concentrations compared to **BT1** likely due to better cell permeability of dasatinib compared to **BT1**, we observed significantly greater impairments in cell proliferation with higher concentrations of BT1 from 1 to 5 μM compared to treatment with dasatinib alone, nimbolide alone, or even dasatinib and nimbolide together at both 24 and 48 h timepoints **(Fig. 3.5c; Supplementary Fig. 3.3).** We postulate that the observed heightened viability impairments observed with **BT1** compared to dasatinib and nimbolide co-treatment are due to the degradation rather than just inhibition of BCR-ABL **(Fig. 3.5c).** We also observed significantly greater anti-proliferative effects with BT1 from 1 to 5 μM, compared to CRBN-dasatinib and VHL-dasatinib PROTACs at 24 and 48 h timepoints **(Fig. 3.5d; Supplementary Fig. 3.3)**. This additional anti-proliferative activity of **BT1**, compared to CRBN- or VHL-dasatinib PROTACs may potentially be due to RNF114-mediated effects such as p21 and p57 stabilization. I have previously shown that dual knockdown of p21 and p57 significantly attenuated the anti-proliferative action of nimbolide in breast cancer cells [79]. Future studies genetically investigating the contributions of RNF114, p21, and p57 to the additional **BT1**-mediated anti-proliferative effects would reveal greater insights into the mechanism of **BT1** action.

3.5 Discussion

Targeted protein degradation has emerged as a formidable and effective drug discovery paradigm for targeting proteins for elimination through the proteasome [80,81]. One of the challenges, however, is that there are only a small number of E3 ligase recruiters that have been developed among the approximately 600 E3 ligases in the human genome [113]. These E3 ligase recruiters include the thalidomide-type immunomodulatory drugs (IMiD) that recruit cereblon, ligands that recruit VHL, nutlins that recruit MDM2, and ligands that recruit BIRC2 (cIAP) [80,81]. Here, I report that nimbolide can be used as a novel RNF114 recruiter for targeted protein degradation applications.

In the initial proof-of-concept study, we demonstrate that nimbolide targeting of C8 on RNF114 can be used to recruit RNF114 for targeted protein degradation applications and degradation of BRD4 with a nimbolide-JQ1 degrader, **XH2**, is possible. Interestingly, degradation of BRD2 and BRD3 was not observed under conditions that led to significant reduction of BRD4 levels, despite the high homology in their respective BET bromodomains. Various levels of selectivity within the BET family members and the structural basis thereof have been reported for JQ1-based degraders with Cereblon and VHL-recruiting modules [83,101,114,115]. While a more detailed investigation of the selectivity of XH2 and its structural basis is outside the scope of this study, it prompted us to investigate how use of nimbolide-based PROTACs might aid in tuning efficacy and selectivity of degraders targeting a given protein of interest.

In following up on these findings, we demonstrate for the first time that covalent E3 ligase recruiters can be used to degrade kinase targets in TPD applications, and that a nimbolide-based BCR-ABL degrader, **BT1**, shows unique degradation specificity profiles compared with initially reported cereblon- or VHL-recruiting degraders. The propensity of RNF114-recruiting nimbolide-based degraders to degrade the oncogenic protein form more selectively is particularly notable.

Additionally, nimbolide-based degraders likely also possess additional anti-cancer effects through heightening the levels of tumor-suppressors such as p21. While complicating mechanistic studies on single targets, such polypharmacological intervention represents a potentially attractive therapeutic strategy.

Though further investigation of nimbolide-based degraders is of high interest, it is beyond the scope of this work. However looking ahead, it should be possible to optimize the performance of this degrader class through further linker modifications, an area of the molecule already determined to be important in the studies at hand. We also set out to utilize more synthetically tractable covalent ligands capable of targeting C8 of RNF114, as RNF114 recruiters as will be discussed in chapter 4 of this work. Additionally, since nimbolide targets a substrate recognition domain within RNF114, it will also be of future interest to determine whether nimbolide may act as a molecular glue to recruit and degrade neo-substrates, as has been reported for the IMiDs [116].

Overall, our results underscore the importance of discovering more E3 ligase recruiters for better tuning the specificity and effects of future clinical candidates and drugs arising from TPD-based approaches. Intriguingly, we show that a natural product can functionally access an E3 ligase protein-protein interaction site for potential cancer therapy and targeted protein degradation applications and remarkably does so in an intrinsically disordered region of the protein. With ready access to supplies of nimbolide through optimized extraction and isolation protocols, a study of the scope of RNF114-mediated protein degradation can begin in earnest.

3.6 Figures

Figure 3.1

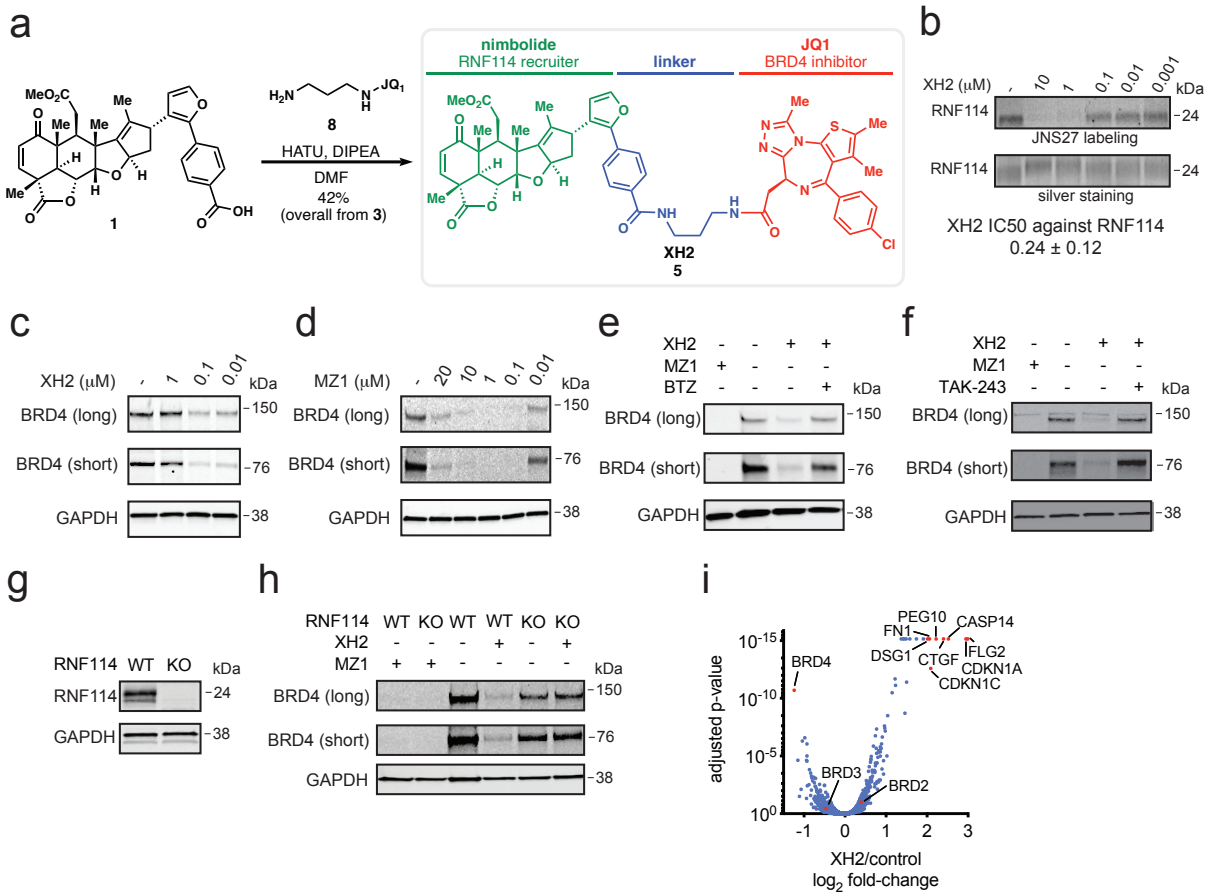

Figure 3.1. Nimbolide can be used to recruit RNF114 for targeted protein degradation of BRD4.

(a) Route for synthesizing XH2, a nimbolide-based degrader consisting of nimbolide as an RNF114 recruiter, a linker, and the BRD4 inhibitor JQ1. **(b)** Gel-based ABPP analysis of XH2 against RNF114. RNF114 was pre-incubated with DMSO vehicle or XH2 for 30 min prior to JNS27 labeling (50 μM) for 1 h followed by appending rhodamine-azide by CuAAC, SDS/PAGE, and analysis of in-gel fluorescence. **(c, d)** BRD4 expression in 231MFP breast cancer cells treated with XH2 **(c)** versus MZ1 **(d)** treatment for 12 h. **(e, f)** BRD4 expression in 231MFP breast cancer cells. Cells were pre-treated with DMSO vehicle or proteasome inhibitor bortezomib (BTZ) (1 μM) **(e)** or E1 ubiquitin activating enzyme inhibitor TAK-243 (10 μM) **(f)** 30 min prior to and also during treatment with MZ1 (1 μM) or XH2 (100 nM) treatment (100 nM) for 12 h. **(g)** RNF114 and loading control GAPDH expression in RNF114 wild-type (WT) and knockout (KO) HAP1 cells. **(h)** RNF114 and BRD4 expression in RNF114 wild-type (WT) or knockout (KO) HAP1 cells treated with DMSO vehicle, MZ1 (1 μM), or XH2 (100 nM) for 12 h. **(i)** Tandem mass tag (TMT)-based quantitative proteomic profiling of 231MFP breast cancer cells treated with DMSO vehicle or XH2 (100 nM) for 12 h. Long and short BRD4 isoforms in **(c-h)** were visualized by SDS/PAGE and Western blotting, quantified by densitometry, and

normalized to GAPDH loading controls. Gels shown in **(b-h)** are representative images from n=3 biologically independent samples/group and quantification for blots in **(c, d, e, f,** and **h)** are shown in **Supplementary Fig. 3.1c, d, e, f,** and **i**. Data shown in **(i)** are for 5797 proteins quantified with 2 or more unique peptides in triplicate treatments, see **Supplementary Dataset 3** for details. Statistical significance in **(i**) are described in the methods section and p-values are reported in **Supplementary Dataset 3.**

Figure 3.2

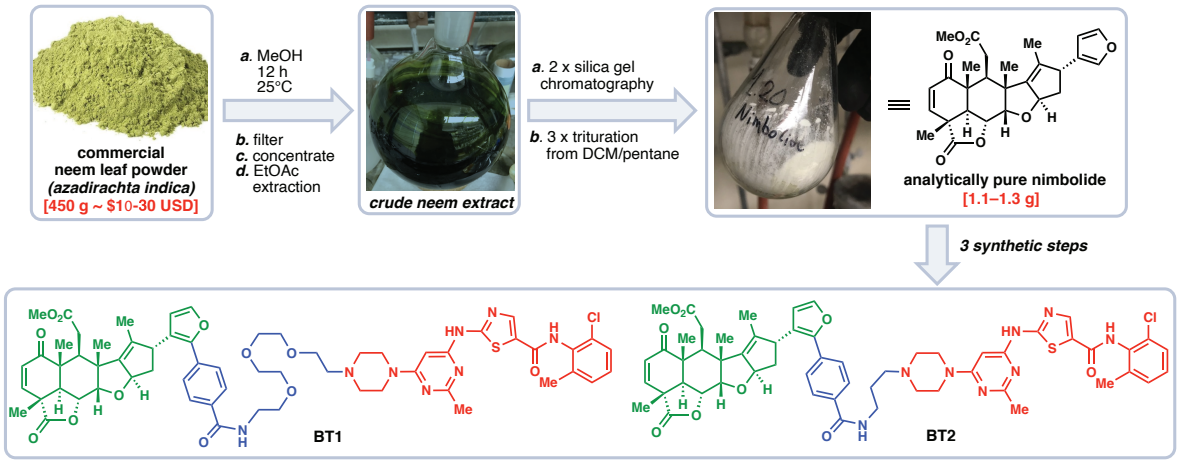

Figure 3.2. Extracting nimbolide from neem and nimbolide-based BCR-ABL degraders.
Efficient method for extracting gram quantities of nimbolide from neem. This procedure is described in detail in Supporting Information. Structures of the nimbolide-based BCR-ABL degraders BT1 and BT2 are shown.

Figure 3.3

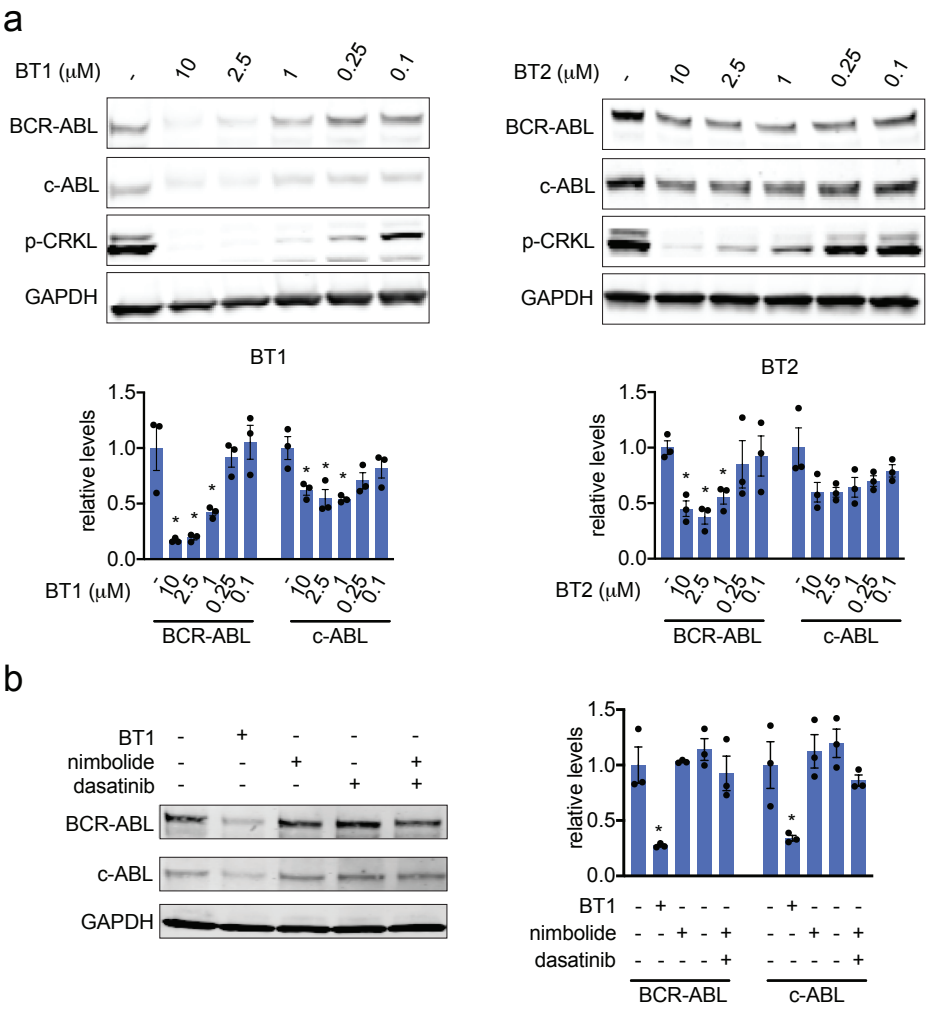

Figure 3.3. Effects of Nimbolide-based BCR-ABL degraders on BCR-ABL and c-ABL.

(a) BCR-ABL, c-ABL, phosphorylated CRKL, and loading control GAPDH levels with DMSO vehicle, BT1, and BT2 treatment in K562 cells for 24 h, assessed by Western blotting and quantified below in bar graphs by densitometry and normalization to GAPDH. **(b)** BCR-ABL, c-ABL, and GAPDH loading control levels in K562 cells treated with BT1 (1 μM), nimbolide (1 μM), or dasatinib (1 μM) for 24 h, assessed by Western blotting and quantified by densitometry normalized to GAPDH. Blots are representative of n=3 biological replicates/group. Quantified data show individual replicate values, average, and sem. Statistical significance is expressed as *p<0.05 compared to vehicle-treated control for each group.

Figure 3.4

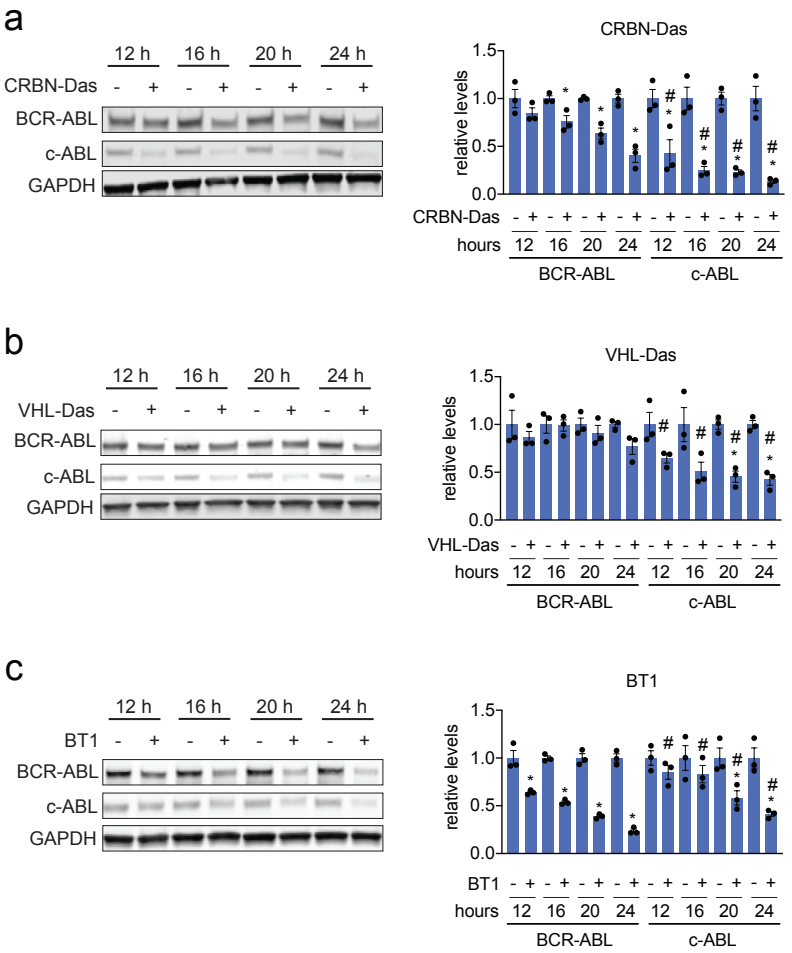

Figure 3.4. Rate of BCR-ABL versus c-ABL degradation with RNF114, CRBN, or VHL-based BCR-ABL degraders.

(a, b, c) BCR-ABL, c-ABL, and loading control GAPDH levels with K562 cell treatment with DMSO vehicle or CRBN (thalidomide)-, VHL (VHL ligand), or RNF114 (nimbolide)-based (BT1) dasatinib BCR-ABL degraders at 2.5 μM for 12, 16, 20, or 24 h, assessed by Western blotting and quantified by densitometry and normalized to GADPH loading control. Structures of all three degraders are show in **Supplementary Fig. 3.2.** Blots are representative of n=3 biological replicates/group. Quantified data show individual replicate values, average, and sem. Statistical significance is expressed as *p<0.05 compared to vehicle-treated control for each group, #p<0.05 compared to the corresponding BCR-ABL treatment comparisons with the individual degraders.

Figure 3.5

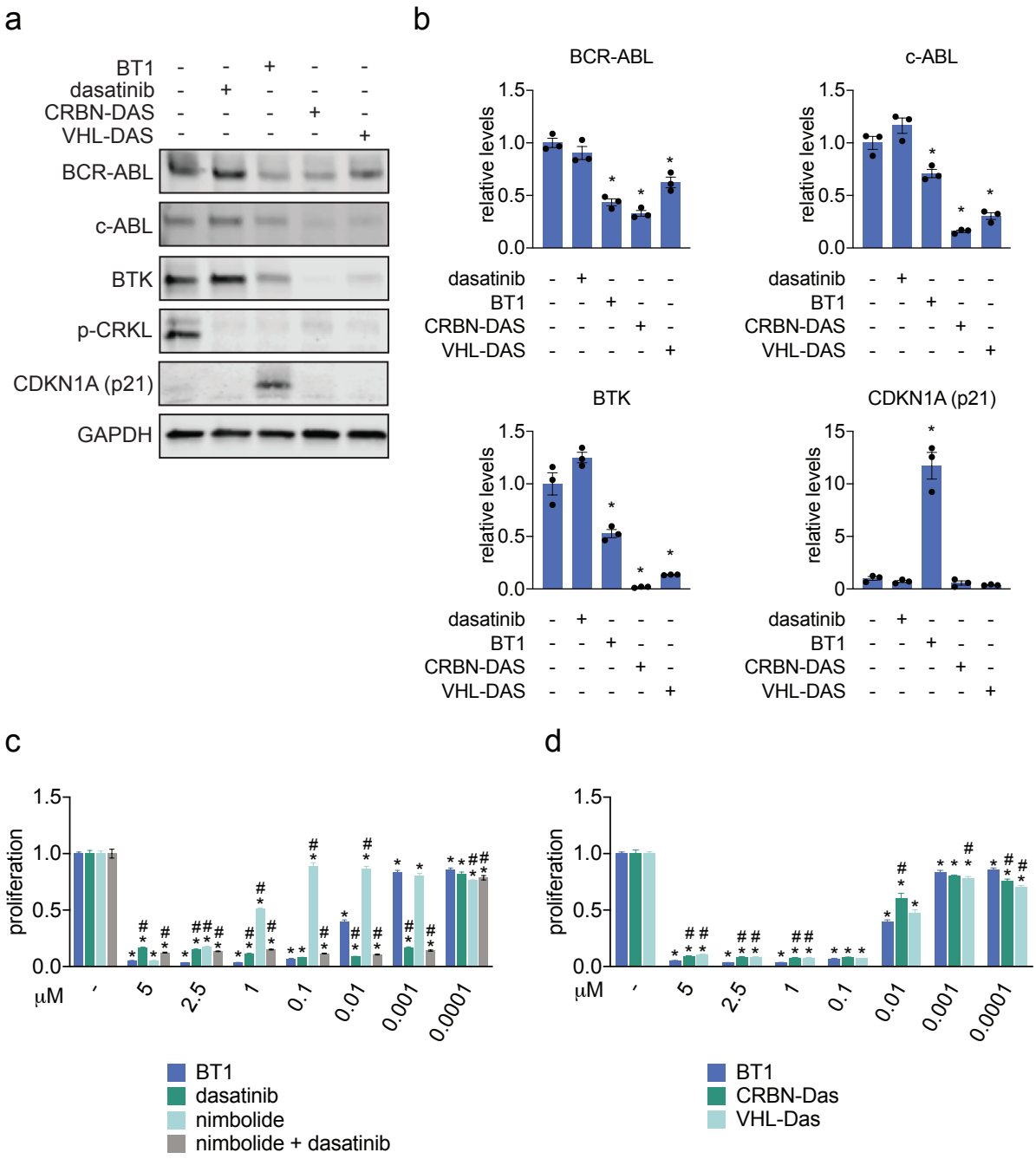

Figure 3.5. Comparing RNF114, CRBN, or VHL-recruiting BCR-ABL degraders. **(a, b)** BCR-ABL, c-ABL, BTK, phosphorylated CRKL, CDKN1A (p21), and loading control GAPDH levels in K562 cells treated with DMSO vehicle or dasatinib (2.5 μM), BT1 (2.5 μM), CRBN-DAS (2.5 μM), and VHL-DAS (2.5 μM) for 24 h, assessed by Western blotting and quantified in **(b)** by densitometry and normalized to GADPH loading control. **(c, d)** Cell proliferation of K562 cells treated with DMSO vehicle, BT1, dasatinib, nimbolide, nimbolide and dasatinib combined, CRBN-dasatinib, or VHL-dasatinib for 48 h. Blots are

representative of n=3 biological replicates/group. Quantified data show individual replicate values, average, and sem. Statistical significance is expressed as *$p<0.05$ compared to vehicle-treated control for each group, #$p<0.05$ compared to BT1 treatment group.

3.7 Acknowledgement of Co-Author Contributions

J.N. Spradlin, T.J. Maimone and D.K. Nomura conceived the project and wrote the papers. J.N. Spradlin, X. Hu, B. Tong, C.C. Ward, M.D. Jones, D.E. Bussiere, J.R. Thomas, J.A. Tallarico, J.M. McKenna, M. Schirle, T.J. Maimone and D.K. Nomura provided intellectual contributions and insights into project directions. J.N. Spradlin, X. Hu, B. Tong, S.M. Busby, M. To, J.A. Olzmann, M. Schirle, T.J. Maimone and D.K. Nomura designed the experiments and analyzed data. C.C. Ward, M.D. Jones developed bioinformatic methods and analyzed data for proteomics experiments. J.N. Spradlin, X. Hu, B. Tong, E. Zhang, S.M. Busby, L. Ou, M.To, A. Proudfoot, E. Ornelas, M. Woldegiorgis, and D.K. Nomura performed experiments and analyzed data. A. Proudfoot, E. Ornelas, M. Woldegiorgis, and D.E. Bussiere provided pure RNF114 protein. J.N. Spradlin, X. Hu, B. Tong and T.J. Maimone designed and synthesized compounds. J.N. Spradlin, S.M. Busby, M.D. Jones, J.A. Olzmann, D.E. Bussiere, J.R. Thomas, JAT, J.A. Tallarico, J.M. McKenna, M. Schirle, T.J. Maimone and D.K. Nomura edited the paper.

3.8 Methods

Cell Culture

The 231MFP cells were obtained from Prof. Benjamin Cravatt and were generated from explanted tumor xenografts of MDA-MB-231 cells as previously described [60]. K562 cells were obtained from the UC Berkeley Cell Culture Facility and were cultured in Iscove's Modified Dulbecco's Medium (IMDM) containing 10% (v/v) fetal bovine serum (FBS), maintained at 37 °C with 5% CO_2. HCC38 and HEK293T cells were obtained from the American Type Culture Collection. HEK293T cells were cultured in DMEM containing 10% (v/v) fetal bovine serum (FBS) and maintained at 37°C with 5% CO_2. 231MFP were cultured in L15 medium containing 10% FBS and maintained at 37°C with 0% CO_2. HCC38 cells were cultured in RPMI medium containing 10% FBS and maintained at 37°C with 5% CO_2. HAP1 RNF114 wild-type and knockout cell lines were purchased from Horizon Discovery. The RNF114 knockout cell line was generated by CRISPR/Cas9 to contain a frameshift mutation in a coding exon of RNF114. HAP1 cells were grown in Iscove's Modified Dulbecco's Medium (IMDM) in the presence of 10 % FBS and penicillin/streptomycin.

Isolation of nimbolide and synthesis of BT1 and BT2.

Isolation of nimbolide and synthesis of BT1 and BT2 are described in Supporting Information.

Proliferation Assays

Cell proliferation assays were performed using WST8 reagent (APExBio, CCK-8) following manufacturer's recommendations. K562 cells were seeded at a density of 100,000 cell/mL in a volume of 100 µL (10,000 cells per well).

Western Blotting

Antibodies to RNF114 (Millipore Sigma, HPA021184), ABL (Santa Cruz Biochemicals, 24-11) , BTK (Cell Signaling Technologies, D3H5), GAPDH (Proteintech Group Inc., 60004-1-Ig), phosphorylated CRKL Y207 (Cell Signaling Technologies,

3181), p21 (Cell Signaling Technology, 12D1), BRD4 (Abcam plc, Ab128874), DYKDDDDK Tag (Cell Signaling Technology, D6W5B) and beta-actin (Proteintech Group Inc., 6609-1-Ig) were obtained from various commercial sources and dilutions were prepared per recommended manufacturers' procedures. K562 cells were seeded for treatment at a density of 500,000 cells/mL, treated with compounds dissolved in DMSO and harvested. Cell pellets were washed with 500 µL phosphate buffered saline and lysed in 75-100 µL Radioimmunoprecipitation assay buffer (RIPA buffer) with protease inhibitor cocktail (Thermo Fisher Scientific, Pierce Protease Inhibitor Mini Tablets, EDTA-free). Supernatant was transferred and total protein was normalized by Pierce BCA Protein Assay. Samples were denatured by addition of 4X Laemmli's Loading dye and 25-50 µg of protein was loaded onto 4-20% TGX Precast gels (BioRad). After gel electrophoresis proteins were transferred to a nitrocellulose membrane. The membrane was then incubated for 1 hour in 5% bovine serum albumin (BSA) in tris-buffered saline containing Tween 20 (TBST) before being incubated with the correct primary antibody overnight at 4 °C. The membranes were washed in TBST before a 1 hour room temperature incubation with secondary antibodies. After a final set of washes blots were imaged on a LiCor CLX imager and band intensities were quantified using ImageJ software.

TMT-Based Quantitative Proteomic Profiling.

Cell Lysis, Proteolysis and Isobaric Labeling. Treated cell-pellets were lysed and digested using the commercially available Pierce™ Mass Spec Sample Prep Kit for Cultured Cells (Thermo Fisher Scientific, P/N 84840) following manufacturer's instructions. Briefly, 100 µg protein from each sample was reduced, alkylated, and digested overnight using a combination of Endoproteinase Lys-C and trypsin proteases. Individual samples were then labeled with isobaric tags using commercially available Tandem Mass Tag™ 6-plex (TMTsixplex™) (Thermo Fisher Scientific, P/N 90061) or TMT11plex (TMT11plex™) isobaric labeling reagent (Thermo Fisher Scientific, P/N 23275) kits, in accordance with manufacturer's protocols.

High pH Reversed Phase Separation. Tandem mass tag labeled (TMT) samples were then consolidated, and separated using high-pH reversed phase chromatography (RP-10) with fraction collection as previously described [77]. Fractions were speed-vac dried, then reconstituted to produce 24 fractions for subsequent on-line nanoLC-MS/MS analysis.

Protein Identification and Quantitation by nanoLC-MS/MS. Reconstituted RP-10 fractions were analyzed on a Thermo Orbitrap Fusion Lumos Mass Spectrometer (Xcalibur 4.1, Tune Application 3.0.2041) coupled to an EasyLC 1200 HPLC system (Thermo Fisher Scientific). The EasyLC 1200 was equipped with a 20 µL loop, set-up for 96 well plates. A Kasil-fritted trapping column (75 µm ID) packed with ReproSil-Pur 120 C18-AQ, 5 µm material (15mm bed length) was utilized together with a 160mm length, 75 µm inner diameter spraying capillary pulled to a tip diameter of approximately 8-10 µm using a P-2000 capillary puller (Sutter Instruments, Novato, CA). The 160mm separation column was packed with ReproSil-Pur 120 C18-AQ, 3 µm material (Dr. Maisch GmbH, Ammerbuch-Entringen, Germany). Mobile phase consisted of A= 0.1% formic acid/2% acetonitrile (v/v), and Mobile phase B= 0.1% formic acid/98% acetonitrile (v/v). Samples (18 µL) were injected on to trapping column using Mobile Phase A at a flow rate of 2.5

μL/min. Peptides were then eluted using an 80 minute gradient (2% Mobile Phase B for 5 min, 2%-40% B from 5-65 min, followed by 70% B from 65-70 minutes, then returning to 2% B from 70-80 min) at a flowrate of 300 nL/min on the capillary separation column with direct spraying into the mass spectrometer. Data was acquired on Orbitrap Fusion Lumos Mass Spectrometer in data-dependent mode using synchronous precursor scanning MS^3 mode (SPS-MS3), with MS^2 triggered for the 12 most intense precursor ions within a mass-to-charge ratio *(m/z)* range of 300-1500 found in the full MS survey scan event. MS scans were acquired at 60,000 mass resolution (*R*) at *m/z* 400, using a target value of 4×10^5 ions, and a maximum fill time of 50 ms. MS^2 scans were acquired as CID ion trap (IT) rapid type scans using a target value of 1×10^4 ions, maximum fill time of 50 ms, and an isolation window of 2 Da. Data-dependent MS^3 spectra were acquired as Orbitrap (OT) scans, using Top 10 MS^2 daughter selection, automatic gain control (AGC) target of 5×10^4 ions, with scan range of *m/z* 100-500. The MS^3 maximum injection time was 86 ms, with HCD collision energy set to 65%. MS^3 mass resolution (*R*) was set to 15,000 at *m/z* 400 for TMT6plex experiments, and 50,000 at *m/z* 400 for TMT11-plex experiments. Dynamic exclusion was set to exclude selected precursors for 60 s with a repeat count of 1. Nanospray voltage was set to 2.2 kV, with heated capillary temperature set to 300 ºC, and an S-lens RF level equal to 30%. No sheath or auxiliary gas flow is applied.

Data Processing and Analysis. Acquired MS data was processed using Proteome Discoverer v. 2.2.0.388 software (Thermo) utilizing Mascot v 2.5.1 search engine (Matrix Science, London, UK) together with Percolator validation node for peptide-spectral match filtering [78]. Data was searched against Uniprot protein database (canonical human and mouse sequences, EBI, Cambridge, UK) supplemented with sequences of common contaminants. Peptide search tolearances were set to 10 ppm for precursors, and 0.8 Da for fragments. Trypsin cleavage specificity (cleavage at K, R except if followed by P) allowed for up to 2 missed cleavages. Carbamidomethylation of cysteine was set as a fixed modification, methionine oxidation, and TMT-modification of N-termini and lysine residues were set as variable modifications. Data validation of peptide and protein identifications was done at the level of the complete dataset consisting of combined Mascot search results for all individual samples per experiment via the Percolator validation node in Proteome Discoverer. Reporter ion ratio calculations were performed using summed abundances with most confident centroid selected from 20 ppm window. Only peptide-to-spectrum matches that are unique assignments to a given identified protein within the total dataset are considered for protein quantitation. High confidence protein identifications were reported using a Percolator estimated <1% false discovery rate (FDR) cut-off. Differential abundance significance was estimated using a background-based ANOVA with Benjamini-Hochberg correction to determine adjusted p-values.

CHAPTER 4

Covalent Ligand Discovery Against Sites Targeted by Anti-Cancer Natural Products

This chapter is based on the *BioRxiv* publication “Chemoproteomics-Enabled Ligand Screening Yields Covalent RNF114-Based Degraders that Mimic Natural Product Function”[27] and the *Cell Chemical Biology* publication “Covalent Ligand Discovery Against Druggable Hotspots Targeted by Anti-Cancer Natural Products”[47], and has been adapted with permission from all co-authors.

4.1 Introduction

Natural products have remained a cornerstone of drug discovery research for decades resulting in numerous FDA-approved medicines and tools for biomedical research across a wide range of therapeutic areas [117]. Historically, a large percentage of natural product-inspired medicines have utilized the natural product as a starting point, wherein the tools of synthetic chemistry are used to fine tune compound properties (i.e a semisynthetic approach). Alternatively, the function of natural products can also serve as motivation for the design of fully synthetic small molecules less constrained by availability, synthetic manipulation limitations, and physicochemical and metabolic liabilities. Modern-day examples of this approach include the translation of the alkaloid cytisine into the smoking cessation drug varenicline, the development of the blockbuster cardiovascular drug atorvastatin from the polyketide lovastatin, and the discovery of the proteasome inhibitor carfilzomib inspired by the natural polypeptide epoxomicin (**Fig. 4.1a-c**). Such approaches, however, are greatly facilitated by an understanding of the binding mode to its protein target as well as the identification of key pharmacophores within the parent natural product.

When structural or binding mode information is not available it becomes considerably more difficult to take these approaches, however, use of ABPP-enabled small molecule screening can facilitate ligand discovery against sites targeted by covalently-acting natural products. Covalently-acting natural products are amenable to rapid target identification through use of chemoproteomic strategies, such as isoTOP-ABPP as has been demonstrated in this work. Insights afforded by knowing specific sites of interaction can enable the pharmacological interrogation of the difficult to predict sites targeted by these natural products. In this work our approach to discovering fully synthetic covalent ligand to mimic biologically active natural products. The simple ABPP screening platform uses pure recombinant protein, on which the natural product binding site was identified, and competes a library of small molecule electrophiles against a fluorescent iodoacetamide probe (IA-rhodamine). This allows fragment binding to be read out on gel as the disappearance of the fluorescent band. While this approach could be considered moderate-throughput, analogous ABPP approaches could be performed on higher throughput using fluorescent polarization or using rapid fire mass spectrometry to directly read out compound binding.

4.2. Discovery of the Synthetic Small Molecule RNF114 Ligand, EN219

As outlined in the previous chapters, I discovered that the anti-cancer natural product nimbolide, covalently reacts with an N-terminal cysteine (C8) within an intrinsically disordered region of the E3 ubiquitin ligase RNF114 in human breast cancer cells [79]. Covalent targeting of RNF114 by nimbolide led to impaired ubiquitination of its endogenous substrate, tumor suppressor p21, through a nimbolide-dependent competition of the RNF114-substrate binding interaction, thus providing a potential mechanism for the anti-cancer effects of this natural product. The realization that nimbolide targeted a substrate recognition domain within RNF114 also lead us to develop

nimbolide as a novel recruiter of RNF114 for targeted protein degradation (TPD) applications. Discovering additional E3 ligase recruiters is an important pursuit in expanding the scope of TPD and may help to address resistance mechanisms [89,90,118], promote differing selectivity or kinetic profiles of degradation [119–121], and lead to cell-type or location-specific degradation. And while recruitment of RNF114 through nimbolide has proven to have advantageous degradation profiles, having a more synthetically tractable RNF114-recruiters would be advantageous. Because the N-terminal region of RNF114, which includes the C8 binding site, is intrinsically disordered, structure-guided ligand discovery and optimization was not possible thus requiring unbiased approaches to ligand discovery.

Activity-based protein profiling (ABPP)-enabled covalent ligand screening has been previously used to discover novel covalent recruiters against E3 ligases RNF4 and DCAF16 [91,122]. Using this technique, we were able to realize the successful translation of the binding mode of nimbolide into a simple, easily manipulated covalent small molecule. Importantly, this early-stage fragment can be used to functionally replace nimbolide as the covalent E3 ligase recruiter in fully synthetic degraders against several oncology targets.

4.2.1 Covalent Ligand Screening Against RNF114

To discover a fully synthetic covalent ligand that could access the same cysteine (C8) targeted by nimbolide on RNF114, we screened 318 cysteine-reactive chloroacetamide and acrylamide ligands in the gel-based competitive activity-based protein profiling (ABPP) assay against pure RNF114 protein **(Fig. 4.2.2a, 4.2.2b, Supplementary Fig. 4.2.1, Supplementary Table 1)** [47,122,123]. Through this screen, chloroacetamide EN219 emerged as the top hit, showing the greatest inhibition of IA-rhodamine binding to RNF114 **(Fig. 4.2.2c).** Dose-response studies showed that EN219 interacted with RNF114 with a 50 % inhibitory concentration (IC50) of 470 nM **(Fig. 4.2.2d, 4.2.2e)**. EN219 also inhibited RNF114-mediated autoubiquitination and p21 ubiquitination *in vitro*, similarly to our previously observed findings with nimbolide **(Fig. 4.2.2f).**

Since EN219 from our screening deck was a racemic mixture, we enantioselectively synthesized *(R)*-EN219 and *(S)*-EN219 and showed that the racemic mixture and both isomers showed similar potency for binding to RNF114 **(Supplementary Fig. 4.2.2a).** We also synthesized a non-reactive acetamide analog of EN219, JNS 2-229, and showed that this compound no longer interacted with RNF114 **(Supplementary Fig. 4.2.2a)**. Mapping the sites of EN219 covalent modification on pure RNF114 protein by LC-MS/MS confirmed C8 as the primary site of covalent modification **(Supplementary Fig. 4.2.2b).** Collectively, these data showed that EN219 reacted with C8 of RNF114, similar to nimbolide, but also that this interaction was likely to be reactivity-driven rather than affinity-mediated. While this compound likely represents an early hit compound that requires further structure-activity relationship (SAR) studies to improve potency and selectivity, we nonetheless pursued further characterization of EN219 as a fully synthetic ligand for RNF114.

To ascertain the selectivity of EN219, we next mapped the proteome-wide cysteine-reactivity of EN219 *in situ* in 231MFP breast cancer cells by competitive isotopic tandem orthogonal proteolysis-ABPP (isoTOP-ABPP) using previously well-validated methods [45,47–49,79]. As in the profiling of nimbolide reactivity, cells were treated *in situ* with vehicle or EN219 and subsequently lysed and labeled with an alkyne-functionalized iodoacetamide probe (IA-alkyne). Only 4 proteins showed >2-fold light versus heavy or control versus EN219-treated probe-modified peptide ratios with adjusted p-value <0.05 out of 686 probe-modified cysteines quantified. These proteins were RNF114 C8, TUBB1 C201, HSPD1 C442, and HIST1H3A C97, among which RNF114 was the only E3 ligase **(Fig. 4.2.2g, Supplementary Dataset 4).**

To further investigate the selectivity of EN219 and to confirm EN219 engagement of RNF114 in cells, we also synthesized an alkyne-functionalized EN219 probe (EN219-alkyne) **(Fig. 4.2.2h)**. We performed Tandem mass-tagging (TMT)-based quantitative proteomic profiling to identify proteins that were enriched by EN219-alkyne *in situ* labeling of 231MFP cells and were competed by EN219 *in situ* treatment **(Supplementary Fig. 4.2.2c, Supplementary Dataset 4)**. While we did not identify RNF114 in this proteomics experiment, likely due to its relatively low abundance, we did identify 7 additional potential off-targets of EN219 that showed >3-fold competition with adjusted p-value <0.05 against EN219-alkyne labeling in cells **(Supplementary Fig. 4.2.2b).** Again, none of these 7 potential EN219 off-targets were E3 ligases. Collectively, our results suggested that EN219 was a moderately selective covalent ligand against C8 of RNF114. While we did not observe RNF114 by TMT-based proteomic experiments, RNF114 was clearly enriched from 231MFP cells treated with EN219-alkyne *in situ* compared to vehicle-treated controls after CuAAC-mediated appendage of biotin-azide and subsequent avidin-pulldown and RNF114 blotting **(Fig. 4.2.2i)**.

4.2.2 EN219-Based RNF114 Recruiter in Targeted Protein Degradation Applications

We next tested whether this fully synthetic RNF114 covalent ligand, EN219, could be exploited for TPD applications. We have demonstrated that nimbolide can be linked to the BET inhibitor ligand JQ1 to selectively degrade BRD4. Thus, we benchmarked our EN219 RNF114 recruiter by linking EN219 to JQ1 with three different linkers—ML 2-14, ML 2-31, and ML 2-32 with C4 alkyl, C7 alkyl, and polyethylene glycol (PEG) 4 linkers, respectively **(Fig. 4.2.3a; Supplementary Fig. 4.2.3a)**. Similar to nimbolide-based degraders, ML 2-14 with the shortest linker showed the most robust degradation of BRD4 in 231MFP breast cancer cells compared to ML 2-31 and ML 2-32 with longer linkers, with 50 % degradation concentration (DC50) values of 36 and 14 nM for the long and short isoforms of BRD4, respectively **(Fig. 4.2.3b, 4.2.3c; Supplementary Fig. 4.2.3b, 4.2.3c)** [79]. EN219 treatment alone did not affect BRD4 levels, compared to ML 2-14 **(Supplementary Fig. 4.2.4a).** This ML 2-14 mediated degradation was fully averted by pre-treating cells with the proteasome inhibitor bortezomib as well as the E1 activating enzyme inhibitor TAK-243 **(Fig. 4.2.3d-4.2.3f, Supplementary Fig. 4.2.4b)**.

To further validate that ML 2-14 degradation of BRD4 was driven through RNF114, we showed that nimbolide pre-treatment completely attenuated BRD4 degradation by ML 2-14 in 231MFP breast cancer cells **(Fig. 4.2.3g-4.2.3h)**. BRD4 degradation in HAP1 cells were also significantly attenuated in RNF114 knockout cells compared to wild-type counterparts in two independent experiments **(Fig. 4.2.3i-4.2.3j, Supplementary Fig. 4.2.4c-4.2.4d)**. We note that these purchased RNF114 knockout cells showed residual RNF114 protein expression, likely indicating a mixed population of cells **(Fig. 4.2.3i-4.2.3j)**. We further showed that this loss of BRD4 protein levels was not due to transcriptional downregulation of BRD4 expression since ML 2-14 treatment in 231MFP cells did not alter BRD4 mRNA levels **(Supplementary Fig. 4.2.4e)**. TMT-based quantitative proteomic profiling of ML 2-14-mediated protein expression changes showed selective degradation of BRD3 and BRD4, but not BRD2. We also observed stabilization of two known or putative RNF114 substrates, including the tumor suppressor CDKN1A (p21) and CTGF **(Fig. 4.2.3k, Supplementary Dataset 6)** [50,79]**.**

To further demonstrate the utility of our newly discovered fully synthetic RNF114 recruiter EN219 in degrading other more challenging protein targets, we synthesized a degrader linking EN219 to the BCR-ABL inhibitor dasatinib, ML 2-23 and ML 2-22, bearing a longer PEG3 linker and a shorter C3 alkyl linker, respectively **(Fig. 4.2.4a, Supplementary Fig. 4.2.4f)**. For this particular target, ML 2-23 with the longer linker showed more robust degradation of BCR-ABL in K562 leukemia cells compared to ML 2-22, consistent with previously observed structure-activity relationships of nimbolide-based BCR-ABL degraders **(Fig. 4.2.4b-4.2.4c, Supplementary Fig. 4.2.4g)** [121]**.** Consistent with ML 2-23 engaging BCR-ABL in cells, we observed inhibition of CRKL phosphorylation, a downstream substrate of BCR-ABL signaling **(Fig. 4.2.4b-4.2.4c).** Interestingly, EN219 showed preferential degradation of BCR-ABL compared to c-ABL, compared to several previous BCR-ABL degraders utilizing cereblon or VHL recruiters that showed opposite selectivity **(Fig. 4.2.4b-4.2.4c)** [124,125]. This preferential degradation was also observed with the equivalent nimbolide-based degrader [9]. We further showed that this loss of BCR-ABL and c-ABL was not due to transcriptional downregulation of these genes, since BCR-ABL mRNA levels remained unchanged and we observed a likely compensatory increase in c-ABL mRNA levels **(Supplementary Fig. 4.2.4h)**. Furthermore, we do not believe that the loss of BCR-ABL shown here is because of general cytotoxicity since ML 2-23 treatment at the timepoints where we assessed BCR-ABL degradation only exerted relatively modest cell viability impairments in K562 cells compared to EN219 treatment alone **(Supplementary Fig. 4.2.4i)**. While rescue experiments with proteasome inhibitors proved challenging due to the cytotoxicity of proteasome inhibitors at the long timepoints required for robust BCR-ABL degradation, we observed significant rescue of early stage ML 2-23-mediated BCR-ABL and c-ABL degradation with pre-treatment of K562 cells with the proteasome inhibitor MG132 at a shorter time point **(Fig. 4.2.4d, 4.2.4e).**

Collectively, we discovered EN219 as a fully synthetic covalent RNF114 recruiter that mimics the action of nimbolide and showed its utility in TPD applications, exemplified by degradation of BRD4 and BCR-ABL.

4.2.3 Discussion

We previously discovered that the natural product nimbolide targets a predicted intrinsically disordered cysteine in RNF114 at a substrate recognition site [79]. Due to limitations of isolation of the natural product and ease of semi-synthetic derivatization, it was desirable to discover fully synthetic ligands for this site. However, given the intrinsically disordered nature of the binding site structure guided ligand design, as is frequently used in translating natural products into synthetic analogs, is not possible. Using the knowledge of this protein hotspot as identified through isoTOP-ABPP it is feasible to take an unbiased structurally naïve approach to ligand discovery using gel-based ABPP screening methods.

Here we report EN219 as a moderately selective covalent ligand that exploits the same binding modality on RNF114 as the natural product nimbolide. We show that EN219 can be linked to the BET inhibitor JQ1 to degrade BRD4 in a nimbolide-sensitive and proteasome- and RNF114-dependent manner. We further show that EN219 can be linked to the kinase inhibitor dasatinib to selectively degrade BCR-ABL over c-ABL in a proteasome-dependent manner in leukemia cells. Thus, EN219 represents a fully synthetic and more tunable chemical scaffold for targeting RNF114 for TPD applications relative to the complex natural product from which it was inspired. These findings also further highlight that moderately selective cysteine-targeting ligands can still lead to robust protein degraders [91,122].

While EN219 represents a promising initial chemical scaffold for RNF114 recruitment, future medicinal chemistry efforts will be required to further optimize the potency and metabolic stability of RNF114 recruiters, but its synthetic tractability compared to nimbolide makes this a realistic endeavor. The synthetic tunability of this scaffold offers possibilities to enhance the selectivity and potency of this RNF114 ligand and also may offer opportunities to alter the solvent exposed region binding to this E3 substrate recognition site in order to enable binding of neo-substrates in a molecular glue mode of action.

Overall, our results highlight the utility of chemoproteomic platforms for discovering new chemical scaffolds that can be used as E3 ligase recruiters for TPD applications. Moreover, these studies further speak to the power of unbiased chemoproteomic approaches in mimicking the function of covalently acting natural products, particularly those in which structural binding information is unavailable [126].

4.2.4 Figures

Figure 4.2.1

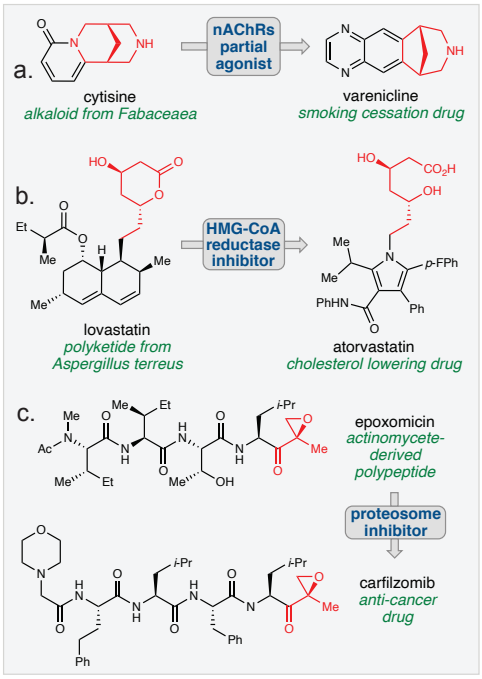

Figure 4.2.1. Translation of natural product function.
Many successful drugs have recapitulated the function of natural products with fully-synthetic chemical scaffolds. Key pharmacophores are shown in red.

Figure 4.2.2

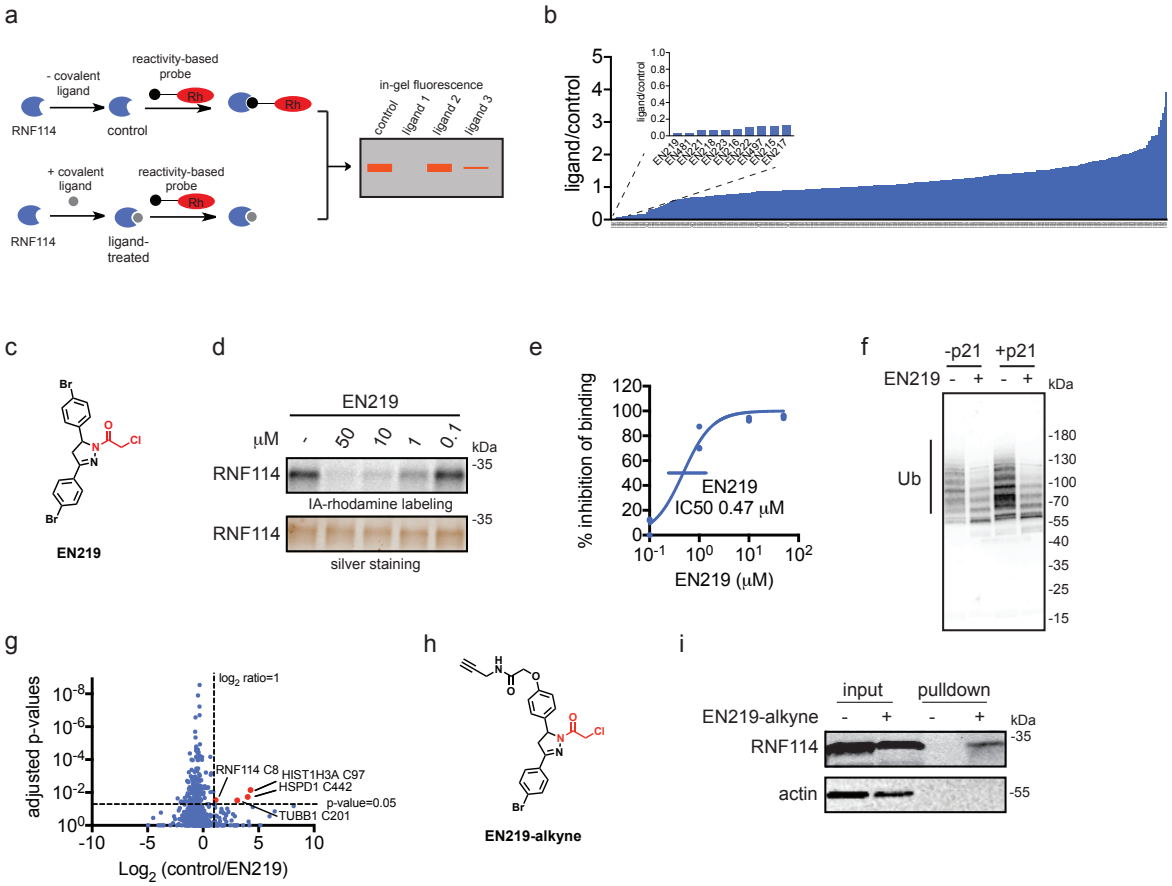

Figure 4.2.2. Covalent ligand screening against RNF114.
(a) Gel-based ABPP assay for screening covalent ligands against IA-rhodamine probe binding to pure RNF114 protein. Loss of fluorescence indicates covalent ligand binding to a cysteine on RNF114. **(b)** Quantified results from gel-based ABPP screen of 318 cysteine-reactive acrylamides and chloroacetamides against IA-rhodamine labeling of RNF114. DMSO vehicle or covalent ligands (50 μM) were pre-incubated with pure RNF114 protein (0.1 μg) for 30 min prior to addition of IA-rhodamine (100 nM) for 30 min at room temperature. Proteins were separated by SDS/PAGE and in-gel fluorescence was quantified. Raw gel-based ABPP data shown in **Supplementary Figure 4.2.1.** Structures of compounds screened can be found in **Table S1.** Data expressed as ligand/control ratio of in-gel fluorescent intensity. Shown in the inlay are the ligand/control ratios for the top 10 hits. **(c)** Structure of top hit EN219 with chloroacetamide cysteine-reactive warhead in red. **(d)** Dose-response of EN219 interaction with RNF114 by competitive gel-based ABPP. DMSO vehicle or covalent ligands were pre-incubated with pure RNF114 protein (0.1 μg) for 30 min prior to addition of IA-rhodamine (100 nM) for 30 min at room temperature. Proteins were separated by SDS/PAGE and in-gel fluorescence was quantified. Gels were also silver-stained as a loading control. **(e)** Percent inhibition of IA-rhodamine binding to RNF114 in **(d)** was quantified and 50 %

inhibitory concentration (IC50) was determined to be 0.47 μM. **(f)** RNF114-mediated autoubiquitination and p21 ubiquitination *in vitro*. DMSO vehicle or EN219 (50 μM) was incubated with pure RNF114 for 30 min prior to addition of PBS or p21, ATP, and FLAG-ubiquitin (Ub) for 60 min. Proteins were separated by SDS/PAGE and blotted for FLAG. Ubiquitinated-RNF114/p21 is noted. **(g)** IsoTOP-ABPP analysis of EN219 in 231MFP breast cancer cells. 231MFP cells were treated *in situ* with DMSO vehicle or EN219 (1 μM) for 90 min. Control and treated cell lysates were labeled with IA-alkyne (100 μM) for 1 h, after which isotopically light (control) or heavy (EN219-treated) biotin-azide bearing a TEV tag was appended by CuAAC. Proteomes were mixed in a 1:1 ratio, probe-labeled proteins were enriched with avidin and digested with trypsin, and probe-modified peptides were eluted by TEV protease and analyzed by LC-MS/MS. Average light-to-heavy (control/EN219) ratios and adjusted p-values were quantified for probe-modified peptides that were present in two out of three biological replicates and plotted. Shown in red are protein and modified cysteine site for peptides that showed >2-fold control/EN219 ratio with adjusted p-value <0.05. Full data can be found in **Supplementary Dataset 3. (h)** Structure of alkyne-functionalized EN219 probe. **(i)** EN219-alkyne pulldown of RNF114. 231MFP cells were treated with DMSO vehicle or EN219-alkyne (50 μM) for 90 min. Biotin-azide was appended to probe-labeled proteins by CuAAC and probe-labeled proteins were avidin enriched and blotted for RNF114 and negative control actin. An aliquot of input proteome from vehicle-and EN219-treated cell lysates was also subjected to blotting as an input control. Data shown in **(e)** are average values and individual replicate values. Data shown are from n=1 in **(b)** and n=3 for **(d-f, i)** biological replicate(s) per group. Gels shown in **(d, i)** are representative gels from n=3 biological replicates per group. This figure is related to **Supplemental Figures 4.2.1-4.2.2.**

Figure 4.2.3

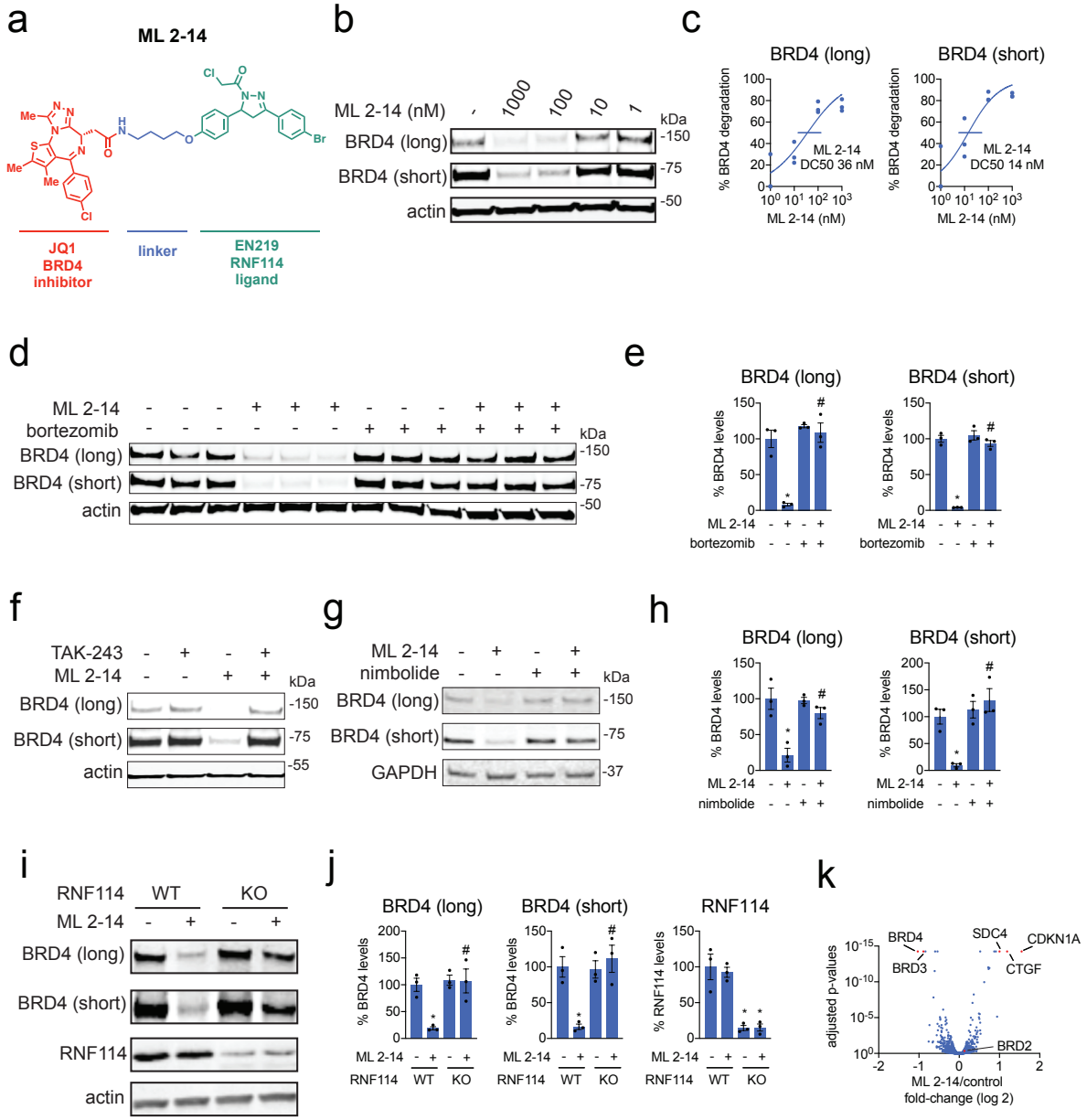

Figure 4.2.3. EN219-based BRD4 degrader.
(a) Structure of ML 2-14, an EN219-based BRD4 degrader linking EN219 to BET inhibitor JQ1. **(b)** Degradation of BRD4 by ML 2-14. 231MFP cells were treated with DMSO vehicle or ML 2-14 for 8 h and the long and short isoforms of BRD4 and loading control actin were detected by Western blotting. **(c)** Percentage of BRD4 degradation quantified from **(b)** show 50 % degradation concentrations of 36 and 14 nM for the long and short isoforms of BRD4, respectively. **(d)** Proteasome-dependent degradation of BRD4 by ML 2-14. 231MFP cells were treated with DMSO vehicle or with proteasome inhibitor bortezomib (1 μM) 30 min prior to DMSO vehicle or ML 2-14 (100 nM) treatment for 8 h. BRD4 and

loading control actin levels were detected by Western blotting. **(e)** Quantification of BRD4 levels from **(d)**. **(f)** Ubiquitin activating enzyme (E1)-dependent degradation of BRD4 by ML 2-14. 231MFP cells were treated with DMSO vehicle or with E1 inhibitor TAK-243 (10 μM) 30 min prior to DMSO vehicle or ML 2-14 (100 nM) treatment for 8 h. BRD4 and loading control actin levels were detected by Western blotting**.** Quantification of blot can be found in **Supplementary Figure 4.2.4b. (g)** BRD4 degradation by ML 2-14 is attenuated by nimbolide. 231MFP cells were treated with DMSO vehicle or with nimbolide (4 μM) 30 min prior to DMSO vehicle or ML 2-14 (100 nM) treatment for 8 h. **(h)** Quantification of BRD4 levels from **(g)**. **(i)** Degradation of BRD4 in RNF114 wild-type (WT) or knockout (KO) HAP1 cells. RNF114 WT or KO HAP1 cells were treated with DMSO vehicle or ML 2-14 (1 μM) for 16 h and BRD4, RNF114, and loading control actin levels were detected by Western blotting. **(j)** Quantification of data from **(i)**. **(k)** TMT-based quantitative proteomic data showing ML 2-14-mediated protein level changes in 231MFP cells. 231MFP cells were treated with DMSO vehicle or ML 2-14 for 8 h. Shown are average TMT ratios for all tryptic peptides identified with at least 2 unique peptides. Shown in red are proteins that showed >2-fold increased or decreased levels with ML 2-14 treatment with adjusted p-values <0.05. Data in **(b-k)** are from n=3 biologically independent replicates/group. Data shown in **(c)** are average and individual replicate values. Data shown in **(e, h, j)** are averages ± sem values and also individual biological replicate values. Blots shown in **(b, d, f, g, i)** are representative of n=3 biologically independent replicates/group. Statistical significance was calculated with unpaired two-tailed Student's t-test and is expressed as *p<0.05 compared to vehicle-treated controls in **(e, h, j)** and #p<0.05 compared to ML 2-14-treated groups in **(e, h)** and compared to ML 2-14-treated RNF114 WT cells in **(j)**. This figure is related to **Supplementary Figures 4.2.3-4.2.4.**

Figure 4.2.4

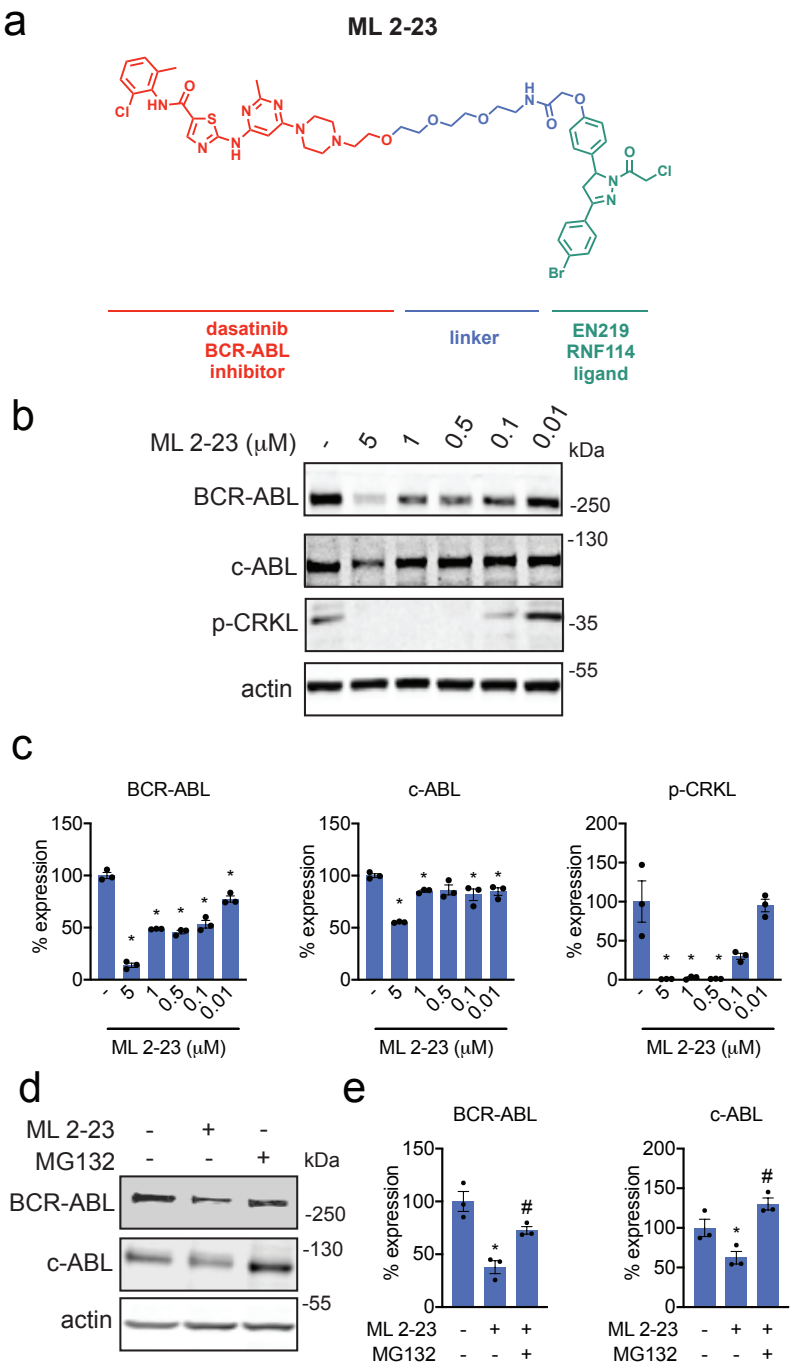

Figure 4.2.4. EN219-based ABL degrader.
(a) Structure of ML 2-23, an EN219-based ABL degrader linking EN219 to ABL inhibitor dasatinib. **(b)** Degradation of BCR-ABL and c-ABL by ML 2-23. K562 cells were treated with DMSO vehicle or ML 2-23 for 16 h and BCR-ABL, c-ABL, p-CRKL, and loading control actin were detected by Western blotting. **(c)** Percentage of BCR-ABL, c-ABL, and

p-CRKL expression quantified from **(b)**. **(d)** Proteasome-dependent degradation of BCR-ABL and c-ABL by ML 2-23. K562 cells were treated with DMSO vehicle or with proteasome inhibitor MG132 (5 μM) 30 min prior to DMSO vehicle or ML 2-23 (1 μM) treatment for 12 h. BCR-ABL, c-ABL, and loading control actin levels were detected by Western blotting. **(e)** Quantification of BCR-ABL and c-ABL levels from **(d)**. Data shown in **(c, e)** are averages ± sem values and also individual biological replicate values. Blots shown in **(b, d)** are representative of n=3 biological replicates/group. Statistical significance was calculated with unpaired two-tailed Student's t-test and is expressed as *$p<0.05$ compared to vehicle-treated controls in **(c, e)** and #$p<0.05$ compared to ML 2-23-treated groups in **(e)**. This figure is related to **Supplementary Figure 4.2.4.**

4.2.5 Acknowledgement of Co-Author Contributions

M. Luo, J.N. Spradlin, and D.K. Nomura conceived the project and wrote the paper. M. Luo, J.N. Spradlin, J.A. Tallarico, J.M. McKenna, M. Schirle, T.J. Maimone and D.K. Nomura provided intellectual contributions and insights into project directions. M. Luo, J.N. Spradlin, S.M. Busby, M. Schirle, T.J. Maimone and D.K. Nomura designed the experiments and analyzed data. M. Luo, J.N. Spradlin and S.M. Busby performed experiments and analyzed data. M. Luo and J.N. Spradlin designed and synthesized compounds. M. Luo, J.N. Spradlin, T.J. Maimone and D.K. Nomura edited the paper.

4.2.6 Methods

Chemicals.

Covalent ligands screened against RNF114 were purchased from Enamine LLC, including EN219. Structures of compounds screened can be found in **Table S1.** See Supplementary Information for synthetic methods and characterization for EN219 and degraders. Nimbolide was purchased from Cayman Chemicals (Item No. 19230).

Cell culture.

The 231MFP cells were obtained from Prof. Benjamin Cravatt and were generated from explanted tumor xenografts of MDA-MB-231 cells as previously described [60]. The 231MFP cells were cultured in L15 medium containing 10% FBS and maintained at 37 °C with 0% CO_2. K562 chronic myeloid leukemia cell lines were purchased from ATCC. The K562 cells were cultured in Iscove's Modified Dµlbecco's Medium containing 10% FBS and maintained at 37 °C with 5% CO_2. HAP1 RNF114 wild-type and knockout cell lines were purchased from Horizon Discovery. The RNF114 knockout cell line was generated by CRISPR/Cas9 to contain a frameshift mutation in a coding exon of RNF114. HAP1 cells were grown in Iscove's Modifed Dµlbecco's Medium in the presence of 10% FBS and penicillin/streptomycin.

Cell-based degrader assays.

For assaying degrader activity, cells were seeded (500,000 cells for 231MFP and HAP1 cells, 1,000,000 for K562 cells) into a 6 cm tissue culture dish (Corning) in 2.0−2.5 mL of media and allowed to adhere overnight for 231MFP and HAP1 cells. The following morning, media was replaced with complete media containing the desired concentration of compound diluted from a 1,000 x stock in DMSO. For rescue studies, the cells were pre-treated with proteasome inhibitors, nimbolide, or E1 activating enzyme inhibitors 30 min prior to the addition of DMSO or degrader compounds. At the specified time point, cells were washed once with PBS on ice, before addition of 120 µL of lysis buffer (20 mM Tris-HCl at pH 7.5, 150 mM NaCl, 1 mM Na_2EDTA, 1 mM EGTA, 1% Triton, 2.5 mM sodium pyrophosphate, 1 mM beta-glycerophosphate, 1 mM Na_3VO_4, 1 µg/ml leupeptin) with Complete Protease Inhibitor Cocktail (Sigma) was added. The cells were incubated in lysis buffer for 5 min before scraping and transferring to microcentrifuge tubes. The lysates were then frozen at −80 °C or immediately processed for Western blotting. To prepare for Western blotting, the lysates were cleared with a 20,000g spin for 10 min and the resulting supernatant protein concentrations were quantified via BCA assay. The

lysates were normalized by dilution with PBS to match the lowest concentration lysate, and the appropriate amount of 4 x Laemmli's reducing buffer was added.

Gel-Based ABPP.

Gel-Based ABPP methods were performed as previously described [122]. Pure recombinant human RNF114 was purchased from Boston Biochem (K-220). RNF114 (0.25 µg) was diluted into 50 µL of PBS and 1 µL of either DMSO (vehicle) or covalently acting small molecule to achieve the desired concentration. After 30 min at room temperature, the samples were treated with 250 nM of tetramethylrhodamine-5-iodoacetamide dihydroiodide (IA-Rhodamine) (Setareh Biotech, 6222, prepared in anhydrous DMSO) for 1 h at room temperature. Incubations were quenched by diluting the incubation with 20 µL of 4 x reducing Laemmli SDS sample loading buffer (Alfa Aesar) and heated at 90 °C for 5 min. The samples were separated on precast 4−20% Criterion TGX gels (Bio-Rad Laboratories, Inc.). Fluorescent imaging was performed on a ChemiDoc MP (Bio-Rad Laboratories, Inc.). Inhibition of target labeling was assessed by densitometry using ImageJ.

EN219-alkyne probe labeling *in situ* and pulldown studies.

Experiments were performed following an adaption of a previously described protocol [127]. The 231MFP cells were treated with either DMSO vehicle or 50 µM EN219-alkyne probe for 90 min. Cells were collected in PBS and lysed by sonication. For preparation of Western blotting samples, the lysate (1 mg of protein in 500 µl) was aliquoted per sample and then the following were added: 10 µl of 5 mM biotin picolylazide (900912 Sigma-Aldrich) and 50 µl of click reaction mix (three parts TBTA 5 mM TBTA in butanol:DMSO (4:1, v/v), one part 50 mM Cu(II)SO_4 solution and one part 50 mM TCEP). Samples were incubated for 1 h at room temperature with gentle agitation. After CuAAC, proteomes were precipitated by centrifugation at 6,500 *g* and washed twice in ice-cold methanol (500 µl). The samples were spun in a prechilled (4 °C) centrifuge at 6,500 *g* for 4 min allowing for aspiration of excess methanol and subsequent reconstitution of protein pellet in 250 µl PBS containing 1.2% SDS by probe sonication. Then the proteome was denatured at 90 °C for 5 min, the insoluble components were precipitated by centrifugation at 6,500*g* and soluble proteome was diluted in 1.2 ml PBS (the final concentration of SDS in the sample was 0.2%) to a total volume of 1450 µl, with 50 µl reserved as input. Then 85 µl of prewashed 50% streptavidin agarose bead slurry was added to each sample and samples were incubated overnight at room temperature with gentle agitation. Supernatant was aspirated from each sample after spinning beads at 6,500 *g* for 2 min at room temperature. Beads were transferred to spin columns and washed three times with PBS. To elute, beads were boiled 5 min in 50 µl LDS sample buffer. Eluents were collected after centrifugation and analyzed by immunoblotting. The resulting samples were also analyzed as described below for TMT-based quantitative proteomic profiling.

LC–MS/MS analysis of pure RNF114 EN219 modification.

Purified RNF114 (10 µg) in 50µl PBS was incubated 30 min at room temperature either with DMSO vehicle or EN219 (50 µM). The DMSO control was then treated with light iodoacetamide while the compound treated sample was incubated with heavy

iodoacetamide for 1h each at room temperature (200 μM final concentration, Sigma-Aldrich, 721328). The samples were precipitated by addition of 12.5 μl of 100% (w/v) trichloroacetic acid and the treated and control groups were combined pairwise, before cooling to −80 °C for 1h. The combined sample was then spun for at max speed for 10 min at 4 °C, supernatant was carefully removed and the sample was washed with ice-cold 0.01 M HCl/90% acetone solution. The pellet was resuspended in 4M urea containing 0.1% Protease Max (Promega Corp. V2071) and diluted in 40 mM ammonium bicarbonate buffer. The samples were reduced with 10 mM TCEP at 60 °C for 30min. The sample was then diluted 50% with PBS before sequencing grade trypsin (1 μg per sample, Promega Corp, V5111) was added for an overnight incubation at 37 °C. The next day, the sample was centrifuged at 13,200 rpm for 30 min. The supernatant was transferred to a new tube and acidified to a final concentration of 5% formic acid and stored at −80 °C until mass spectrometry analysis.

IsoTOP-ABPP.

IsoTOP-ABPP studies were done as previously reported [79]. Cells were lysed by probe sonication in PBS and protein concentrations were measured by BCA assay35. For in situ experiments, cells were treated for 90 min with either DMSO vehicle or covalently acting small molecμle (from 1,000× DMSO stock) before cell collection and lysis. Proteomes were subsequently labeled with *N*-5-Hexyn-1-yl-2-iodoacetamide (IA-alkyne) labeling (100 μM) for 1 h at room temperature. CuAAC was used by sequential addition of tris(2-carboxyethyl) phosphine (1 mM, Sigma), tris[(1-benzyl-1H-1,2,3-triazol-4-yl)methyl]amine (34 μM, Sigma), copper(II) sμlfate (1 mM, Sigma) and biotin-linker-azide—the linker functionalized with a tobacco etch virus (TEV) protease recognition sequence as well as an isotopically light or heavy valine for treatment of control or treated proteome, respectively. After CuAAC, proteomes were precipitated by centrifugation at 6,500*g*, washed in ice-cold methanol, combined in a 1:1 control:treated ratio, washed again, then denatured and resolubilized by heating in 1.2% SDS–PBS to 80 °C for 5 min. Insoluble components were precipitated by centrifugation at 6,500*g* and soluble proteome was diluted in 5 ml 0.2% SDS–PBS. Labeled proteins were bound to avidin-agarose beads (170 μl resuspended beads per sample, Thermo Pierce) while rotating overnight at 4 °C. Bead-linked proteins were enriched by washing three times each in PBS and water, then resuspended in 6 M urea and PBS (Sigma), and reduced in TCEP (1 mM, Sigma), alkylated with iodoacetamide (18 mM, Sigma), before being washed and resuspended in 2 M urea and trypsinized overnight with 0.5 μg μl^{-1} sequencing grade trypsin (Promega). Tryptic peptides were eluted off. Beads were washed three times each in PBS and water, washed in TEV buffer solution (water, TEV buffer, 100 μM dithiothreitol) and resuspended in buffer with Ac-TEV protease and incubated overnight. Peptides were diluted in water and acidified with formic acid (1.2 M, Spectrum) and prepared for analysis.

Mass spectrometry analysis.

Total peptides from TEV protease digestion for isoTOP-ABPP or tryptic peptides for mapping EN219 site of modification on pure RNF114 were pressure loaded onto 250 mm tubing packed with Aqua C18 reverse phase resin (Phenomenex no. 04A-4299), which was previously equilibrated on an Agilent 600 series high-performance liquid chromatograph using the gradient from 100% buffer A to 100% buffer B over 10 min,

followed by a 5 min wash with 100% buffer B and a 5 min wash with 100% buffer A. The samples were then attached using a MicroTee PEEK 360 µm fitting (Thermo Fisher Scientific no. p-888) to a 13 cm laser pµlled column packed with 10 cm Aqua C18 reverse-phase resin and 3 cm of strong-cation exchange resin for isoTOP-ABPP studies. Samples were analyzed using an Q Exactive Plus mass spectrometer (Thermo Fisher Scientific) using a five-step Mµltidimensional Protein Identification Technology (MudPIT) program, using 0, 25, 50, 80 and 100% salt bumps of 500 mM aqueous ammonium acetate and using a gradient of 5–55% buffer B in buffer A (buffer A: 95:5 water:acetonitrile, 0.1% formic acid; buffer B 80:20 acetonitrile:water, 0.1% formic acid). Data were collected in datadependent acquisition mode with dynamic exclusion enabled (60 s). One fµll mass spectrometry (MS^1) scan (400–1,800 mass-to-charge ratio (m/z)) was followed by 15 MS^2 scans of the nth most abundant ions. Heated capillary temperature was set to 200 °C and the nanospray voltage was set to 2.75 kV, as previously described.
Data were extracted in the form of MS^1 and MS^2 files using Raw Extractor v.1.9.9.2 (Scripps Research Institute) and searched against the Uniprot human database using ProLuCID search methodology in IP2 v.3 (Integrated Proteomics Applications, Inc.) [128]. Probe-modified cysteine residues were searched with a static modification for carboxyaminomethylation (+57.02146) and up to two differential modifications for methionine oxidation and either the light or heavy TEV tags (+464.28596 or +470.29977, respectively) or the mass of the EN219 adduct. Peptides were required to be fully tryptic peptides and to contain the TEV modification. ProLUCID data was filtered through DTASelect to achieve a peptide false-positive rate below 5%. Only those probe-modified peptides that were evident across two out of three biological replicates were interpreted for their isotopic light to heavy ratios. Light versus heavy isotopic probe-modified peptide ratios are calculated by taking the mean of the ratios of each replicate paired light vs. heavy precursor abundance for all peptide spectral matches (PSM) associated with a peptide. The paired abundances were also used to calculate a paired sample t-test p-value in an effort to estimate constancy within paired abundances and significance in change between treatment and control. P-values were corrected using the Benjamini/Hochberg method.

TMT-based quantitative proteomic profiling.

TMT proteomic profiling was performed as previously described [79].

RNF114 ubiquitination assay.

Recombinant Myc-Flag-RNF114 proteins were purchased from Origene (Origene Technologies Inc., TP309752) or were purified as described previously[79]. For in vitro auto-ubiquitination assay, 0.2 µg of RNF114 in 25 µl of TBS was pre-incubated with DMSO vehicle or the covalently acting compound for 30 min at room temperature. Subsequently, 0.1 µg of UBE1 (Boston Biochem. Inc., E-305), 0.1 µg UBE2D1 (Boston Bichem. Inc., e2-615), 5 µg of Flag-ubiquitin (Boston Bichem. Inc., u-120) in a total volume of 25 µl Tris buffer containing 2 mM ATP, 10 mM DTT and 10 mM $MgCl_2$ were added to achieve a final volume of 50 µl. For substrate-protein ubiquitination assays, 0.1 µg of p21 (Origene) was added at this stage. The mixture was incubated at 37 °C with agitation for 1.5 h. Then, 20 µl of Laemmli's buffer was added to quench the reaction and proteins were analyzed by Western blot assay.

Western blotting.

Antibodies to RNF114 (Millipore Sigma, HPA021184), c-ABL (Santa Crus, 24-11), p-CRKL (Tyr207, Cell Signaling Technology, 3181), GAPDH (Proteintech Group Inc., 60004-1-Ig), BRD4 (Abcam plc, Ab128874), and beta-actin (Proteintech Group Inc., 6609-1-Ig) were obtained from various commercial sources and dilutions were prepared per the recommended manufacturers' procedures. Proteins were resolved by SDS–PAGE and transferred to nitrocellulose membranes using the iBlot system (Invitrogen). Blots were blocked with 5% BSA in Tris-buffered saline containing Tween 20 (TBST) solution for 1 h at room temperature, washed in TBST and probed with primary antibody diluted in diluent, as recommended by the manufacturer, overnight at 4 °C. Following washes with TBST, the blots were incubated in the dark with secondary antibodies purchased from Ly-Cor and used at 1:10,000 dilution in 5% BSA in TBST at room temperature. Blots were visualized using an Odyssey Li-Cor scanner after additional washes. If additional primary antibody incubations were required, the membrane was stripped using ReBlot Plus Strong Antibody Stripping Solution (EMD Millipore, 2504), washed and blocked again before being re-incubated with primary antibody. Blots were quantified and normalized to loading controls using Image J.

Proliferation Assays:

Cell proliferation assays were performed using WST8 reagent (APExBio, CCK-8), following the manufacturer's recommendations. K562 cells were seeded at a density of 100,000 cell/mL in a volume of 100 µL. 231MFP cells were seeded at a density of 50,000 cell/mL in a volume of 100 µL. Cells were seeded in full media and allowed to rest overnight before being treated with 50 µL of treated media (0.1% DMSO vehicle for each condition). After the appropriate compound treatment time 15 µL of WST8 reagent was added and cells were returned to 37 °C incubator for 90 min before reading absorbance at 450 nM.

Gene expression by quantitative PCR:

Total RNA was extracted from cells using Monarch Total RNA Miniprep Kit (NEB, T2010S). Complementary DNA was synthesized using ProtoScript II reverse transcriptase (NEB, M0368L) and gene expression was confirmed by quantitative PCR (qPCR) using the manufacturer's protocol for DyNAmo HS SYBR Green (Fisher Scientific, F-410L) on the CFX Connect Real-Time PCR Detection System (Bio-Rad). Primer sequences for Fisher Maxima SYBR Green were derived from Primer Bank. Sequences of primers are as follows:

BRD4 Forward: ACCTCCAACCCTAACAAGCC
BRD4 Reverse: TTTCCATAGTGTCTTGAGCACC
ABL1 Forward: TGAAAAGCTCCGGGTCTTAGG
ABL1 Reverse: TTGACTGGCGTGATGTAGTTG
BCR-ABL Forward: TCCGCTGACCATCAATAAGGA
BCR-ABL Reverse: CACTCAGACCCTGAGGCTCAA
PPIA (Cyclophilin) Forward: CCC ACC GTG TTC TTC GAC ATT
PPIA (Cyclophilin) Reverse: GGA CCC GTA TGC TTT AGG ATG A

4.3 Discovery of a Synthetic PPP2R1A Ligand, JNS-1-40

The profiling of the anti-cancer natural product Withaferin A offers another prime example of how chemoproteomic profiling of covalent natural products uncovers unconventional druggable modalities. Withaferin A was found to covalently modify a cysteine at the protein interaction interface of the regulatory subunit of the PP2A complex, stabilizing the complex to activate PP2A activity and impair cancer proliferation. Uncovering this druggable node allowed for the same target-directed fragment screening approach to identify a simple synthetic scaffold capable of *in vivo* engagement of the druggable site for cancer growth impairment and PP2A activation. Early medicinal chemistry efforts demonstrate the potential to increase binding affinity and selectivity of the initial lead compound, yielding a useful and synthetically scalable tool compound for PP2A complex application. Additionally, this compound offers a starting point for the development of a PP2A complex recruiter for the expansion of heterobifunctional therapeutic modalities.

4.3.1 Chemoproteomic Profiling Uncovers Interaction of Withaferin A with PPP2R1A

This study began by testing the anti-cancer activity of withaferin A across several breast cancer cell lines including the receptor-positive MCF7 cells and triple-negative breast cancer (TNBC) cells 231MFP and HCC38 devoid in estrogen, progesterone, and HER2 receptors. Consistent with previous studies, we show that withaferin A impairs serum-free cell survival and proliferation in MCF7, 231MFP, and HCC38 breast cancer cells **(Fig. 4.3.1b-4.3.1d)**. We show that withaferin A impairs 231MFP cell proliferation in a dose-dependent manner with a 50 % effective concentration (EC50) of 7.5 μM **(Supplementary Fig. 4.3.1a)**.

We next used competitive isoTOP-ABPP platforms to map the proteome-wide cysteine-reactivity of withaferin A in 231MFP breast cancer cell proteomes. To ascertain the direct targets of withaferin A without potential confounding effects from protein expression changes, we initially performed isoTOP-ABPP studies *in vitro* in 231MFP breast cancer cell proteomes **(Fig. 4.3.2a)**. Out of the >3000 total probe-modified peptides identified, we only interpreted those peptides that were present in at least 2 out of 3 biological replicates. Through this analysis, we identified C377 of PPP2R1A, a regulatory subunit of PP2A, as the primary and only target that showed a light to heavy ratio >5 across all three biological replicates **(Fig. 4.3.2b)**. We also confirmed that C377 of PPP2R1A was the primary *in situ* target of withaferin A in 231MFP cells showing an isotopically light to heavy ratio of 4.0. **(Supplementary Fig. 4.3.1b).**

PP2A is a tumor suppressor that dephosphorylates and inactivates oncogenic signaling pathways such as AKT. There has been considerable interest in developing direct or indirect activators of PP2A for cancer therapy [129]. While our IAyne probe labeled both C377 and C390 on PPP2R1A, withaferin A specifically targets C377 but not C390 on PPP2R1A **(Fig. 4.3.2b).** We confirmed this interaction as demonstrated by competition of withaferin A against IAyne labeling of pure human PPP2R1A protein using gel-based

ABPP methods **(Fig. 4.3.2c)**. In these gel-based studies, we used a lower concentration of IAyne than our isoTOP-ABPP studies, which may explain why we observe full competition of withaferin A against IAyne labeling. C377 sits at an interface between three subunits of the core PP2A complex based on previously solved crystal structures of the PP2A heterotrimeric holoenzyme complex **(Fig. 4.3.2d)** [130]. We postulated that withaferin A activates PP2A activity through targeting C377 on PPP2R1A to impair 231MFP breast cancer cell proliferation. Consistent with this premise, we showed that withaferin A activated PP2A activity in a reconstituted *in vitro* biochemical assay with purified human wild-type PPP2R1A protein and the regulatory and catalytic subunits PPP2R2A and PPP2CA, respectively, but not with the PPP2R1A C377A mutant protein **(Fig. 4.3.2e)**. Treatment of 231MFP cells with withaferin A also reduced phosphorylated AKT levels and this effect was rescued by co-treatment with the PP2A-selective inhibitor cantharidin **(Fig. 4.3.2f)**. Further confirming that targeting of PPP2R1A is involved in withaferin A effects, PPP2R1A knockdown with short interfering RNA (siPPP2R1A) significantly attenuated the anti-proliferative effects observed with withaferin A treatment in 231MFP breast cancer cells **(Supplementary Fig. 4.3.1d, 4.3.1e)**. The lack of complete attenuation of withaferin A-induced anti-proliferative effects in siPPP2R1A cells may be due to residual PPP2R1A protein expression in the knockdown cells or the contribution of additional withaferin A targets to the anti-proliferative effects. Nonetheless, our data indicate that withaferin A targeting of C377 of PPP2R1A and activation of PP2A activity is in-part involved in the observed anti-proliferative effects.

4.3.2 Covalent Ligand Screening Against PPP2R1A

To identify more synthetically tractable covalent ligands against C377 of PPP2R1A, we took a different approach than with RNF114, screening the library of cysteine-reactive small molecule ligands in 231MFP breast cancer cells to identify any compounds that recapitulated the phenotypes of withaferin A in impairing 231MFP cell proliferation, rather than for direct *in vitro* binders **(Fig. 4.3.3a, 4.3.3b; Supplementary Table 2)**. The top hit that arose from this screen was the chloroacetamide DKM 2-90 **(Fig. 4.3.3b-4.3.3c, 4.3.4a)**.

We next performed competitive isoTOP-ABPP experiments to identify the targets of DKM 2-90 through competition of this lead fragment against IAyne labeling of 231MFP proteomes. While this ligand was not potent, only showing anti-proliferative effects at 100 μM, we found that DKM 2-90 showed considerable selectivity in targeting C377 of PPP2R1A *in vitro* **(Fig. 4.3.4b; Supplementary Dataset 7)**. We also confirmed this through gel-based ABPP methods, showing significant competition of DKM 2-90 against IAyne labeling of pure human PPP2R1A protein with a 50 % inhibitory concentration (IC50) of 10 μM. **(Fig. 4.3.4c).** We also show that other chloroacetamide ligands of similar structures do not bind to PPP2R1A, suggesting that DKM 2-90 interacts with PPP2R1A *in vitro* relatively specifically, despite its simple structure **(Supplementary Fig. 4.3.1f).** IsoTOP-ABPP analysis of DKM 2-90 treatment in 231MFP cells *in situ* also showed targeting of C377 of PPP2R1A with an isotopically light to heavy ratio of 5.9. However, four additional targets were also evident that showed an isotopically light to heavy ratio >5, including TXNDC17 C43, CLIC4 C35, ACAT1 C196, and SCP2 C307

(Supplementary Fig. 4.3.1g). Nonetheless, while DKM 2-90 was a very simple and non-potent covalent ligand, it showed remarkable overall selectivity with only 5 total sites showing >5 ratio out of >1000 cysteines profiled **(Supplementary Fig. 4.3.1g; Supplementary Dataset 7)**. Despite additional targets of DKM 2-90, we still observed an attenuation of DKM 2-90-mediated anti-proliferative effects in siPPP2R1A 231MFP cells compared to DKM 2-90-treated siControl cells **(Supplementary Fig. 4.3.1h)**. We also recapitulated the reduced levels of phosphorylated AKT and cantharidin rescue with DKM 2-90 treatment in 231MFP cells **(Fig. 4.3.4d).**

While DKM 2-90 was not a potent ligand against PPP2R1A, we showed that much simpler covalent ligands could be identified that hit the same druggable hotspots targeted by complex natural products like withaferin A with decent selectivity and cell penetration. We next sought to optimize the potency of DKM 2-90. We found that replacing the benzodioxan ring with a tetralin with JNS 1-37 dramatically reduced potency with an IC50 value of 300 μM **(Supplementary Fig. 4.3.2a)** compared to 10 μM with DKM 2-90**.** Adding an N-benzyl group to DKM 2-90 with JNS 1-40 improved potency towards PPP2R1A by 16-fold with an IC50 of 630 nM **(Fig. 4.3.5a)**. We thus moved forward with further characterization of JNS 1-40. Both *in vitro* and *in situ* isoTOP-ABPP analysis showed that JNS 1-40 selectively targets C377 of PPP2R1A in both 231MFP complex proteome and cells, and is the only target exhibiting an isotopically light to heavy ratio >5 **(Fig. 4.3.5b; Supplementary Fig. 4.3.2b; Supplementary Dataset 7)**. Much like withaferin A, JNS 1-40 activated PP2A activity *in vitro* with purified PP2A complex proteins with wild-type PPP2R1A, but not with the PPP2R1A C377A mutant protein **(Fig. 4.3.5c)**. Similarly, JNS 1-40 treatment in 231MFP cells significantly reduced phosphorylated AKT levels and impaired proliferation and survival **(Fig. 4.3.5d-4.3.5f)**. The anti-proliferative effects observed with JNS 1-40 were also attenuated in siPPP2R1A 231MFP cells compared to siControl cells **(Fig. 4.3.2c)**.

With the improved potency and selectivity observed with JNS 1-40, we next sought to determine whether JNS 1-40 targeting of PPP2R1A could reduce breast cancer tumor growth *in vivo*. Daily treatment of mice with JNS 1-40 (50 mg/kg ip) *in vivo* began 15 days after 231MFP tumor xenograft initiation and significantly attenuated tumor growth **(Fig. 4.3.5g)**. Daily treatment with JNS 1-40 for >30 days did not cause any overt toxicity or body weight loss, suggesting that this compound is well tolerated *in vivo* (data not shown). To confirm target engagement, we also performed *ex vivo* isoTOP-ABPP analysis of 231MFP tumor xenografts from *in vivo* JNS 1-40 treated mice. We demonstrated that JNS 1-40 selectively targeted C377 of PPP2R1A *in vivo* in 231MFP tumors showing an isotopically light to heavy ratio of 5.7 **(Fig. 4.3.5h, Supplementary Dataset 7)**. Collectively, our data indicated that the improved covalent ligand JNS 1-40 selectively targeted C377 of PPP2R1A to activate PP2A activity and impair breast cancer cell proliferation and *in vivo* tumor growth.

4.3.3 Discussion

In conclusion, we showed once again that isoTOP-ABPP platforms can be used to identify the druggable hotspots targeted by bioactive covalently-acting natural products,

which can in-turn be pharmacologically interrogated with more synthetically tractable covalent ligands. In this study, we revealed that withaferin A targets C377 of PPP2R1A, a unique druggable hotspot within the PP2A tumor suppressor complex, to activate PP2A activity, inhibit AKT signaling, and impair breast cancer cell proliferation. Through screening a library of fragment-based covalent ligands, we identified a much simpler covalent ligand DKM 2-90 that also targeted the same site as withaferin A. We further optimized this hit to generate JNS 1-40, a lead covalent ligand with nanomolar potency that selectively targets C377 of PPP2R1A *in vitro*, *in situ*, and *in vivo* to recapitulate the effects observed with withaferin A: activating PP2A, inactivating AKT signaling, and impairing breast cancer pathogenicity.

While there are countless natural products that exhibit therapeutic activity, translating these natural products into drugs has been hindered by difficulty in synthesis and isolation of these compounds. Here, we show that isoTOP-ABPP based chemoproteomic platforms and covalent ligand discovery approaches can be coupled to discover synthetically tractable covalent ligands that target druggable hotspots targeted by more complex covalently-acting natural products, offering an alternative strategy for translating natural products into therapeutics, by developing simpler covalent ligands that hit the same druggable hotspots. In the case of PPP2R1A-targeting synthetic ligands, this has enabled use of the newly discovered covalent ligand as a PP2A activating tool compound in studies of small cell lung cancer[131]. Additionally, with the advent of new heterobifunctional therapeutic modalities, including proof-of-concept work for the recruitment of phosphatases for targeted dephosphorylation, one could imagine a use for ligands like JNS 1-40 for the recruitment of the activated PP2A complex via its interaction with C377 on PPP2R1A[34].

4.3.4 Figures

Figure 4.3.1

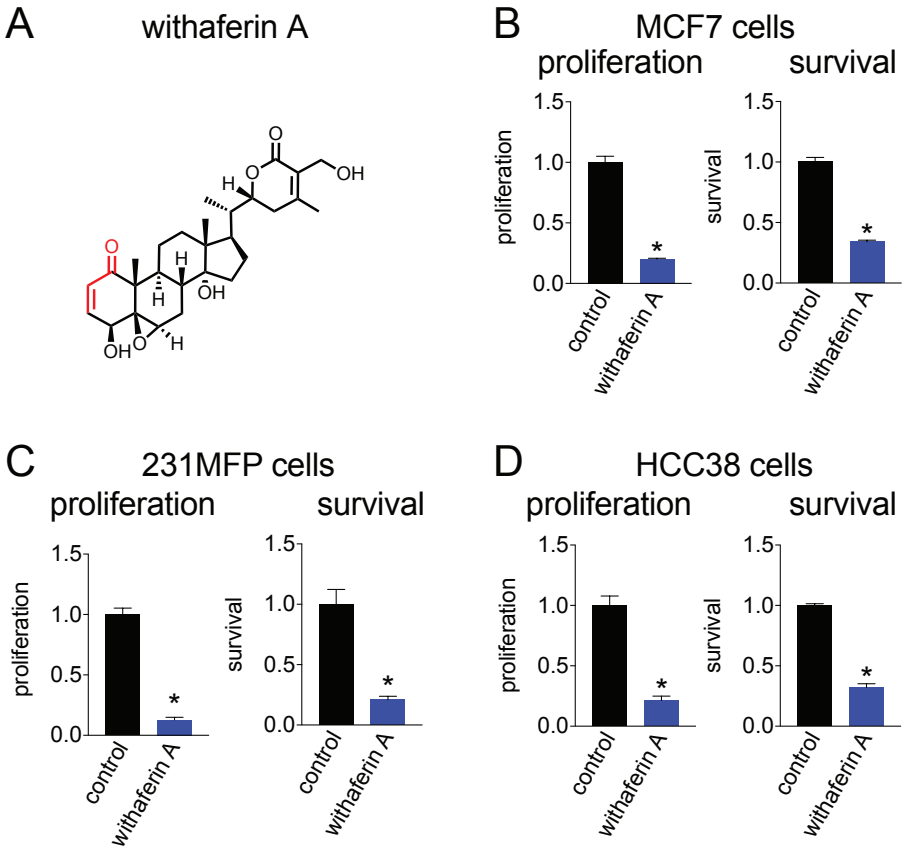

Figure 4.3.1. Withaferin A impairs breast cancer cell pathogenicity.
(A) Structure of withaferin A. Reactive Michael acceptor is indicated in red. **(B)** Withaferin A (10 μM) impairs cell proliferation and serum-free cell survival after 48 h in MCF7, 231MFP, and HCC38 cells compared to DMSO-treated controls. Data are presented as mean ± sem, n=5. Significance is shown as *p<0.05 compared to vehicle-treated controls.

Figure 4.3.2

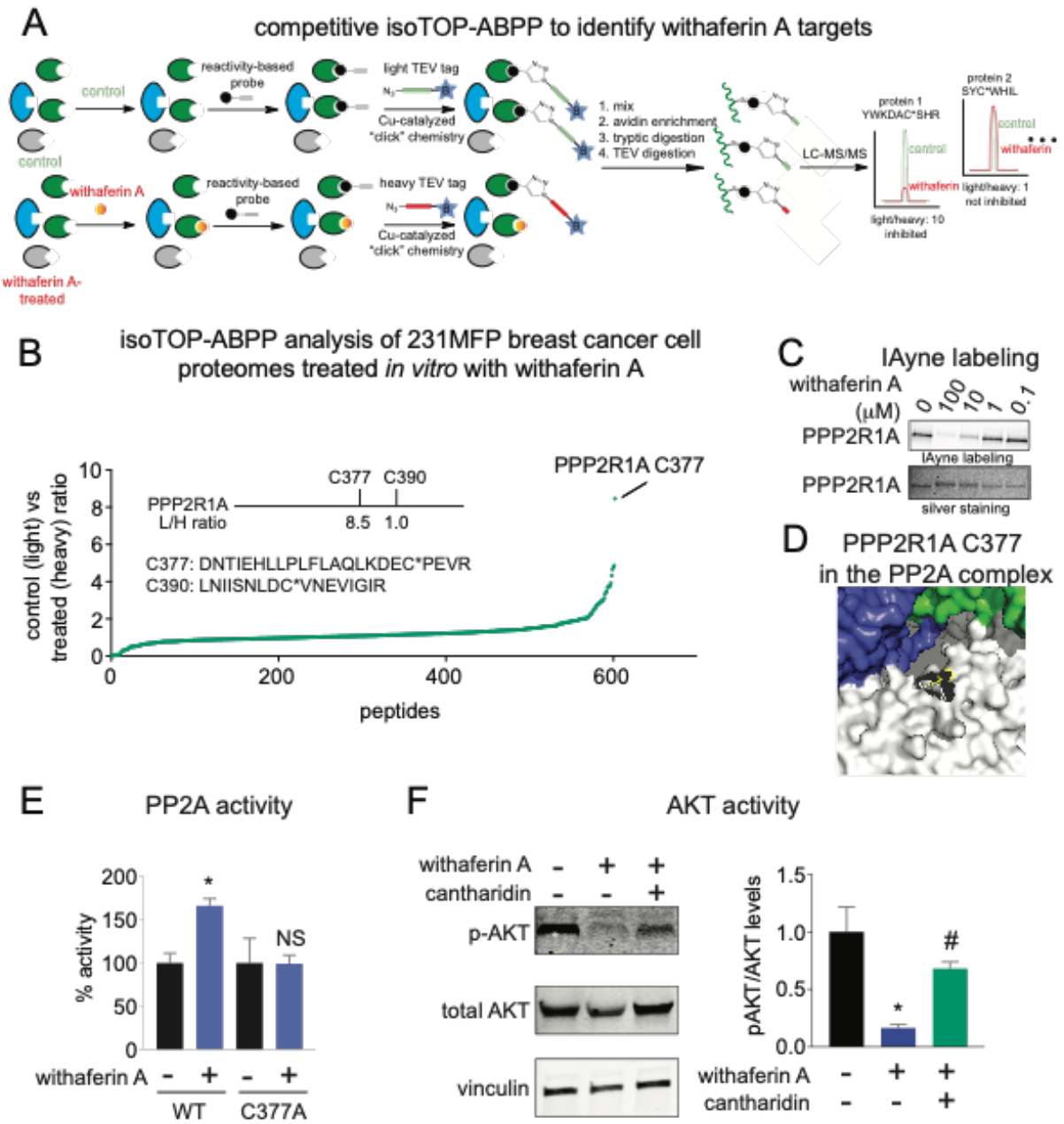

Figure 4.3.2. Using isoTOP-ABPP platforms to map proteome-wide targets of withaferin A in breast cancer cells.

(A) Competitive isoTOP-ABPP method. We mapped the cysteine-reactivity of withaferin A by pre-incubating withaferin A (10 μM) for 30 min in 231MFP breast cancer cell proteomes, prior to labeling with the cysteine-reactive iodoacetamide-alkyne (IAyne) probe (100 μM, 30 min). Probe labeled proteins were then tagged with an isotopically light (for control) or heavy (for withaferin A-treated) biotin-azide tag bearing a TEV protease

recognition site by CuAAC. Control and treated proteomes were then mixed in a 1:1 ratio, probe labeled proteins were avidin-enriched and tryptically digested, probe-labeled tryptic peptides were avidin-enriched again, and released by TEV protease and analyzed by quantitative proteomic methods and light to heavy peptide ratios were quantified. **(B)** Competitive isoTOP-ABPP analysis of withaferin A cysteine-reactivity in 231MFP breast cancer cell proteomes *in vitro*. Light to heavy ratios of ~1 indicate peptides that were labeled by IAyne, but not bound by withaferin A. We designate light to heavy ratios of >5 as targets that were bound by withaferin A. Also shown are the peptide sequences and sites of modification of probe-modified peptides identified for PPP2R1A and the light to heavy ratios of C377 and C390 on PPP2R1A. **(C)** Validation of PPP2R1A as a target of withaferin A. Withaferin A was pre-incubated with pure human PPP2R1A protein followed by IAyne. Probe-labeled proteins conjugated to rhodamine-azide by CuAAC and analyzed by SDS/PAGE and in-gel fluorescence. Shown above is fluorescence detection of IAyne labeling and shown below is silver staining of the gel showing PPP2R1A protein expression. **(D)** Crystal structure of PP2A complex showing C377 of PPP2R1A (shown in white), the catalytic subunit shown in blue, and another regulatory subunit shown in green. PDB structure used is 2IAE. **(E)** PP2A activity assay with PP2A complex proteins PPP2R1A wild-type (WT) or C377A mutant and PPP2R2A and PPP2CA subunits measuring phosphate release from a PP2A substrate phosphopeptide. This PP2A complex was treated *in vitro* with DMSO or withaferin A (10 μM) for 30 min prior to initiation of the assay. **(F)** Withaferin A (10 μM, 4 h) treatment significantly reduces phospho-AKT levels in 231MFP breast cancer cells and this reduction is rescued by cotreatment with cantharidin (10 μM, 4 h). Data in **(B)** is average ratios from n=3. Gel in **(C)** is a representative gel from n=3. Data in **(E-F)** are presented as mean ± sem, n=3. Significance expressed as *$p<0.05$ compared to vehicle-treated controls and #$p<0.05$ compared to withaferin A-treated control. NS refers to not significant compared to the vehicle-treated C377A PPP2R1A group. Raw isoTOP-ABPP proteomic data can be found in **Supplementary Dataset 7.** Withaferin A *in situ* isoTOP-ABPP analysis can be found in **Supplementary Fig. 4.3.1**. **Figure 4.3.1** is related to **Supplementary Figure 4.3.1** and **Supplementary Dataset 7**.

Figure 4.3.3

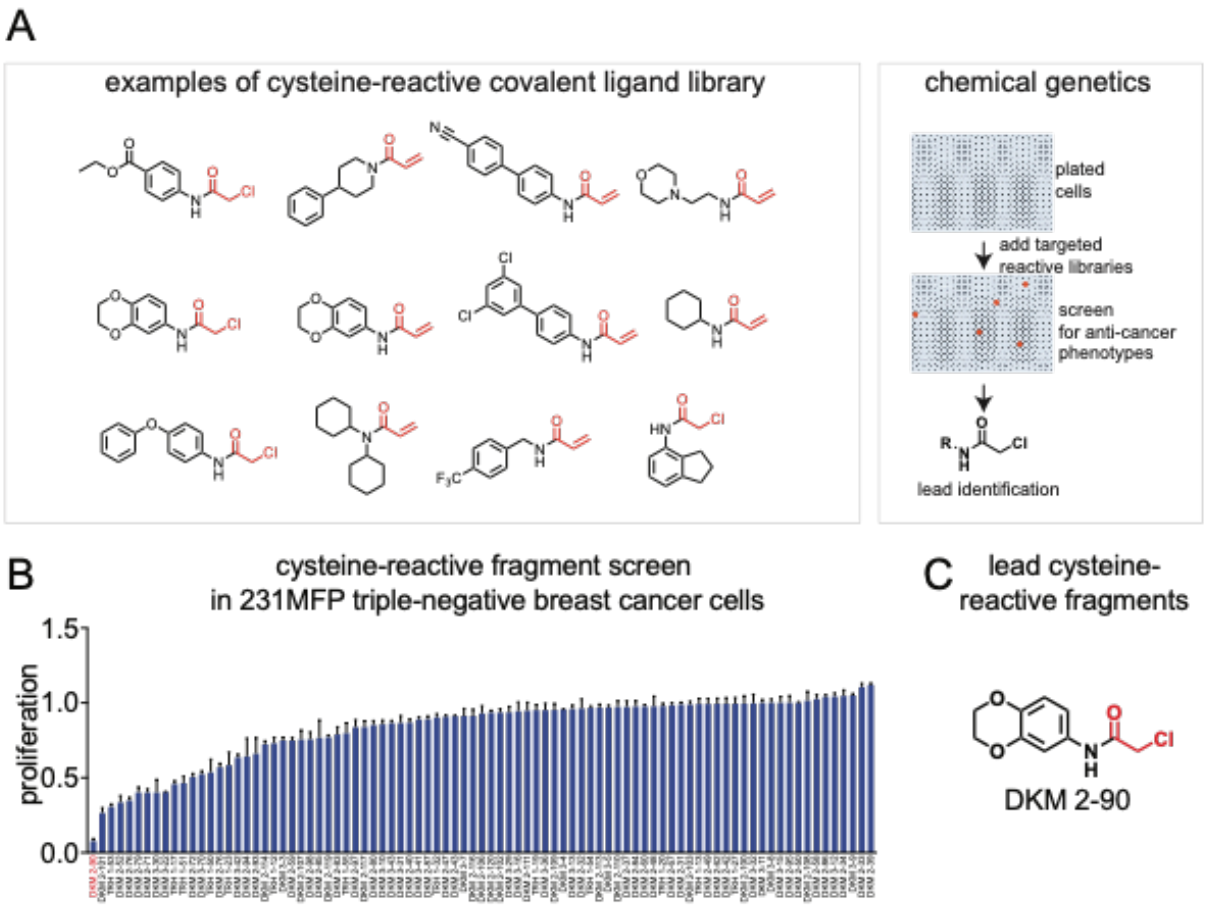

Figure 4.3.3. Screening of covalent ligand libraries in breast cancer cells.
(A) Coupled screening of a cysteine-reactive covalent ligand library in 231MFP breast cancer cells with competitive isoTOP-ABPP platforms to identify anti-cancer lead compounds, targets, and ligandable hotspots within these targets. **(B)** We screened a cysteine-reactive fragment library consisting of acrylamides and chloroacetamides in 231MFP breast cancer cells (100 μM) to identify any leads that significantly impaired 231MFP breast cancer cell proliferation. Cell viability was assessed 48 h after treatment by Hoescht staining. **(C)** Shown is the structure of the lead covalent ligand DKM 2-90. Reactive chloroacetamide warheads are designated in red. Data in **(B)** are presented as mean ± sem, n=3. Significance expressed as *p<0.05 compared to vehicle-treated controls. **Figure 4.3.3** is related to **Supplementary Table 2**.

Figure 4.3.4

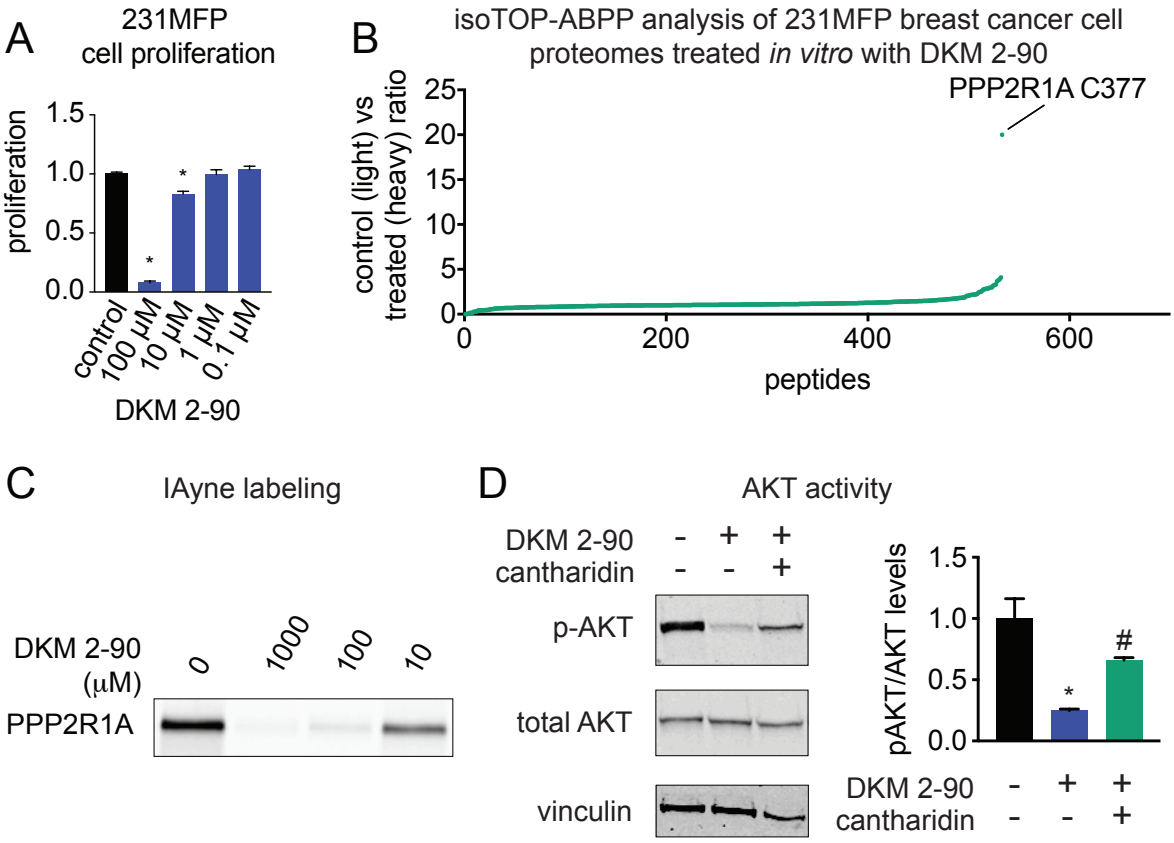

Figure 4.3.4. Target identification of DKM 2-90 using competitive isoTOP-ABPP platforms.
(A) Dose-responsive effects of DKM 2-90 on cell proliferation in 231MFP breast cancer cells. 231MFP cells were treated with DMSO or DKM 2-90 and proliferation was assessed 48 h after treatment by Hoechst staining. **(B)** IsoTOP-ABPP analysis of DKM 2-90 in 231MFP cell proteomes *in vitro*. 231MFP proteomes were pre-treated with DMSO or DKM 2-90 (100 μM) for 30 min prior to labeling proteomes with IAyne (100 μM) and subjected to the isoTOP-ABPP method. A light to heavy ratio of 1 indicates that the probe-labeled cysteine-bearing peptide was not bound by the covalent ligand, whereas a ratio >5 indicates bound sites. **(C)** Competition of DKM 2-90 against IAyne labeling of pure human PPP2R1A protein. DKM 2-90 was pre-incubated with pure PPP2R1A protein for 30 min prior to labeling with IAyne (100 μM) for 30 min. Rhodamine-azide was appended on by copper-catalyzed azide-alkyne cycloaddition and proteins were separated by SDS/PAGE and analyzed by in-gel fluorescence. **(D)** Levels of total and phosphorylated AKT (p-AKT) and vinculin as a loading control in 231MFP breast cancer cells. 231MFP cells were treated with vehicle, DKM 2-90 (100 μM), or cantharidin (10 μM) and DKM 2-90 (100 μM) for 5 h. Proteins were blotted for p-AKT, total AKT, and vinculin loading control. All data shown represents n=3-5/group. Raw data for **(B)** can be found in **Supplementary Dataset 7.** IsoTOP-ABPP analysis of DKM 2-90 *in situ* can be found in **Supplementary**

Figure 4.3.1. Figure 4.3.4 is associated with **Supplementary Figure 4.3.1** and **Supplementary Dataset 7**.

Figure 4.3.5

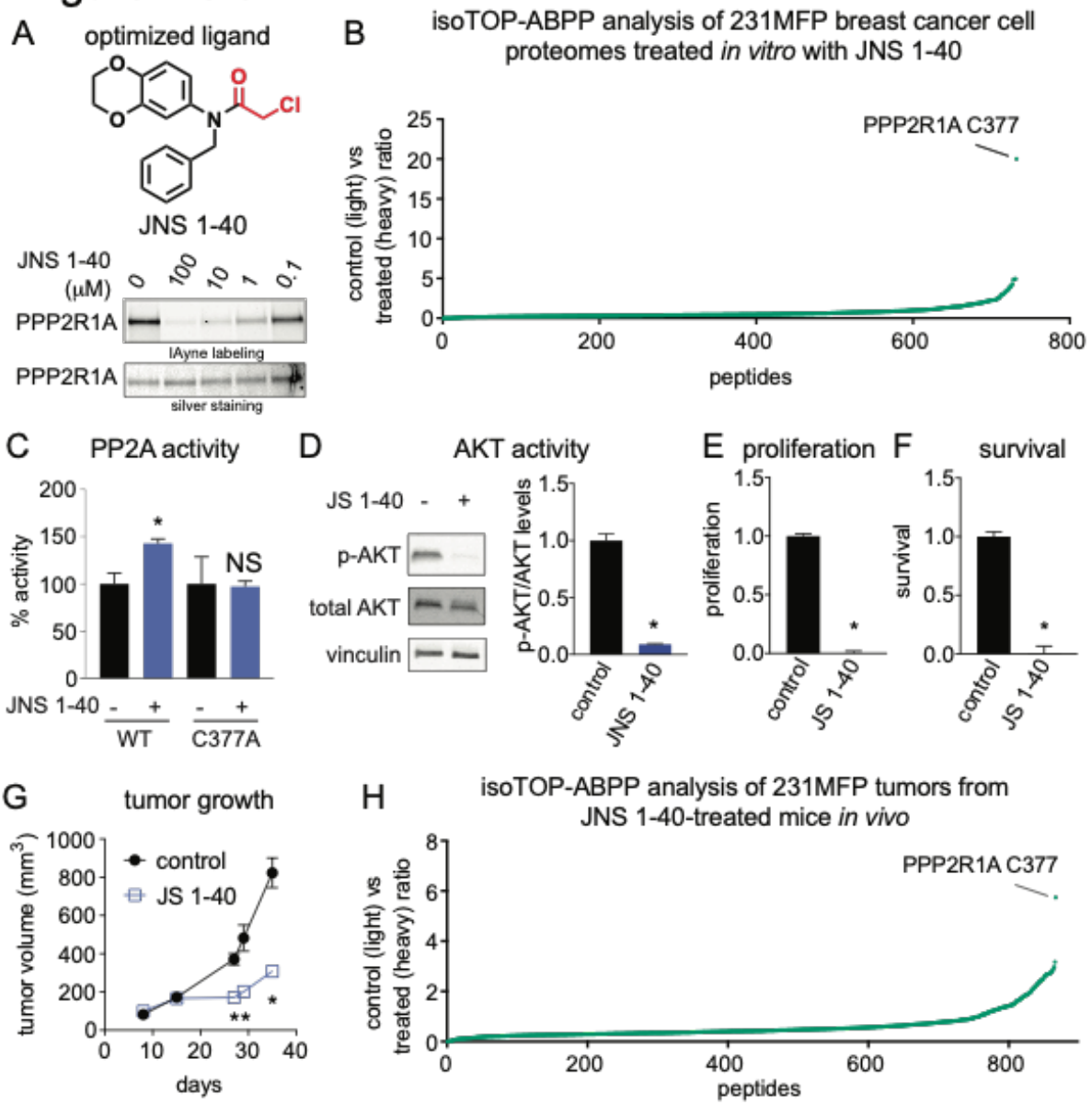

Figure 4.3.5. Optimized covalent ligand JNS 1-40 selectively targets C377 of PPP2R1A to activate PP2A activity and impair breast cancer pathogenicity.
(A) Structure of JNS 1-40 and gel-based ABPP analysis of its potency against PPP2R1A. Reactive chloroacetamide is shown in red. Pure human PPP2R1A was pre-treated with DMSO or JNS 1-40 for 30 min at 37 °C prior to IAyne labeling for 30 min at room temperature. Probe-labeled proteins were appended to rhodamine-azide by CuAAC and analyzed by SDS/PAGE and in-gel fluorescence. Shown above is fluorescence detection of IAyne labeling and shown below is silver staining of the gel showing PPP2R1A protein expression. **(B)** IsoTOP-ABPP analysis of JNS 1-40 treatment in 231MFP cells. 231MFP proteomes were treated *in vitro* with DMSO or JNS 1-40 (100 μM) for 30 min prior to IAyne labeling for 1 h and subjected to the isoTOP-ABPP method. Light to heavy ratios of probe-modified peptides are shown. **(C)** PP2A activity assay with PP2A complex proteins

PPP2R1A wild-type (WT) or C377A mutant and PPP2R2A and PPP2CA subunits measuring phosphate release from a PP2A substrate phosphopeptide. This PP2A complex was treated *in vitro* with DMSO or JNS 1-40 (100 μM) for 30 min prior to initiation of the assay. **(D)** Levels of total and phosphorylated AKT (p-AKT) and vinculin as a loading control in 231MFP breast cancer cells. 231MFP cells were treated with vehicle or JNS 1-40 (100 μM) for 75 min. **(E, F)** JS 1-40 (100 μM) impairs cell proliferation and serum-free cell survival after 48 h in 231MFP cells. **(G)** 231MFP tumor xenograft growth in immune-deficient SCID mice. 231MFP cells were subcutaneously injected into mice. Daily once per day treatment with vehicle or JNS 1-40 (50 mg/kg ip) was initiated 15 days after tumor implantation. **(H)** isoTOP-ABPP analysis of 231MFP tumor xenografts from JNS 1-40-treated mice *in vivo*. Tumors harvested from the end of the study shown in **(G)** were labeled with IAyne *ex vivo* and subjected to the isoTOP-ABPP methodology. Data in **(C-G)** are presented as mean ± sem, n=3-7/group. Data in **(B, H)** is average ratios from n=3. Significance is shown as *$p<0.05$ compared to vehicle-treated controls. NS indicates not significant ($p>0.05$) compared to the vehicle-treated C377A PPP2R1A group. Raw proteomic data can be found in **Supplementary Dataset 7**. IsoTOP-ABPP analysis of JNS 1-40 *in situ* can be found in **Supplementary Figure 4.3.2. Figure 4.3.5** is associated with **Supplementary Figure 4.3.2** and **Supplementary Dataset 7.**

4.3.5 Acknowledgement of Co-Author Contributions

E.A. Moore (neé Grossman) and C.C. Ward are co-first authors and contributed equally to the paper adapted for this chapter section; E.A. Moore (neé Grossman), C.C. Ward, J.N. Spradlin, J.I. Kleinman, and D.K. Nomura performed experiments, analyzed and interpreted data, and wrote the paper. J.N. Spradlin, L.A. Bateman, T.R. Hoffman, D.K. Myamoto synthesized compounds and chemical reagents for this study.

4.3.6 Methods

Cellular Phenotype Studies.

Cell survival and proliferation assays were performed as previously described using Hoechst 33342 dye (Invitrogen) according to manufacturer's protocol [132]. Cells were seeded into 96-well plates (40,000 for survival and 20,000 for proliferation) in a volume of 150 µl and allowed to adhere overnight. Cells were treated with an additional 50 µL of media containing 1:250 dilution of 1000x compound stock in DMSO. Medium was removed from each well and 100 µl of staining solution containing 10% formalin and Hoechst 33342 dye was added to each well and incubated for 15 min in the dark at room temperature. After incubation, staining solution was removed and wells were washed with PBS before imaging. Studies with HCC38 cells were also performed as above but were seeded with 20,000 cells for survival and 10,000 cells for proliferation.

Western Blotting.

Antibodies to vinculin, phospho-Akt (Ser473), and Akt were obtained from Cell Signaling Technology and proteomes were blotted per recommended manufacturer's' procedure. Cells were lysed in lysis buffer (containing the following: 20 mM Tris pH 7.5, 150 mM NaCl, 1 mM EDTA, 1 mM EGTA, 1% Triton X-100, 2.5 mM pyrophosphate, 50 mM NaF, 5 mM β-glycero-phosphate, 1 mM Na3VO4, 50 nM calyculin A (EMD Millipore), and protease inhibitors (Roche)). Lysate was incubated on a rotator at 4°C for 30 min, and insoluble material was removed via centrifugation at max speed for 10 min. Proteins were resolved by SDS/PAGE and transferred to nitrocellulose membranes using the iBlot system (Invitrogen). Blots were blocked with 5% nonfat milk in Tris-buffered saline containing Tween 20 (TBST) solution for 1 hour at room temperature, washed in TBST, and probed with primary antibody diluted in recommended diluent per manufacturer overnight at 4°C. Following washes with TBST, the blots were incubated in the dark with secondary antibodies purchased from Rockland and used at 1:10 000 dilution in 5% nonfat milk in TBST at room temperature. Blots were visualized using an Odyssey Li-Cor scanner after additional washes.

Purification of PPP2R1A and PPP2R2A Subunits.

Wild-type mammalian expression plasmids with C-terminal FLAG tag were purchased from Origene (PPP2R1A: RC200056; PPP2R2A, MR207137). The PPP2R1A C337A mutant was generated with Agilent QuickChange Lightning site-directed mutagenesis kit according to manufacturer's instructions. HEK293T cells (ATCC CRL-11268) were grown to 60% confluency in DMEM (Corning) supplemented with 10% FBS (Corning) and 2mM L-glutamine (Life Technologies) and maintained at 37˚C with 5% CO_2.

Immediately prior to transfection, media was replaced with DMEM + 5% FBS. Each plate was transfected with 20 µg of overexpression plasmid with 100 µg PEI (Sigma). After 48hrs cells were collected in TBS, lysed by sonication, and batch bound with anti-DYKDDDDK resin (GenScript) for 1hr. Lysate and resin was loaded onto a gravity flow column and washed, followed by elution with 250ng/uL 3xFLAG peptide (ApexBio A6001). Purity and concentration were verified by PAGE, UV/Spectroscopy, and BCA assay.

In Vitro PP2A Activity Assay.

Recombinant PPP2CA (40 nM, Origene TP301334) was combined with pulled-down WT or mutant PPP2R1A (50 nM) as well as PPP2R2A (50 nM) and incubated with 10 µM withaferin A, JS 1-40, or vehicle for 30 min at RT in TBS. Activity was assayed by addition of 60 µM Thr phosphopeptide (KRpTIRR, Millipore, 12-219) at 37º C for 25 min, and free phosphate was detected colorimetrically by malachite green kit (Cayman 10009325) per manufacturer's instructions.

PPP2R1A Knockdown Studies.

PPP2R1A was transiently knocked down with siRNA using previously described methods [133]. siRNA for a scrambled RNA oligonucleotide control and pooled RNA oligonucleotides targeting PPP2R1A were purchased from Dharmacon.

IsoTOP-ABPP.

IsoTOP-ABPP studies were done as previously reported [45,48,134]. Cells were lysed by probe sonication in PBS and protein concentrations were measured by BCA assay. Proteome samples diluted in PBS (4 mg of proteome per biological replicate) were treated with a covalently-acting small molecule or vehicle for 30 min at 37°C. Then, IAyne labeling (100 □M) was performed for 1 h at room temperature. CuAAC was used by sequential addition of tris(2-carboxyethyl)phosphine (1 mM, Sigma), tris[(1-benzyl-1H-1,2,3-triazol-4-yl)methyl]amine (34 µM, Sigma), copper (II) sulfate (1 mM, Sigma), and biotin-linker-azide, the linker functionalized with a TEV protease recognition sequence along with an isotopically light or heavy valine for treatment of control or treated proteome, respectively. After click reactions, proteomes were precipitated by centrifugation at 6500 x *g*, washed in ice-cold methanol, combined in a 1:1 control/treated ratio, washed again, then denatured and resolubilized by heating in 1.2% SDS/PBS to 80°C for 5 minutes. Insoluble components were precipitated by centrifugation at 6500 x *g* and soluble proteome was diluted in 5 ml 0.2% SDS/PBS. Labeled proteins were bound to avidin-agarose beads (170 µ¬ resuspended beads/sample, Thermo Pierce) while rotating overnight at 4°C. Bead-linked proteins were enriched by washing three times each in PBS and water, then resuspended in 6 M urea/PBS (Sigma) and reduced in TCEP (1 mM, Sigma), alkylated with iodoacetamide (18 mM, Sigma), then washed and resuspended in 2 M urea and trypsinized overnight with 0.5 µg/µL sequencing grade trypsin (Promega). Tryptic peptides were eluted off. Beads were washed three times each in PBS and water, washed in TEV buffer solution (water, TEV buffer, 100 µM dithiothreitol) and resuspended in buffer with Ac-TEV protease and incubated overnight. Peptides were diluted in water and acidified with formic acid (1.2 M, Spectrum) and prepared for analysis.

MS Analysis.

Peptides from all proteomic experiments were pressure-loaded onto a 250 μm inner diameter fused silica capillary tubing packed with 4 cm of Aqua C18 reverse-phase resin (Phenomenex # 04A-4299) which was previously equilibrated on an Agilent 600 series HPLC using gradient from 100% buffer A to 100% buffer B over 10 min, followed by a 5 min wash with 100% buffer B and a 5 min wash with 100% buffer A. The samples were then attached using a MicroTee PEEK 360 μm fitting (Thermo Fisher Scientific #p-888) to a 13 cm laser pulled column packed with 10 cm Aqua C18 reverse-phase resin and 3 cm of strong-cation exchange resin for isoTOP-ABPP studies. Samples were analyzed using an Q Exactive Plus mass spectrometer (Thermo Fisher Scientific) using a 5-step Multidimensional Protein Identification Technology (MudPIT) program, using 0 %, 25 %, 50 %, 80 %, and 100 % salt bumps of 500 mM aqueous ammonium acetate and using a gradient of 5-55 % buffer B in buffer A (buffer A: 95:5 water:acetonitrile, 0.1 % formic acid; buffer B 80:20 acetonitrile:water, 0.1 % formic acid). Data was collected in data-dependent acquisition mode with dynamic exclusion enabled (60 s). One full MS (MS1) scan (400-1800 m/z) was followed by 15 MS2 scans (ITMS) of the nth most abundant ions. Heated capillary temperature was set to 200º C and the nanospray voltage was set to 2.75 kV.

Data was extracted in the form of MS1 and MS2 files using Raw Extractor 1.9.9.2 (Scripps Research Institute) and searched against the Uniprot mouse database using ProLuCID search methodology in IP2 v.3 (Integrated Proteomics Applications, Inc) [135]. Cysteine residues were searched with a static modification for carboxyaminomethylation (+57.02146) and up to two differential modifications for methionine oxidation and either the light or heavy TEV tags (+464.28596 or +470.29977, respectively). Peptides were required to have at least one tryptic end and to contain the TEV modification. ProLUCID data was filtered through DTASelect to achieve a peptide false-positive rate below 1%. Only those probe-modified peptides that were evident in two out of three biological replicates were interpreted for their isotopic light to heavy ratios. MS1 peak shapes were confirmed to be of good quality for interpreted peptides. Targets of covalently-acting molecules are defined here as targets that showed >4 light to heavy ratios across all three biological replicates.

Gel-Based ABPP.

Gel-based ABPP methods were performed as previously described [136,137]. Recombinant pure human proteins were purchased from Origene. Pure proteins (0.2 μg) were pre-treated with DMSO or covalently-acting small molecules for 30 min at 37ºC in an incubation volume of 50 μL PBS, and were subsequently treated with IAyne (10 μM final concentration) for 30 min at room temperature. CuAAC was performed to append rhodamine-azide (1 μM final concentration) onto IAyne probe-labeled proteins. The samples were separated by SDS/PAGE and scanned using a ChemiDoc MP (Bio-Rad Laboratories, Inc). Inhibition of target labeling was assessed by densitometry using ImageJ.

General synthetic methods

Chemicals and reagents were purchased from major commercial suppliers and used without further purification. Reactions were performed under a nitrogen atmosphere

unless otherwise noted. Silica gel flash column chromatography was performed using EMD or Sigma Aldrich silica gel 60 (230-400 mesh). Proton and carbon nuclear magnetic resonance (^{1}H NMR and ^{13}C NMR) data was acquired on a Bruker AVB 400, AVQ 400, or AV 600 spectrometer at the University of California, Berkeley. High resolution mass spectrum were obtained from the QB3 mass spectrometry facility at the University of California, Berkeley using positive or negative electrospray ionization (+ESI or -ESI). Yields are reported as a single run.

General Procedure A: The amine (1 eq.) was dissolved in DCM (5 mL/mmol) and cooled to 0^{o}C. To the solution was added acryloyl chloride (1.2 eq.) followed by triethylamine (1.2 eq.). The solution was warmed to room temperature and stirred overnight. The solution was then washed with brine and the crude product was purified by silica gel chromatography (and recrystallization if necessary) to afford the corresponding acrylamide.

General Procedure B: The amine (1 eq.) was dissolved in DCM (5 mL/mmol) and cooled to 0^{o}C. To the solution was added chloroacetyl chloride (1.2 eq.) followed by triethylamine (1.2 eq.). The solution was warmed to room temperature and stirred overnight. The solution was then washed with brine and the crude product was purified by silica gel chromatography (and recrystallization if necessary) to afford the corresponding chloroacetamide.

Quantification and Statistical Analysis

Microsoft Excel and Graphpad Prism software were used for statistical analysis. Statistical and quantification details of experiments can be found in the figure legends. Significance was defined a $p<0.05$ between comparison groups.

CONCLUDING REMARKS

Collectively the work complied in this dissertation demonstrates the great promise of using chemoproteomic profiling to better understand the targets of covalently-acting natural products. Using this approach on the anti-cancer natural product nimbolide I was able to identify a unique and difficult to predict druggable site within the N-terminal intrinsically disordered region of the E3 ligase RNF114. Identifying C8 of RNF114 as a target of nimbolide, enabled mechanistic studies to understand the role of RNF114 inhibition and stabilization of its native substrates in the anti-cancer phenotypes elicited with nimbolide treatment. Furthermore, biochemical studies of the nimbolide-RNF114 interaction unveiled the function of this site in the recognition of tumor suppressing substrates of RNF114, including the tumor suppressors p21 and p27. This discovery in turn catalyzed the development of nimbolide-based bifunctional degrader molecules (PROTACs), which successfully demonstrated the ability of this natural product to recruit RNF114 to non-native substrates to induce their ubiquitination and proteasomal degradation. Our work further demonstrated the utility of having RNF114 recruiters in the TPD toolbox, as RNF114-recruting degraders displayed unique degradation selectivity of the oncogenic BCR-ABL fusion protein as compared to other E3 recruiters.

One powerful advantage of using chemoproteomic methods to identify covalent targets of natural products is that after identifying these reactive hotspots covalent fragment libraries can be screened for ability to target these same sites. This allows for unbiased identification on synthetically accessible and scalable ligands of the identified sites, even when structural information is not available for the protein target. This was a useful approach to identify EN219 as a lead candidate capable of binding C8 on RNF114, which falls within an intrinsically disordered region of the protein preventing structure-guided ligand discovery effort. As this ligand was found to mimic nimbolide's ability to covalently modify C8 of RNF114 and recruit RNF114 for TPD when incorporated into bifunctional degrader molecules, this will greatly enable future efforts to use RNF114 in PROTACs. In an additional example of this approach to translating the functions of natural products into synthetic mimics, I report a successful screen identifying JNS 1-40 as a simple covalent scaffold to recapitulate withaferin A's ability to bind C377 of PPP2R1A. After identifying this ligandable site through chemoproteomic mapping of withaferin A, we showed that synthetic ligands could also bind this site to activate PP2A phosphatase activity and inhibit tumor growth *in vivo* with engagement of this site. Again discovery of this simple ligand greatly enables future studies of PP2A activation and allows for opportunities to incorporate PPP2R1A ligands into future bifunctional therapies without the synthetic limitation imposed by the natural product.

Chemoproteomic methods have rapidly advanced over the last two decades, showing promise to fill the unmet need for rapid and versatile strategies to go after diverse classes of traditionally undruggable therapeutic targets. This approach allows for rapid identification of unique druggable sites targeted by targeted by covalently-acting natural products, facilitating study of their biological effects and enabling discovery of simple synthetic ligands. As emphasis in modern drug discovery shifts from inhibitor development towards multivalent, induced-proximity therapies, such as targeted protein degradation, there is need to discover ligandable sites on effector proteins as well as on therapeutic targets. The utility of chemoproteomics towards this end has been

demonstrated in this work through the discovery of covalent recruiters of the E3 ligase RNF114 for the advancement of targeted protein. With the discovery of a wider variety of chemoproteomic probes and the advancement of mass spectrometry methods, the depth and breadth of chemoproteomic profiling continues to grow. Employing chemoproteomic methods to ligandable site discovery will make the challenge of undruggable targets a thing of the past.

REFERENCES

1. Bailey, M. H. *et al.* Comprehensive Characterization of Cancer Driver Genes and Mutations. *Cell* **173**, 371-385.e18 (2018).
2. Swinney, D. C. & Anthony, J. How were new medicines discovered? *Nat. Rev. Drug Discov.* **10**, 507–519 (2011).
3. Ferreira, L., dos Santos, R., Oliva, G. & Andricopulo, A. Molecular Docking and Structure-Based Drug Design Strategies. *Molecules* **20**, 13384–13421 (2015).
4. Hopkins, A. L. & Groom, C. R. The druggable genome. *Nat. Rev. Drug Discov.* **1**, 727–730 (2002).
5. Makley, L. N. & Gestwicki, J. E. Expanding the Number of 'Druggable' Targets: Non-Enzymes and Protein-Protein Interactions: **Expanding the Number of 'Druggable' Targets**. *Chem. Biol. Drug Des.* **81**, 22–32 (2013).
6. Dang, C. V., Reddy, E. P., Shokat, K. M. & Soucek, L. Drugging the 'undruggable' cancer targets. *Nat. Rev. Cancer* **17**, 502–508 (2017).
7. Kessler, D. *et al.* Drugging an undruggable pocket on KRAS. *Proc. Natl. Acad. Sci.* **116**, 15823–15829 (2019).
8. Ostrem, J. M., Peters, U., Sos, M. L., Wells, J. A. & Shokat, K. M. K-Ras(G12C) inhibitors allosterically control GTP affinity and effector interactions. *Nature* **503**, 548–551 (2013).
9. Gehringer, M. & Laufer, S. A. Emerging and Re-Emerging Warheads for Targeted Covalent Inhibitors: Applications in Medicinal Chemistry and Chemical Biology. *J. Med. Chem.* **62**, 5673–5724 (2019).

10. Deshaies, R. J. Multispecific drugs herald a new era of biopharmaceutical innovation. *Nature* **580**, 329–338 (2020).
11. Nalawansha, D. A. & Crews, C. M. PROTACs: An Emerging Therapeutic Modality in Precision Medicine. *Cell Chem. Biol.* **27**, 998–1014 (2020).
12. Sutanto, F., Konstantinidou, M. & Dömling, A. Covalent inhibitors: a rational approach to drug discovery. *RSC Med. Chem.* **11**, 876–884 (2020).
13. Evans, M. J. & Cravatt, B. F. Mechanism-Based Profiling of Enzyme Families. *Chem. Rev.* **106**, 3279–3301 (2006).
14. Speers, A. E. & Cravatt, B. F. Activity-Based Protein Profiling (ABPP) and Click Chemistry (CC)–ABPP by MudPIT Mass Spectrometry. *Curr. Protoc. Chem. Biol.* **1**, 29–41 (2009).
15. Roberts, A. M., Ward, C. C. & Nomura, D. K. Activity-based protein profiling for mapping and pharmacologically interrogating proteome-wide ligandable hotspots. *Curr. Opin. Biotechnol.* **43**, 25–33 (2017).
16. Speers, A. E. & Cravatt, B. F. A Tandem Orthogonal Proteolysis Strategy for High-Content Chemical Proteomics. *J. Am. Chem. Soc.* **127**, 10018–10019 (2005).
17. Liu, Y., Patricelli, M. P. & Cravatt, B. F. Activity-based protein profiling: The serine hydrolases. *Proc. Natl. Acad. Sci.* **96**, 14694–14699 (1999).
18. Weerapana, E. *et al.* Quantitative reactivity profiling predicts functional cysteines in proteomes. *Nature* **468**, 790–795 (2010).
19. Maurais, A. J. & Weerapana, E. Reactive-cysteine profiling for drug discovery. *Curr. Opin. Chem. Biol.* **50**, 29–36 (2019).

20. Backus, K. M. *et al.* Proteome-wide covalent ligand discovery in native biological systems. *Nature* **534**, 570–574 (2016).
21. Vinogradova, E. V. *et al.* An Activity-Guided Map of Electrophile-Cysteine Interactions in Primary Human T Cells. *Cell* **182**, 1009-1026.e29 (2020).
22. Chung, C. Y.-S. *et al.* Covalent targeting of the vacuolar H+-ATPase activates autophagy via mTORC1 inhibition. *Nat. Chem. Biol.* **15**, 776–785 (2019).
23. Boike, L. *et al.* Discovery of a Functional Covalent Ligand Targeting an Intrinsically Disordered Cysteine within MYC. *Cell Chem. Biol.* S2451945620303421 (2020) doi:10.1016/j.chembiol.2020.09.001.
24. Spradlin, J. N. *et al.* Harnessing the anti-cancer natural product nimbolide for targeted protein degradation. *Nat. Chem. Biol.* **15**, 747–755 (2019).
25. Tong, B. *et al.* A Nimbolide-Based Kinase Degrader Preferentially Degrades Oncogenic BCR-ABL. *ACS Chem. Biol.* **15**, 1788–1794 (2020).
26. Grossman, E. A. *et al.* Covalent Ligand Discovery against Druggable Hotspots Targeted by Anti-cancer Natural Products. *Cell Chem. Biol.* **24**, 1368-1376.e4 (2017).
27. Luo, M. *et al. Chemoproteomics-Enabled Ligand Screening Yields Covalent RNF114-Based Degraders that Mimic Natural Product Function*. http://biorxiv.org/lookup/doi/10.1101/2020.07.12.198150 (2020) doi:10.1101/2020.07.12.198150.
28. Huang, H.-T. *et al.* A Chemoproteomic Approach to Query the Degradable Kinome Using a Multi-kinase Degrader. *Cell Chem. Biol.* **25**, 88-99.e6 (2018).

29. Lai, A. C. *et al.* Modular PROTAC Design for the Degradation of Oncogenic BCR-ABL. *Angew. Chem. Int. Ed.* **55**, 807–810 (2016).

30. Zeng, M. *et al.* Exploring Targeted Degradation Strategy for Oncogenic KRASG12C. *Cell Chem. Biol.* **27**, 19-31.e6 (2020).

31. Bond, M. J., Chu, L., Nalawansha, D. A., Li, K. & Crews, C. M. Targeted Degradation of Oncogenic KRAS ^{G12C} by VHL-Recruiting PROTACs. *ACS Cent. Sci.* acscentsci.0c00411 (2020) doi:10.1021/acscentsci.0c00411.

32. Weng, G. *et al.* PROTAC-DB: an online database of PROTACs. *Nucleic Acids Res.* gkaa807 (2020) doi:10.1093/nar/gkaa807.

33. Banik, S. M. *et al.* Lysosome-targeting chimaeras for degradation of extracellular proteins. *Nature* **584**, 291–297 (2020).

34. Yamazoe, S. *et al.* Heterobifunctional Molecules Induce Dephosphorylation of Kinases–A Proof of Concept Study. *J. Med. Chem.* **63**, 2807–2813 (2020).

35. Costales, M. G. *et al.* Small-molecule targeted recruitment of a nuclease to cleave an oncogenic RNA in a mouse model of metastatic cancer. *Proc. Natl. Acad. Sci.* **117**, 2406–2411 (2020).

36. Nomura, D. K. & Maimone, T. J. Target Identification of Bioactive Covalently Acting Natural Products. *Curr. Top. Microbiol. Immunol.* (2018) doi:10.1007/82_2018_121.

37. Drahl, C., Cravatt, B. F. & Sorensen, E. J. Protein-reactive natural products. *Angew. Chem. Int. Ed Engl.* **44**, 5788–5809 (2005).

38. Liu, J. *et al.* Calcineurin is a common target of cyclophilin-cyclosporin A and FKBP-FK506 complexes. *Cell* **66**, 807–815 (1991).

39. Cohen, E., Quistad, G. B. & Casida, J. E. Cytotoxicity of nimbolide, epoxyazadiradione and other limonoids from neem insecticide. *Life Sci.* **58**, 1075–1081 (1996).

40. Bodduluru, L. N., Kasala, E. R., Thota, N., Barua, C. C. & Sistla, R. Chemopreventive and therapeutic effects of nimbolide in cancer: the underlying mechanisms. *Toxicol. Vitro Int. J. Publ. Assoc. BIBRA* **28**, 1026–1035 (2014).

41. Subramani, R. *et al.* Nimbolide inhibits pancreatic cancer growth and metastasis through ROS-mediated apoptosis and inhibition of epithelial-to-mesenchymal transition. *Sci. Rep.* **6**, 19819 (2016).

42. Hao, F., Kumar, S., Yadav, N. & Chandra, D. Neem components as potential agents for cancer prevention and treatment. *Biochim. Biophys. Acta* **1846**, 247–257 (2014).

43. Gupta, S. C., Prasad, S., Tyagi, A. K., Kunnumakkara, A. B. & Aggarwal, B. B. Neem (Azadirachta indica): An indian traditional panacea with modern molecular basis. *Phytomedicine Int. J. Phytother. Phytopharm.* **34**, 14–20 (2017).

44. Bianchini, G., Balko, J. M., Mayer, I. A., Sanders, M. E. & Gianni, L. Triple-negative breast cancer: challenges and opportunities of a heterogeneous disease. *Nat. Rev. Clin. Oncol.* **13**, 674–690 (2016).

45. Weerapana, E. *et al.* Quantitative reactivity profiling predicts functional cysteines in proteomes. *Nature* **468**, 790–795 (2010).

46. Roberts, A. M., Ward, C. C. & Nomura, D. K. Activity-based protein profiling for mapping and pharmacologically interrogating proteome-wide ligandable hotspots. *Curr. Opin. Biotechnol.* **43**, 25–33 (2017).

47. Grossman, E. A. *et al.* Covalent Ligand Discovery against Druggable Hotspots Targeted by Anti-cancer Natural Products. *Cell Chem. Biol.* **24**, 1368-1376.e4 (2017).

48. Backus, K. M. *et al.* Proteome-wide covalent ligand discovery in native biological systems. *Nature* **534**, 570–574 (2016).

49. Wang, C., Weerapana, E., Blewett, M. M. & Cravatt, B. F. A chemoproteomic platform to quantitatively map targets of lipid-derived electrophiles. *Nat. Methods* **11**, 79–85 (2014).

50. Han, J. *et al.* ZNF313 is a novel cell cycle activator with an E3 ligase activity inhibiting cellular senescence by destabilizing p21(WAF1.). *Cell Death Differ.* **20**, 1055–1067 (2013).

51. Lee, M.-G. *et al.* XAF1 directs apoptotic switch of p53 signaling through activation of HIPK2 and ZNF313. *Proc. Natl. Acad. Sci. U. S. A.* **111**, 15532–15537 (2014).

52. Huang, S. *et al.* The UbL-UBA Ubiquilin4 protein functions as a tumor suppressor in gastric cancer by p53-dependent and p53-independent regulation of p21. *Cell Death Differ.* (2018) doi:10.1038/s41418-018-0141-4.

53. Abbas, T. & Dutta, A. p21 in cancer: intricate networks and multiple activities. *Nat. Rev. Cancer* **9**, 400–414 (2009).

54. Guo, H., Tian, T., Nan, K. & Wang, W. p57: A multifunctional protein in cancer (Review). *Int. J. Oncol.* **36**, 1321–1329 (2010).

55. Havens, C. G. & Walter, J. C. Mechanism of CRL4(Cdt2), a PCNA-dependent E3 ubiquitin ligase. *Genes Dev.* **25**, 1568–1582 (2011).

56. Kitagawa, K., Kotake, Y. & Kitagawa, M. Ubiquitin-mediated control of oncogene and tumor suppressor gene products. *Cancer Sci.* **100**, 1374–1381 (2009).

57. Biswas, K. *et al.* The E3 Ligase CHIP Mediates p21 Degradation to Maintain Radioresistance. *Mol. Cancer Res. MCR* **15**, 651–659 (2017).

58. Rodriguez, M. S. *et al.* The RING ubiquitin E3 RNF114 interacts with A20 and modulates NF-κB activity and T-cell activation. *Cell Death Dis.* **5**, e1399 (2014).

59. Yang, Y. *et al.* The E3 ubiquitin ligase RNF114 and TAB1 degradation are required for maternal-to-zygotic transition. *EMBO Rep.* **18**, 205–216 (2017).

60. Jessani, N. *et al.* Carcinoma and stromal enzyme activity profiles associated with breast tumor growth in vivo. *Proc. Natl. Acad. Sci. U. S. A.* **101**, 13756–13761 (2004).

61. Anderson, K. E., To, M., Olzmann, J. A. & Nomura, D. K. Chemoproteomics-Enabled Covalent Ligand Screening Reveals a Thioredoxin-Caspase 3 Interaction Disruptor That Impairs Breast Cancer Pathogenicity. *ACS Chem. Biol.* **12**, 2522–2528 (2017).

62. Smith, P. K. *et al.* Measurement of protein using bicinchoninic acid. *Anal. Biochem.* **150**, 76–85 (1985).

63. Xu, T. *et al.* ProLuCID: An improved SEQUEST-like algorithm with enhanced sensitivity and specificity. *J. Proteomics* **129**, 16–24 (2015).

64. Roberts, A. M. *et al.* Chemoproteomic Screening of Covalent Ligands Reveals UBA5 As a Novel Pancreatic Cancer Target. *ACS Chem. Biol.* **12**, 899–904 (2017).

65. Counihan, J. L., Wiggenhorn, A. L., Anderson, K. E. & Nomura, D. K. Chemoproteomics-Enabled Covalent Ligand Screening Reveals ALDH3A1 as a Lung Cancer Therapy Target. *ACS Chem. Biol.* (2018) doi:10.1021/acschembio.8b00381.

66. Bateman, L. A. *et al.* Chemoproteomics-enabled covalent ligand screen reveals a cysteine hotspot in reticulon 4 that impairs ER morphology and cancer pathogenicity. *Chem. Commun. Camb. Engl.* **53**, 7234–7237 (2017).

67. Kokosza, K., Balzarini, J. & Piotrowska, D. G. Novel 5-Arylcarbamoyl-2-methylisoxazolidin-3-yl-3-phosphonates as Nucleotide Analogues. *Nucleosides Nucleotides Nucleic Acids* **33**, 552–582 (2014).

68. Talaty, E. R., Young, S. M., Dain, R. P. & Stipdonk, M. J. V. A study of fragmentation of protonated amides of some acylated amino acids by tandem mass spectrometry: observation of an unusual nitrilium ion. *Rapid Commun. Mass Spectrom.* **25**, 1119–1129 (2011).

69. Timokhin, V. I., Gastaldi, S., Bertrand, M. P. & Chatgilialoglu, C. Rate Constants for the β-Elimination of Tosyl Radical from a Variety of Substituted Carbon-Centered Radicals. *J. Org. Chem.* **68**, 3532–3537 (2003).

70. Cee, V. J. *et al.* Systematic Study of the Glutathione (GSH) Reactivity of N-Arylacrylamides: 1. Effects of Aryl Substitution. *J. Med. Chem.* **58**, 9171–9178 (2015).

71. Le Sann, C., Huddleston, J. & Mann, J. Synthesis and preliminary evaluation of novel analogues of quindolines as potential stabilisers of telomeric G-quadruplex DNA. *Tetrahedron* **63**, 12903–12911 (2007).

72. Ikoma, M., Oikawa, M. & Sasaki, M. Synthesis and domino metathesis of functionalized 7-oxanorbornene analogs toward cis-fused heterocycles. *Tetrahedron* **64**, 2740–2749 (2008).

73. Cho, S.-D. *et al.* A One-Pot Synthesis of Pyrido[2,3-b][1,4]oxazin-2-ones. *J. Org. Chem.* **68**, 7918–7920 (2003).

74. Magolan, J., Carson, C. A. & Kerr, M. A. Total Synthesis of (±)-Mersicarpine. *Org. Lett.* **10**, 1437–1440 (2008).

75. Longo, P. A., Kavran, J. M., Kim, M.-S. & Leahy, D. J. Transient mammalian cell transfection with polyethylenimine (PEI). *Methods Enzymol.* **529**, 227–240 (2013).

76. Li, C. *et al.* FastCloning: a highly simplified, purification-free, sequence- and ligation-independent PCR cloning method. *BMC Biotechnol.* **11**, 92 (2011).

77. Thomas, J. R. *et al.* A Photoaffinity Labeling-Based Chemoproteomics Strategy for Unbiased Target Deconvolution of Small Molecule Drug Candidates. *Methods Mol. Biol. Clifton NJ* **1647**, 1–18 (2017).

78. Käll, L., Canterbury, J. D., Weston, J., Noble, W. S. & MacCoss, M. J. Semi-supervised learning for peptide identification from shotgun proteomics datasets. *Nat. Methods* **4**, 923–925 (2007).

79. Spradlin, J. N. *et al.* Harnessing the anti-cancer natural product nimbolide for targeted protein degradation. *Nat. Chem. Biol.* **15**, 747–755 (2019).

80. Lai, A. C. & Crews, C. M. Induced protein degradation: an emerging drug discovery paradigm. *Nat. Rev. Drug Discov.* **16**, 101–114 (2017).

81. Burslem, G. M. & Crews, C. M. Small-Molecule Modulation of Protein Homeostasis. *Chem. Rev.* **117**, 11269–11301 (2017).

82. Mullard, A. First targeted protein degrader hits the clinic. *Nat. Rev. Drug Discov.* **18**, 237–239 (2019).

83. Winter, G. E. *et al.* DRUG DEVELOPMENT. Phthalimide conjugation as a strategy for in vivo target protein degradation. *Science* **348**, 1376–1381 (2015).

84. Zengerle, M., Chan, K.-H. & Ciulli, A. Selective Small Molecule Induced Degradation of the BET Bromodomain Protein BRD4. *ACS Chem. Biol.* **10**, 1770–1777 (2015).

85. Bondeson, D. P. *et al.* Catalytic in vivo protein knockdown by small-molecule PROTACs. *Nat. Chem. Biol.* **11**, 611–617 (2015).

86. Buckley, D. L. *et al.* Targeting the von Hippel-Lindau E3 ubiquitin ligase using small molecules to disrupt the VHL/HIF-1α interaction. *J. Am. Chem. Soc.* **134**, 4465–4468 (2012).

87. Hines, J., Lartigue, S., Dong, H., Qian, Y. & Crews, C. M. MDM2-Recruiting PROTAC Offers Superior, Synergistic Antiproliferative Activity via Simultaneous Degradation of BRD4 and Stabilization of p53. *Cancer Res.* **79**, 251–262 (2019).

88. Okuhira, K. *et al.* Development of hybrid small molecules that induce degradation of estrogen receptor-alpha and necrotic cell death in breast cancer cells. *Cancer Sci.* **104**, 1492–1498 (2013).

89. Zeng, M. *et al.* Exploring Targeted Degradation Strategy for Oncogenic KRASG12C. *Cell Chem. Biol.* **27**, 19-31.e6 (2020).

90. Ottis, P. *et al.* Cellular Resistance Mechanisms to Targeted Protein Degradation Converge Toward Impairment of the Engaged Ubiquitin Transfer Pathway. *ACS Chem. Biol.* **14**, 2215–2223 (2019).

91. Zhang, X., Crowley, V. M., Wucherpfennig, T. G., Dix, M. M. & Cravatt, B. F. Electrophilic PROTACs that degrade nuclear proteins by engaging DCAF16. *Nat. Chem. Biol.* **15**, 737–746 (2019).

92. Ward, C. C. *et al.* Covalent Ligand Screening Uncovers a RNF4 E3 Ligase Recruiter for Targeted Protein Degradation Applications. *ACS Chem. Biol.* **14**, 2430–2440 (2019).

93. Hantschel, O. & Superti-Furga, G. Regulation of the c-Abl and Bcr-Abl tyrosine kinases. *Nat. Rev. Mol. Cell Biol.* **5**, 33–44 (2004).

94. Burslem, G. M. *et al.* Targeting BCR-ABL1 in Chronic Myeloid Leukemia by PROTAC-Mediated Targeted Protein Degradation. *Cancer Res.* **79**, 4744–4753 (2019).

95. Lai, A. C. *et al.* Modular PROTAC Design for the Degradation of Oncogenic BCR-ABL. *Angew. Chem. Int. Ed Engl.* **55**, 807–810 (2016).

96. Demizu, Y. *et al.* Development of BCR-ABL degradation inducers via the conjugation of an imatinib derivative and a cIAP1 ligand. *Bioorg. Med. Chem. Lett.* **26**, 4865–4869 (2016).

97. Shibata, N. *et al.* Development of protein degradation inducers of oncogenic BCR-ABL protein by conjugation of ABL kinase inhibitors and IAP ligands. *Cancer Sci.* **108**, 1657–1666 (2017).

98. Shibata, N., Ohoka, N., Hattori, T. & Naito, M. Development of a Potent Protein Degrader against Oncogenic BCR-ABL Protein. *Chem. Pharm. Bull. (Tokyo)* **67**, 165–172 (2019).

99. Shimokawa, K. *et al.* Targeting the Allosteric Site of Oncoprotein BCR-ABL as an Alternative Strategy for Effective Target Protein Degradation. *ACS Med. Chem. Lett.* **8**, 1042–1047 (2017).

100. Zhao, Q. *et al.* Discovery of SIAIS178 as an Effective BCR-ABL Degrader by Recruiting Von Hippel-Lindau (VHL) E3 Ubiquitin Ligase. *J. Med. Chem.* **62**, 9281–9298 (2019).

101. Zengerle, M., Chan, K.-H. & Ciulli, A. Selective Small Molecule Induced Degradation of the BET Bromodomain Protein BRD4. *ACS Chem. Biol.* **10**, 1770–1777 (2015).

102. Zhu, H.-Q. & Gao, F.-H. Regulatory Molecules and Corresponding Processes of BCR-ABL Protein Degradation. *J. Cancer* **10**, 2488–2500 (2019).

103. Bondeson, D. P. *et al.* Lessons in PROTAC Design from Selective Degradation with a Promiscuous Warhead. *Cell Chem. Biol.* **25**, 78-87.e5 (2018).

104. Brand, M. *et al.* Homolog-Selective Degradation as a Strategy to Probe the Function of CDK6 in AML. *Cell Chem. Biol.* **26**, 300-306.e9 (2019).

105. Cromm, P. M., Samarasinghe, K. T. G., Hines, J. & Crews, C. M. Addressing Kinase-Independent Functions of Fak via PROTAC-Mediated Degradation. *J. Am. Chem. Soc.* **140**, 17019–17026 (2018).

106. Huang, H.-T. *et al.* A Chemoproteomic Approach to Query the Degradable Kinome Using a Multi-kinase Degrader. *Cell Chem. Biol.* **25**, 88-99.e6 (2018).

107. Jaime-Figueroa, S., Buhimschi, A. D., Toure, M., Hines, J. & Crews, C. M. Design, synthesis and biological evaluation of Proteolysis Targeting Chimeras (PROTACs) as a BTK degraders with improved pharmacokinetic properties. *Bioorg. Med. Chem. Lett.* **30**, 126877 (2020).

108. Li, Z. *et al.* Development and Characterization of a Wee1 Kinase Degrader. *Cell Chem. Biol.* **27**, 57-65.e9 (2020).

109. Olson, C. M. *et al.* Pharmacological perturbation of CDK9 using selective CDK9 inhibition or degradation. *Nat. Chem. Biol.* **14**, 163–170 (2018).

110. Powell, C. E. *et al.* Chemically Induced Degradation of Anaplastic Lymphoma Kinase (ALK). *J. Med. Chem.* **61**, 4249–4255 (2018).

111. Tovell, H. *et al.* Design and Characterization of SGK3-PROTAC1, an Isoform Specific SGK3 Kinase PROTAC Degrader. *ACS Chem. Biol.* **14**, 2024–2034 (2019).

112. You, I. *et al.* Discovery of an AKT Degrader with Prolonged Inhibition of Downstream Signaling. *Cell Chem. Biol.* **27**, 66-73.e7 (2020).

113. Rape, M. Ubiquitylation at the crossroads of development and disease. *Nat. Rev. Mol. Cell Biol.* **19**, 59–70 (2018).

114. Gadd, M. S. *et al.* Structural basis of PROTAC cooperative recognition for selective protein degradation. *Nat. Chem. Biol.* **13**, 514–521 (2017).

115. Nowak, R. P. *et al.* Plasticity in binding confers selectivity in ligand-induced protein degradation. *Nat. Chem. Biol.* (2018) doi:10.1038/s41589-018-0055-y.

116. Hughes, S. J. & Ciulli, A. Molecular recognition of ternary complexes: a new dimension in the structure-guided design of chemical degraders. *Essays Biochem.* **61**, 505–516 (2017).

117. Newman, D. J. & Cragg, G. M. Natural Products as Sources of New Drugs from 1981 to 2014. *J. Nat. Prod.* **79**, 629–661 (2016).

118. Bond, M. J., Chu, L., Nalawansha, D. A., Li, K. & Crews, C. Targeted Degradation of Oncogenic KRASG12C by VHL-recruiting PROTACs. (2020) doi:10.26434/chemrxiv.12091176.v1.

119. Huang, H.-T. *et al.* A Chemoproteomic Approach to Query the Degradable Kinome Using a Multi-kinase Degrader. *Cell Chem. Biol.* **25**, 88-99.e6 (2018).

120. Bondeson, D. P. *et al.* Lessons in PROTAC Design from Selective Degradation with a Promiscuous Warhead. *Cell Chem. Biol.* **25**, 78-87.e5 (2018).

121. Tong, B. *et al.* A Nimbolide-Based Kinase Degrader Preferentially Degrades Oncogenic BCR-ABL. *bioRxiv* 2020.04.02.022541 (2020) doi:10.1101/2020.04.02.022541.

122. Ward, C. C. *et al.* Covalent Ligand Screening Uncovers a RNF4 E3 Ligase Recruiter for Targeted Protein Degradation Applications. *ACS Chem. Biol.* **14**, 2430–2440 (2019).

123. Bachovchin, D. A. *et al.* Superfamily-wide portrait of serine hydrolase inhibition achieved by library-versus-library screening. *Proc. Natl. Acad. Sci. U. S. A.* **107**, 20941–20946 (2010).

124. Burslem, G. M. *et al.* Targeting BCR-ABL1 in Chronic Myeloid Leukemia by PROTAC-Mediated Targeted Protein Degradation. *Cancer Res.* **79**, 4744–4753 (2019).

125. Lai, A. C. *et al.* Modular PROTAC Design for the Degradation of Oncogenic BCR-ABL. *Angew. Chem. Int. Ed Engl.* **55**, 807–810 (2016).

126. Nomura, D. K. & Maimone, T. J. Target Identification of Bioactive Covalently Acting Natural Products. *Curr. Top. Microbiol. Immunol.* **420**, 351–374 (2019).

127. Thomas, J. R. *et al.* A Photoaffinity Labeling-Based Chemoproteomics Strategy for Unbiased Target Deconvolution of Small Molecule Drug Candidates. *Methods Mol. Biol. Clifton NJ* **1647**, 1–18 (2017).

128. Xu, T. *et al.* ProLuCID: An improved SEQUEST-like algorithm with enhanced sensitivity and specificity. *J. Proteomics* **129**, 16–24 (2015).

129. Sangodkar, J. *et al.* All roads lead to PP2A: exploiting the therapeutic potential of this phosphatase. *FEBS J.* **283**, 1004–1024 (2016).

130. Cho, U. S. & Xu, W. Crystal structure of a protein phosphatase 2A heterotrimeric holoenzyme. *Nature* **445**, 53–57 (2007).

131. Coles, G. L. *et al.* Unbiased Proteomic Profiling Uncovers a Targetable GNAS/PKA/PP2A Axis in Small Cell Lung Cancer Stem Cells. *Cancer Cell* **38**, 129-143.e7 (2020).

132. Louie, S. M. *et al.* GSTP1 Is a Driver of Triple-Negative Breast Cancer Cell Metabolism and Pathogenicity. *Cell Chem. Biol.* **23**, 567–578 (2016).

133. Benjamin, D. I. *et al.* Inositol phosphate recycling regulates glycolytic and lipid metabolism that drives cancer aggressiveness. *ACS Chem. Biol.* **9**, 1340–1350 (2014).

134. Bateman, L. A. *et al.* Chemoproteomics-enabled covalent ligand screen reveals a cysteine hotspot in reticulon 4 that impairs ER morphology and cancer pathogenicity. *Chem. Commun. Camb. Engl.* (2017) doi:10.1039/c7cc01480e.

135. Xu, T. *et al.* ProLuCID: An improved SEQUEST-like algorithm with enhanced sensitivity and specificity. *J. Proteomics* **129**, 16–24 (2015).

136. Bateman, L. A. *et al.* Covalent Ligand Screening Reveals Cysteine Hotspot within RTN4 that Impairs ER Morphology and Colorectal Cancer Pathogenicity. *Submitt. ACS Chem. Biol.* (2017).

137. Medina-Cleghorn, D. *et al.* Mapping Proteome-Wide Targets of Environmental Chemicals Using Reactivity-Based Chemoproteomic Platforms. *Chem. Biol.* **22**, 1394–1405 (2015).

APPENDICES

Chapter 2 Supplementary Information
Supplementary Figures

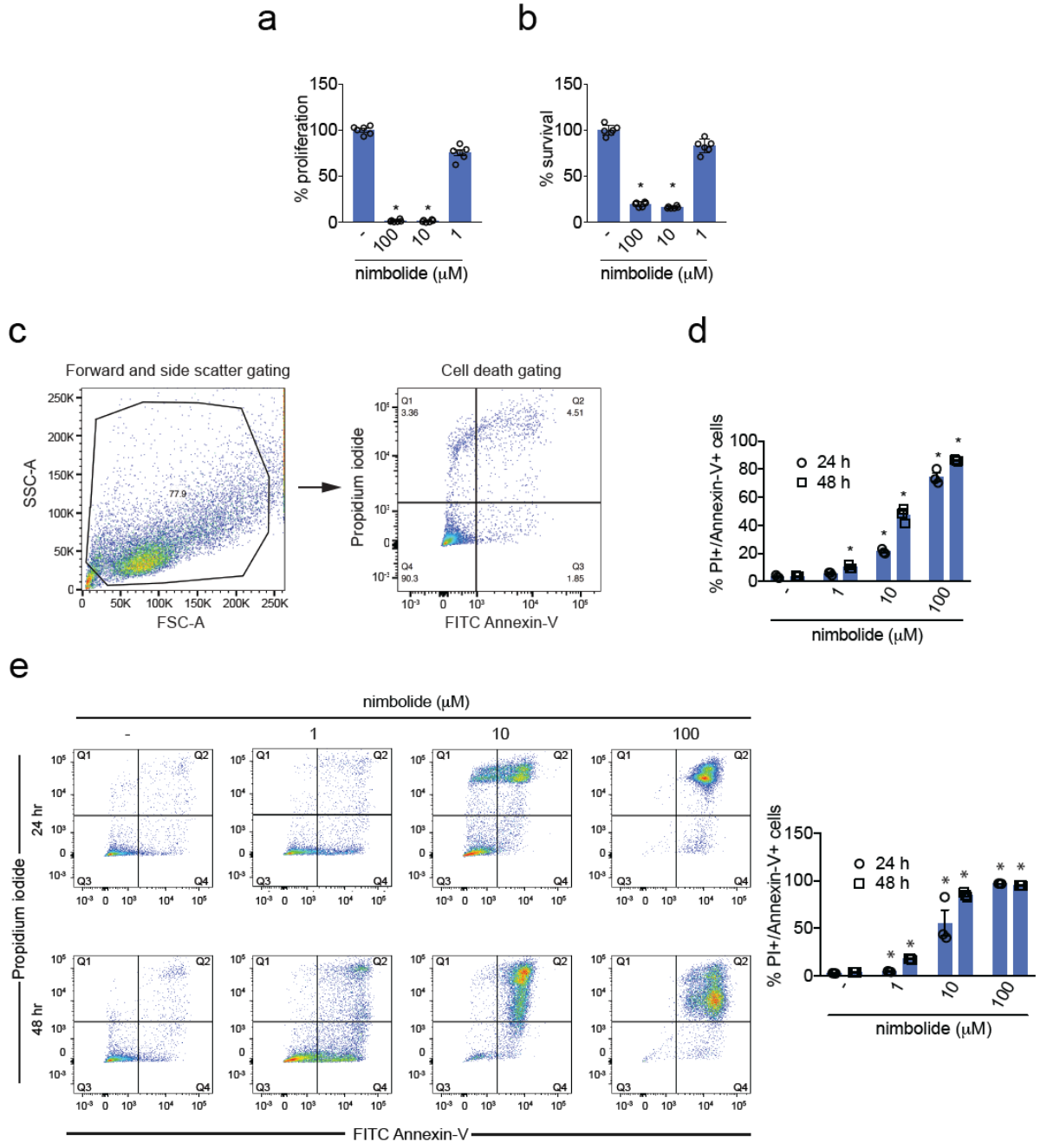

Supplementary Figure 2.1. Nimbolide impairs breast cancer cell proliferation and survival and induces apoptosis.
(a, b) HCC38 breast cancer cell proliferation in serum-containing media **(a)** and serum-free cell survival **(b)**. Cells were treated with DMSO vehicle or nimbolide and cell viability was assessed after 48 h.

(c) Shown is the gating strategy for the flow cytometry data. We used two gating steps--the first step we gated by forward and side scatter. The second gate was based on separation into quadrants by cell death stains (PI / annexin). **(d, e)** Percent of propidium iodide and Annexin-V-positive (PI+/Annexin-V+) cells assessed by flow cytometry after treating 231MFP **(d)** and HCC38 **(e)** cells with DMSO vehicle or nimbolide for 24 or 48 h. Representative FACS data from 231MFP cells in **(d)** in shown in **Fig. 2.1d** and from HCC38 cells are shown in **(e)** on the left panels. Bar graphs in **(d, e)** are percentage of late-stage apoptotic cells defined as defined as PI+/Annexin-V+ cells. Data shown in **(a**, **b, d, e)** are average ± sem, n=6 in **(a, b)** and n=3 in **(d, e)** biologically independent samples/group. Statistical significance was calculated with unpaired two-tailed Student's t-tests. Significance is expressed as *p=$1.64x10^{-13}$ and $2.05x10^{-13}$ for 100 and 10 μM, respectively for **(a)** and *p=$2.09x10^{-11}$ and $7.07x10^{-12}$ for 100 and 10 μM, respectively for **(b)**, *p=$9.05x10^{-5}$ and $1.87x10^{-5}$ for 10 and 100 μM, respectively for 24 h data for **(d)**, *p=0.00139, 0.000142, and $7.97x10^{-9}$ for 1, 10 and 100 μM, respectively for 48 h data for **(e),** *p=0.00424, 0.0182, and $2.22x10^{-11}$ for 1, 10 and 100 μM, respectively for 24 h data for **(e),** and *p=$6.68x10^{-6}$, $4.70x10^{-7}$, and $9.00x10^{-11}$ for 1, 10 and 100 μM, respectively for 48 h data for **(e),** compared to vehicle-treated controls.

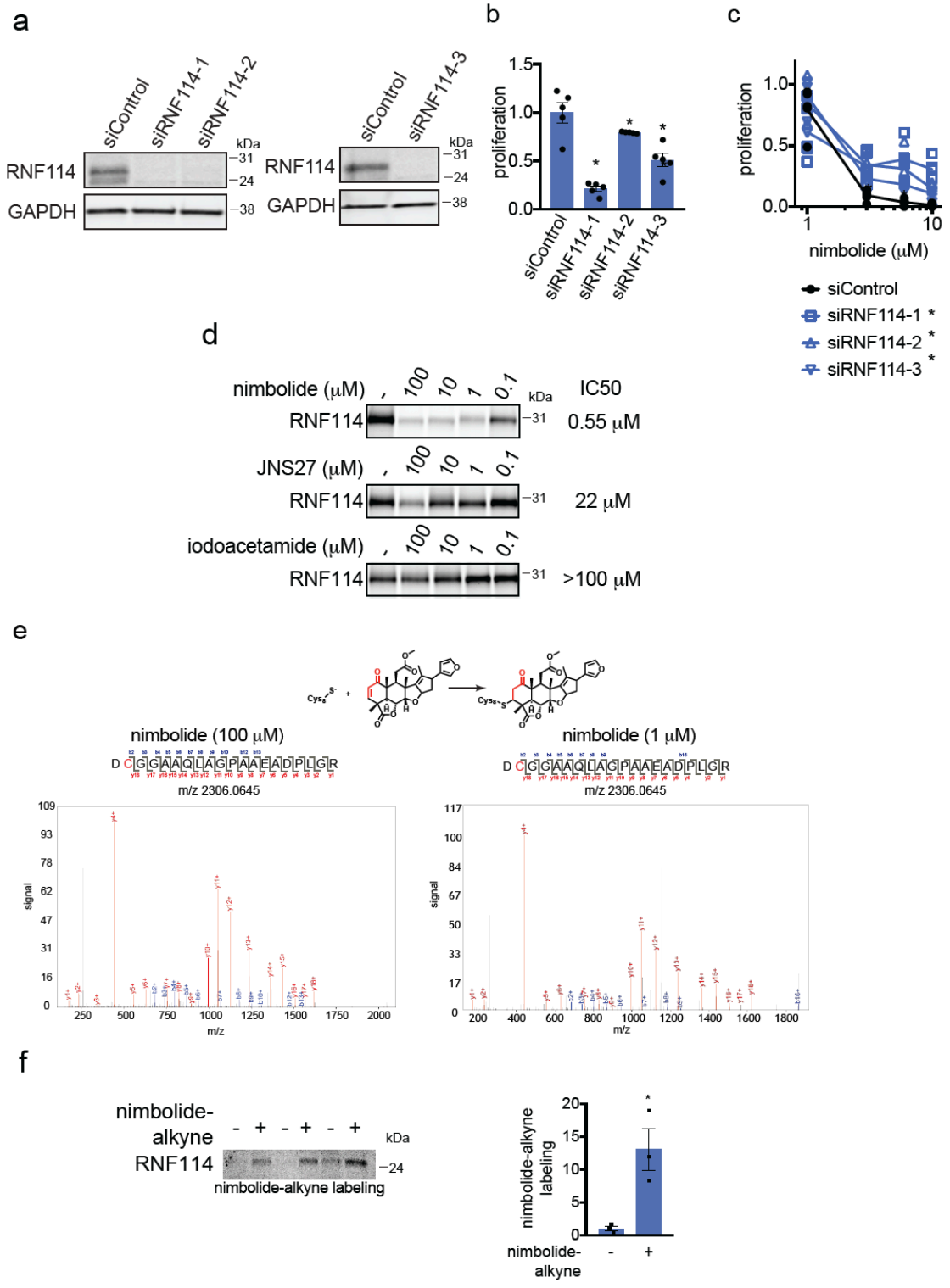

Supplementary Figure 2.2. Elucidating the Role of RNF114 in nimbolide-mediated effects.

(a) RNF114 knockdown by 3 independent siRNAs targeting RNF114 validated by Western blotting of RNF114 compared to siControl 231MFP cells. GAPDH expression is

shown as a loading control. Full length and replicate blots are shown in **Supplementary Fig. 2.4a. (b)** 231MFP cell proliferation after 24 h in siControl and siRNF114 cells assessed by Hoechst stain. **(c)** Nimbolide effects on 231MFP siControl and siRNF114 231MFP breast cancer cells. Cells were treated with DMSO vehicle or nimbolide for 24 h after which proliferation was assessed by Hoechst stain. Data for each siControl or siRNF114 group was normalized to the respective DMSO vehicle control in each group. Individual biologically independent sample data is shown and the lines indicate mean values. **(d)** Gel-based ABPP analysis of nimbolide, JNS27, and iodoacetamide competition against IA-rhodamine labeling of recombinant human RNF114 protein. RNF114 protein was pre-treated with DMSO vehicle or nimbolide, JNS27, or iodoacetamide for 30 min prior to labeling of RNF114 with IA-rhodamine (100 nM) for 30 min. RNF114 IA-rhodamine labeling was assessed by SDS/PAGE and in-gel fluorescence. Full length and replicate blots are shown in **Supplementary Fig. 2.4b.** Data shown are from an n=1 biological replicates. **(e)** Pure RNF114 protein was labeled with nimbolide (100 or 1 μM, 1 h) and subjected to tryptic digestion and LC-MS/MS analysis. Shown is the nimbolide-modified adduct on C8 of RNF114. We have repeated these experiments twice. **(f)** Nimbolide-alkyne *in situ* labeling. 231MFP cells stably expressing a Flag-tagged RNF114 were treated with DMSO vehicle or nimbolide-alkyne (100 nM) for 4 h. RNF114 was subsequently enriched from harvested cell lysates and then rhodamine-azide was appended onto probe-labeled proteins by CuAAC, after which nimbolide-alkyne labeling was visualized by SDS/PAGE and in-gel fluorescence. RNF114 labeling by the nimbolide-alkyne probe were quantified by densitometry. Full length and replicate blots are shown in **Supplementary Fig. 2.4c.** Data shown are from n=3 biologically independent samples/group. Gels shown in **(a** and **d)** are representative gels from n=3 biologically independent samples/group. Data shown in **(b, f)** are average ± sem, n=5 for **(b)** and n=3 for **(f)** biologically independent samples/group. Statistical significance was calculated with unpaired two-tailed Student's t-tests in **(b, c, f)**. Significance is expressed in **(b)** as *p=4.52x10^{-5}, 0.0429, and 0.00230 for siRNF114-1, siRNF114-2, and siRNF114-3, respectively compared to siControl cells. Significance in **(c)** is expressed as *p=1.90x10^{-5}, 0.000272, 0.00101 for 10, 6, and 3 μM, respectively for siRNF114-1; *p=0.000626, 0.00139, 3.66x10^{-5} for 10, 6, and 3 μM, respectively for siRNF114-2; and *p=0.00134, 9.15x10^{-5}, 0.00769 for 10, 6, and 3 μM, respectively for siRNF114-3 compared to corresponding concentration of nimbolide treatment in siControl cells. Significance in **(f)** is expressed as *p=0.0188 compared to vehicle-treated controls.

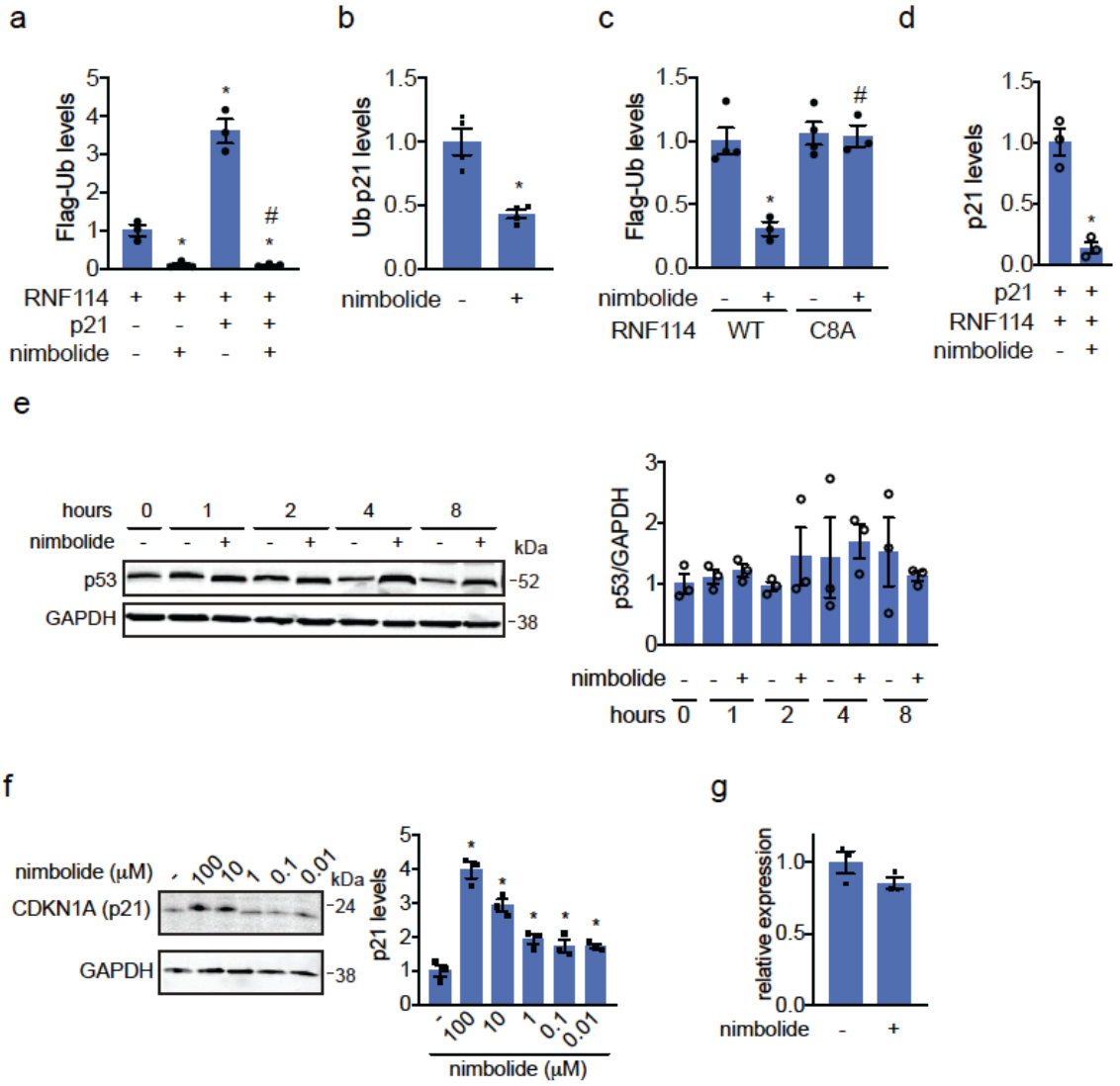

Supplementary Figure 2.3. Levels of p53 and p21 in nimbolide-treated 231MFP breast cancer cells.

(a-d) Quantification of ubiquitinated protein blots shown in **Fig. 2.4a-c** and p21 levels in **Fig. 2.4d**, respectively. **(e)** p53 levels in 231MFP breast cancer cells treated with DMSO vehicle or nimbolide (100 μM) assessed by Western blotting alongside GAPDH as a loading control. **(f)** Dose-response of p21 elevation with DMSO vehicle or nimbolide treatment for 1 h, assessed by Western blotting alongside GAPDH as a loading control. Full length and replicate blots are shown in **Supplementary Fig. 2.4b. (g)** p21 mRNA expression levels in 231MFP cells treated with nimbolide (100 μM) for 1 h assessed by qPCR. Gels shown in **(e** and **f)** are representative of an n=3 biologically independent samples /group. Blots were quantified by densitometry and normalized to loading control. Data shown in bar graphs are average ± sem from n=3 biologically independent samples/group for **(a-g)**. Statistical significance was calculated with unpaired two-tailed Student's t-tests in **(a-g)**. Significance is expressed as *p=0.0265, 0.00461, 0.0247 for RNF114/nimbolide, RNF114/p21, and RNF114/p21/nimbolide groups compared to

RNF114 DMSO vehicle treated control groups for Flag-Ub blot in **(a)**; *p=0.00201385 compared to RNF114/p21 DMSO vehicle control group for **(b)**; *p=0.00334 for WT nimbolide groups compared to WT DMSO vehicle-treated control in **(c)**; *p=0.00102 compared to the p21/RNF114 group in **(d)**; and *p=0.00518, 0.00161, 0.0145, 0.0452, 0.0187 for 100, 10, 1, 0.1, and 0.01 μM, respectively, compared to vehicle-treated controls in **(f)**. Significance expressed as #p=0.00202 compared to RNF114/p21 vehicle-treated control group in **(a)**, #p=0.0294 compared to WT nimbolide-treated group in **(c)**.

Synthetic Methods and Characterization

Synthesis and characterization of the nimbolide-alkyne probe (5) and degraders XH1 (9) and XH2 (10)

General Procedures

Unless otherwise stated, all reactions were performed in oven-dried or flame-dried Fisherbrand® borosilicate glass tubes (Fisher Scientific, 1495925A, 13 × 100 mm) with a black phenolic screw cap (13-425) under an atmosphere of dry nitrogen. Dry *N*,*N*-dimethylformamide (DMF), toluene, and acetonitrile were obtained by passing these previously degassed solvents through activated alumina columns. Nimbolide was purchased from Sigma-Aldrich or Cayman Chemical, and used directly without further purification. Propargylamine and *N*-methylpropargylamine were purchased from Fisher Scientific and used directly without further purification. Reactions were monitored by thin layer chromatography (TLC) on TLC silica gel 60 F_{254} glass plates (EMD Millipore) and visualized by UV irradiation and staining with *p*-anisaldehyde, phosphomolybdic acid, or potassium permanganate. Volatile solvents were removed under reduced pressure using a rotary evaporator. Flash column chromatography was performed using Silicycle F60 silica gel (60Å, 230-400 mesh, 40-63 μm). Ethyl acetate and hexanes were purchased from Fisher Chemical and used for chromatography without further purification. Proton nuclear magnetic resonance (^{1}H NMR) and carbon nuclear magnetic resonance (^{13}C NMR) spectra were recorded on Bruker AV-600 and AV-700 spectrometers operating at 600 and 700 MHz for ^{1}H, and 150 and 175 MHz for ^{13}C. Chemical shifts are reported in parts per million (ppm) with respect to the residual solvent signal $CDCl_3$ (^{1}H NMR: δ = 7.26; ^{13}C NMR: δ = 77.16), CD_2Cl_2 (^{1}H NMR: δ = 5.32; ^{13}C NMR: δ = 53.84). Peak multiplicities are reported as follows: *s* = singlet, *d* = doublet, *t* = triplet, *dd* = doublet of doublets, *tt* = triplet of triplets, *m* = multiplet, *br* = broad signal, *app* = apparent. IR spectra were recorded on a Nicolet 380 FT-IR spectrometer. High-resolution mass spectra (HRMS) were obtained by the QB3/chemistry mass spectrometry facility at the University of California, Berkeley. Optical rotations were measured on a Perkin-Elmer 241 polarimeter.

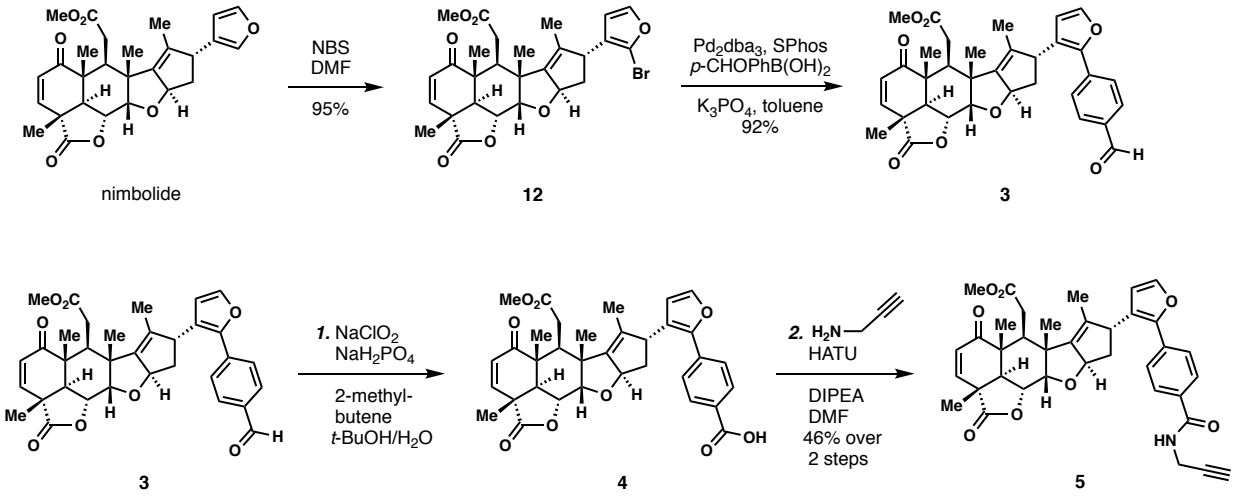

Scheme S1. Synthesis of the nimbolide-alkyne probe (**5**).

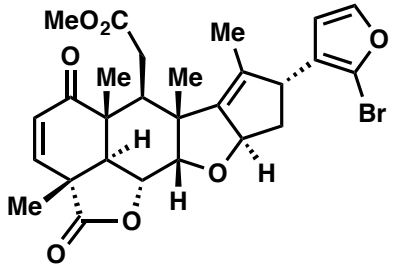

Bromonimbolide (**12**): Nimbolide (100 mg, 0.214 mmol) was divided evenly into four reaction tubes (Fisher Scientific, 13 × 100 mm), each charged with a stir bar. The tubes were evacuated and back-filled with nitrogen, dry DMF (0.25 mL each) was added, and the resulting solutions were cooled to 0 °C in an ice bath. Recrystallized *N*-bromosuccinimide (40.0 mg, 0.225 mmol) was dissolved in dry DMF (4 mL), and the solution was slowly added to each reaction tube (1 mL each). The reaction mixture was stirred at 0 °C for 1 hour and then quenched by the addition of saturated *aq*. $Na_2S_2O_3$ (5 mL each). The resulting mixtures were combined and extracted with EtOAc (3 X 20 mL). The combined organic layer was washed with H_2O (50 mL) and brine (50 mL), dried over $MgSO_4$, and concentrated *in vacuo*. The crude mixture was purified by column chromatography (EtOAc:hexane = 1:3 to 1:1), affording **(12)** (111 mg, 95%) as a white foam: $[\alpha]_D^{20}$ = +190.3° (c 0.010 g/ml, $CHCl_3$); ^{1}H NMR (700 MHz, $CDCl_3$) δ 7.34 (d, *J* = 2.1 Hz, 1H), 7.28 (d, *J* = 9.7 Hz, 1H), 6.29 (d, *J* = 2.1 Hz, 1H), 5.92 (d, *J* = 9.7 Hz, 1H), 5.56 (app. tt, *J* = 7.4, 1.8 Hz, 1H), 4.62 (dd, *J* = 12.5, 3.7 Hz, 1H), 4.27 (d, *J* = 3.7 Hz, 1H), 3.67 (brd, *J* = 7.0 Hz, 1H), 3.56 (s, 3H), 3.24 (dd, *J* = 16.3, 5.5 Hz, 1H), 3.18 (d, *J* = 12.5 Hz, 1H), 2.75 (dd, *J* = 5.5, 5.5 Hz, 1H), 2.36 (dd, *J* = 16.3, 5.5 Hz, 1H), 2.18 – 2.13 (m, 2H), 1.66 (d, *J* = 1.4 Hz, 3H), 1.47 (s, 3H), 1.36 (s, 3H), 1.22 (s, 3H); ^{13}C NMR (175 MHz, $CDCl_3$) δ 200.9, 175.0, 173.2, 149.8, 145.4, 144.2, 136.1, 131.2, 125.2, 120.3, 112.1, 88.5, 83.1, 73.5, 52.0, 50.5, 50.0, 47.9, 45.4, 43.8, 41.2, 40.4, 32.2, 18.7, 17.3, 15.3, 13.0; IR (thin film, cm^{-1}) 2974, 2929, 2875, 1783, 1734, 1678, 1594, 1438, 1394, 1373; HRMS (ESI) *calcd.* for $[C_{27}H_{29}O_7BrNa]^+$ $(M+Na)^+$: m/z 567.0989, found 567.0990.

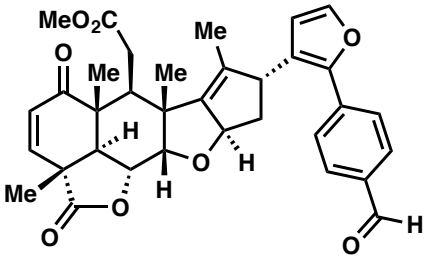

Aldehyde (**3**): A reaction tube (Fisher Scientific, 13 × 100 mm) was charged with a stir bar, (**12**) (12 mg, 0.022 mmol, 1 equiv), $Pd_2(dba)_3$ (10 mg, 0.011 mmol, 0.5 equiv), SPhos (10 mg, 0.024 mmol, 1 equiv), anhydrous K_3PO_4 (35 mg, 0.17 mmol, 7.5 equiv) and 4-formylphenylboronic acid (16 mg, 0.11 mmol, 5 equiv). The tube was evacuated and back-filled with nitrogen and dry toluene (0.5 mL) added. The resulting mixture was heated at 60 ºC for 48 h, cooled to room temperature, and passed through a plug of Celite®. The filtrate was concentrated *in vacuo* and purified by column chromatography (EtOAc:hexane = 1:3 to 1:1) to afford aldehyde (**3**) (11.5 mg, 92%) as a light yellow oil: $[\alpha]_D^{20}$ = +4.8° (c 0.005 g/mL, $CHCl_3$); ^{1}H NMR (600 MHz, $CDCl_3$) δ 10.01 (s, 1H), 7.92 (d, *J* = 8.3 Hz, 2H), 7.71 (d, *J* = 8.3 Hz, 2H), 7.42 (d, *J* = 1.9 Hz, 1H), 7.29 (d, *J* = 9.7 Hz, 1H), 6.39 (d, *J* = 1.9 Hz, 1H), 5.93 (d, *J* = 9.7 Hz, 1H), 5.60 (app. tt, *J* = 7.3, 1.7 Hz, 1H), 4.64 (dd, *J* = 12.5, 3.6 Hz, 1H), 4.32 (d, *J* = 3.6 Hz, 1H), 4.17 – 4.13 (m, 1H), 3.69 (s, 3H), 3.23 (dd, *J* = 16.4, 5.5 Hz, 1H), 3.20 (d, *J* = 12.5 Hz, 1H), 2.78 (dd, *J* = 5.5, 5.5 Hz, 1H), 2.41 (dd, *J* = 16.4, 5.5 Hz, 1H), 2.31 – 2.27 (m, 2H), 1.69 (d, *J* = 1.7 Hz, 3H), 1.49 (s, 3H), 1.38 (s, 3H), 1.25 (s, 3H); ^{13}C NMR (150 MHz, $CDCl_3$) δ 200.8, 191.7, 175.0, 173.2, 149.8, 147.9, 146.3, 143.1, 137.0, 136.1, 134.8, 131.1, 130.3, 126.1, 126.0, 112.6, 88.4, 83.3, 73.4, 52.1, 50.8, 50.0, 47.9, 45.5, 43.8, 41.3, 32.5, 18.8, 17.5, 15.3, 13.4; IR (thin film, cm^{-1}) 2977, 2935, 2873, 1782, 1733, 1702, 1677, 1608, 1438, 1393, 1372; HRMS (ESI) *calcd.* for $[C_{34}H_{34}O_8Na]^+$ $(M+Na)^+$: m/z 593.2146, found 593.2154.
[Note: Aldehyde **(3))** is not stable under preparative TLC conditions]

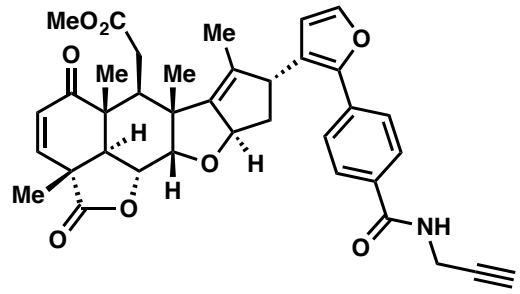

Nimbolide Alkyne Probe (**5**)**:** *i.* A reaction tube (Fisher Scientific, 13 × 100 mm) was charged with a stir bar, aldehyde (**3**) (7.0 mg, 0.012 mmol, 1 equiv), and a mixture of *t*-BuOH and 2-methyl-2-butene (0.6 mL, 3:5 v/v). A solution of $NaClO_2$ (3.3 mg, 3 equiv) and NaH_2PO_4 (13.2 mg, 9 equiv) in H_2O (0.2 mL) was added in one portion and the resulting mixture was stirred at room temperature for 6 hours. After the reaction was complete as judged by TLC (EtOAc:hexane = 2:1), the mixture was diluted with EtOAc (10 mL) and saturated *aq.* NH_4Cl (10 mL), and the aqueous phase was extracted by EtOAc (10 mL × 2). The combined organic layer was washed with brine (20 mL), dried over $MgSO_4$, and concentrated *in vacuo*. The resulting crude carboxylic acid (**4**) was used directly without further purification.
ii. A reaction tube (Fisher Scientific, 13 × 100 mm) charged with a stir bar, crude acid (**4**) (0.012 mmol assumed), and HATU (13.7 mg, 0.036 mmol, 3 equiv) was added a solution of DIPEA (6.4 μL, 0.036 mmol, 3 equiv) in DMF (0.1 mL). The resulting mixture was cooled to 0 ºC and stirred for 10 minutes. A solution of propargylamine (1.6 μL, 0.024 mmol, 2 equiv) in DMF (0.2 mL) was then added and the reaction mixture was further stirred at 0–4 ºC for 12 hours. After the reaction was complete, as judged by TLC (EtOAc:hexane = 2:1), the mixture was diluted with EtOAc (10 mL) and saturated *aq.* NH_4Cl (10 mL), and the aqueous phase was extracted by EtOAc (10 mL × 2). The combined organic layer

was washed with H_2O (20 mL), brine (20 mL), dried over $MgSO_4$, and concentrated *in vacuo*. The resulting crude was purified by preparative TLC (EtOAc:hexane = 2:1), affording amide (**5**) (3.5 mg, 46% over 2 steps) as a white solid: $[\alpha]_D^{20}$ = +21.5° (c 0.002 g/mL, $CHCl_3$); ^{1}H NMR (600 MHz, $CDCl_3$) δ 7.83 (d, *J* = 8.2 Hz, 2H), 7.61 (d, *J* = 8.2 Hz, 2H), 7.39 (d, *J* = 1.8 Hz, 1H), 7.29 (d, *J* = 9.7 Hz, 1H), 6.36 (d, *J* = 1.8 Hz, 1H), 6.27 (t, *J* = 5.2 Hz, 1H), 5.93 (d, *J* = 9.7 Hz, 1H), 5.60 (app. t, *J* = 7.6 Hz, 1H), 4.64 (dd, *J* = 12.6, 3.7 Hz, 1H), 4.31 (d, *J* = 3.7 Hz, 1H), 4.28 (dd, *J* = 5.2, 2.6 Hz, 2H), 4.11 (brd, *J* = 7.6 Hz, 1H), 3.68 (s, 3H), 3.25 – 3.18 (m, 2H), 2.78 (dd, *J* = 5.5, 5.5 Hz, 1H), 2.40 (dd, *J* = 16.4, 5.5 Hz, 1H), 2.32 – 2.24 (m, 3H), 1.67 (brs, 3H), 1.49 (s, 3H), 1.38 (s, 3H), 1.24 (s, 3H); ^{13}C NMR (150 MHz, $CDCl_3$) δ 200.8, 175.0, 173.2, 166.6, 149.8, 148.2, 146.1, 142.5, 136.3, 134.7, 132.1, 131.2, 127.6, 126.1, 124.8, 112.3, 88.5, 83.2, 79.6, 73.5, 72.2, 52.1, 50.8, 50.0, 48.0, 45.5, 43.8, 41.3, 41.3, 32.5, 30.0, 18.8, 17.5, 15.3, 13.4; IR (thin film, cm^{-1}) 3337, 2954, 2921, 2852, 1781, 1734, 1663, 1609; HRMS (ESI) *calcd.* for $[C_{37}H_{37}NO_8Na]^+$ $(M+Na)^+$: m/z 646.2417, found 646.2417.

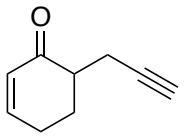

JNS27 (**6**)**.** i. To a stirring solution of lithium diisopropylamide (6.0 mL, 1.2 equiv) at -78 °C under nitrogen atmosphere, was added a solution of cyclohexenone (0.48mL, 1 equiv) in THF (5.0 mL) drop wise. After 45 minutes, a solution of 3-bromo-1-(trimethylsilyl)-propyne (0.85 mL, 2.4 equiv) in THF (5.0 mL) was added gradually, before allowing the reaction to come to room temperature overnight. The reaction was quenched with saturated NH_4Cl (20mL) and extracted with EtOAc (20 mL × 3). The combined organic layers were washed with brine, dried with Na_2SO_4, and concentrated *in vacuo*. Flash chromatography of the crude residue on silica gel (10-20% EtOAc in hexanes) gave the TMS-protected alkyne in 25% yield (261 mg). ii. To a solution of this material (261 mg, 1 equiv) in THF (5.0 mL) under N_2 was added a solution of TBAF (0.44 mL, 1 equiv). After 4 hours of stirring at room temperature, the reaction was quenched by the addition of saturated NH_4Cl (15 mL). The mixture was extracted with EtOAc (3 x15 mL). The combined organic layers were washed with brine, dried with Na_2SO_4, and concentrated *in vacuo*. Flash chromatography of the residue on silica gel (0-20% EtOAc in hexanes) gave JNS-27 as a pale-yellow waxy solid in 81% yield (168 mg, 21% over 2 steps). ^{1}H NMR (400 MHz, $CDCl_3$) δ 6.99 (m, 1H), 6.03 (dt, *J* = 10.02, 1.97 Hz, 1H), 2.78 (m, 1H), 2.48 (m, 3H), 2.33 (m, 2H), 1.98 (t, *J* = 2.68, 1H), 1.88 (m, 1H); ^{13}C NMR (400 MHz, $CDCl_3$) δ 150.30, 129.34, 45.74, 27.68, 25.78, 20.27; HRMS (ESI) *calcd.* for $[C_9H_{10}ONa]^+$ $(M+Na)^+$: m/z 134.0732, found 134.0728.

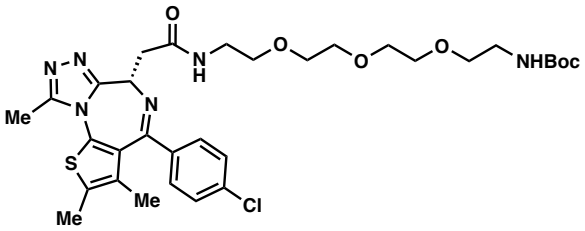

This compound (**7**) was prepared according to the conditions reported by Bradner and co-workers (PCT Int. Appl. 2017, WO 2017091673 A2).

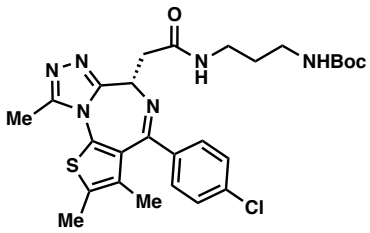

This compound (**8**) was prepared according to conditions reported by Waring and coworkers (*J. Med. Chem.*, **2016**, *59*, 7801).

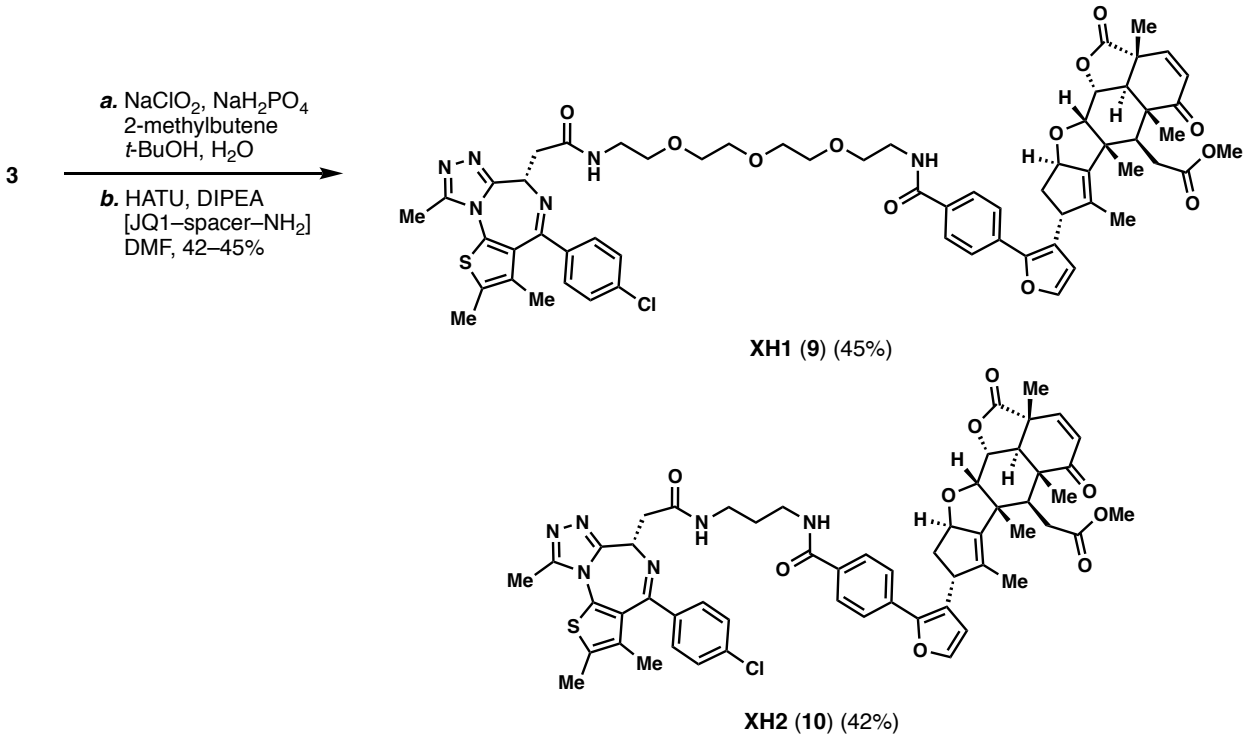

XH1 (**9**) (45%)

XH2 (**10**) (42%)

Scheme S2. Synthesis of nimbolide-derived bifunctional degraders **XH1** (**9**) **and XH2** (**10**).

General procedure for the synthesis of bifunctional degraders XH1 (9) and XH2 (10):

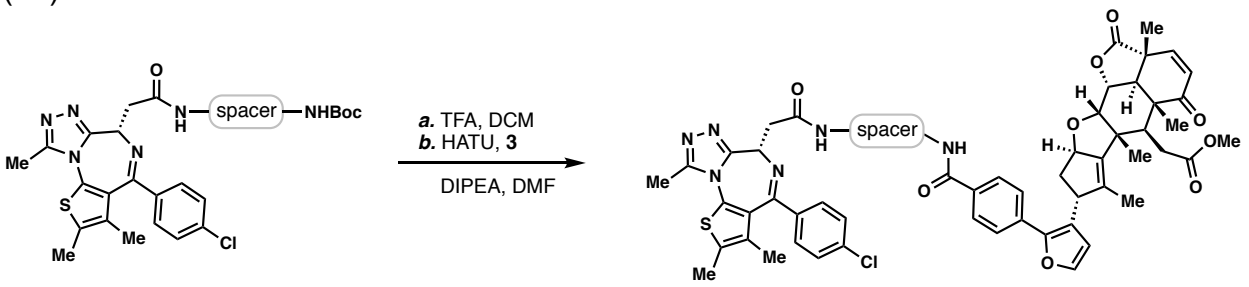

i. A reaction tube (Fisher Scientific, 13 × 100 mm) was charged with a stir bar, the Boc-protected amine (**7**) or (**8**) (0.04 mmol), triethylsilane (12 μL, 0.075 mmol), and DCM (0.4 mL). The resulting mixture was cooled to 0 ºC, followed by the dropwise addition of TFA (0.12 mL). The reaction mixture was allowed to warm to room temperature and further stirred for 2 hours. After the reaction was complete as judged by TLC (MeOH:DCM = 1:10), the mixture was diluted with toluene (2 mL), and concentrated *in vacuo*. The resulting crude was dried under high vacuum for 30 minutes, and directly used in the next step without further purification. Carboxylic acid (**4**) was prepared from aldehyde (**3**) according to the aforementioned procedure, and used without further purification.

ii. A reaction tube (Fisher Scientific, 13 × 100 mm) was charged with a stir bar, the crude amine (0.04 mmol assumed), unpurified acid (**4**) (0.02 mmol assumed), and DMF (0.6 mL). The resulting mixture was cooled to 0 ºC in an ice bath, followed by the addition of HATU (23.0 mg, 0.06 mmol) and DIPEA (11 μL, 0.06 mmol). The reaction mixture was stirred at 4 ºC for 16 hours. After the reaction was complete as judged by TLC (MeOH:DCM = 1:10), the mixture was diluted with EtOAc (10 mL) and saturated *aq.* NH_4Cl (10 mL), and the aqueous phase extracted with EtOAc (2 x 10 mL). The combined organic layer was washed with H_2O (20 mL), brine (20 mL), dried over $MgSO_4$, and concentrated *in vacuo*. The resulting crude material was purified by preparative TLC (MeOH:DCM = 1:15, developed twice), affording the bifunctional degraders **XH1** or **XH2**.

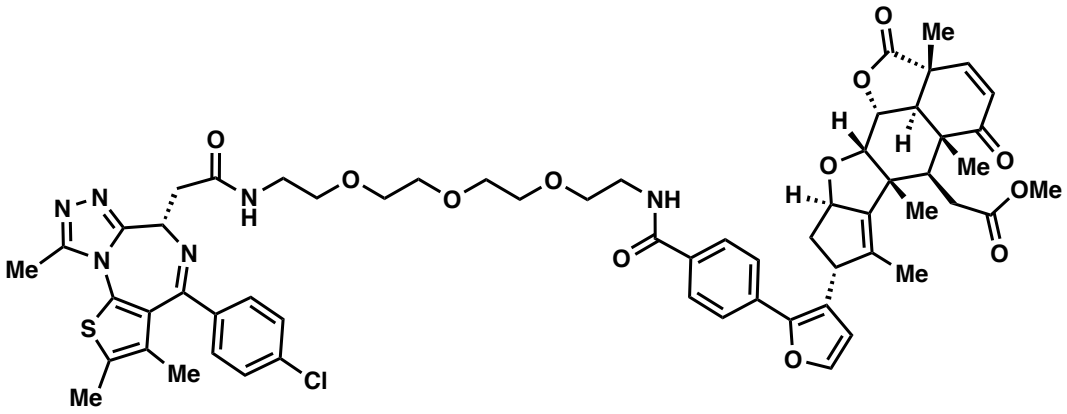

XH1 (**9**) (45% yield from (**3**)), a white foam: $[\alpha]_D^{20}$ = +48.7° (c 0.0052 g/mL, $CHCl_3$); ^1H NMR (600 MHz, $CDCl_3$) δ 7.87 (d, *J* = 8.5 Hz, 2H), 7.53 (d, *J* = 8.5 Hz, 2H), 7.40 (d, *J* =

8.2 Hz, 3H), 7.36 (d, *J* = 1.9 Hz, 1H), 7.34 – 7.29 (m, 2H), 7.28 (d, *J* = 9.7 Hz, 1H), 6.33 (d, *J* = 1.9 Hz, 1H), 5.93 (d, *J* = 9.7 Hz, 1H), 5.61 – 5.55 (m, 1H), 4.73 (app. t, *J* = 7.1 Hz, 1H), 4.64 (dd, *J* = 12.5, 3.7 Hz, 1H), 4.30 (d, *J* = 3.6 Hz, 1H), 4.12 – 4.08 (m, 1H), 3.75 – 3.64 (m, 15H), 3.64 – 3.53 (m, 3H), 3.51 – 3.40 (m, 3H), 3.25 – 3.16 (m, 2H), 2.77 (app. t, *J* = 5.5 Hz, 1H), 2.70 (s, 3H), 2.42 – 2.36 (m, 4H), 2.26 – 2.20 (m, 2H), 1.68 – 1.65 (m, 3H), 1.65 (d, *J* = 1.8 Hz, 3H), 1.48 (s, 3H), 1.37 (s, 3H), 1.24 (s, 3H); ^{13}C NMR (150 MHz, $CDCl_3$) δ 200.6, 174.8, 173.0, 170.1, 167.0, 164.4, 155.3, 149.9, 149.6, 148.3, 146.1, 145.6, 142.1, 137.2, 136.3, 135.8, 133.8, 133.0, 131.6, 131.2, 131.0, 130.6, 130.0, 130.0, 128.7, 128.7, 127.6, 127.6, 125.7, 125.7, 124.1, 112.0, 88.3, 83.0, 73.3, 70.5, 70.5, 70.3, 70.2, 69.7, 69.6, 54.1, 51.9, 50.5, 49.7, 47.8, 45.3, 43.6, 41.1, 41.1, 39.7, 39.4, 38.5, 32.3, 18.6, 17.3, 15.1, 14.4, 13.1, 13.1, 11.6; IR (thin film, cm^{-1}) 3339, 2923, 2866, 1781, 1734, 1659, 1540, 1487, 1437, 1419, 1300; HRMS (ESI) *calcd.* for $[C_{61}H_{67}N_6O_{12}Cl_1S_1Na]^+$ $(M+Na)^+$: m/z 1165.4118, found 1165.4142.

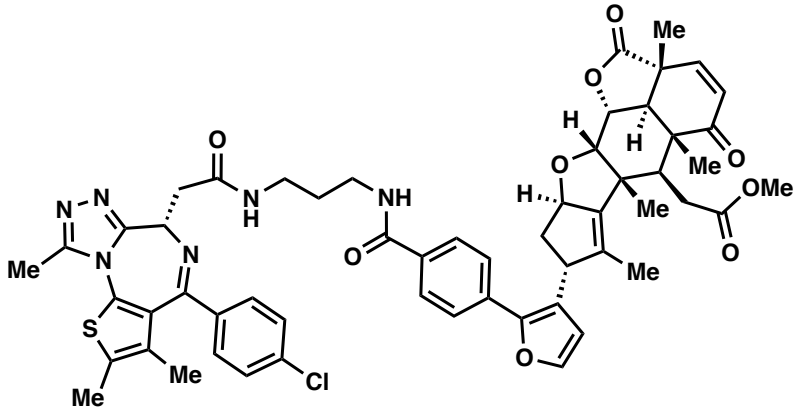

XH2 (**10**) (42% yield from (**3**)), a white foam: $[\alpha]_D^{20}$ = +18.6° (c 0.004 g/mL, $CHCl_3$); ^{1}H NMR (600 MHz, CD_2Cl_2) δ 7.90 (d, *J* = 8.3 Hz, 2H), 7.65 – 7.57 (m, 3H), 7.44 – 7.39 (m, 3H), 7.33 (d, *J* = 8.5 Hz, 2H), 7.25 (d, *J* = 9.7 Hz, 1H), 7.07 (t, *J* = 6.5 Hz, 1H), 6.36 (d, *J* = 1.9 Hz, 1H), 5.89 (d, *J* = 9.7 Hz, 1H), 5.52 (app. t, *J* = 7.6 Hz, 1H), 4.66 – 4.59 (m, 2H), 4.26 (d, *J* = 3.6 Hz, 1H), 4.12 (brd, *J* = 7.6 Hz, 1H), 3.63 (s, 3H), 3.52 – 3.45 (m, 2H), 3.44 – 3.34 (m, 4H), 3.20 (dd, *J* = 16.4, 5.5 Hz, 1H), 3.15 (d, *J* = 12.5 Hz, 1H), 2.74 (app. t, *J* = 5.5 Hz, 1H), 2.63 (s, 3H), 2.45 – 2.37 (m, 4H), 2.25 – 2.21 (m, 2H), 1.75 – 1.70 (m, 2H), 1.65 (s, 6H), 1.46 (s, 3H), 1.36 (s, 3H), 1.22 (s, 3H); ^{13}C NMR (150 MHz, CD_2Cl_2) δ 201.2, 175.6, 173.5, 171.9, 166.7, 164.5, 156.1, 150.5, 149.9, 148.8, 146.3, 142.5, 137.1, 137.0, 136.6, 134.2, 133.7, 132.7, 131.6, 131.3, 131.2, 130.8, 130.3, 130.3, 129.0, 129.0, 127.8, 127.8, 126.2, 126.2, 124.8, 112.6, 88.6, 83.4, 73.9, 54.9, 52.1, 51.0, 50.2, 48.2, 45.8, 44.1, 41.6, 41.5, 39.7, 36.5, 36.2, 32.7, 29.9, 18.8, 17.5, 15.4, 14.6, 13.4, 13.3, 12.0; IR (thin film, cm^{-1}) 3308, 3023, 2930, 2867, 1782, 1734, 1654, 1540, 1488, 1437, 1301; HRMS (ESI) *calcd.* for $[C_{56}H_{57}ClN_6O_9S]^+$ $(M+H)^+$: m/z 1025.3669, found 1025.3669.

Synthesis and characterization of cysteine-reactive covalent ligands previously not reported

General synthetic methods

Chemicals and reagents were purchased from major commercial suppliers and used without further purification. Reactions were performed under a nitrogen atmosphere

unless otherwise noted. Silica gel flash column chromatography was performed using EMD or Sigma Aldrich silica gel 60 (230-400 mesh). Proton and carbon nuclear magnetic resonance (^{1}H NMR and ^{13}C NMR) data was acquired on a Bruker AVB 400, AVQ 400, or AV 600 spectrometer at the University of California, Berkeley. High resolution mass spectrum were obtained from the QB3 mass spectrometry facility at the University of California, Berkeley using positive or negative electrospray ionization (+ESI or -ESI). Yields are reported as a single run.

General Procedure A
The amine (1 eq.) was dissolved in DCM (5 mL/mmol) and cooled to 0˚C. To the solution was added acryloyl chloride (1.2 eq.) followed by triethylamine (1.2 eq.). The solution was warmed to room temperature and stirred overnight. The solution was then washed with brine and the crude product was purified by silica gel chromatography (and recrystallization if necessary) to afford the corresponding acrylamide.

General Procedure B
The amine (1 eq.) was dissolved in DCM (5 mL/mmol) and cooled to 0˚C. To the solution was added chloroacetyl chloride (1.2 eq.) followed by triethylamine (1.2 eq.). The solution was warmed to room temperature and stirred overnight. The solution was then washed with brine and the crude product was purified by silica gel chromatography (and recrystallization if necessary) to afford the corresponding chloroacetamide.

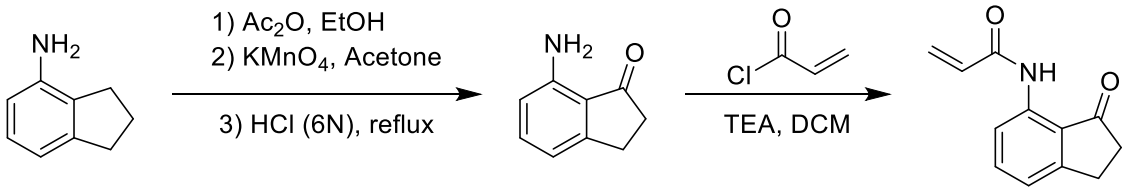

***N*-(3-oxo-2,3-dihydro-1*H*-inden-4-yl)acrylamide (TRH 1-129)** (**13**)
i. To a solution of 4-aminoindane (1.0 g, 7.5 mmol) in ethanol (20 mL) at 0 °C was added acetic anhydride (1.4 mL, 15.0 mmol). The solution was then warmed to room temperature and stirred overnight at which point the solvent was evaporated *in vacuo*. The residue was then dissolved in acetone (50 mL) and 15% aqueous magnesium sulfate (1.2 g in 6.75 mL of water) followed by potassium permanganate (3.4 g, 17.0 mmol) were added. The resulting solution was stirred for 24 hours and then filtered through a pad of celite, eluting with chloroform and then water. The eluent was separated, and the aqueous layer was extracted several times with additional chloroform. The combined organics were dried over magnesium sulfate, filtered and evaporated *in vacuo*. The residue was then dissolved in 6N HCl (20 mL) and heated to 90 °C. After stirring for 5 hours, the solution was cooled, neutralized with small portions of potassium carbonate, and extracted with ethyl acetate. The combined organics were dried with magnesium sulfate, filtered, and evaporated *in vacuo* to give the crude **7-aminoindan-1-one** (610 mg, 55% over 3 steps) which was used without further purification.
ii. To a solution of the crude 7-aminoindan-1-one in dichloromethane (15 mL) was added acryloyl chloride (0.39 mL, 4.8 mmol) followed by triethylamine (0.67 mL, 4.8 mmol) at 0˚C under an atmosphere of N_2. The reaction mixture was warmed to room temperature and stirred overnight. The reaction mixture was then washed with 1M HCl solution twice,

brine, and concentrated *in vacuo*. The crude material was purified by silica gel chromatography (10% to 20% ethyl acetate in hexanes) to yield (**13**) the product (390 mg, 47% yield, 26% combined yield over 4 steps) as a white solid.
^{1}H NMR (400MHz, $CDCl_3$): δ 10.64 (s, 1H), 8.45 (d, *J* = 8.2 Hz, 1H), 7.55 (t, *J* = 7.9 Hz, 1H), 7.12 (d, *J* = 7.6 Hz, 1H), 6.45 (dd, *J* = 1.0, 17.0 Hz, 1H), 6.33 (dd, *J* = 10.1, 17.0 Hz, 1H), 5.82 (dd, *J* = 1.0, 10.1 Hz, 1H), 3.11 (t, *J* = 11.5 Hz, 2H), 2.74-2.71 (m, 2H).
^{13}C NMR (100MHz, $CDCl_3$): δ 209.3, 164.4, 155.9, 138.7, 137.0, 131.7, 128.0, 123.1, 120.8, 116.9, 36.5, 25.5.
HRMS (+ESI): Calculated: 202.0863 ($C_{12}H_{12}NO_2$). Observed: 202.0860.

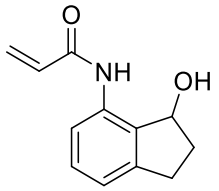

***N*-(3-hydroxy-2,3-dihydro-1*H*-inden-4-yl)acrylamide (TRH 1-133)** (**14**)
To a solution of **(13)** (201 mg, 1.0 mmol) in anhydrous methanol (7 mL) under nitrogen atmosphere was added sodium borohydride (46.1 mg, 1.2 mmol). After 30 minutes of stirring, the reaction was quenched with saturated sodium bicarbonate solution and extracted three times with DCM. The combined organic layers were dried with magnesium sulfate, filtered, and concentrated *in vacuo*. The crude material was purified by silica gel chromatography (30 to 50% ethyl acetate in hexanes) affording (**14**) (190 mg, 94% yield) as a white solid.
^{1}H NMR (400 MHz, $CDCl_3$): δ 8.93 (s, 1H), 7.98 (d, *J* = 7.8 Hz, 1H), 7.19 (t, *J* = 7.9 Hz, 1H), 6.95 (d, *J* = 7.4 Hz, 1H), 6.29 (d, *J* = 16.8 Hz, 1H), 6.15 (dd, *J* = 10.2, 16.9 Hz, 1H), 5.66 (d, *J* = 10.2 Hz, 1H), 5.32 (q, *J* = 6.9 Hz, 1H), 3.60 (d, *J* = 6.7 Hz, 1H), 2.96 (ddd, *J* = 2.4, 9.0, 15.7 Hz), 2.73 (quint, *J* = 8.1 Hz, 1H), 2.56-2.48 (m, 1H), 1.96-1.86 (m, 1H).
^{13}C NMR (100 MHz, $CDCl_3$): δ 164.1, 143,7 ,135.6, 132.8, 131.6, 129.5, 127.3, 121.0, 118.5, 76.2, 36.0, 29.8.
HRMS (-ESI): Calculated: 202.0874 ($C_{12}H_{12}NO_2$). Observed: 202.0874.

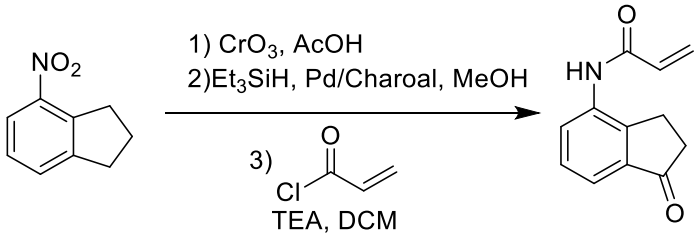

***N*-(1-oxo-2,3-dihydro-1*H*-inden-4-yl)acrylamide (TRH 1-134)** (**15**)
i. To a solution of 4-nitroindane (5.38 g, 33 mmol) in acetic acid (250 mL) was slowly added chromium trioxide (8.95 g, 90 mmol). After stirring for 24 hours, the reaction was neutralized with 2M NaOH and extracted five times with ethyl acetate. The combined organics were washed with a saturated sodium bicarbonate solution and brine, dried over

magnesium sulfate, filtered, and concentrated *in vacuo*. The crude material was purified by silica gel chromatography (10-20% ethyl acetate in hexanes) to give 1.26 g (ca. 7.1 mmol) of 4-nitroindanone as a white solid.
ii. This intermediate was then combined with palladium on activated charcoal (125 mg, 10 wt%) dissolved in anhydrous methanol (21 mL) under an atmosphere of a nitrogen. Triethylsilane (11.3 mL, 71 mmol) was slowly added by addition funnel over the course of 10 minutes to the reaction in a room temperature water bath. After an additional 20 minutes of stirring, the reaction mixture was filtered through a pad of celite and concentrated *in vacuo* to give 4-aminoindanone which was used without further purification.
iii. The aforementioned crude aminoindanone was dissolved in DCM (21 mL) under an atmosphere of nitrogen and cooled to 0 ˚C at which point acryloyl chloride (0.77 mL, 9.5 mmol) and triethylamine (1.19 mL, 8.5 mmol) were slowly added dropwise. The reaction mixture was warmed to room temperature, stirred overnight, washed twice with brine, dried over magnesium sulfate, filtered, and concentrated *in vacuo*. The crude material was purified by silica gel chromatography (30-50% ethyl acetate in hexanes) affording **(15)** (989 mg, 15% yield over 3 steps) as a white solid.
^{1}H NMR (400 MHz, $CDCl_3$): δ 8.20 (d, *J* = 5.8 Hz, 1H), 7.63 (s, 1H), 7.56 (d, *J* = 7.5 Hz, 1H), 7.39 (t, *J* = 7.7 Hz, 1H), 6.48 (d, *J* = 16.7 Hz, 1H), 6.37 (dd, *J* = 10.0 Hz, 16.8 Hz, 1H), 5.83 (d, *J* = 10.1 Hz, 1H), 3.04 (t, *J* = 5.6 Hz, 2H), 2.70 (t, *J* = 5.7 Hz, 2H).
^{13}C NMR (100 MHz, $CDCl_3$): δ 206.3, 163.9, 146.0, 138.0, 135.4, 130.7, 128.8, 128.7, 127.6, 120.4, 36.1, 23.4.
HRMS (-ESI): Calculated: 200.0717 ($C_{12}H_{10}NO_2$). Observed: 200.0715.

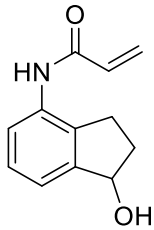

***N*-(1-hydroxy-2,3-dihydro-1*H*-inden-4-yl)acrylamide (TRH 1-135)** (**16**)
To a solution of (**15)** (1.26 g, 6.25 mmol) in anhydrous methanol (50 mL) under nitrogen atmosphere was added sodium borohydride (292.7 mg, 7.7 mmol). After 30 minutes of stirring, the reaction was quenched with water and the methanol was removed *in vacuo*. The residue was saturated with NaCl and extracted five times with a 2:1 chloroform:methanol solution. The combined organic layers were dried over 3Å molecular sieves, filtered, and concentrated *in vacuo*. The crude material was purified by silica gel chromatography (40 to 70% ethyl acetate in hexanes) to give (**16**) (1.05 g, 83% yield) as a white solid.
^{1}H NMR (400 MHz, MeOD): δ 7.50 (dd, *J* = 2.3, 6.3 Hz, 1H), 7.25-7.20 (m, 2H), 6.51 (dd, *J* = 10.2, 17.0 Hz, 1H), 6.35 (dd, *J* = 1.7, 17.0 Hz, 1H), 5.77 (dd, *J* = 1.7, 10.2 Hz, 1H), 5.17 (t, *J* = 6.3 Hz, 1H), 2.97 (ddd, *J* = 4.5, 8.6, 16.2, 1H), 2.74 (quint, *J* = 7.8 Hz, 1H), 2.47-2.39 (m, 1H), 1.95-1.86 (m, 1H).
^{13}C NMR (100 MHz, MeOD): δ 166.3, 148.0, 137.8, 134.8, 132.1, 128.3, 127.9, 124.0, 122.7, 76.9, 36.1, 28.6.
HRMS (-ESI): Calculated: 202.0874 ($C_{12}H_{12}NO_2$). Observed: 202.0872.

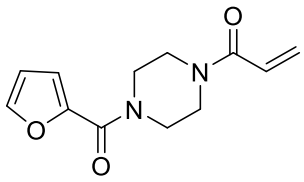

1-(4-(furan-2-carbonyl)piperazin-1-yl)prop-2-en-1-one (TRH 1-145) (**17**)

To a solution 1-(2-furoyl)piperazine (362 mg, 2.0 mmol) in dichloromethane (10 mL) was added acryloyl chloride (0.20 mL, 2.4 mmol) followed by triethylamine (0.34 mL, 2.4 mmol) at 0˚C under an atmosphere of nitrogen. After stirring for 20 minutes, the reaction mixture was warmed to room temperature and was stirred an additional 24 hours. The reaction mixture was washed twice with brine, dried over magnesium sulfate, and concentrated *in vacuo*. The resulting crude material was purified by silica gel chromatography (70% to 100% ethyl acetate in hexanes) to yield (**17**) (446 mg, 95%) as a yellow solid.

^{1}H NMR (400 MHz, $CDCl_3$): δ 7.53 (m, 1H), 7.06 (dd, *J* = 0.7, 3.5 Hz, 1H), 6.61 (dd, *J* = 10.5, 16.8 Hz, 1H), 6.52 (dd, *J* = 1.8, 3.5 Hz, 1H), 6.33 (dd, *J* = 1.9, 16.8 Hz, 1H), 5.75 (dd, *J* = 1.9, 10.5 Hz, 1H), 3.84-3.67 (m, 8H).

^{13}C NMR (100 MHz, $CDCl_3$): δ 165.5, 159.1, 147.5, 144.0, 128.5, 127.1, 117.0, 111.5, 45.6, 41.9.

HRMS (+ESI): Calculated: 235.1077 ($C_{12}H_{15}N_2O_3$). Observed: 235.1075.

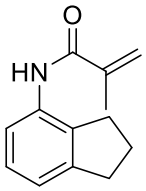

***N*-(2,3-dihydro-1*H*-inden-4-yl)methacrylamide (TRH 1-149)** (**18**)

To a solution 4-aminoindane (0.24 mL, 2.0 mmol) in dichloromethane (10 mL) was added methacryloyl chloride (0.23 mL, 2.4 mmol) followed by triethylamine (0.34 mL, 2.4 mmol) at 0˚C under an atmosphere of nitrogen. After stirring for 20 minutes, the reaction mixture was warmed to room temperature and stirred for an additional 3.5 hours. The reaction mixture was then washed twice with brine, dried over magnesium sulfate, and concentrated *in vacuo*. The resulting crude material was purified by silica gel chromatography (35% to 40% ethyl acetate in hexanes) to yield (**18**) (378 mg, 94%) as an off-white solid.

^{1}H NMR (400 MHz, $CDCl_3$): δ 7.72 (d, *J* = 8.0 Hz, 1H), 7.55 (s, 1H), 7.12 (t, *J* = 7.7 Hz, 1H), 7.01 (d, *J* = 7.4 Hz, 1H), 5.79 (s, 1H), 5.42 (s, 1H), 2.93 (t, *J* = 7.5 Hz, 2H), 2.79 (t, *J* =7.4 Hz, 2H), 7.12-2.06 (m, 2H), 2.04 (s, 3H).

^{13}C NMR (100 MHz, $CDCl_3$): δ 166.3, 145.1, 140.6, 134.5, 133.7, 127.0, 120.7, 119.8, 118.9, 33.1, 29.9, 24.7, 18.6.

HRMS (+ESI): Calculated: 202.1226 ($C_{13}H_{16}NO$). Observed: 202.1224.

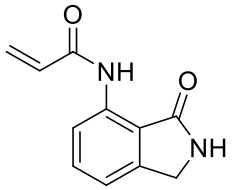

***N*-(3-oxoisoindolin-4-yl)acrylamide (TRH 1-152)** (**19**)

To a solution of 7-aminoisoindolin-1-one (99 mg, 0.67 mmol) in dichloromethane (4 mL) was added acryloyl chloride (0.07 mL, 0.8 mmol) followed by triethylamine (0.11 mL, 0.8 mmol) at 0˚ C under N_2 atmosphere. After stirring for 20 minutes, the reaction mixture was warmed to room temperature and stirred overnight. The reaction mixture was washed twice with brine, dried over magnesium sulfate, and concentrated *in vacuo*. The resulting crude material was purified by silica gel chromatography (50 to 60% ethyl acetate in hexanes) to afford the title compound (58 mg, 43%) as a white solid.

^{1}H NMR (400 MHz, $CDCl_3$): δ 10.50 (s, 1H), 8.58 (d, *J* = 8.2 Hz, 1H), 7.55 (t, *J* = 7.9 Hz, 1H), 7.15 (d, *J* = 7.5 Hz, 1H), 6.82 (s, 1H), 6.46 (dd, *J* = 1.3, 17.0 Hz, 1H), 6.36 (dd, *J* = 10.0, 17.0 Hz, 1H), 5.81 (dd, *J* = 1.3, 10.0 Hz, 1H), 4.46 (s, 2H).

^{13}C NMR (100 MHz, $CDCl_3$): δ 172.9, 164.2, 143.9, 138.2, 133.8, 131.8, 127.8, 118.0, 117.7, 117.6, 45.6.

HRMS (+ESI): Calculated: 203.0815 ($C_{11}H_{11}N_2O_2$). Observed: 203.0814.

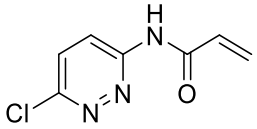

***N*-(6-chloropyridazin-3-yl)acrylamide (TRH 1-155)** (**20**)

To a solution 3-amino-6-chloropyridazine (261 mg, 2.0 mmol) in dichloromethane (10 mL) was added acryloyl chloride (0.20 mL, 2.4 mmol) followed by triethylamine (0.34 mL, 2.4 mmol) at 0˚C under an atmosphere of nitrogen. After stirring for 20 minutes, the reaction mixture was warmed to room temperature and stirred overnight. The solution was washed twice with brine, dried over magnesium sulfate, and concentrated *in vacuo*. The resulting crude material was purified by silica gel chromatography (40% to 50% ethyl acetate in hexanes) to yield **(20)** (23 mg, 6%) as a pale-yellow solid.

^{1}H NMR (400 MHz, $CDCl_3$): δ 10.06 (s, 1H), 8.70 (d, *J* = 9.4 Hz, 1H), 7.57 (d, *J* = 9.4 Hz, 1H), 6.73 (dd, *J* = 10.2, 16.8 Hz, 1H) 6.56 (dd, *J* = 1.2, 16.8, 1H), 5.94 (dd, *J* = 1.2, 10.2 Hz, 1H).

^{13}C NMR (100 MHz, $CDCl_3$): δ 164.8, 155.2, 152.3, 130.7, 130.4, 130.3, 122.0.

HRMS (+ESI): Calculated: 182.0127 ($C_7H_5N_3OCl$). Observed: 182.0126

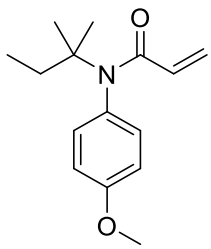

***N*-(4-methoxyphenyl)-*N*-(*tert*-pentyl)acrylamide (TRH 1-170)** (**21**)

To a solution of 4-methoxy-*N*-(*tert*-pentyl)aniline (94 mg, 0.49 mmol) in dichloromethane (5 mL) was added acryloyl chloride (0.05 mL, 0.6 mmol) followed by triethylamine (0.09 mL, 0.6 mmol) at 0˚C under an atmosphere of nitrogen. After stirring for 15 minutes, the reaction mixture was warmed to room temperature and stirred an additional 18 hours. The reaction mixture was then washed with saturated aqueous sodium bicarbonate solution, brine, dried over magnesium sulfate, and concentrated *in vacuo*. The resulting crude material was purified by silica gel chromatography (0% to 20% ethyl acetate in hexanes) to yield the title compound (82 mg, 68%) as a pale-yellow oil.
^{1}H NMR (400 MHz, $CDCl_3$): δ 6.99 (d, *J* = 8.7 Hz, 2H), 6.85 (d, *J* = 8.7 Hz, 2H), 6.17 (dd, *J* = 1.9, 16.7 Hz, 1H), 5.76 (dd, *J* = 10.3, 16.7 Hz, 1H), 5.28 (dd, *J* = 1.9, 10.3 Hz, 1H), 3.81 (s, 3H), 2.11 (q, *J* = 7.5 Hz, 2H), 1.20 (s, 6H), 0.91 (t, *J* = 7.5 Hz, 3H).
^{13}C NMR (100 MHz, $CDCl_3$): δ 166.3, 159.0, 134.3, 131.49, 131.45, 125.6, 114.1, 61.7, 55.5, 32.0, 27.4, 9.4.
HRMS (+ESI): Calculated: 247.1572 ($C_{15}H_{21}NO_2$). Observed: 247.1577.

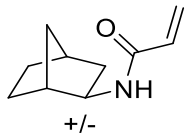

+/-

***N*-(*exo*-norborn-2-yl)acrylamide (TRH 1-176)** (**22**)
To a solution of *exo*-2-aminonorbornane (0.24 mL, 2 mmol) in dichloromethane (10 mL) was added acryloyl chloride (0.20 mL, 2.4 mmol) followed by triethylamine (0.33 mL, 2.4 mmol) at 0˚C under an atmosphere of nitrogen. After stirring for 20 minutes, the reaction mixture was warmed to room temperature and stirred for an additional 18 hours. The reaction mixture was then washed with saturated aqueous sodium bicarbonate solution, brine, dried over magnesium sulfate, and concentrated *in vacuo*. The resulting crude material was purified by silica gel chromatography (30% ethyl acetate in hexanes) to yield the title compound (271 mg, 82%) as a white solid.
^{1}H NMR (400 MHz, $CDCl_3$): δ 6.42 (s, 1H), 6.25 (dd, *J* = 2.3, 17.0 Hz, 1H), 6.18 (dd, *J* = 9.5, 17.0 Hz, 1H), 5.58 (dd, *J* = 2.3, 9.5 Hz, 1H), 3.8-3.77 (m, 1H), 2.27-2.24 (m, 2H), 1.78 (ddd, *J* = 2.1, 8.1, 13.0 Hz, 1H), 1.55-1.38 (m, 3H), 1.30-1.10 (m, 4H).
^{13}C NMR (100 MHz, $CDCl_3$): δ 165.0, 131.4, 125.8, 52.9, 42.4, 40.0, 35.7, 35.6, 28.2, 26.6.
HRMS (+EI): Calculated:165.1154 ($C_{10}H_{15}NO$). Observed: 165.1155.

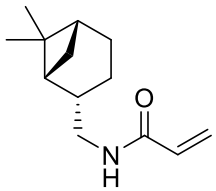

***N*-(((1*R*,2*S*,5*R*)-6,6-dimethylbicyclo[3.1.1]heptan-2-yl)methyl)acrylamide (TRH 1-178)** (**23**)
To a solution of (-)-*cis*-myrtanylamine (0.34 mL, 2 mmol) in dichloromethane (10 mL) was added acryloyl chloride (0.20 mL, 2.4 mmol) followed by triethylamine (0.33 mL, 2.4 mmol) at 0˚C under an atmosphere of nitrogen. After stirring for 20 minutes, the reaction mixture was warmed to room temperature and stirred for an additional 21 hours. The

reaction mixture was then washed with saturated aqueous sodium bicarbonate solution, brine, dried over magnesium sulfate, and concentrated *in vacuo*. The resulting crude material was purified by silica gel chromatography (20 to 30% ethyl acetate in hexanes) to yield the title compound (369 mg, 89%) as a white solid.
^{1}H NMR (600 MHz, $CDCl_3$): δ 6.26 (dd, *J* = 1.5, 17.0 Hz, 1H), 6.11 (dd, *J* = 10.3, 17.0 Hz, 1H) 5.85 (s, 1H), 5.61 (dd, *J* = 1.5, 10.3 Hz, 1H), 3.39-3.29 (m, 2H), 2.38-2.34 (m, 1H), 2.26-2.21 (m, 1H), 1.98-1.90 (m, 4H), 1.88-1.83 (m, 1H), 1.53-1.47 (m, 1H), 1.19 (s, 3H), 1.04 (s, 3H), 0.89 (d, *J* = 9.6 Hz, 1H).
^{13}C NMR (150 MHz, $CDCl_3$): δ 165.7, 131.2, 126.2, 45.3, 43.9, 41.5, 38.8, 33.3, 28.1, 26.1, 23.3, 19.9.
HRMS (-ESI): Calculated: 206.1550 ($C_{13}H_{20}NO$). Observed: 206.1551.

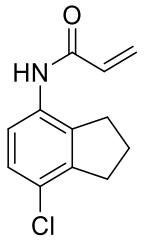

N-(7-chloro-2,3-dihydro-1H-inden-4-yl)acrylamide (YP 1-1) (**24**)
A solution of *N*-(2,3-dihydro-1H-inden-4-yl)acrylamide (187 mg, 1.0 mmol) in PEG 400 (5.2 mL) was cooled to 0˚C and *N*-chlorosuccinimide (140 mg, 1.0 mmol) added. After 30 minutes, the mixture was warmed to room temperature and stirred overnight. The reaction mixture was diluted with ethyl acetate, washed with brine twice, and dried over magnesium sulfate. The volatiles were removed *in vacuo* and the crude product purified by silica gel chromatography (30% ethyl acetate in hexanes). The obtained mixture of isomers were recrystallized to afford the title compound (47 mg, 22% yield) as a white solid.
^{1}H NMR (400MHz, $CDCl_3$): δ 7.78 (d, *J* = 8.8 Hz, 1H), 7.15-7.11 (m, 2H), 6.42 (dd, *J* = 1.4, 16.8 Hz, 1H), 6.26 (dd, *J* = 10.2, 16.8 Hz, 1H), 5.77 (dd, *J* = 1.4, 10.2 Hz, 1H), 2.98 (t, *J* = 7.6 Hz, 2H), 2.87 (t, *J* = 7.5 Hz, 2H), 2.12 (quint, *J* = 7.5 Hz, 2 H).
^{13}C NMR (100MHz, $CDCl_3$): δ 163.4, 143.1, 136.1, 132.2, 131.0, 128.0, 127.2, 126.7, 120.9, 32.7, 31.1, 24.0.
HRMS (+ESI): Calculated: 220.0535 ($C_{12}H_{11}ClNO$). Observed: 220.0533.

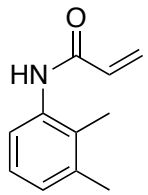

N-(2,3-dimethylphenyl)acrylamide (YP 1-18) (**25**)
A solution of 2,3-dimethylaniline (121 mg, 1.0 mmol) in DCM (10 mL) was cooled to 0˚C and acryloyl chloride (109 mg, 1.2 mmol) and triethylamine (121 mg, 1.2 mmol) were added sequentially. The reaction mixture was maintained at this temperature for 30 minutes and then warmed to room temperature and stirred overnight. The reaction

mixture was washed twice with brine and dried over magnesium sulfate. Volatiles were removed *in vacuo* and the crude material purified by silica gel chromatography (30% to 40% ethyl acetate in hexanes) to afford the product (154 mg, 88%) as a white solid.
^{1}H NMR (400MHz, $CDCl_3$): δ 7.49 (d, *J* = 7.9 Hz, 1H), 7.29 (s, 1H), 7.11-7.07 (m, 1H), 7.01 (d, *J* = 7.7, 1H) 6.40 (d, *J* = 17.1, 1H), 6.30 (dd, *J* = 7.3, 17.1 Hz, 1H), 5.74 (d, *J* = 10.1 Hz, 1H), 2.29 (s, 1H), 2.13 (s, 1H).
^{13}C NMR (100MHz, $CDCl_3$): δ 135.1, 131.2, 127.6, 127.3, 125.9, 122.3, 20.6, 13.9.
HRMS (+ESI): Calculated: 176.1070 ($C_{11}H_{14}NO$). Observed: 176.1068.

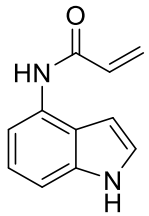

N-(1H-indol-4-yl)acrylamide (YP 1-19) (**26**)
A solution of 4-aminoindole (132 mg, 1 mmol) in DCM/DMF (1:1 *v:v*, 10 mL) was cooled to 0˚C and acryloyl chloride (109 mg, 1.2 mmol) and triethylamine (121 mg, 1.2 mmol) added sequentially. The reaction mixture was stirred at this temperature for 26 minutes and then warmed to room temperature and stirred overnight. The reaction mixture was washed twice with brine and dried over magnesium sulfate. Volatiles were removed *in vacuo* and the crude product purified by basic alumina chromatography (60% to 75% ethyl acetate in hexanes) to afford the title compound (56mg, 30%) as a white-grey solid.
^{1}H NMR (600MHz, MeOD): δ 7.51 (d, *J* = 7.6 Hz, 1H), 7.24-7.22 (m, 2H), 7.08 (t, *J* = 7.6 Hz, 1H), 6.64 (dd, *J* = 10.1, 16.7 Hz, 2H), 6.38 (dd, *J* = 1.7, 16.9 Hz, 1H), 5.78 (dd, *J* = 1.7, 10.3 Hz, 1H), 4.6 (s, 1H).
^{13}C NMR (150MHz, MeOD): δ 165.0, 137.2, 131.1, 129.2, 126.0, 123.8, 121.5, 120.9, 112.2, 108.4, 98.5.
HRMS (+ESI): Calculated: 187.0866 ($C_{11}H_{11}N_2O$). Observed: 187.0865.

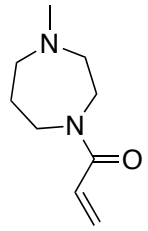

1-(4-methyl-1,4-diazepan-1-yl)prop-2-en-1-one (YP 1-23) (**27**)
A solution of 1-methylhomopiperazine (114 mg, 1.0 mmol) in DCM (10 mL) was cooled to 0˚C and acryloyl chloride (109 mg, 1.2 mmol) and triethylamine (121 mg, 1.2 mmol) added sequentially. The solution was maintained at this temperature for 30 minutes and then warmed to room temperature and stirred overnight. The reaction mixture was washed twice with brine and dried over magnesium sulfate. After removal of the volatiles in *vacuo*, the crude product was purified via silica gel chromatography (1% to 10%

methanol in DCM) affording the title compound (58 mg, 51%) as a yellow oil (mixture of rotamers)
^{1}H NMR (400MHz, $CDCl_3$): δ 6.61-6.53 (m, 1H), 6.35-6.29 (m, 1H), 5.70-5.66 (m, 1H), 3.74-3.72 (m, 1 H), 3.69 (t, *J* = 6.4 Hz, 1H), 3.65-3.61 (m, 2H), 2.66-2.63 (m, 2H), 2.59-2.54 (m, 2H), 2.37 (s, 3H), 1.94 (quint, *J* = 6.2 Hz, 2H).
^{13}C NMR (100MHz, $CDCl_3$): δ 166.4, 166.3, 128.0, 127.9, 127.8, 127.6, 59.1, 58.0, 57.1, 56.8, 47.4, 47.1, 46.7, 46.6, 45.3, 44.8, 28.1, 26.9.
HRMS (+ESI): Calculated: 169.1335 ($C_9H_{17}N_2O$). Observed: 169.1333.

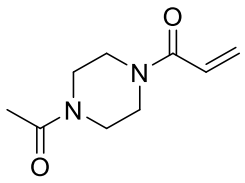

1-(4-acetylpiperazin-1-yl)prop-2-en-1-one (YP 1-24) (**28**)
A solution of 1-acetylpiperazine (128 mg, 1.0 mmol) in DCM (10 mL) was cooled to 0˚C and acryloyl chloride (109 mg, 1.2 mmol) and triethylamine (121 mg, 1.2 mmol) added sequentially. The solution was stirred at this temperature for 23 minutes and then warmed to room temperature and stirred an additional two hours. The reaction mixture was washed twice with brine, dried over magnesium sulfate, and the volatiles removed *in vacuo*. The crude material was purified via silica gel chromatography (0% to 10% methanol in DCM) to afford the title compound (40 mg, 18%) as a yellow oil.
^{1}H NMR (400MHz, $CDCl_3$): δ 6.57 (dd, *J* = 10.5, 16.8 Hz, 1H), 6.33 (dd, *J* = 1.8, 16.8 Hz, 1H), 5.75 (dd, *J* = 1.9, 10.5 Hz, 1H), 3.72 (s, 1H), 3.66-3.64 (m, 3H), 3.57 (s, 1H), 3.51-3.49 (m, 2H), 2.13 (s, 3H).
^{13}C NMR (100MHz, $CDCl_3$): δ 169.0, 165.6, 128.7, 127.0, 41.9, 41.4, 21.4.
HRMS (+ESI): Calculated: 183.1128 ($C_9H_{15}N_2O_2$). Observed: 183.1126.

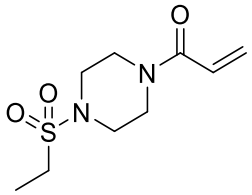

1-(4-(Ethylsulfonyl)piperazin-1-yl)prop-2-en-1-one (YP 1-25) (**29**)
A solution of 1-(ethanesulfonyl)piperazine (178 mg, 1.0 mmol) in DCM (10 mL) was cooled to 0 ˚C and acryloyl chloride (109 mg, 1.2 mmol) and triethylamine (121 mg, 1.2 mmol) added sequentially. The solution was stirred at this temperature for 27 minutes and then warmed to room temperature and stirred for an additional two hours. The solution was washed twice with brine and dried over magnesium sulfate. The crude material was purified by silica gel chromatography (1% to 10% methanol in DCM) to afford the title compound (163 mg, 70%) as a white-yellow solid.
^{1}H NMR (400MHz, $CDCl_3$): δ 6.57 (dd, *J* = 10.5, 16.8 Hz, 1H), 6.32 (dd, *J* = 1.9, 16.8 Hz, 1H), 5.76 (dd, *J* = 1.8, 10.5 Hz, 1H), 3.77 (s, 2H), 3.67 (s, 2H), 3.32 (t, *J* = 5.2 Hz, 4H), 2.98 (q, *J* = 7.5 Hz, 2H), 1.37 (t, *J* = 7.4, 3H).
^{13}C NMR (100MHz, $CDCl_3$): δ 165.5, 128.8, 127.0, 77.4, 45.9, 45.6, 44.2, 41.9, 7.8.

HRMS (+ESI): Calculated: 233.0954 ($C_9H_{17}N_2O_3S_1$). Observed: 233.0953.

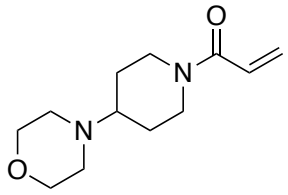

1-(4-morpholinopiperidin-1-yl)prop-2-en-1-one (YP 1-42) (**30**)
Following **General Procedure A** using 4-morpholinopiperidine (336 mg, 2.0 mmol), the product was obtained after silica gel chromatography (1% methanol and 80% ethyl acetate in hexanes) as a colorless oil (259 mg, 58%).
^{1}H NMR (400MHz, $CDCl_3$): δ 6.42 (dd, *J* = 10.6, 16.8 Hz, 1H), 6.06 (dd, *J* = 2.0, 16.8 Hz, 1H), 5.49 (dd, *J* = 2.0, 10.6 Hz, 1H), 4.45 (d, *J* = 12.8 Hz, 1H), 3.86 (d, *J* = 12.8 Hz, 1H), 3.52 (t, *J* = 4.7 Hz, 4H), 2.90 (t, *J* = 12.8 Hz, 1H), 2.55-2.48 (m, 1H), 2.37-2.35 (m, 4H), 2.26 (tt, *J* = 3.7, 11.0 Hz, 1H), 1.72 (d, *J* = 12.8 Hz, 2H), 1.30-1.20 (m, 2H).
^{13}C NMR (100MHz, $CDCl_3$): δ 165.0, 127.7, 127.3, 67.1, 61.6, 49.6, 44.9, 41.1, 28.9, 27.8.
HRMS (+ESI): Calculated: 225.1598 ($C_{12}H_{21}N_2O_2$). Observed: 225.1595.

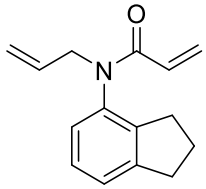

N-allyl-N-(2,3-dihydro-1H-inden-4-yl)acrylamide (IGA 1-12) (**31**)
To a solution of sodium hydride (96 mg, 4.0 mmol) in tetrahydrofuran (8 mL) was added *N*-(2,3-dihydro-1H-inden-4-yl)acrylamide (187 mg, 1.0 mmol) in tetrahydrofuran (2 mL) under an atmosphere of nitrogen. The reaction mixture was cooled to 0°C and 3-bromoprop-1-ene (484 mg, 4.0 mmol) was and the mixture warmed to room temperature and stirred overnight. The reaction was quenched by the addition of water and extracted with ethyl acetate. The crude product was purified by silica gel chromatography (20% ethyl acetate in hexanes) to afford the product (151 mg, 67%) as a yellow crystalline solid.
^{1}H NMR (400MHz, $CDCl_3$): δ 7.06-7.18 (m, 2H), 6.80-6.88 (m, 1H), 6.26-6.37 (dd, *J* = 16.8, 2.0 Hz, 1H), 5.76-5.96 (m, 2H), 5.38-5.48 (dd, *J* = 10.3, 2.1 Hz, 1H), 4.98-5.08 (m, 2H), 4.40-4.52 (ddt, *J* = 14.5, 6.3, 1.3 Hz, 1H), 4.00-4.11 (ddt, *J* = 14.5, 6.8, 1.2 Hz, 1H), 2.82-2.98 (m, 2H), 2.59-2.79 (m, 2H), 1.92-2.07 (m, 2H).
^{13}C NMR (100MHz, $CDCl_3$): δ 165.1, 146.5, 142.4, 137.9, 133.0, 128.4, 127.8, 127.48, 126.1, 124.3, 118.1, 51.6, 33.3, 30.9, 25.0.
HRMS (+ESI): Calculated: 228.13 ($C_{15}H_{17}NO$). Observed: 228.1381.

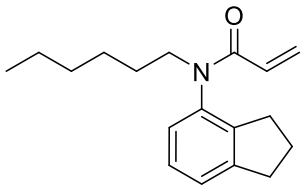

N-allyl-N-(2,3-dihydro-1H-inden-4-yl)acrylamide (IGA 1-15) (**32**)

To a solution of sodium hydride (96 mg, 4.0 mmol) in tetrahydrofuran (8 mL) was added *N*-(2,3-dihydro-1H-inden-4-yl)acrylamide (187 mg, 1.0 mmol) in tetrahydrofuran (2 mL) under an atmosphere of nitrogen. The solution was cooled to 0°C and 1-bromohexane (660 mg, 4.0 mmol) was added after which point the solution was warmed to room temperature and stirred overnight. The solution was quenched with water and extracted with ethyl acetate. The crude product was purified via silica gel chromatography (20% ethyl acetate in hexanes) to afford the product in 34% yield as a yellow oil (92 mg).
^{1}H NMR (400MHz, $CDCl_3$): δ 7.11-7.25 (m, 2H), 6.86-6.96 (dd, *J* = 7.5, 1.2 Hz, 1H), 6.30-6.40 (dd, *J* = 16.8, 2.1 Hz, 1H), 5.86-6.00 (m, 1H), 5.41-5.51 (dd, *J* = 10.3, 2.1 Hz, 1H), 3.82-3.96 (m, 1H), 3.42-3.56 (m, 1H), 2.90-3.04 (m, 2H), 2.65-2.85 (m, 2H), 1.98-2.16 (m, 2H), 1.47-1.63 (m, 2H), 1.20-1.36 (m, 6H), 0.80-0.90 (m, 3H).
^{13}C NMR (100MHz, $CDCl_3$): δ 165.2, 146.5, 142.4, 138.2, 128.6, 127.5, 127.4, 126.1, 124.1, 48.7, 33.3, 31.6, 30.9, 27.9, 26.7, 25.0, 22.6, 14.1.
HRMS (+ESI): Calculated: 272.19 ($C_{18}H_{25}NO$). Observed: 272.2007.

Chapter 3 Supplementary Information
Supplementary Figures

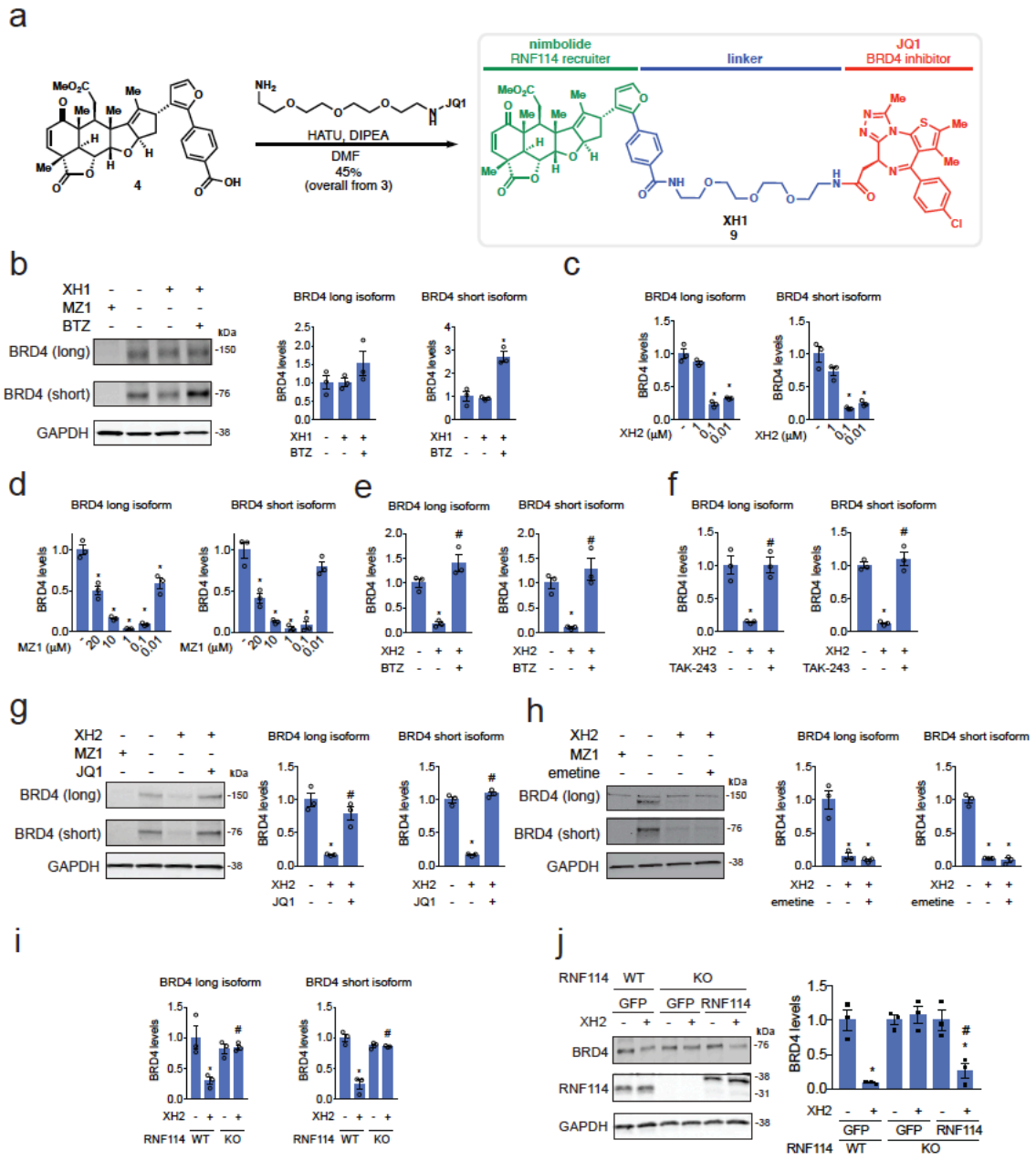

Supplementary Figure 3.1. Characterization of nimbolide-based degraders.
(a) Synthetic route for XH1 degrader. **(b)** BRD4 levels in 231MFP breast cancer cells pre-treated with DMSO vehicle or proteasome inhibitor bortezomib (1 μM) for 30 min prior to and also during XH1 treatment (100 nM) for 12 h, assessed by Western blotting alongside GAPDH loading control. **(c-f)** Shown in **(c, d, e, f)** are quantification for experiments in **Fig. 3.1c, d, e,** and **f. (g, h)** BRD4 levels in 231MFP breast cancer cells pre-treated with DMSO vehicle, JQ1 (1 μM) **(g)**, or emetine (75 μM) **(h)** for 30 min prior to and also during XH2 treatment (100 nM) for 12 h, assessed by Western blotting alongside a GAPDH

loading control. **(i)** Quantification for experiments shown in **Fig. 5h. (j)** Effect of DMSO vehicle or XH2 (100 nM) treatment for 12 h on BRD4 expression in HAP1 RNF114 wild-type and knockout cells transiently transfected with GFP control or wild-type Flag-tagged RNF114. BRD4, RNF114, and GAPDH expression were assessed by Western blotting. Data were normalized to DMSO vehicle controls for each group. Gels shown in **(b, g, h,** and **j)** are representative images. Data shown in **(b-j)** are average ± sem from n=3 biologically independent samples/group. Statistical significance was calculated with unpaired two-tailed Student's t-tests. Significance is expressed as:

*p=0.00231 for BRD4 short isoform XH1/BTZ group compared to vehicle-treated control groups in **(b);** *p=0.000665, 0.000902 for BRD4 long isoform 0.1 and 0.01 μM, respectively, and *p=0.0019925, 0.00303 for BRD4 short isoform 0.1 and 0.01 μM, respectively, compared to vehicle-treated control groups in **(c)**; *p=0.00400, 0.000187, $9.81x10^{-5}$, 0.000129, 0.01 for BRD4 long isoform for 20, 10, 1, 0.1, 0.01 μM, respectively, and *p=0.00673, 0.000902, 0.000666, 0.00104 for BRD4 short isoform for 20, 10, 1, 0.1 μM, respectively, compared to vehicle-treated control groups in **(d);** *p=0.00098186 and p=0.0169 for XH2 compared to vehicle-treated control groups for BRD4 long and short isoforms, respectively, in **(e)**; *p=0.00174, $2.55x10^{-5}$ for XH2-treated groups compared to vehicle treated groups for BRD4 long and short isoforms, respectively, in **(f)**; *p=0.00143, $6.23x10^{-5}$ for XH2-treated groups compared to vehicle treated groups for BRD4 long and short isoforms, respectively, in **(g)**; *p=0.00246, 0.00171 for XH2- and XH2/emetine-treated groups, respectively, compared to vehicle treated groups for BRD4 long isoform, and *p=$3.47x10^{-5}$, $5.71x10^{-5}$ for XH2- and XH2/emetine-treated groups, respectively, compared to vehicle treated groups for BRD4 short isoform in **(h)**; *p=0.0236, 0.00165 for WT XH2-treated groups compared to WT control groups for BRD4 long and short isoforms, respectively, in **(i);** *p=0.00344 for WT GFP/XH2 groups compared WT GFP vehicle-treated control group and *p=0.0154 for KO RNF114/XH2 groups compared to KO RNF114 vehicle-treated control groups in **(j);** #p=0.00197 and 0.00557 for XH2/BTZ groups compared to XH2-treated groups for BRD4 long and short isoforms, respectively, in **(e)**; #p=0.000817 and 0.000437 for XH2/TAK-243 groups compared to XH2-treated groups for BRD4 long and short isoforms, respectively, in **(f)**; #p=0.00389 and $1.21x10^{-5}$ for XH2/JQ1 groups compared to XH2-treated groups for BRD4 long and short isoforms, respectively, in **(g)**; #p=0.00166, 0.00159 for KO XH2-treated groups compared to WT XH2-treated groups for BRD4 long and short isoforms, respectively, in **(i)**; #p=0.00814 for KO RNF114/XH2-treated groups compared to KO GFP/XH2-treated groups in **(j).**

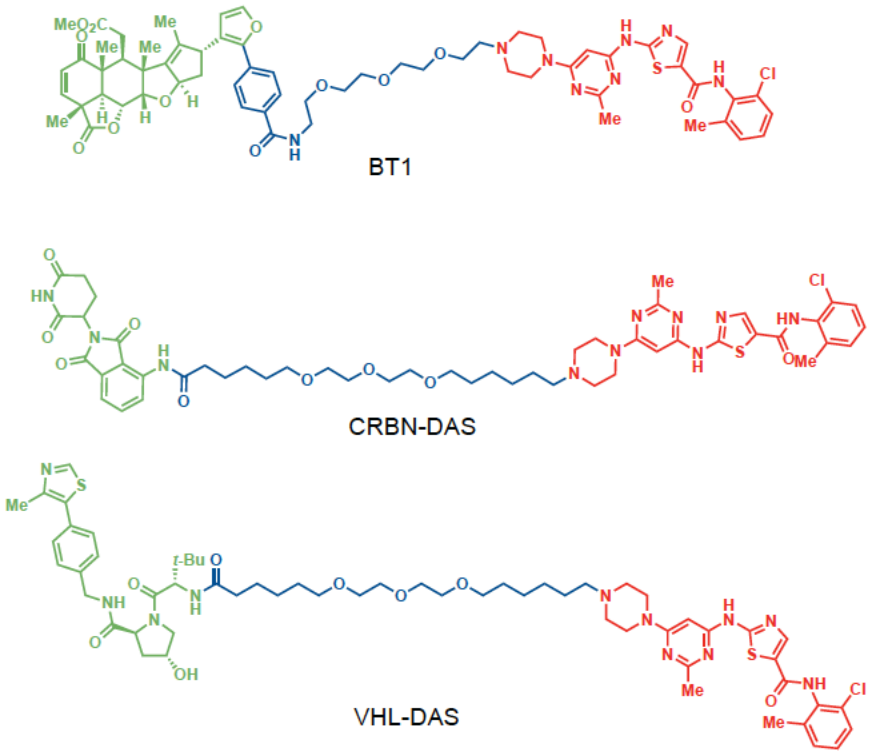

Supplementary Figure 3.2. Structures of BT1, CRBN-dasatinib, and VHL-dasatinib. This figure is related to **Figure 3.4.**

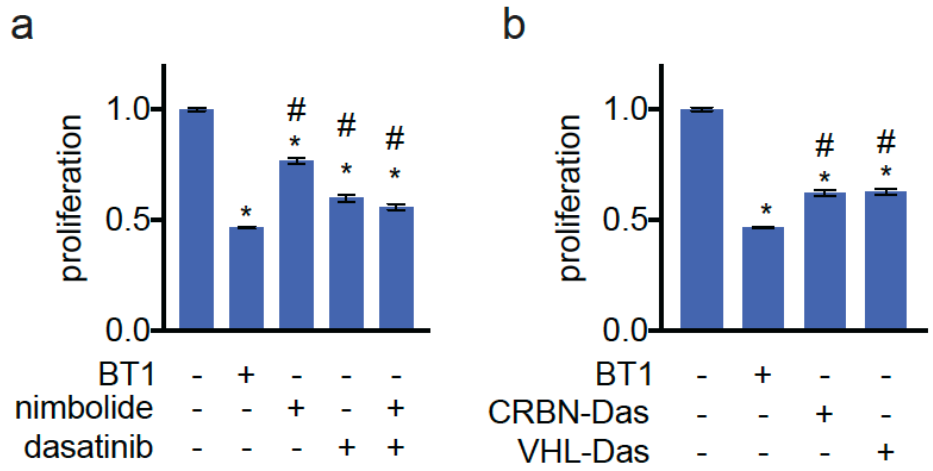

Supplementary Figure 3.3. Anti-proliferative benefit of BT1 treatment.
Cell proliferation of K562 cells treated with DMSO vehicle, BT1, dasatinib, nimbolide, nimbolide and dasatinib combined, CRBN-dasatinib, or VHL-dasatinib for 24 h at 1 μM. Data are from n=6-18 biological replicates/group. Statistical significance is expressed as *p<0.05 compared to vehicle-treated control for each group, #p<0.05 compared to BT1 treatment group.

Synthetic Methods and Characterization

General Procedures

Unless otherwise noted, all reactions were performed in flame-dried glassware under positive pressure of nitrogen or argon. Air- and moisture-sensitive liquids were transferred via syringe. Dry dichloromethane, *N*,*N*-Dimethylformamide and tetrahydrofuran were obtained by passing these previously degassed solvents through activated alumina columns. Organic Neem leaf powder from Organic Veda™ (16 Oz. can, https://www.organicveda.com/neem-leaf-powder.htm?product_id=83) was purchased through Amazon.com. *N*-(2-Chloro-6-methylphenyl)-2-[(6-chloro-2-methyl-4-pyrimidinyl)amino]-5-thiazolecarboxamide was purchased from Combi-Blocks Inc. All reagents were used as received from commercial sources, unless stated otherwise. Reactions were monitored by thin layer chromatography (TLC) on TLC silica gel 60 F_{254} glass plates (EMD Millipore) and visualized by UV irradiation and staining with *p*-anisaldehyde, phosphomolybdic acid, or Ninhydrin. Volatile solvents were removed under reduced pressure using a rotary evaporator. Flash column chromatography was performed using Silicycle F60 silica gel (60Å, 230-400 mesh, 40-63 μm). Proton nuclear magnetic resonance (^{1}H NMR) and carbon nuclear magnetic resonance (^{13}C NMR) spectra were recorded on Bruker AV-600 and AV-700 spectrometers operating at 600 and 700 MHz for ^{1}H NMR, and 151 and 176 MHz for ^{13}C NMR. Chemical shifts are reported in parts per million (ppm) with respect to the residual solvent signal $CDCl_3$ (^{1}H NMR: δ 7.26; ^{13}C NMR: δ 77.16), CD_2Cl_2 (^{1}H NMR: δ 5.32; ^{13}C NMR: δ 53.84), $(CD_3)_2CO$ (^{1}H NMR: δ 2.05; ^{13}C NMR: δ 29.84), $(CD_3)_2SO$ (^{1}H NMR: δ 2.50; ^{13}C NMR: δ 39.52). Peak multiplicities are reported as follows: *s* = singlet, *d* = doublet, *t* = triplet, *dd* = doublet of doublets, *tt* = triplet of triplets, *m* = multiplet, *br* = broad signal. IR spectra were recorded on a Bruker Vertex 80 FTIR spectrometer. High-resolution mass spectra (HRMS) were obtained by the QB3/chemistry mass spectrometry facility at the University of California, Berkeley using a Thermo LTQ-FT mass spectrometer with electrospray ionization (ESI) technique. Microwave reactions were performed in a Biotage Initiator EXP microwave reactor.

Supplementary Procedure 1. Isolation of nimbolide from commercial neem leaf powder

Initial Extraction. To a 3 L round bottom flask containing 1 lb. (~450 g) of Organic Veda™ neem leaf powder and a large stir bar was added 1.5 L of anhydrous methanol and the resulting suspension was stirred for 12 hours at room temperature in a fumehood with the lights off. The mixture was then filtered through a short pad of Celite® (typically in 5 portions for faster filtering, filtration takes >1 hour) and the solid was washed with additional methanol until the Celite® layer was white colored (see SI-figure 1B). The filtrate was concentrated *in vacuo* at 30 °C to provide a dark green oil which was partitioned between EtOAc (500 mL) and water (300 mL). The phases were separated, and the aqueous layer was extracted with additional EtOAc (250 mL). The combined organic layers were washed with a mixture of saturated aqueous $NaHCO_3$ and $Na_2S_2O_3$ (9:1 v/v, 250 mL), dried over Na_2SO_4 and concentrated *in vacuo* to afford a dark green oil. Thin layer chromatographic (TLC) analysis of this mixture is shown in SI-Figure 1D.

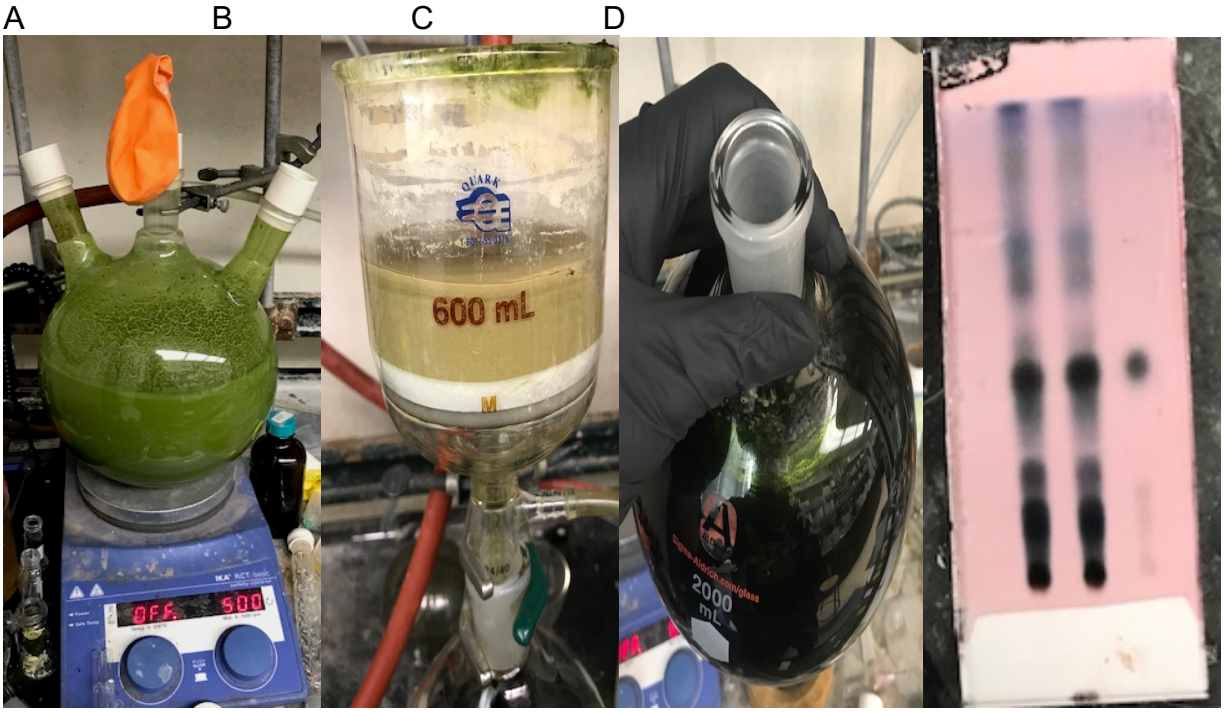

SI-Figure 1. Initial extraction step of nimbolide from neem leaf powder. A) extraction set-up. B) completed filtration through celite. C) crude residue obtained. D) Thin layer chromatographic analysis (50:50 EtOAc/Hexane, *p*-anisaldehyde stain) of the crude residue. Pure nimbolide is shown in the far-right lane, unpurified mixture in the left lane, and a co-spot in the center lane.

First Column Chromatography. The dark green oil was purified by silica gel flash column chromatography according to the following procedure. A column of silica gel (7 cm diameter X 25 cm height) was packed and flushed with hexanes/EtOAc/Et_3N (75:25:1 v/v/v). Next, 100 mL of hexanes was loaded on the top and a solution of the green residue

in 50 mL of EtOAc was loaded mixing with the neat hexanes layer. The column was eluted using the following gradient: Hexanes/EtOAc 75:25 (1 L), 65:35 (1 L), 60:40 (2 L), 55:45 (2.5 L). At the end of 75:25 gradient, a yellow fraction elutes, and during the 60:40 elution a dark blue fraction emerges (NOTE: Neem powder from other brands sometimes does not contain this blue pigment). Nimbolide elutes at the tail end of the blue fraction. After removal of the solvent *in vacuo*, crude nimbolide is obtained as a dark green solid or thick oil, the TLC analysis of which is shown in SI-Figure 2D.

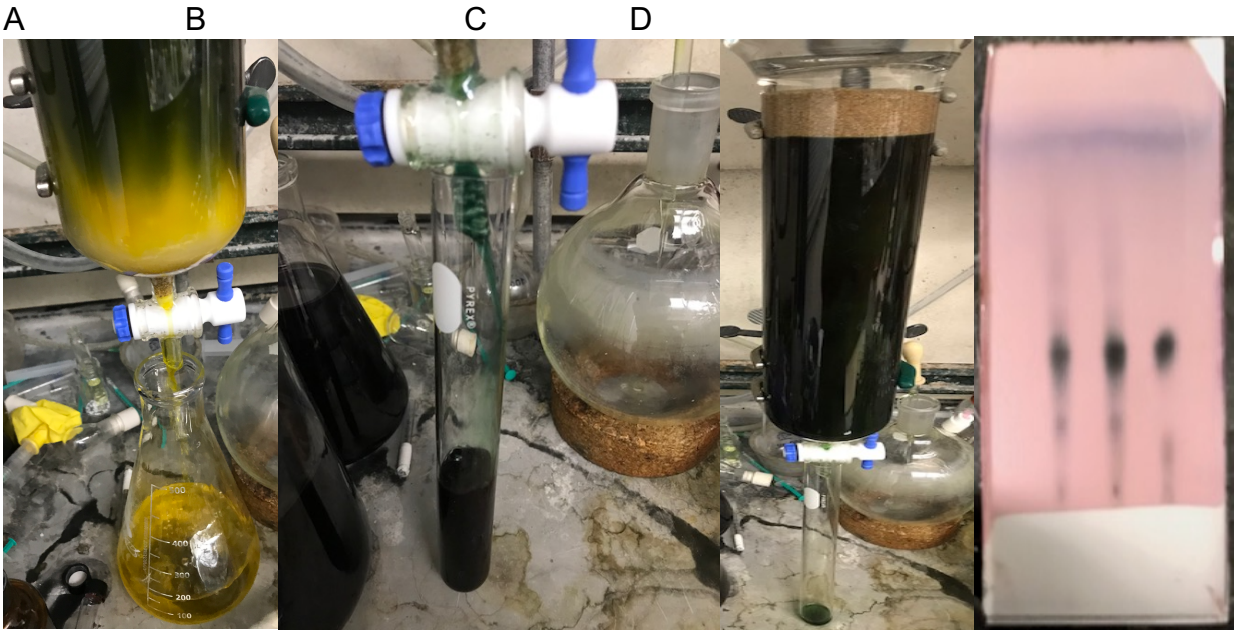

SI-Figure 2. Initial chromatographic event. A) Elution of the yellow fraction. B) elution of the blue fraction C) final column color (dark green). D) Thin layer chromatographic analysis (50:50 EtOAc/Hexane, *p*-anisaldehyde stain) of the combined nimbolide-containing fractions. Pure nimbolide is shown in the far-right lane, the column purified material in the left lane, and a co-spot in the center lane.

Second Column Chromatography: A column of silica gel (7 cm of diameter X 20 cm height) was packed and flushed with CH_2Cl_2/Et_3N (100:1 v/v). Next, a solution of the green residue obtained after the 1st column in 25 mL of CH_2Cl_2 was loaded on the top. The column was eluted with the following gradient: CH_2Cl_2 (800 mL) CH_2Cl_2/acetone 60:1 (600 mL), 50:1 (1 L), 45:1 (2 L), 40:1 (3 L). Note that the green pigment should not move during this chromatographic event. After combining the fractions that contained nimbolide (as determined by TLC) and removal of solvent *in vacuo*, nimbolide is obtained as a dark brown solid, the TLC analysis of which is shown in SI-Figure 3C.

A B C

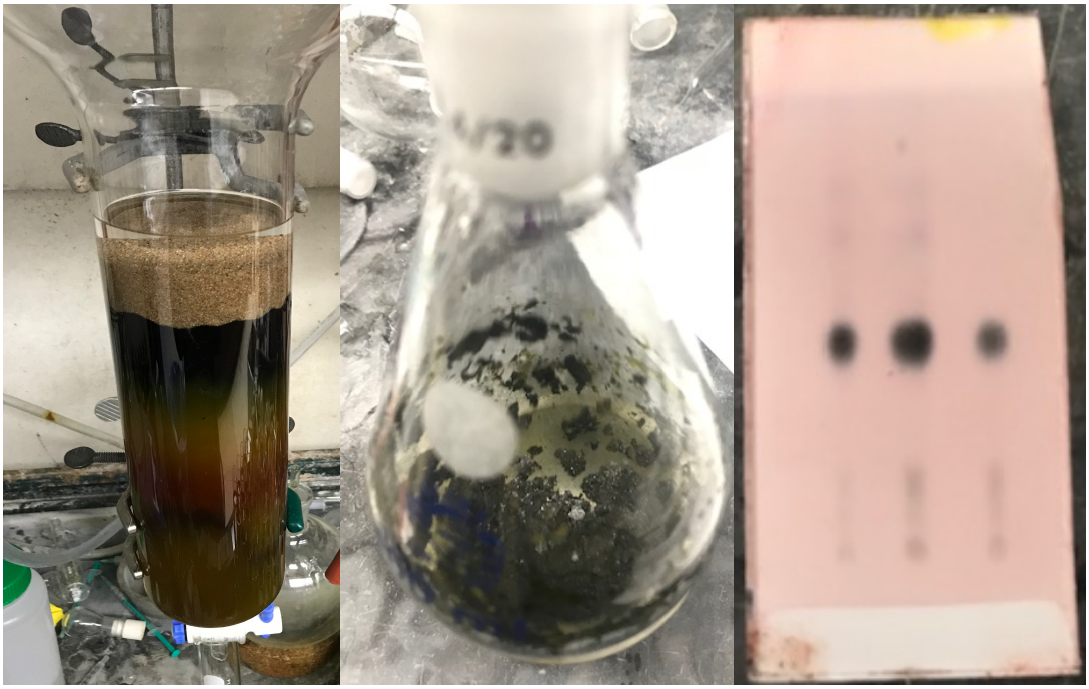

SI-Figure 3. Second chromatographic event. A) Column at the end of the elution. B) nimbolide obtained. C) Thin layer chromatographic analysis (50:50 EtOAc/Hexane, *p*-anisaldehyde stain) of the crude residue. Pure nimbolide is shown in the far-right lane, the column purified material in the left lane, and a co-spot in the center lane.

Trituration to obtain analytically pure nimbolide. The dark brown solid obtained after the 2nd column was diluted with 3 mL of CH_2Cl_2, followed by the addition of 20 mL of pentane. A brown solid precipitated out of solution and the liquid phase was removed by pipette. The solid was triturated 2 additional times in the same way (3 mL of CH_2Cl_2 then 20 mL of pentane) to furnish nimbolide as a white solid. A range of 1.1 g – 1.3 g of pure nimbolide was isolated using this procedure. No attempts were made to further purify the mother liquor which still contains significant quantities of nimbolide.

A B C

D E F

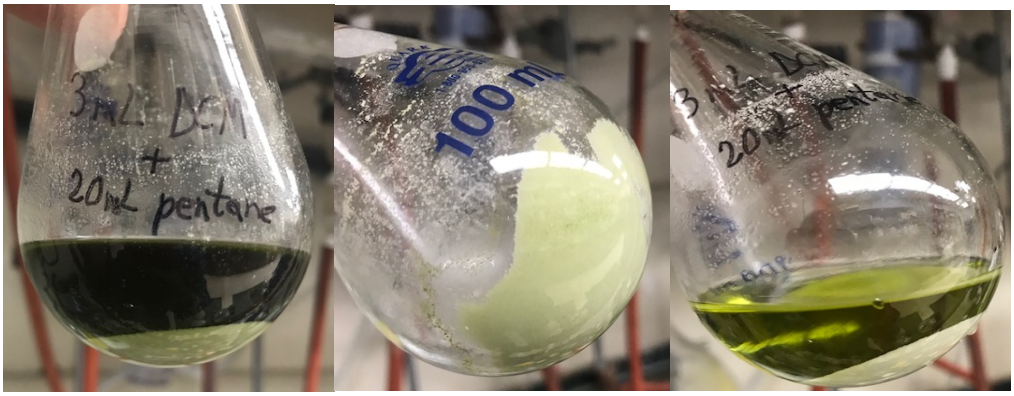

G H

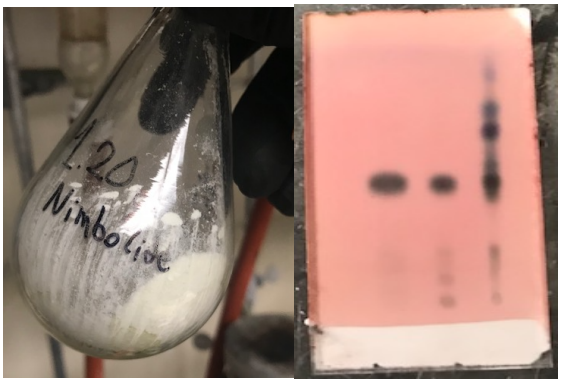

SI-Figure 4. Final trituration process. A) nimbolide in 3 ml of DCM. B) solid formed after addition of 20 ml of pentane. C) Removal of solvent from first trituration. D-F) final two triturations. G) Final pure nimbolide obtained. H) Thin layer chromatographic analysis (50:50 EtOAc/Hexane, *p*-anisaldehyde stain) of the trituration process. The final, pure nimbolide obtained is shown in the far-left lane, an authentic standard in the middle lane, and the mother liquor is shown in the far-right lane.

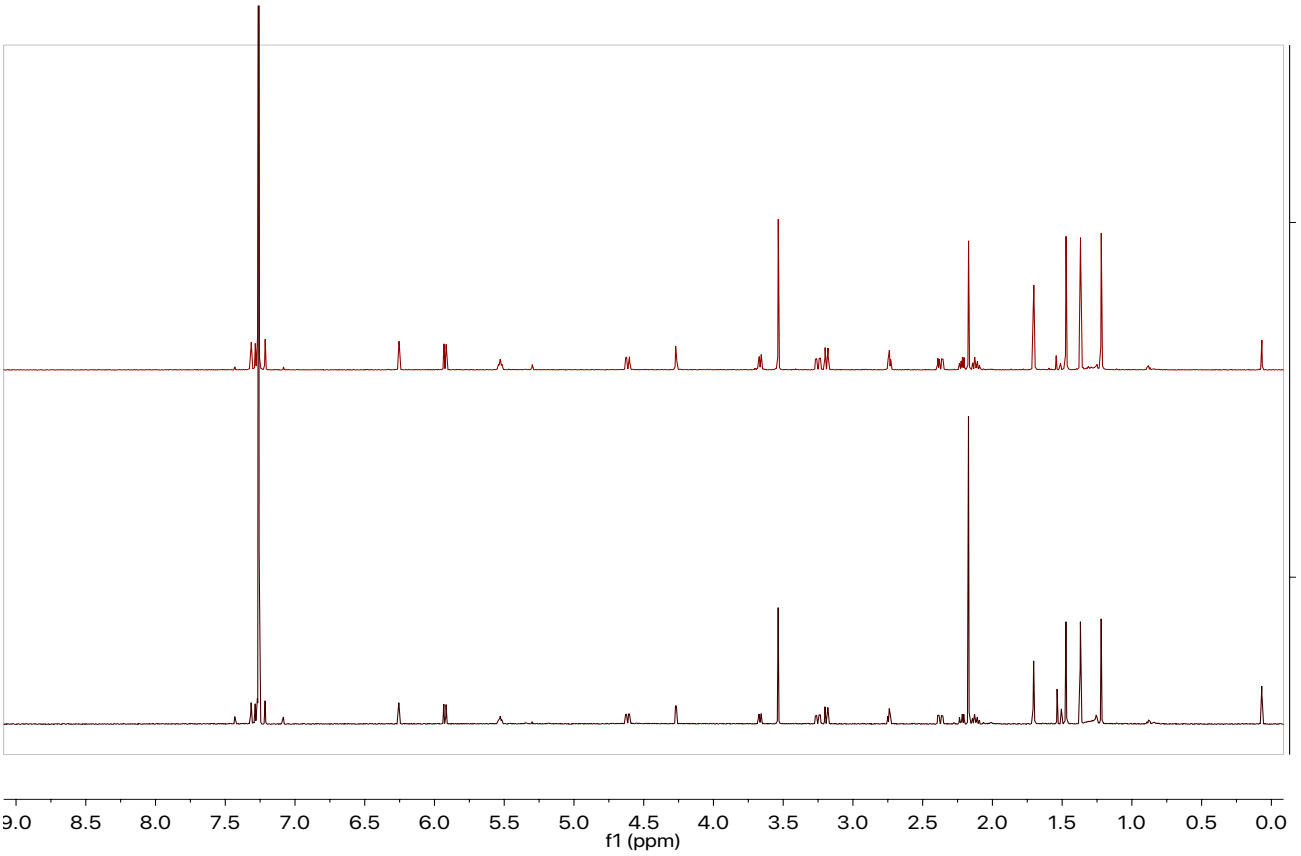

SI-Figure 5. 600 MHz ^{1}H NMR Comparison of nimbolide in $CDCl_3$. (Top) Material obtained using the extraction protocol reported herein. (Bottom) Commercial nimbolide obtained from Sigma. (NOTE: nimbolide is quite acid sensitive and the $CDCl_3$ used was stored over K_2CO_3 prior to use).

Synthesis and Characterization of Nimbolide-Dasatinib degraders BT1 and BT2

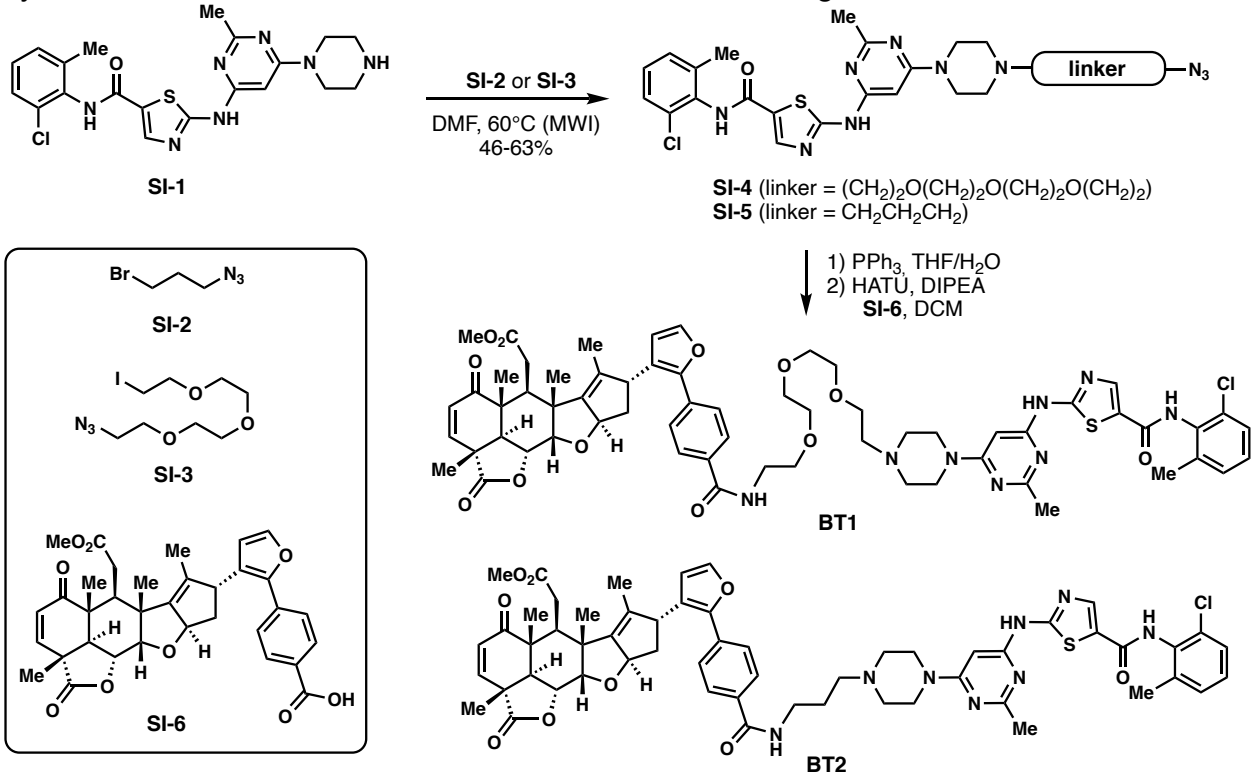

Scheme SI-1. Synthesis of nimbolide-dasatinib based degraders BT1 and BT2.

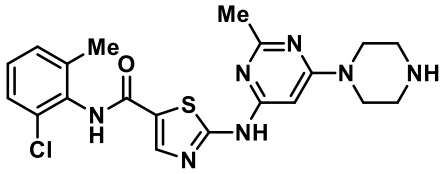

Compound SI-1: This compound was synthesized according to the procedure reported by Veach and coworkers.[1] (*J. Med. Chem.* 2007, *50*, 5853-5857)

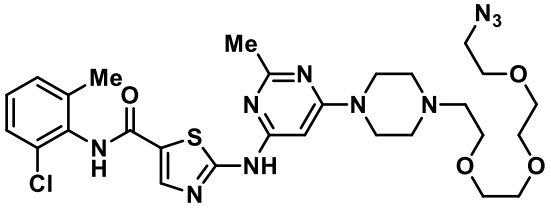

Compound SI-4: A 5 mL microwave tube equipped with a magnetic stir bar was charged with compound SI-1 (111 mg, 0.25 mmol, 1 equiv), DMF (1.5 mL), DIPEA (65.0 µL, 0.375 mmol, 1.5 equiv) and iodide SI-3 (51 □L, 0.25 mmol, 1.0 equiv). The tube was sealed and placed in a microwave reactor. The microwave reaction was performed at 60 °C for 1 h. After cooling to room temperature, the reaction mixture was transferred to a 50 mL round-bottom flask and the volatiles were remove under high vacuum. The remaining white solid was purified by column chromatography (CH_2Cl_2:MeOH = 95:5 to 93:7) to afford SI-4 (101 mg, 63% yield) as a white solid: ^{1}H NMR (600 MHz, CD_3OD) δ 8.15 (s, 1H), 7.35 (d, *J* = 7.2 Hz, 1H), 7.30 – 7.18 (m, 2H), 6.02 (s, 1H), 3.72 – 3.62 (m, 16H), 3.37 (t, *J* = 4.8 Hz, 2H), 2.70 (t, *J* = 5.4 Hz, 2H), 2.68 (br, 4H), 2.48 (s, 3H), 2.32 (s, 3H); ^{13}C NMR (151 MHz, CD_3OD) δ 167.5, 165.3, 164.5,

163.3, 158.6, 142.2, 140.4, 134.4, 134.3, 130.1, 129.5, 128.3, 126.8, 83.9, 71.7 (two resonances), 71.6, 71.4, 71.2, 69.4, 58.7, 54.1, 51.8, 44.7, 25.6, 18.7; IR (thin film) vmax 3182, 3061, 2925, 2870, 2094, 1718, 1616, 1536, 1189, 1144, 1010, 952, 781 cm^{-1}; HRMS (ESI) *calcd.* for $[C_{28}H_{38}O_4N_{10}ClS]^+$ ($[M+H]^+$) *m/z* 645.2481, found: 645.2476.

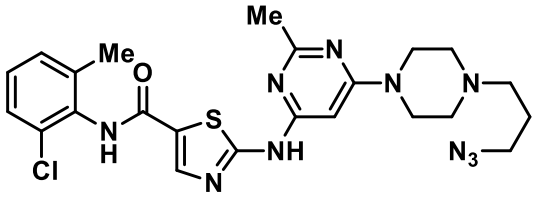

Compound SI-5: A 30 mL microwave tube equipped with a magnetic stir bar was charged with compound SI-1 (533 mg, 1.20 mmol, 1 equiv), DMF (12 mL), DIPEA (0.418 mL, 2.4 mmol, 2 equiv) and bromide SI-2 (0.178 mL, 1.44 mmol, 1.2 equiv). The tube was sealed and placed in the microwave reactor. The microwave reaction was performed at 60 °C for 1.5 h. After cooling to room temperature, the reaction mixture was transferred into a 100 mL round-bottom flask and the DMF and other volatiles were removed *in vacuo*. The resulting white solid was then suspended in CH_2Cl_2/MeOH (90:10 v/v), passed through a short column of silica gel and eluted with CH_2Cl_2/MeOH (90:10). The resulting solution was concentrated *in vacuo* to afford the crude product, which was further purified by column chromatography (CH_2Cl_2:MeOH = 95:5) to yield SI-5 (290 mg, 46% yield) as a white solid: ^{1}H NMR (600 MHz, $(CD_3)_2SO$) δ 11.47 (s, 1H), 9.88 (s, 1H), 8.22 (s, 1H), 7.40 (d, *J* = 7.7 Hz, 1H), 7.33 – 7.22 (m, 2H), 6.05 (s, 1H), 3.51 (br, 4H), 3.39 (t, *J* = 6.7 Hz, 2H), 2.43 (br, 4H), 2.40 (s, 3H), 2.38 (t, *J* = 6.9 Hz, 2H), 2.24 (s, 3H), 1.73 (p, *J* = 6.8 Hz, 2H); ^{13}C NMR (151 MHz, $(CD_3)_2SO$) δ 165.2, 162.6, 162.4, 159.9, 156.9, 140.8, 138.8, 133.5, 132.4, 129.0, 128.1, 127.0, 125.7, 82.6, 54.6, 52.2, 48.9, 43.6, 25.61, 25.58, 18.3; IR (thin film) vmax 3205, 3060, 2938, 2847, 2093, 1715, 1621, 1536, 1182, 1142, 998, 862 cm^{-1}; HRMS (ESI) *calcd* for $[C_{23}H_{28}ON_{10}ClS]^+$ ($[M+H]^+$): *m/z* 527.1851, found: 527.1850.

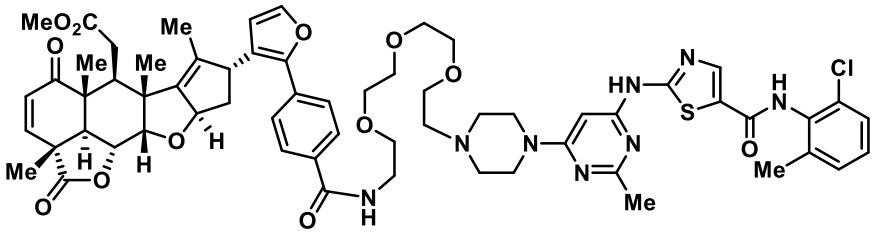

Degrader BT1: *i.* To a 10 mL reaction tube was added SI-4 (10.6 mg, 0.0164 mmol, 1.0 equiv), triphenylphosphine (8.6 mg, 0.033 mmol, 2.0 equiv), THF (0.6 mL) and H_2O (0.06 mL). The resulting solution was heated in a 50 °C oil bath for 12 hours. After full consumption of the starting material was indicated by TLC, all the volatiles in the reaction mixture was removed by rotary evaporation at 60 °C. The resulting crude pale-yellow solid containing the primary amine was further dried under high vacuum for 12 hours before being subjected to the next step.

ii. To a separate 10 mL reaction tube was added acid SI-6 (0.016 mmol, 1.0 equiv),[2] HATU (6.1 mg, 0.016 mmol, 1.0 equiv), DIPEA (5.6 µL, 0.032 mmol, 2.0 equiv) and CH_2Cl_2 (0.4 mL). After stirring at room temperature for 10 hours, the reaction was quenched with saturated *aq*. NH_4Cl and extracted with CH_2Cl_2 (3 × 1 mL). The combined organic layer was dried over Na_2SO_4 and concentrated *in vacuo*. The resulting activated

ester was then transferred into the reaction tube containing the crude primary amine, DIPEA (5.6 μL, 0.032 mmol, 2.0 equiv) and CH_2Cl_2 (0.4 mL). The reaction mixture was allowed to stir at room temperature for 12 hours before quenching with saturated aq. NH_4Cl. The layers were separated, and the aqueous phase was extracted with CH_2Cl_2 (3×1 mL). The combined organic layer was dried over Na_2SO_4 and concentrated *in vacuo*. The residue was purified by column chromatography (7% MeOH/CH_2Cl_2 with 0.2% Et_3N) to afford degrader BT1 (10.5 mg, 54% yield) as a colorless oil which slowly solidifies. ^{1}H NMR (600 MHz, $(CD_3)_2CO$) δ 10.38 (br, 1H), 9.03 (br, 1H), 8.20 (s, 1H), 8.03 (d, *J* = 8.4 Hz, 2H), 7.83 (br, 1H), 7.67 (d, *J* = 8.4 Hz, 2H), 7.56 (d, *J* = 1.8 Hz, 1H), 7.34 (d, *J* = 7.7 Hz, 1H), 7.30 (d, *J* = 9.7 Hz, 1H), 7.28 – 7.20 (m, 2H), 6.45 (d, *J* = 1.8 Hz, 1H), 6.17 (s, 1H), 5.88 (d, *J* = 9.7 Hz, 1H), 5.51 (ddd, *J* = 8.6, 3.6, 1.8 Hz, 1H), 5.00 (dd, *J* = 12.4, 3.7 Hz, 1H), 4.28 (d, *J* = 3.6 Hz, 1H), 4.20 (d, *J* = 9.0 Hz, 1H), 3.68 (t, *J* = 5.7 Hz, 2H), 3.64 – 3.55 (m, 16H), 3.62 (s, 3H), 3.26 (dd, *J* = 16.7, 5.4 Hz, 1H), 3.12 (d, *J* = 12.5 Hz, 1H), 2.78 (t, *J* = 5.4 Hz, 1H), 2.55 (br, 6H), 2.48 (dd, *J* = 16.7, 5.4 Hz, 1H), 2.44 (s, 3H), 2.33 (s, 3H), 2.24 (ddd, *J* = 12.0, 8.6, 8.4 Hz, 1H), 2.18 (dd, *J* = 12.0, 6.9 Hz, 1H), 1.68 (d, *J* = 1.5 Hz, 3H), 1.50 (s, 3H), 1.44 (s, 3H), 1.30 (s, 3H); ^{13}C NMR (151 MHz, $(CD_3)_2CO$) δ 201.6, 176.1, 173.9, 167.1, 166.6, 163.9, 160.9, 158.2, 150.7, 149.0, 147.4, 143.3, 141.5, 140.1, 136.4, 134.7, 134.6, 134.2, 133.5, 131.5, 129.8, 128.9, 128.7, 128.5, 127.8, 127.4, 126.4, 125.6, 113.2, 88.7, 84.0, 83.4, 74.1, 71.3, 71.2, 71.08, 71.06, 70.3, 70.1, 58.5, 54.0, 51.9, 51.5, 50.5, 49.1, 46.3, 44.8, 44.7, 41.9, 41.90, 40.6, 32.8, 25.9, 18.9, 18.7, 17.2, 15.2, 13.4; IR (thin film) vmax 3385, 2923. 2852, 1733, 1611,1563, 1449, 1417, 1290, 1197, 1117, 824, 714 cm^{-1}; HRMS (ESI) *calcd* for $[C_{62}H_{72}O_{12}N_8ClS]^+$ ($[M+H]^+$): *m/z* 1187.4673, found: 1187.4663.

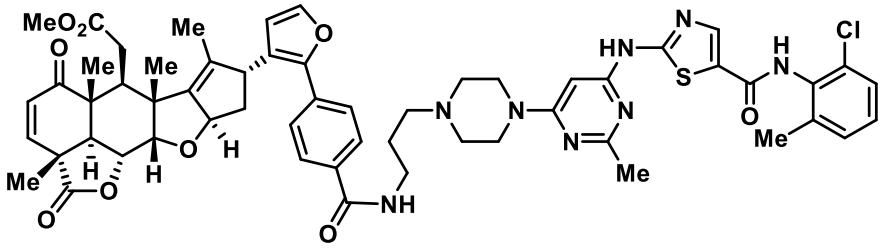

Degrader BT2: *i.* To a 10 mL reaction tube was added SI-5 (14.8 mg, 0.0281 mmol, 1.0 equiv), triphenylphosphine (14.7 mg, 0.056 mmol, 2.0 equiv), THF (1.0 mL) and H_2O (0.1 mL). The resulting solution was heated in a 50 °C oil bath for 12 hours. After fully consumption of the starting material was indicated by TLC, all the volatiles in the reaction mixture was removed by rotary evaporation at 60 °C. The resulting crude pale-yellow solid containing the primary amine was further dried under high vacuum overnight before being subjected to the next step.

ii. To another 10 mL reaction tube was added acid SI-6 (0.0261 mmol, 0.93 equiv), HATU (9.6 mg, 0.025 mmol, 0.9 equiv), DIPEA (9.8 □L) and CH_2Cl_2 (0.6 mL). After stirring at room temperature for 1 hour, this reaction mixture was transferred via syringe into the reaction tube containing the crude primary amine and CH_2Cl_2 (0.2 mL). The resulting mixture was stirred for 12 hours before quenching with saturated aq. NH_4Cl. The layers were separated, and the aqueous phase was extracted with CH_2Cl_2 (3×1 mL). The combined organic layer was dried over Na_2SO_4 and concentrated *in vacuo*. The residue

was purified by column chromatography (5% MeOH/CH_2Cl_2 with 0.2% Et_3N), followed by HPLC to afford degrader BT2 (7.8 mg, 26% yield) as a colorless oil which slowly solidifies. ^{1}H NMR (600 MHz, $(CD_3)_2CO$) δ 9.06 (br, 1H), 8.25 (br, 1H), 8.20 (br, 1H), 7.97 (d, *J* = 8.4 Hz, 2H), 7.66 (d, *J* = 8.4 Hz, 2H), 7.55 (d, *J* = 1.7 Hz, 1H), 7.34 (d, *J* = 7.6 Hz, 1H), 7.30 (d, *J* = 9.7 Hz, 1H), 7.28 – 7.20 (m, 2H), 6.43 (d, *J* = 1.8 Hz, 1H), 6.18 (s, 1H), 5.87 (d, *J* = 9.7 Hz, 1H), 5.49 (t, *J* = 7.2 Hz, 1H), 4.98 (dd, *J* = 12.5, 3.6 Hz, 1H), 4.26 (d, *J* = 3.6 Hz, 1H), 4.14 (t, *J* = 4.8 Hz, 1H), 3.67 (br, 4H), 3.61 (s, 3H), 3.58 – 3.47 (m, 2H), 3.24 (dd, *J* = 16.5, 5.1 Hz, 1H), 3.10 (d, *J* = 12.4 Hz, 1H), 2.76 (t, *J* = 5.4 Hz, 1H), 2.63 (br, 6H), 2.46 (s, 3H), 2.45 (dd, *J* = 16.5, 5.5 Hz, 1H), 2.33 (s, 3H), 2.17 (dd, *J* = 7.4, 5.1 Hz, 2H), 1.88 (quint, *J* = 6.0 Hz, 2H), 1.63 (d, *J* = 1.3 Hz, 3H), 1.50 (s, 3H), 1.39 (s, 3H), 1.28 (s, 3H); ^{13}C NMR (151 MHz, $(CD_3)_2CO$) δ 201.6, 176.1, 173.9, 166.8, 166.7, 164.0, 160.9, 158.2, 150.8, 149.0, 147.3, 143.3, 141.4, 140.1, 136.4, 134.62, 134.59, 134.52, 133.5, 131.5, 129.8, 128.9, 128.5, 128.5, 127.8, 127.5, 126.4, 125.6, 113.2, 88.7, 83.9, 83.5, 74.1, 57.6, 53.6, 51.9, 51.5, 50.5, 49.1, 46.2, 44.7, 44.6, 41.91, 41.88, 39.8, 32.8, 26.5, 25.9, 18.9, 18.7, 17.2, 15.3, 13.3; IR (thin film) ν_{max} 3252, 2923, 2853, 1781, 1735, 1611, 1577, 1508, 1463, 1416, 1290, 1198, 851, 750 cm^{-1}; HRMS (ESI) *calcd.* for $[C_{57}H_{62}O_9N_8ClS]^+$ ($[M+H]^+$): *m/z* 1069.4044, found: 1069.4047.

Chapter 4.2 Supplementary Information
Supplementary Figures

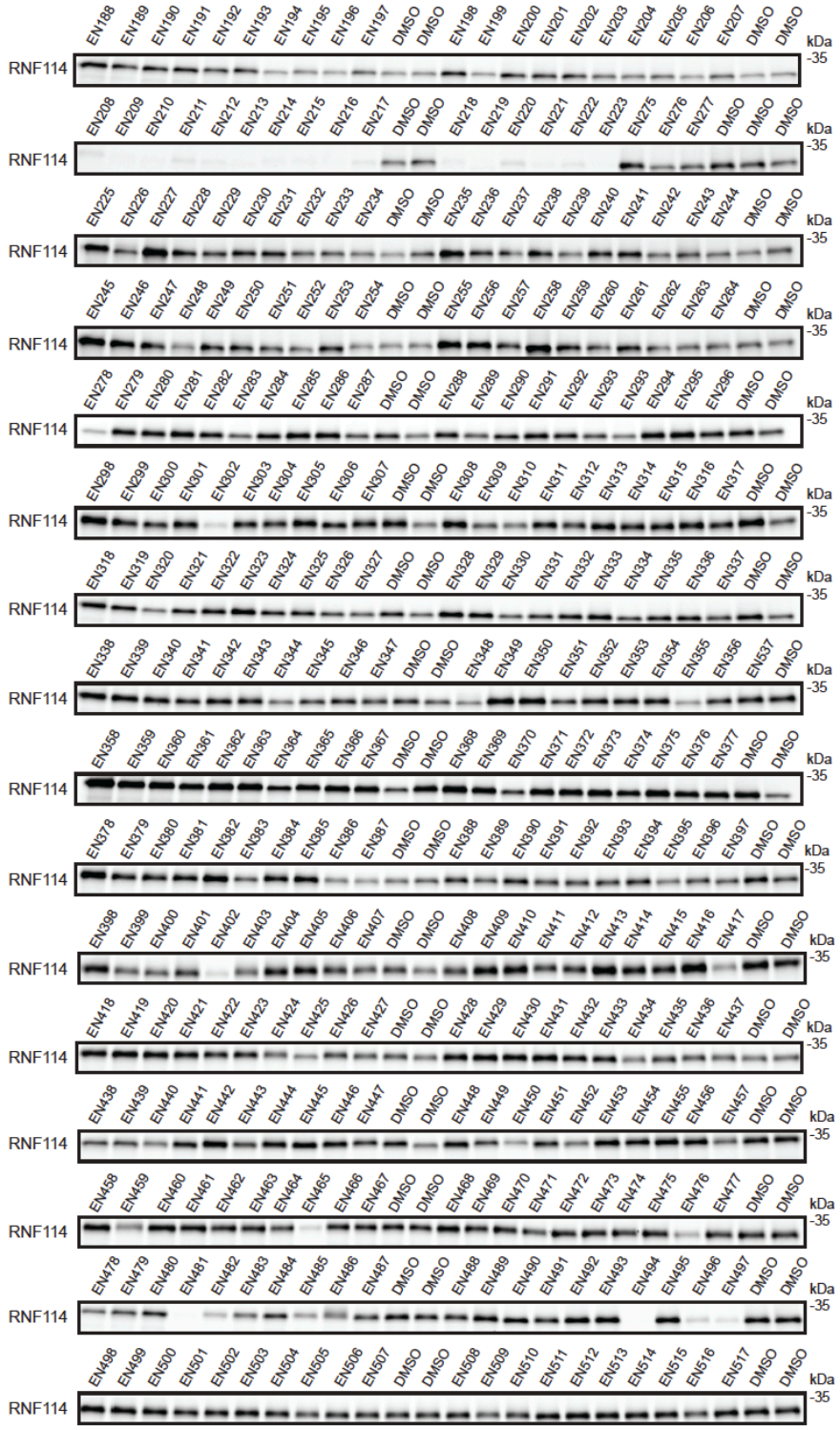

Supplementary Figure 4.2.1. Gel-based ABPP assay for screening covalent ligands against IA-rhodamine probe binding to pure RNF114 protein.

Related to Figure 4.2.2. Loss of fluorescence indicates covalent ligand binding to a cysteine on RNF114. DMSO vehicle or covalent ligands (50 μM) were pre-incubated with pure RNF114 protein (0.1 μg) for 30 min prior to addition of IA-rhodamine (100 nM) for 30 min at room temperature. Proteins were separated by SDS/PAGE and in-gel fluorescence was quantified. The structures of all the compounds screened can be found in **Table S1.**

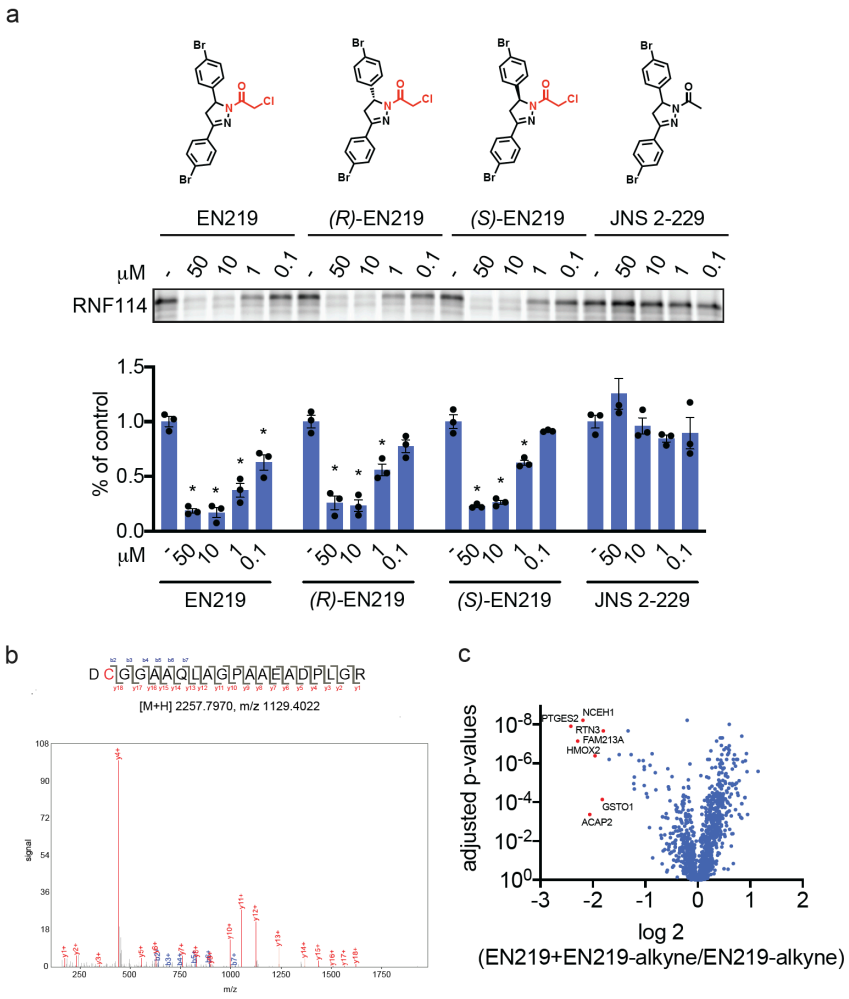

Supplementary Figure 4.2.2. EN219 reactivity with RNF114 pure protein and TMT-based quantitative proteomic profiling of EN219-alkyne-enriched targets in 231MFP cells.

Related to Figure 4.2.2. **(a)** Dose-response of racemic EN219, *(R)*-EN219, *(S)*-EN219, and non-reactive analog JNS 2-229 interactions with RNF114 by competitive gel-based ABPP. DMSO vehicle or ligands were pre-incubated with pure RNF114 protein (0.1 μg) for 30 min prior to addition of IA-rhodamine (100 nM) for 30 min at room temperature. Proteins were separated by SDS/PAGE and in-gel fluorescence was quantified. Gels shown in **(a)** are representative of n=3 biological replicates/group and bar graphs show average ± sem and individual replicate values from quantitation of IA-rhodamine labeling.

Statistical significance was calculated with unpaired two-tailed Student's t-test and is expressed as *p<0.05 compared to vehicle-treated controls. **(b)** Pure RNF114 protein was incubated with EN219 (50 μM) for 1 h and subsequent tryptic digests of RNF114 protein were analyzed by LC-MS/MS to look for EN219 covalent modification. The Cysteine 8 highlighted in red was found to be modified. Shown is the mass spectra of the EN219 covalent adduct on the RNF114 tryptic peptide. **(c)** 231MFP cells were treated with DMSO vehicle or EN219 (20 μM) 30 min prior to treating cells with DMSO or EN219-alkyne probe (2 μM) for 90 min. Resulting cell lysates were subjected to CuAAC with biotin-azide to append a biotin enrichment handle onto EN219-alkyne labeled proteins *ex situ*. EN219-alkyne labeled proteins were subsequently avidin-enriched, digested with trypsin, and resulting tryptic peptides from each treatment group were labeled with TMT reagents and combined and fractionated for LC-MS/MS analysis. Shown are average TMT ratios and adjusted p-values comparing EN219 pre-treated EN219-alkyne labeled groups to EN219-alkyne labeled groups to identify EN219-alkyne-labeled proteins that are competed by the parent compound EN219. Shown in red are proteins that show EN219+EN219-alkyne versus EN219-alkyne ratios <0.33 with adjusted p<0.05. The full dataset can be found in **Supplementary Dataset 5.**

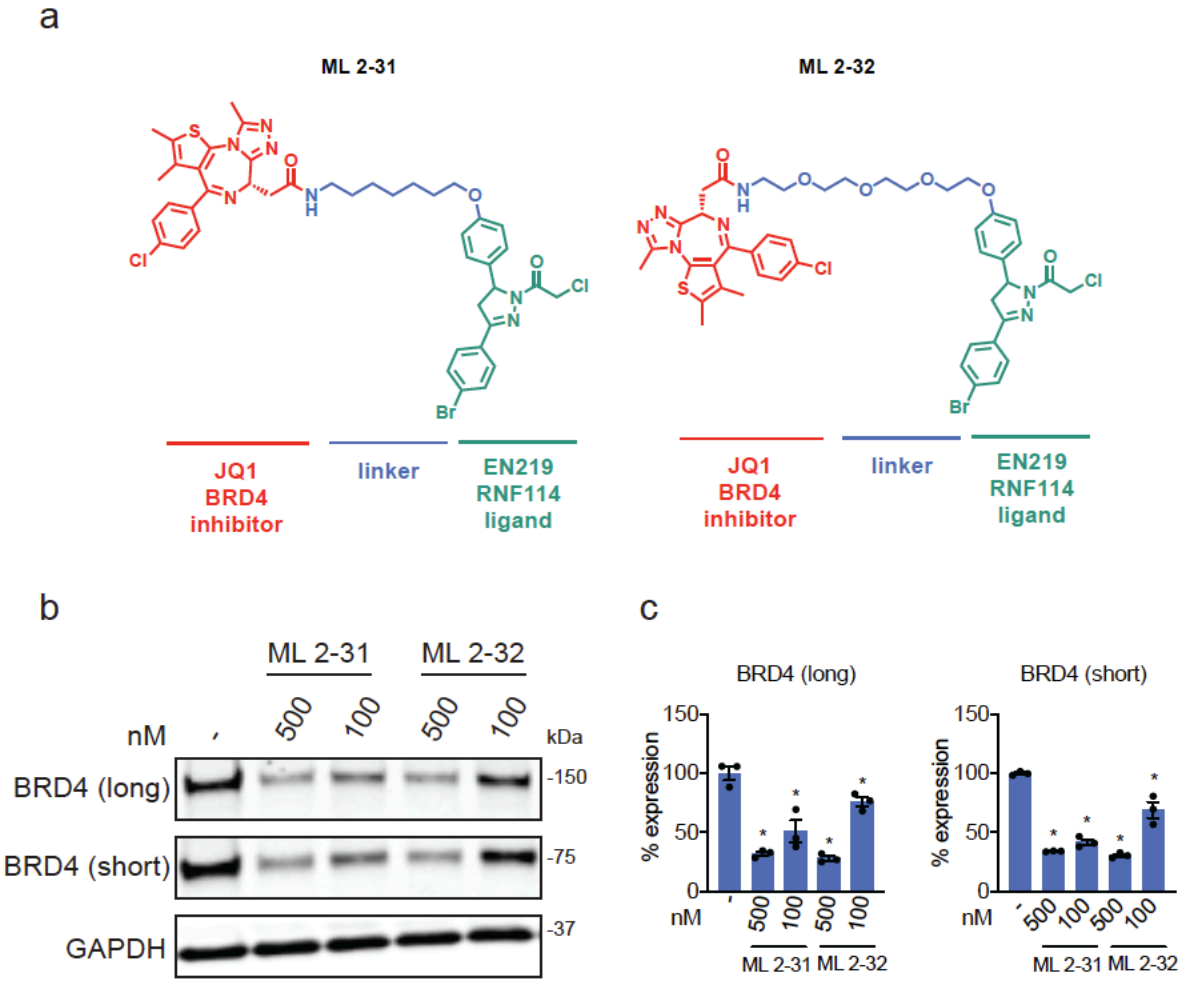

Supplementary Figure 4.2.3. EN219-based BRD4 degraders.
Related to Figure 4.2.3. **(a)** Structure of ML 2-31 and ML 2-32, EN219-based BRD4 degraders linking EN219 to BET inhibitor JQ1 with two different linkers. **(b)** Degradation of BRD4 by ML 2-31 and ML 2-32. 231MFP cells were treated with DMSO vehicle or ML 2-31 or ML 2-32 for 8 h and the long and short isoforms of BRD4 and loading control GAPDH were detected by Western blotting. **(c)** Percentage of BRD4 degradation quantified from **(b)**. Data shown in **(c)** are average and individual replicate values. Blots shown in **(b)** are representative of n=3 biological replicates/group.

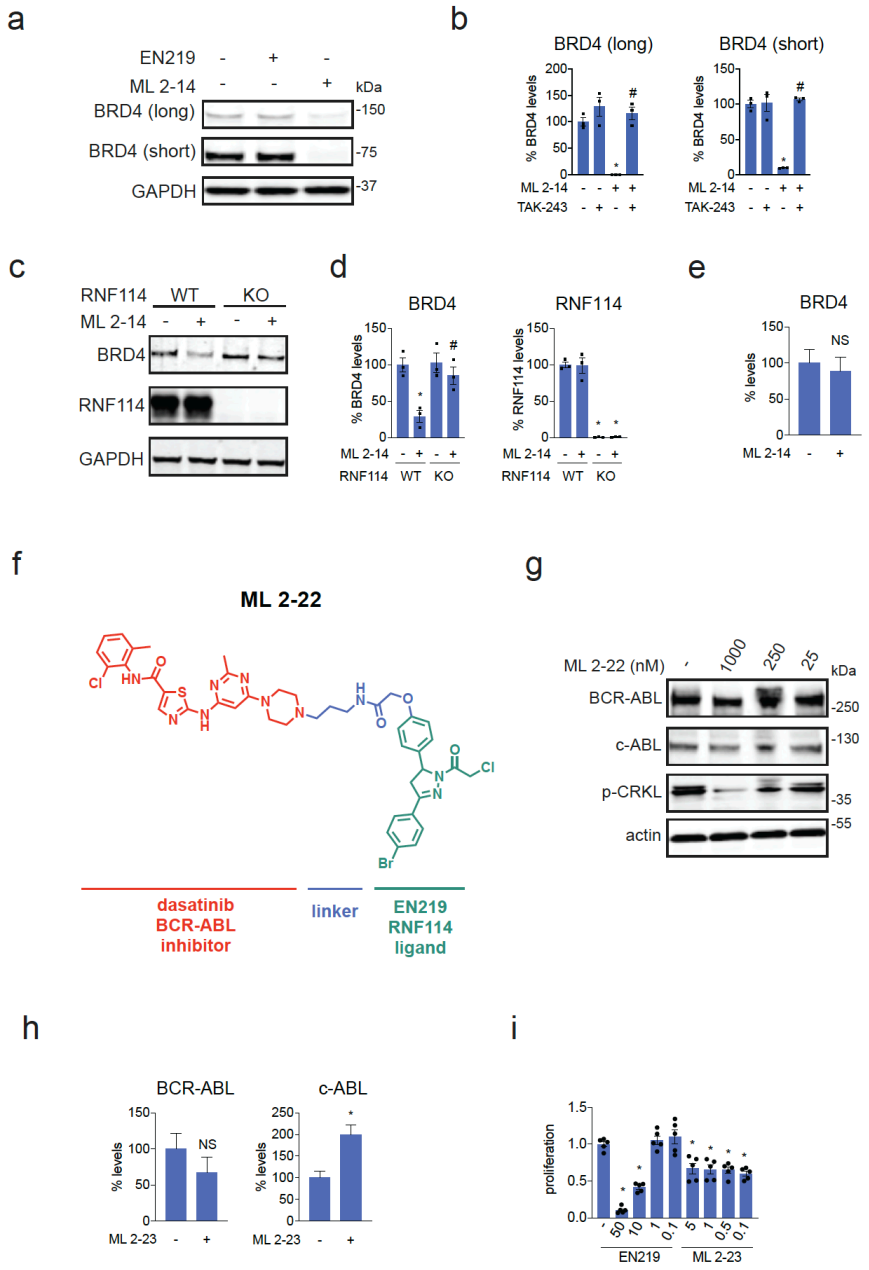

Supplementary Figure. 4.2.4. ML 2-14 and ML 2-22 mediated degradation of BRD4 and BCR-ABL, respectively.

Related to Figures 4.2.3 and 4.2.4. (a) BRD4 and loading control GAPDH expression in 231MFP cells treated with DMSO, EN219 (100 nM), and ML 2-14 (100 nM) for 20 h detected by Western blotting. (b) Quantification of data from Figure 3f. (c) Degradation of BRD4 (long isoform) in RNF114 wild-type (WT) or knockout (KO) HAP1 cells in a distinct separate experiment from the data shown in Figure 3i. RNF114 WT or KO HAP1 cells were treated with DMSO vehicle or ML 2-14 (1 □M) for 16 h and BRD4, RNF114, and loading control GAPDH levels were detected by Western blotting. (d) Quantification of data from (c). (e) Quantitative PCR data of BRD4 mRNA expression in 231MFP cells treated with vehicle or ML 2-14 (100 nM, 16 h). (f) Structure of ML 2-22 degrader that

linked EN219 to dasatinib. **(g)** BCR-ABL, c-ABL, p-CRKL, and loading control actin levels assessed by Western blot from K562 cells treated with DMSO vehicle or ML 2-22 for 20 h. **(h)** Quantitative PCR data of BCR-ABL and c-ABL mRNA expression in K562 cells treated with vehicle or ML 2-23 (5 μM, 16 h). **(i)** Cell proliferation of K562 cells treated with DMSO vehicle, EN219, or ML 2-23 for 16 h, assessed by WST reagent. Blots in **(a, c, g)** are a representative from n=3 biological replicates/group. Data shown in **(b, d, e, h, i)** are average ± sem with n=3 biological replicates/group for **(b, d, e, h)** and n=5 biological replicates/group in **(i)**. Statistical significance was calculated with unpaired two-tailed Student's t-test and is expressed as *p<0.05 compared to vehicle-treated controls or vehicle-treated wild-type controls in **(b, d, e, h, i**) and #p<0.05 compared to ML 2-14 treated groups or ML 2-14-treated wild-type groups. NS denotes not significant.

Synthetic Methods and Characterization

SI Scheme 1. Synthetic route to degrader ML 2-14.

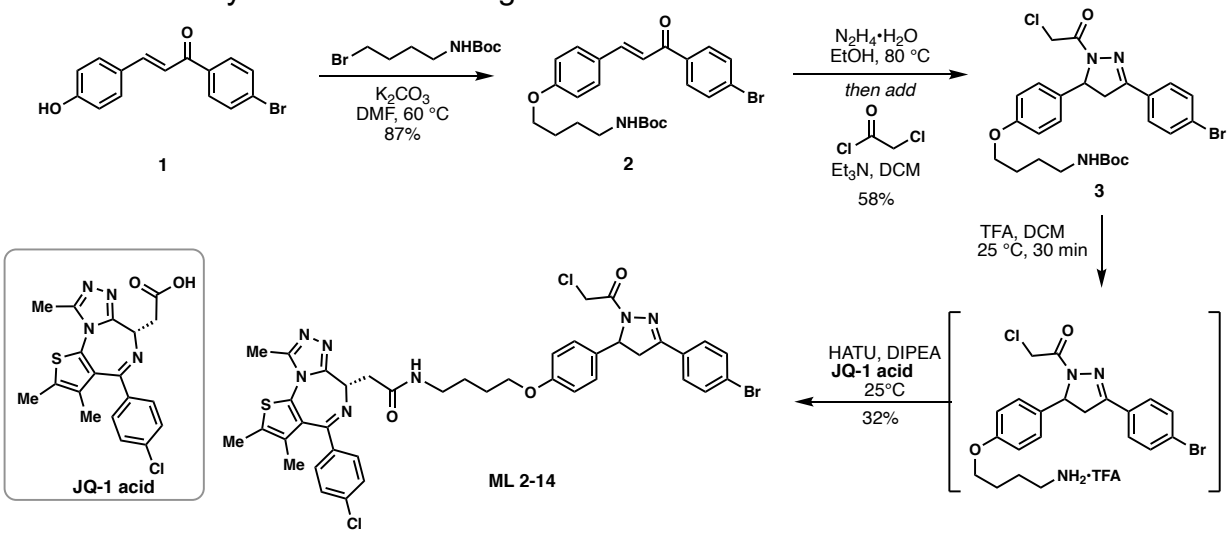

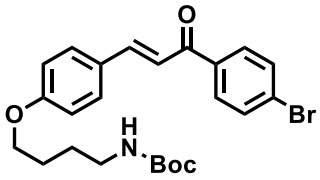

(*E*)-tert-butyl (4-(4-(3-(4-bromophenyl)-3-oxoprop-1-en-1-yl)phenoxy)butyl)carbamate **(2):**

To a solution of enone **1**[X] (226 mg, 0.75 mmol) in anhydrous DMF (8 mL) was added 4-(Boc-amino)butyl bromide (376 mg, 1.5 mmol) and K_2CO_3 (414 mg, 3 mmol) and the reaction mixture was stirred at 60 °C for 5 h under an atmosphere of nitrogen. Upon cooling, the inorganic salts were filtered off, the solution was diluted with EtOAc, washed with water, and the volatiles removed *in vacuo*. The crude material was purified by silica gel chromatography (25% EtOAc/hexanes) to yield 310 mg (87%) of **2**: **^{1}H NMR (400 MHz, $CDCl_3$):** δ 7.96 – 7.88 (m, 2H), 7.83 (d, *J* = 15.6 Hz, 1H), 7.72 – 7.59 (m, 4H), 7.39

(d, *J* = 15.6 Hz, 1H), 7.01 – 6.91 (m, 2H), 4.66 (s, 1H), 4.07 (t, *J* = 6.2 Hz, 2H), 3.25 (q, *J* = 6.8 Hz, 2H), 1.94 – 1.82 (m, 2H), 1.79 – 1.64 (m, 3H), 1.49 (s, 9H).

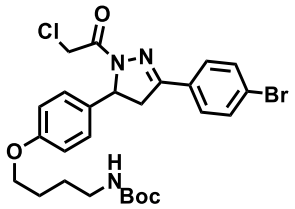

tert-butyl (4-(4-(3-(4-bromophenyl)-1-(2-chloroacetyl)-4,5-dihydro-1*H*-pyrazol-5-yl)phenoxy)butyl)carbamate **(3):**

To a solution of enone **2** (550 mg, 1.16 mmol) in EtOH was added hydrazine monohydrate (116 mg, 2.32 mmol) and the reaction mixture heated at 80 °C for 5 h under a nitrogen atmosphere. The reaction was cooled to room temperature, diluted with water, and extracted with DCM. The combined organic phase was dried over anhydrous magnesium sulfate and then concentrated *in vacuo* to ~ 5 mL. [NOTE: All of the workup procedures should be performed quickly (<1.5 h total time) and the rotovap bath kept cool as the crude product can easily undergo autooxidation]. To the concentrated DCM solution was immediately added chloroacetyl chloride (157 mg, 1.39 mmol) and triethylamine (152 mg, 1.5 mmol) at 0°C. The reaction mixture was stirred in ice bath for 30 min, then warmed to room temperature and stirred overnight under an N_2 atmosphere. Upon reaction completion, the reaction solution was diluted with EtOAc, washed with brine, and concentrated *in vacuo*. The crude was purified by silica gel chromatography (40% EtOAc/hexanes) to yield 381 mg (58%) of **3**: **^{1}H NMR (400 MHz, $CDCl_3$):** δ 7.60 (q, *J* = 8.8 Hz, 4H), 7.19 – 7.10 (m, 2H), 6.87 – 6.77 (m, 2H), 5.55 (dd, *J* = 11.7, 4.7 Hz, 1H), 4.55 (s, 2H), 3.94 (t, *J* = 6.2 Hz, 2H), 3.74 (dd, *J* = 17.8, 11.7 Hz, 1H), 3.24 – 3.11 (m, 3H), 1.85 – 1.75 (m, 2H), 1.65 (p, *J* = 7.1 Hz, 2H), 1.44 (s, 9H).

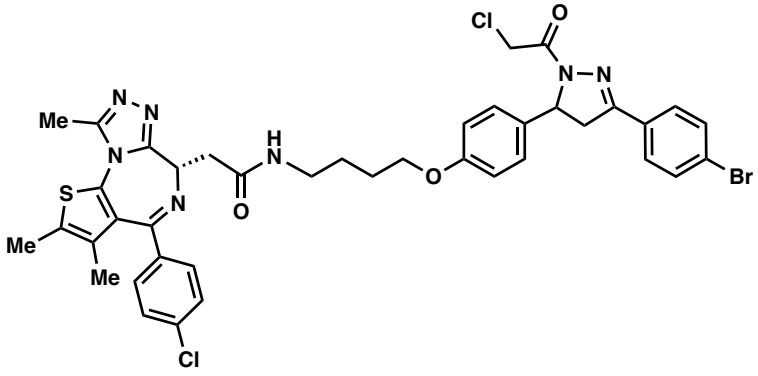

ML 2-14:

i. Chloroacetamide **3** (185 mg, 0.327 mmol) was dissolved in DCM (2.5 mL) and trifluoroacetic acid (2.5 mL) was added dropwise slowly over 20 minutes. After an

additional 20 minutes of stirring, the solvent was removed in *in vacuo,* and the crude material three times with 3mL DCM to remove excess TFA. The deprotected amine was used in the next step without purification.
ii. The resulting TFA salt was dissolved in DCM (8 mL) and **JQ1-acid** (157 mg, 0.4 mmol), 1- [Bis(dimethylamino)methylene]-1H-1,2,3-triazolo[4,5-b]pyridinium 3-oxid hexafluorophosphate (HATU) (202 mg, 0.530 mmol), and *N,N*-Diisopropylethylamine (168 mg, 1.31 mmol) were added. The mixture was stirred overnight with monitoring by TLC (5% MeOH in DCM, 100% EtOAc). Upon completion, the reaction mixture was concentrated *in vacuo* and directly purified by silica gel flash column chromatography (1-5% MeOH/DCM). The eluted fractions were insufficiently pure and those containing product were combined, concentrated and purified again by flash silica chromatography (100-0% EtOAc/DCM followed by 0-5% MeOH/DCM) to afford 88.4 mg (32%) of **ML 2-14**: **^{1}H NMR (400 MHz, $CDCl_3$):** δ 7.66 – 7.46 (m, 4H), 7.39 (d, *J* = 8.2 Hz, 2H), 7.29 (d, *J* = 8.3 Hz, 2H), 7.13 (d, *J* = 8.3 Hz, 2H), 6.86 (t, *J* = 5.9 Hz, 1H), 6.80 (d, *J* = 8.3 Hz, 2H), 5.54 (dt, *J* = 11.7, 4.1 Hz, 1H), 4.63 (t, *J* = 7.0 Hz, 1H), 4.54 (s, 2H), 3.90 (t, *J* = 6.1 Hz, 2H), 3.72 (dd, *J* = 17.8, 11.7 Hz, 1H), 3.54 (dd, *J* = 14.3, 7.5 Hz, 1H), 3.33 (ddt, *J* = 30.5, 13.3, 6.8 Hz, 3H), 3.17 (dd, *J* = 17.9, 4.7 Hz, 1H), 2.64 (s, 3H), 2.39 (s, 3H), 1.84 – 1.72 (m, 2H), 1.69 (d, *J* = 7.4 Hz, 2H), 1.65 (s, 3H); **^{13}C NMR (151 MHz, $CDCl_3$)** δ 169.6, 163.1, 160.4, 157.8, 154.8, 153.5, 150.5, 149.0, 135.9, 135.7, 131.9, 131.3, 131.2, 130.1, 130.0, 129.6, 129.0, 129.0, 127.9, 127.4, 126.2, 124.3, 119.8, 114.1, 66.6, 59.4, 53.7, 41.3, 41.2, 38.7, 38.4, 25.7, 25.4, 13.5, 13.3, 12.2, 11.0, 10.6; **HRMS (ESI):** *calcd*. $C_{40}H_{39}BrCl_2N_7O_3S$ ($[M+H]^+$): *m/z* 846.1390, found: 846.1399.

SI Scheme 2. Synthetic route to degraders **ML 2-22** and **ML 2-23**.

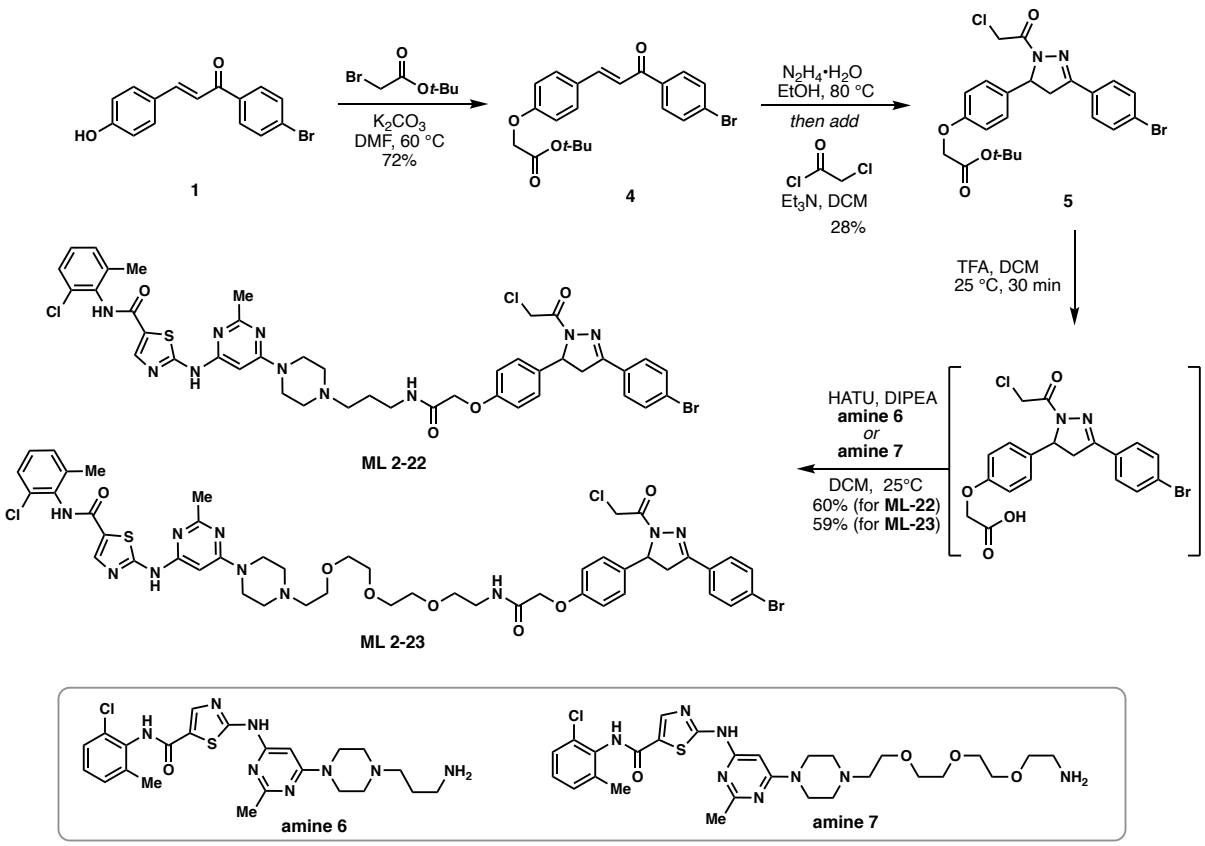

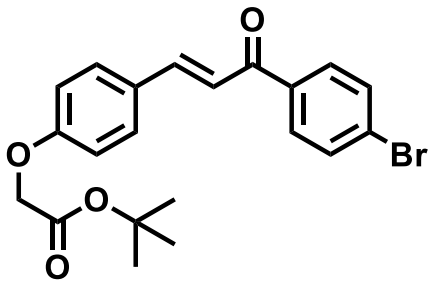

(*E*)-tert-butyl 2-(4-(3-(4-bromophenyl)-3-oxoprop-1-en-1-yl)phenoxy)acetate (**4**):

To a solution of **1** (153 mg, 0.50 mmol) in anhydrous DMF (8 mL) was added *tert*-Butyl bromoacetate (146 mg, 0.75 mmol) and K_2CO_3 (138 mg, 1 mmol) and the reaction mixture was heated to 60 °C for 5 hours under an atmosphere of nitrogen. Upon cooling, the inorganic salts were filtered off, the solution was diluted with EtOAc, washed with water, and concentrated *in vacuo*. The crude was purified by silica gel chromatography (25% EtOAc/hexanes) to yield 150 mg (72%) of **4**: **^{1}H NMR (400 MHz, $CDCl_3$):** δ 7.97 – 7.89 (m, 2H), 7.82 (d, *J* = 15.6 Hz, 1H), 7.73 – 7.60 (m, 4H), 7.41 (d, *J* = 15.6 Hz, 1H), 7.01 – 6.93 (m, 2H), 4.61 (s, 2H), 1.54 (s, 9H).

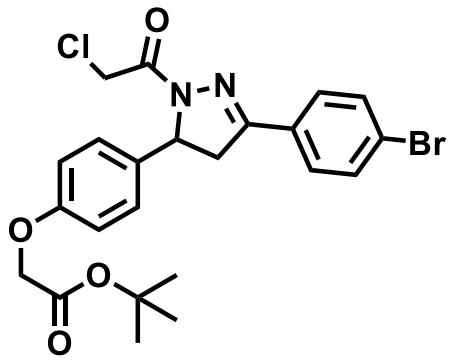

tert-butyl 2-(4-(3-(4-bromophenyl)-1-(2-chloroacetyl)-4,5-dihydro-1*H*-pyrazol-5-yl)phenoxy)acetate (**5**):

To a solution of **4** (417 mg, 1.00 mmol) in EtOH was added hydrazine monohydrate (250 mg, 5.00 mmol) and the reaction mixture was heated at 80 °C for 5 hours under an atmosphere of nitrogen. The reaction was cooled to room temperature, diluted by water, and extracted with DCM. The combined organic phase was dried over anhydrous magnesium sulfate and then concentrated *in vacuo* to ~ 5 mL [NOTE: All of the workup procedures should be performed quickly (<1.5 h total time) and the rotovap bath kept cool as the crude product can easily undergo autooxidation]. To the concentrated DCM solution was immediately added chloroacetyl chloride (169 mg, 1.50 mmol) and triethylamine (303 mg, 3.00 mmol) at 0 °C under an atmosphere of nitrogen. The reaction was maintained at this temperature for 30 minutes and then warmed to room temperature and stirred overnight under N_2. The reaction mixture was diluted with EtOAc, washed with brine, and concentrated *in vacuo*. The crude material was purified by silica gel chromatography (35 – 40 % EtOAc/hexanes) to yield 140 mg (28%) of **5**: **^{1}H NMR (400 MHz, $CDCl_3$):** δ 7.60 – 7.54 (m, 2H), 7.25 – 7.17 (m, 2H), 7.02 – 6.94 (m, 2H), 6.92 – 6.84 (m, 2H), 6.77 (s, 1H), 5.60 (dd, *J* = 11.7, 4.6 Hz, 1H), 4.60 (s, 2H), 4.51 (s, 2H), 3.77 (dd, *J* = 17.8, 11.7 Hz, 1H), 3.22 (dd, *J* = 17.8, 4.6 Hz, 1H), 1.54 (s, 9H).

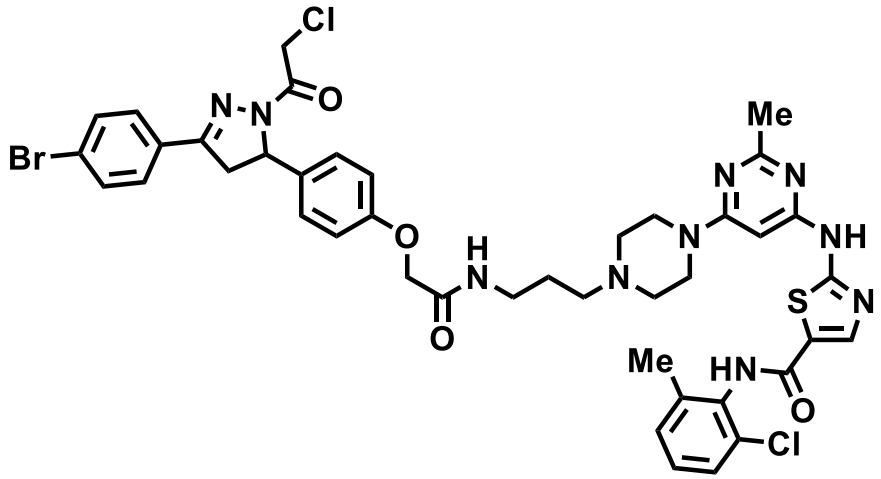

ML 2-22:

i. Compound **5** (15.2 mg, 0.030 mmol) was dissolved in DCM (1.5 mL) and trifluoroacetic acid (0.5 mL) added slowly over the course of 20 minutes. After stirring for an additional 20 minutes, the solvent was removed in *vacuo,* and chases three times with 3mL DCM to remove excess TFA The crude material was used directly in the next step.
ii. The aforementioned crude carboxylic acid was dissolved in 2 mL DCM and **amine 6** (15.0 mg, 0.030 mmol), 1- [Bis(dimethylamino)methylene]-1H-1,2,3-triazolo[4,5-b]pyridinium 3-oxid hexafluorophosphate (HATU) (17.1 mg, 0.045 mmol), and *N,N*-Diisopropylethylamine (193.5 mg, 1.50 mmol) were added. The reaction was stirred overnight monitoring by TLC (20% Methanol in DCM). Upon completion, the reaction mixture was diluted with EtOAc, washed with brine, and concentrated *in vacuo*. The crude material was purified by silica gel flash column chromatography (1-5% MeOH/DCM). The eluted fractions were insufficiently pure and those containing product were combined, concentrated and purified again by flash silica chromatography (100-0% EtOAc/DCM followed by 10-35% MeOH/DCM) to afford 17.1 mg (60%) of **ML 2-22**: **^{1}H NMR (600 MHz, DMSO-d$_6$)** δ 11.47 (s, 1H), 9.88 (s, 1H), 8.23 (s, 1H), 8.11 (d, *J* = 18.3 Hz, 1H), 7.84 – 7.71 (m, 2H), 7.71 – 7.64 (m, 2H), 7.40 (dd, *J* = 7.8, 1.6 Hz, 1H), 7.34 – 7.22 (m, 2H), 7.22 – 7.09 (m, 2H), 6.99 – 6.85 (m, 2H), 6.06 (s, 1H), 5.54 (dd, *J* = 11.7, 4.8 Hz, 1H), 4.79 – 4.59 (m, 2H), 4.46 (s, 2H), 3.93 – 3.79 (m, 1H), 3.51 (d, *J* = 9.8 Hz, 4H), 3.26 – 3.07 (m, 3H), 2.41 (s, 6H), 2.31 (s, 2H), 2.25 (s, 3H), 1.67 (d, *J* = 4.6 not 40.6? Hz, 2H); **^{13}C NMR (151 MHz, DMSO)** δ 167.0, 164.7, 162.8, 162.1, 161.9, 159.5, 156.6, 156.5, 154.3, 140.4, 138.4, 133.8, 133.1, 132.0, 131.4, 129.5, 129.0, 128.6, 128.4, 127.7, 126.5, 125.3, 123.7, 114.4, 82.2, 66.7, 59.2, 55.1, 54.5, 51.9, 43.1, 42.0, 41.4, 36.5, 29.5, 28.0, 25.1, 23.0, 22.0, 17.9, 13.5, 10.5; **HRMS (ESI):** *calcd*. $C_{42}H_{44}BrCl_2N_{10}O_4S$ ([M+H]$^+$): *m/z* 933.1823, found: 933.1814.

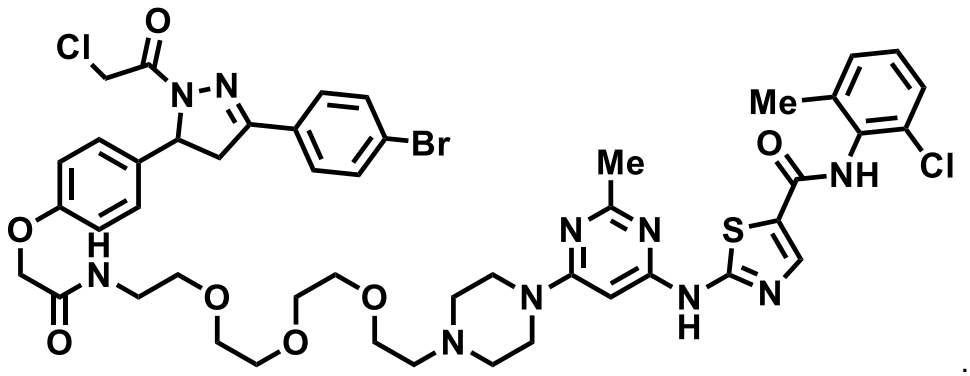

ML 2-23:

i. Compound **5** (16.2 mg, 0.032 mmol) was dissolved in DCM (1.5 mL) and trifluoroacetic acid (0.5 mL) added slowly over the course of 20 minutes. After stirring for an additional 20 minutes, the solvent was removed in *vacuo,* and chases three times with 3mL DCM to remove excess TFA. The crude material was used directly in the next step.

ii. The aforementioned crude carboxylic acid was dissolved in DCM (2 mL) and **amine 7** (19.8 mg, 0.032 mmol), 1- [Bis(dimethylamino)methylene]-1H-1,2,3-triazolo[4,5-b]pyridinium 3-oxid hexafluorophosphate (HATU) (18.2 mg, 0.048 mmol), and *N,N*-Diisopropylethylamine (206.0 mg, 1.60 mmol) were added. The reaction mixture was stirred overnight with monitoring by TLC (20% Methanol in DCM). Upon completion, the reaction mixture was diluted with EtOAc, washed with brine, and concentrated *in vacuo*. The crude material was purified by silica gel flash column chromatography (1-5% MeOH/DCM). The eluted fractions were insufficiently pure and those containing product were combined, concentrated and purified again by flash silica chromatography (100-0% EtOAc/DCM followed by 10-35% MeOH/DCM) to afford 20.1 mg (59%) of **ML 2-23**:
^{1}H NMR (400 MHz, Methanol-d_4) δ 8.16 (s, 1H), 7.77 – 7.71 (m, 2H), 7.61 (dd, *J* = 8.8, 2.3 Hz, 2H), 7.40 – 7.34 (m, 1H), 7.31 – 7.15 (m, 4H), 7.00 – 6.90 (m, 2H), 6.00 (s, 1H), 5.57 (dd, *J* = 11.7, 4.7 Hz, 1H), 4.73 (d, *J* = 13.8 Hz, 1H), 4.60 (d, *J* = 13.9 Hz, 1H), 4.52 (s, 2H), 4.12 (q, *J* = 7.1 Hz, 1H), 3.88 (dd, *J* = 18.2, 11.7 Hz, 1H), 3.62 (tdd, *J* = 13.9, 10.2, 6.7 Hz, 16H), 3.48 (t, *J* = 5.5 Hz, 2H), 3.19 (dd, *J* = 18.1, 4.8 Hz, 1H), 2.66 (dd, *J* = 11.8, 5.7 Hz, 6H), 2.47 (s, 3H), 2.34 (s, 3H); **^{13}C NMR (151 MHz, DMSO)** δ 167.2, 164.6, 162.8, 161.9, 159.5, 156.6, 154.4, 140.4, 137.6, 133.3, 133.1, 132.0, 131.4, 131.3, 129.1, 128.6, 128.4, 127.3, 126.5, 114.4, 69.3, 69.2, 68.4, 66.7, 59.3, 53.6, 42.0, 41.4, 41.3, 37.8, 35.3, 30.3, 29.5, 27.4, 25.1, 23.0, 22.0, 17.9, 17.6, 15.6, 13.5, 11.9, 10.5; **HRMS (ESI):** *calcd*. $C_{47}H_{54}BrCl_2N_{10}O_4S$ ($[M+H]^+$): *m/z* 1051.2453, found: 1051.2445

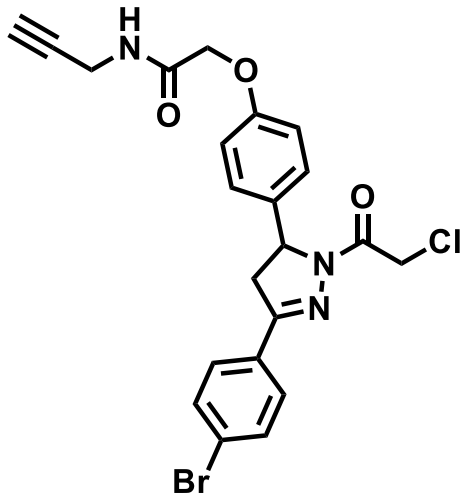

ML 2-24:

i. Compound **5** (17.6 mg, 0.035 mmol) was dissolved in DCM (1.5 mL) and trifluoroacetic acid (0.5 mL) added slowly over the course of 20 minutes. After stirring for an additional 20 minutes, the solvent was removed in *vacuo,* and chases three times with 3mL DCM to remove excess TFA. The crude material was used directly in the next step.
ii. The aforementioned crude carboxylic acid was dissolved in DCM (2 mL) and propargylamine (2.3 mg, 0.042 mmol), 1- [Bis(dimethylamino)methylene]-1H-1,2,3-triazolo[4,5-b]pyridinium 3-oxid hexafluorophosphate (HATU) (19.8 mg, 0.052 mmol), and *N,N*-Diisopropylethylamine (223.9 mg, 1.750 mmol) were added. The reaction mixture

was stirred overnight with monitoring by TLC (60% EtOAc in hexane). Upon completion, the reaction mixture was diluted with DCM, washed with brine, and concentrated *in vacuo*. The crude material was purified by silica gel chromatography (25 – 70 % EtOAc/hexanes) to yield 14.6 mg (88%) of **ML 2-24**: **^{1}H NMR (400 MHz, $CDCl_3$):** δ 7.68 – 7.60 (m, 4H), 7.27 – 7.21 (m, 2H), 6.95 – 6.89 (m, 2H), 6.81 (s, 1H), 5.60 (dd, *J* = 11.8, 4.8 Hz, 1H), 4.64 – 4.54 (m, 2H), 4.52 (s, 2H), 4.18 (dd, *J* = 5.6, 2.6 Hz, 2H), 3.81 (dd, *J* = 17.8, 11.8 Hz, 1H), 3.22 (dd, *J* = 17.9, 4.8 Hz, 1H), 2.31 (t, *J* = 2.6 Hz, 1H); **^{13}C NMR (101 MHz, $CDCl_3$):** δ 167.9, 164.1, 156.9, 154.5, 134.7, 132.3, 128.4, 127.6, 125.5, 115.3, 77.5, 77.2, 76.8, 72.1, 67.4, 60.2, 42.2, 42.1, 28.9; **HRMS (ESI):** *calcd*. $C_{22}H_{19}BrCl_1N_3O_3Na$ ($[M+Na]^+$): *m/z* 510.0191, found: 510.0186.

SI Scheme 3. Synthetic route to degrader **ML 2-31**.

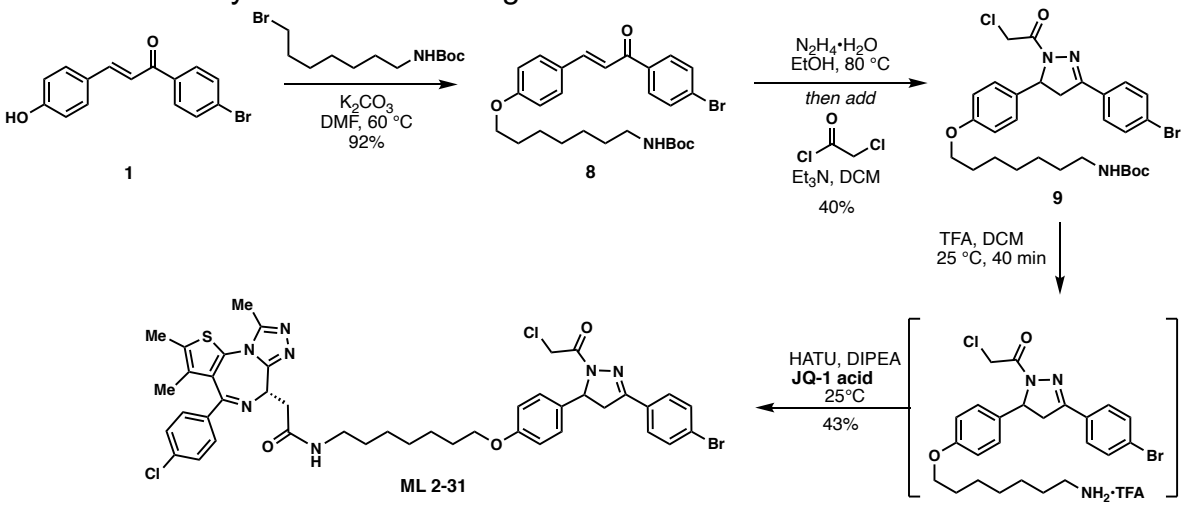

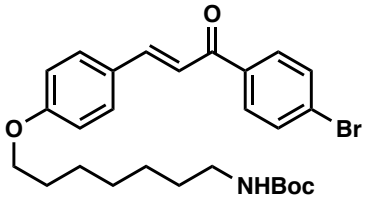

(*E*)-*tert*-butyl (7-(4-(3-(4-bromophenyl)-3-oxoprop-1-en-1-yl)phenoxy)heptyl)carbamate (**8**)**:**

To a solution of **1** (153 mg, 0.50 mmol) in anhydrous DMF (8 mL) was added *N*-Boc-7-bromoheptan-1-amine (300 mg, 1.00 mmol) and K_2CO_3 (276 mg, 2.00 mmol). The reaction mixture was heated at 60 °C for 5 hours under an atmosphere of nitrogen. Upon cooling to room temperature, the inorganic salts were filtered off, the solution was diluted with EtOAc, washed with water, and the volatiles removed *in vacuo*. The crude material was purified by silica gel chromatography (25% EtOAc/hexanes) to yield 238 mg (92%) of **8**: **^{1}H NMR (400 MHz, $CDCl_3$):** δ 7.97 – 7.89 (m, 2H), 7.83 (d, *J* = 15.6 Hz, 1H), 7.73 – 7.59 (m, 4H), 7.39 (d, *J* = 15.6 Hz, 1H), 7.00 – 6.92 (m, 2H), 4.55 (s, 1H), 4.04 (t, *J* = 6.5

Hz, 2H), 3.16 (q, *J* = 6.8 Hz, 2H), 1.94 – 1.76 (m, 2H), 1.57 – 1.50 (m, 4H), 1.49 (s, 9H), 1.44 – 1.37 (m, 4H).

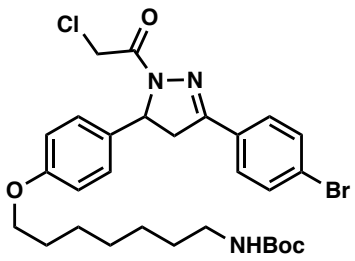

tert-butyl (7-(4-(3-(4-bromophenyl)-1-(2-chloroacetyl)-4,5-dihydro-1*H*-pyrazol-5-yl)phenoxy)heptyl)carbamate (**9**):

To a solution of **8** (223 mg, 0.43 mmol) in EtOH was added hydrazine monohydrate (43 mg, 0.86 mmol) and the reaction mixture heated at 80 °C for 3 h under an atmosphere of nitrogen. The reaction mixture was cooled to room temperature, diluted with water and extracted with DCM. The combined organic phase was dried over anhydrous magnesium sulfate and then concentrated *in vacuo* to ~ 5 mL [NOTE: All of the workup procedures should be performed quickly (<1.5 h total time) and the rotovap bath kept cool as the crude product can easily undergo autooxidation]. To the concentrated solution was quickly added chloroacetyl chloride (58 mg, 0.52 mmol) and triethylamine (57 mg, 0.56 mmol) at 0 °C. The reaction mixture was stirred in an ice bath for 30 minutes, then warmed to room temperature and stirred overnight under N_2. The reaction mixture was diluted with EtOAc, washed with brine, and concentrated *in vacuo*. The crude was purified by silica gel chromatography (25 – 40 % EtOAc/hexanes) to yield 104 mg (40%) of **9**: **^{1}H NMR (400 MHz, $CDCl_3$):** δ 7.69 – 7.53 (m, 4H), 7.23 – 7.12 (m, 2H), 6.89 – 6.82 (m, 2H), 5.57 (dd, *J* = 11.7, 4.7 Hz, 1H), 4.57 (s, 2H), 3.93 (t, *J* = 6.5 Hz, 2H), 3.76 (dd, *J* = 17.8, 11.7 Hz, 1H), 3.21 (dd, *J* = 17.9, 4.7 Hz, 1H), 3.13 (q, *J* = 6.8 Hz, 2H), 1.85 – 1.70 (m, 2H), 1.55 – 1.46 (m, 4H), 1.47 (s, 9H), 1.41 – 1.32 (m, 4H).

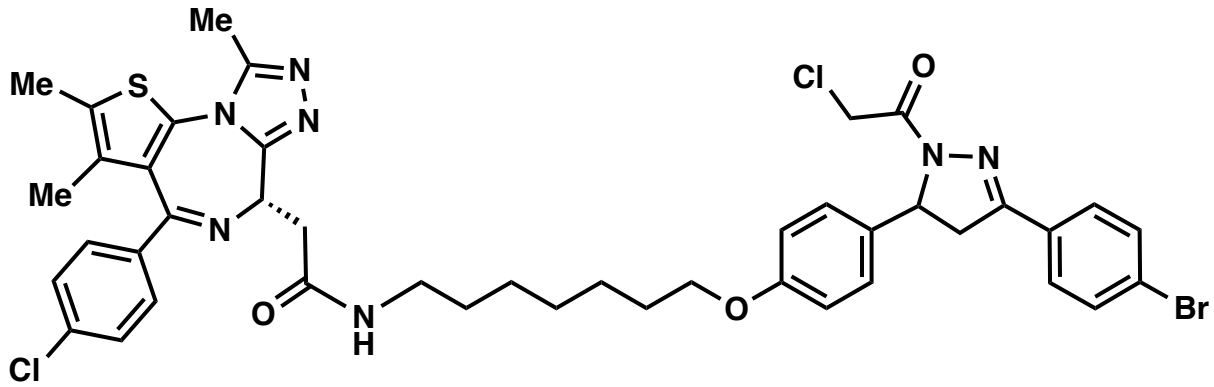

ML 2-31:

i. Compond **9** (104 mg, 0.171 mmol) was dissolved in DCM (2.5 mL) and TFA (2.5 mL) was added slowly over 20 minutes followed by stirring for an additional 20 minutes. The

solvent was removed in *vacuo,* and chases three times with 3mL DCM to remove excess TFA. The crude material was used without further purification for amide coupling.
ii. The aforementioned TFA salt was dissolved in DCM (8 mL) and **JQ1-acid** (82 mg, 0.205 mmol), 1- [Bis(dimethylamino)methylene]-1H-1,2,3-triazolo[4,5-b]pyridinium 3-oxid hexafluorophosphate (HATU) (97.5 mg, 0.257 mmol), and *N,N*-Diisopropylethylamine (552 mg, 4.28 mmol) were added. The reaction mixture was stirred overnight with monitoring by TLC (5% MeOH in DCM, 100% EtOAc). Upon completion, the reaction mixture was directly concentrated *in vacuo* and the crude material purified by silica gel flash chromatography (1-5% MeOH/DCM). The eluted fractions were insufficiently pure and those containing product were combined, concentrated and purified again by flash silica chromatography (100-0% EtOAc/DCM followed by 0-5% MeOH/DCM) to afford 66 mg (43%) of **ML 2-31**: **^{1}H NMR (400 MHz, $CDCl_3$):** δ 7.68 – 7.57 (m, 4H), 7.48 – 7.39 (m, 2H), 7.39 – 7.32 (m, 2H), 7.22 – 7.11 (m, 2H), 6.90 – 6.81 (m, 2H), 6.67 (t, *J* = 5.8 Hz, 1H), 5.58 (ddd, *J* = 11.8, 4.7, 2.1 Hz, 1H), 4.69 – 4.61 (m, 1H), 4.59 (d, *J* = 2.5 Hz, 2H), 3.93 (t, *J* = 6.4 Hz, 2H), 3.84 – 3.67 (m, 2H), 3.56 (dd, *J* = 14.3, 7.4 Hz, 1H), 3.42 – 3.30 (m, 2H), 3.28 – 3.16 (m, 3H), 2.70 (s, 3H), 2.47 – 2.35 (m, 3H), 1.82 – 1.71 (m, 2H), 1.71 – 1.67 (m, 3H), 1.56 (p, *J* = 7.0 Hz, 2H), 1.45 – 1.43 (m, 4H); **^{13}C NMR (151 MHz, $CDCl_3$)** δ 170.4, 163.9, 158.9, 155.7, 154.6, 149.9, 136.8, 136.6, 132.6, 132.1, 132.1, 130.9, 130.9, 130.5, 129.8, 128.7, 128.2, 127.0, 125.2, 115.1, 115.1, 114.9, 67.9, 60.2, 54.9, 54.5, 43.0, 42.2, 42.1, 39.6, 39.4, 29.7, 29.4, 29.1, 29.0, 26.8, 25.9, 18.5, 17.2, 14.4, 13.1, 12.4, 11.8; **HRMS (ESI):** *calcd*. $C_{43}H_{45}BrCl_2N_7O_3S$ ([M+H]$^+$): *m/z* 888.1865, found: 888.1858.

SI Scheme 4. Synthetic route to degrader **ML 2-32**.

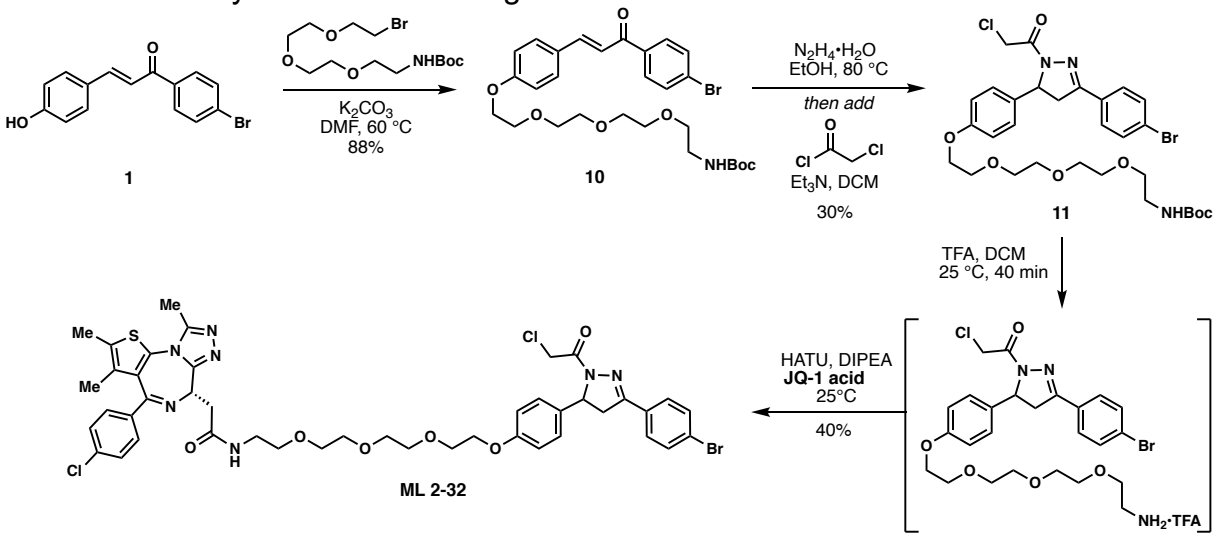

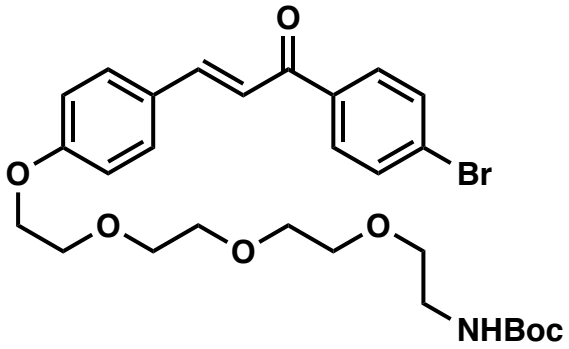

(*E*)-tert-butyl (2-(2-(2-(2-(4-(3-(4-bromophenyl)-3-oxoprop-1-en-1-yl)phenoxy)ethoxy)ethoxy)ethoxy)ethyl)carbamate (**10**):

To a solution of **1** (153 mg, 0.50 mmol) in anhydrous DMF (8 mL) was added *tert*-Butyl (2-(2-(2-(2-bromoethoxy)ethoxy)ethoxy)ethyl)carbamate (344 mg, 0.97 mmol) and K_2CO_3 (276 mg, 2.00 mmol), and the reaction mixture was stirred at 60 °C for 5 hours under an atmosphere of nitrogen. Upon cooling, the inorganic salts were filtered off, the solution was diluted with EtOAc, washed with water, and the volatiles removed *in vacuo*. The crude was purified by silica gel chromatography (50% EtOAc/hexanes) to yield 251 mg (88%) of **10**: **^{1}H NMR (400 MHz, $CDCl_3$):** δ 7.97 – 7.89 (m, 2H), 7.89 – 7.78 (m, 1H), 7.72 – 7.55 (m, 4H), 7.40 (d, *J* = 15.6 Hz, 1H), 7.04 – 6.95 (m, 2H), 5.07 (s, 1H), 4.23 (dd, *J* = 5.7, 4.0 Hz, 2H), 3.97 – 3.84 (m, 2H), 3.83 – 3.77 (m, 2H), 3.76 – 3.72 (m, 2H), 3.71 – 3.64 (m, 4H), 3.58 (t, *J* = 5.1 Hz, 2H), 3.35 (d, *J* = 6.3 Hz, 2H), 1.48 (s, 9H).

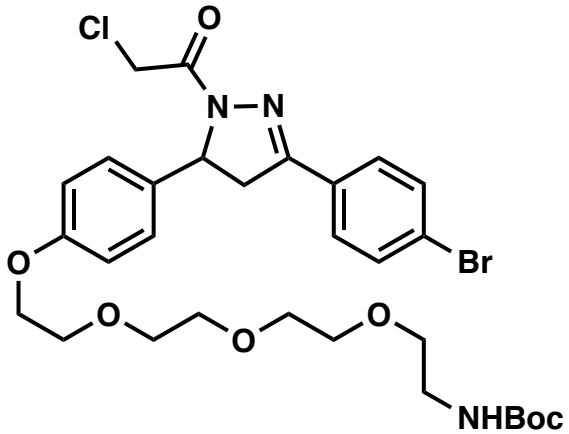

tert-butyl (2-(2-(2-(2-(4-(3-(4-bromophenyl)-1-(2-chloroacetyl)-4,5-dihydro-1*H*-pyrazol-5-yl)phenoxy)ethoxy)ethoxy)ethoxy)ethyl)carbamate (**11**):

To a solution of **10** (244 mg, 0.42 mmol) in EtOH was added hydrazine monohydrate (42 mg, 0.84 mmol) and the reaction solution was heated at 80 °C for 5 h under an atmosphere of nitrogen. Upon cooling to room temperature, the solution was diluted with water, extracted with DCM, and dried over anhydrous magnesium sulfate. The combined

organic phase was concentrated *in vacuo* to ~ 5 mL [NOTE: All of the workup procedures should be performed quickly (<1.5 h total time) and the rotovap bath kept cool as the crude product can easily undergo autooxidation]. To the concentrated solution was quickly added chloroacetyl chloride (58 mg, 0.52 mmol) and triethylamine (57 mg, 0.56 mmol) at 0°C. The reaction mixture was stirred for 30 minutes in an ice bath and then warmed to room temperature and stirred overnight under N_2. Upon completion of the reaction, the mixture was diluted with EtOAc, washed with brine, and concentrated *in vacuo*. The crude material was purified by silica gel chromatography (30 – 65 % EtOAc/hexanes) to yield 82 mg (30%) of **11**:
^{1}H NMR (400 MHz, $CDCl_3$): δ 7.67 – 7.58 (m, 4H), 7.21 – 7.14 (m, 2H), 6.92 – 6.85 (m, 2H), 5.57 (dd, *J* = 11.7, 4.7 Hz, 1H), 4.57 (d, *J* = 1.1 Hz, 2H), 4.12 (dd, *J* = 5.6, 4.2 Hz, 2H), 3.88 – 3.83 (m, 2H), 3.75 – 3.73 (m, 2H), 3.72 – 3.69 (m, 2H), 3.67 – 3.62 (m, 4H), 3.55 (t, *J* = 5.1 Hz, 2H), 3.32 (q, *J* = 4.3, 3.4 Hz, 2H), 3.21 (dd, *J* = 17.8, 4.7 Hz, 1H), 1.46 (s, 9H).

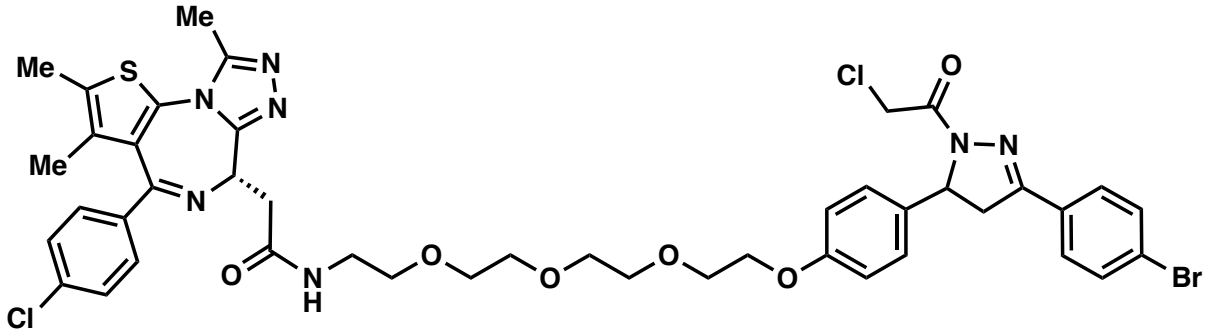

ML 2-32:

i. Compound **11** (81.7 mg, 0.120 mmol) was dissolved in DCM (2.5 mL) and trifluoroacetic acid (2.5 mL) added slowly over 20 minutes followed by an additional 20 minutes of stirring. The solvent was removed in *vacuo,* and chases three times with 3mL DCM to remove excess TFA. The crude material was used directly in the next step.
ii. The aforementioned crude material was dissolved in DCM (8 mL) and **JQ1-acid** (57.6 mg, 0.150 mmol), 1- [Bis(dimethylamino)methylene]-1H-1,2,3-triazolo[4,5-b]pyridinium 3-oxid hexafluorophosphate (HATU) (68.4 mg, 0.180 mmol), and *N,N*-Diisopropylethylamine (774 mg, 6.00 mmol) were added. The reaction was stirred overnight with monitoring by TLC (10% MeOH in DCM, 100% EtOAc). Upon completion, the reaction mixture was concentrated *in vacuo* and purified by silica gel flash chromatography (1-10% MeOH/DCM). The eluted fractions were insufficiently pure and those containing product were combined, concentrated and purified again by flash silica chromatography (100-0% EtOAc/DCM followed by 0-10% MeOH/DCM) to afford 46 mg (40%) of **ML 2-32**: **^{1}H NMR (400 MHz, $CDCl_3$):** δ 7.66 – 7.57 (m, 4H), 7.45 – 7.41 (m, 2H), 7.34 (d, *J* = 8.5 Hz, 2H), 7.16 (dq, *J* = 7.9, 3.1 Hz, 2H), 6.98 (d, *J* = 5.1 Hz, 1H), 6.92 – 6.83 (m, 2H), 5.57 (ddd, *J* = 11.8, 7.3, 4.7 Hz, 1H), 4.68 (t, *J* = 6.9 Hz, 1H), 4.57 (s, 2H), 4.12 (dd, *J* = 5.7, 4.0 Hz, 2H), 3.90 – 3.84 (m, 2H), 3.78 – 3.66 (m, 10H), 3.65 – 3.58 (m,

2H), 3.54 – 3.50 (m, 2H), 3.44 – 3.37 (m, 1H), 3.20 (dd, *J* = 17.8, 4.7 Hz, 1H), 2.68 (d, *J* = 1.5 Hz, 3H), 2.42 (s, 3H), 1.69 (s, 3H); **^{13}C NMR (151 MHz, $CDCl_3$)** δ 170.4, 163.8, 163.7, 158.4, 155.6, 154.3, 149.7, 145.2, 136.6, 136.6, 132.9, 132.1, 131.9, 131.7, 130.8, 130.6, 130.3, 130.2, 129.9, 129.8, 128.6, 128.1, 126.9, 125.0, 114.9, 70.7, 70.5, 70.5, 70.3, 69.7, 69.6, 67.4, 60.1, 54.3, 54.3, 42.1, 41.9, 39.3, 39.0, 29.6, 14.3, 13.0, 11.7; **HRMS (ESI):** *calcd*. $C_{44}H_{47}BrCl_2N_7O_6S$ ([M+H]$^+$): *m/z* 950.1863, found: 950.1852.

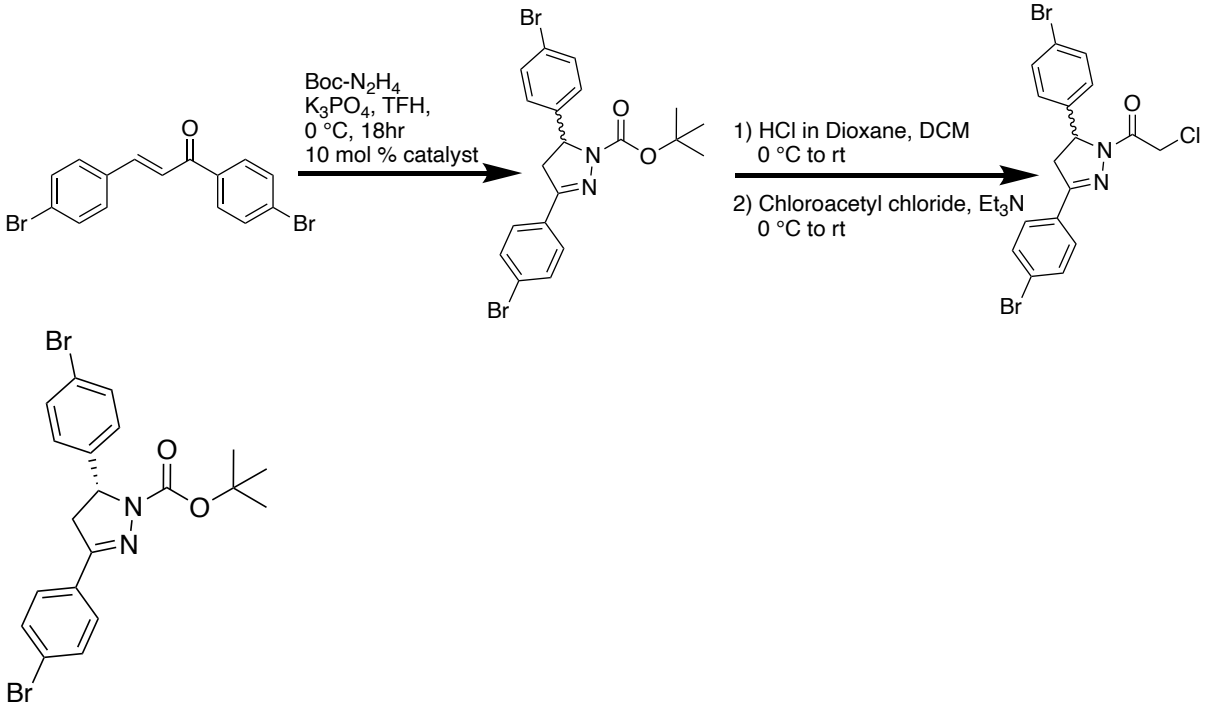

***tert*-butyl (*R*)-3,5-bis(4-bromophenyl)-4,5-dihydro-1*H*-pyrazole-1-carboxylate (JNS-2-128A)**

(*E*)-1,3-bis(4-bromophenyl)prop-2-en-1-one (Princeton Bio, 109.8 mg, 0.3 mmol, 1.0 eq.), tert-butyl carbazate (43.6 mg, 0.33 mmol, 1.1 eq.), potassium phosphate (82.8 mg, 0.39

mmol, 1.3 eq.), and catalyst A (prepared according to Mahé et. al., 13.3 mg, 0.03 mmol, 10 mol%) were combined in THF (0.6 mL, 0.5 M) under nitrogen and stirred at 0 ºC for 18h. The mixture was diluted with EtOAc, filtered to remove salts, concentrated and purified by silica gel chromatography to provide the stereoenriched pyrazoline. (Mahé et. al. Angew. Chem. Int. Ed. 2010. 49. 39. 7072-7075.)

^{1}H NMR (400 MHz, Chloroform-*d*): δ 7.61 (d, *J* = 8.6 Hz, 2H), 7.55 – 7.43 (m, 4H), 7.14 – 7.08 (m, 2H), 5.31 (dd, *J* = 11.9, 5.1 Hz, 1H), 3.73 (dd, *J* = 17.5, 12.1 Hz, 1H), 3.08 (dd, *J* = 17.5, 5.5 Hz, 1H), 1.35 (s, 9H).

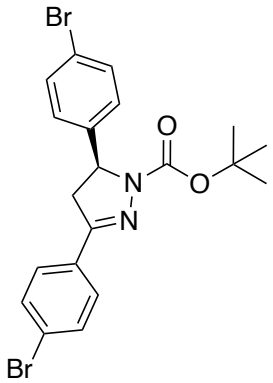

***tert*-butyl (*S*)-3,5-bis(4-bromophenyl)-4,5-dihydro-1*H*-pyrazole-1-carboxylate (JNS-2-128B)**

(*E*)-1,3-bis(4-bromophenyl)prop-2-en-1-one (Princeton Bio, 109.8 mg, 0.3 mmol, 1.0 eq.), tert-butyl carbazate (43.6 mg, 0.33 mmol, 1.1 eq.), potassium phosphate (82.8 mg, 0.39 mmol, 1.3 eq.), and catalyst B (prepared according to Mahé et. al., 13.3 mg, 0.03 mmol, 10 mol%) were combined in THF (0.6 mL, 0.5 M) under nitrogen and stirred at 0 ºC for 18h. The mixture was diluted with EtOAc, filtered to remove salts, concentrated and purified by silica gel chromatography to provide the stereoenriched pyrazoline. (Mahé et. al. Angew. Chem. Int. Ed. 2010. 49. 39. 7072-7075.)

^{1}H NMR (400 MHz, Chloroform-*d*): δ 7.61 (d, *J* = 8.6 Hz, 2H), 7.54 – 7.43 (m, 4H), 7.14 – 7.09 (m, 2H), 5.31 (dd, *J* = 12.0, 5.5 Hz, 1H), 3.73 (dd, *J* = 17.6, 12.1 Hz, 1H), 3.08 (dd, *J* = 17.5, 5.5 Hz, 1H), 1.34 (s, 9H).

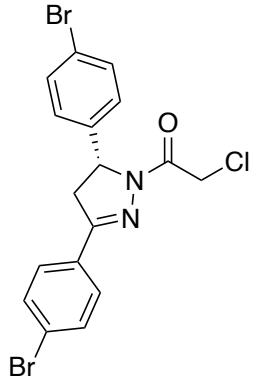

(*R*)-1-(3,5-bis(4-bromophenyl)-4,5-dihydro-1*H*-pyrazol-1-yl)-2-chloroethan-1-one (JNS-2-130A)

Boc-protected pyrazoline, JNS-2-128A, (45 mg, 0.094 mmol, 1.0 eq) was dissolved in DCM (0.47 mL, 0.2 M), cooled to 0 ºC, and 4.0 M HCl in dioxane (0.234 mL, 0.94 mmol, 10.0 eq.) was added under nitrogen. The mixture was stirred at rt until starting material was consumed (1.5h), then additional DCM was added (0.47 mL, reducing to 0.1 M) and the mixture cooled to 0 ºC. Chloroacetyl chloride (22 µL, 0.28 mmol, 3.0 eq.) was added followed by TEA (0.17 mL, 1.22 mmol, 13.0 eq.), and the reaction allowed to warm to room temperature and stirred for 1h. Crude was concentrated and purified by silica gel chromatography. (Mahé et. al. Angew. Chem. Int. Ed. 2010. 49. 39. 7072-7075.)

^{1}H NMR (400 MHz, Chloroform-*d*): δ 7.63 – 7.55 (m, 4H), 7.49 – 7.43 (m, 2H), 7.11 (d, *J* = 8.5 Hz, 2H), 5.55 (dd, *J* = 11.8, 4.9 Hz, 1H), 4.60 – 4.48 (m, 2H), 3.77 (dd, *J* = 17.9, 11.8 Hz, 1H), 3.16 (dd, *J* = 17.9, 4.9 Hz, 1H).
^{13}C NMR (101 MHz, $CDCl_3$): δ 154.40, 152.10, 139.71, 132.29, 132.25, 129.60, 128.31, 127.59, 125.52, 122.14, 60.22, 42.05, 42.02.
HRMS (+ESI): calc. 454.9156 for $C_{17}H_{14}ON_2{}^{79}Br_2{}^{35}Cl$, found 454.9160.

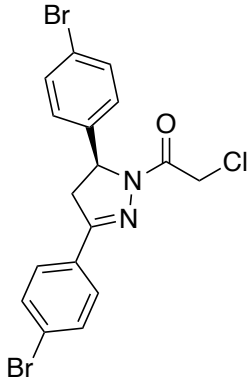

(*S*)-1-(3,5-bis(4-bromophenyl)-4,5-dihydro-1*H*-pyrazol-1-yl)-2-chloroethan-1-one (JNS-2-130B)

Boc-protected pyrazoline, JNS-2-128B, (45 mg, 0.094 mmol, 1.0 eq) was dissolved in DCM (0.47 mL, 0.2 M), cooled to 0 ºC, and 4.0 M HCl in dioxane (0.234 mL, 0.94 mmol, 10.0 eq.) was added under nitrogen. The mixture was stirred at rt until starting material was consumed (1.5h), then additional DCM was added (0.47 mL, reducing to 0.1 M) and the mixture cooled to 0 ºC. Chloroacetyl chloride (22 µL, 0.28 mmol, 3.0 eq.) was added followed by TEA (0.17 mL, 1.22 mmol, 13.0 eq.), and the reaction allowed to warm to room temperature and stirred for 1h. Crude was concentrated and purified by silica gel chromatography. (Mahé et. al. Angew. Chem. Int. Ed. 2010. 49. 39. 7072-7075.)

^{1}H NMR (400 MHz, Chloroform-*d*): δ 7.64 – 7.55 (m, 4H), 7.50 – 7.42 (m, 2H), 7.15 – 7.08 (m, 2H), 5.55 (dd, *J* = 11.8, 4.9 Hz, 1H), 4.61 – 4.48 (m, 2H), 3.78 (dd, *J* = 17.9, 11.8 Hz, 1H), 3.16 (dd, *J* = 17.9, 4.9 Hz, 1H).
^{13}C NMR (101 MHz, $CDCl_3$): δ 164.21, 154.46, 139.54, 132.18, 132.14, 129.45, 128.21, 127.47, 125.45, 122.05, 60.12, 41.93, 41.91, 21.63.
HRMS (+ESI): calc. 454.9156 for $C_{17}H_{14}ON_2{}^{79}Br_2{}^{35}Cl$, found 454.9159.

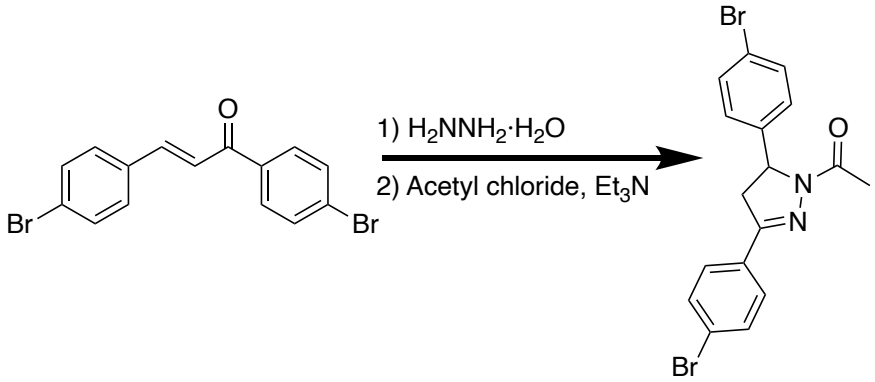

1-(3,5-bis(4-bromophenyl)-4,5-dihydro-1*H*-pyrazol-1-yl)ethan-1-one (JNS 2-229)
Hydrazine monohydrate (50% conc., 80.16 µL, 0.8 mmol, 2.0 eq.) was added to a suspension of (*E*)-1,3-bis(4-bromophenyl)prop-2-en-1-one (Princeton Bio, 146.4 mg, 0.4 mmol, 1.0 eq.) in EtOH (1.33 mL, 0.3 M). The resulting reaction mixture was stirred at reflux temperature for 4 h before it was concentrated under reduced pressure. The crude pyrazoline was then dissolved in CH_2Cl_2 (2mL, 0.2 M) and cooled to 0 °C. Triethylamine (167 µL, 1.2 mmol, 3.0 eq.) was added dropwise, followed by chloroacetyl chloride (42.6 µL, 0.6 mmol, 1.5 eq.). The resulting reaction mixture was stirred at ambient temperature for 1 hr before it was diluted with CH_2Cl_2. The organic phase was sequentially washed with $NaHCO_3$ solution (sat. aqueous) and NaCl solution (sat. aqueous), dried over Na_2SO_4, filtered and concentrated under reduced pressure. Purification by column chromatography afforded the corresponding chloroacetamide.

^{1}H NMR (400 MHz, $CDCl_3$): δ 7.61 (q, *J* = 8.6 Hz, 4H), 7.49 (d, *J* = 8.4 Hz, 2H), 7.24 – 7.10 (m, 2H), 5.58 (dd, *J* = 12.3, 4.9 Hz, 1H), 3.77 (dd, *J* = 17.6, 12.0 Hz, 1H), 3.24 – 3.06 (m, 1H), 2.44 (s, 3H).
^{13}C NMR (101 MHz, $CDCl_3$): δ 168.94, 152.66, 140.71, 132.10, 132.06, 130.17, 128.03, 127.42, 124.82, 121.68, 59.63, 42.04, 21.94.
HRMS (+ESI): calc. 420.9546 for $C_{17}H_{15}ON_2{}^{79}Br_2{}^{35}$, found 420.9550.

Chapter 4.3 Supplementary Information
Supplementary Figures

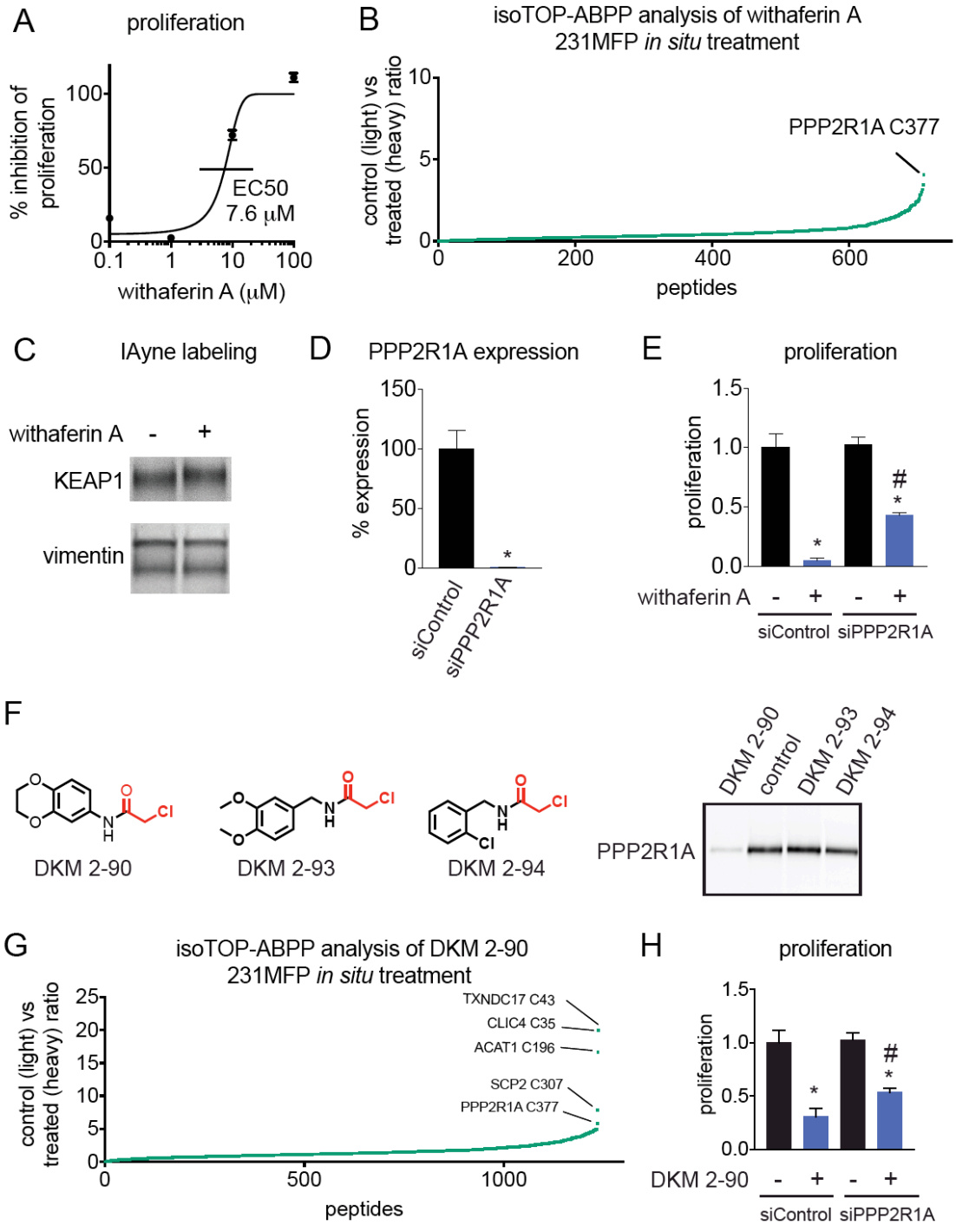

Supplementary Figure 4.3.1. Investigating the interactions of withaferin A and DKM 2-90.

Related to Figures 4.3.1, 2, 3, and 4. (A) Anti-proliferative dose-response of withaferin A in 231MFP cells. Cells were treated with DMSO or withaferin A for 48 h in serum-

containing media and cell viability was assessed by Hoechst staining. **(B)** IsoTOP-ABPP analysis of withaferin A treatment in 231MFP cells. 231MFP cells were treated with DMSO or withaferin A (10 μM) for 4 h. Proteomes were subsequently labeled *ex situ* with IAyne for 1 h and subjected to the isoTOP-ABPP method. Light to heavy ratios of probe-modified peptides are shown. **(C)** Gel-based ABPP analysis of withaferin A competition against IAyne labeling of pure human KEAP1 and vimentin. Purified proteins were pre-treated with DMSO or withaferin A (10 μM) for 30 min at 37 °C before IAyne labeling (10 μM) for 30 min at room temperature. Probe labeled proteins were subsequently appended to rhodamine-azide by CuAAC and analyzed by SDS/PAGE and in-gel fluorescence. **(D)** PPP2R1A expression as assessed by qPCR. 231MFP cells were transfected with siControl or siPPP2R1A oligonucleotides and cells were harvested for qPCR analysis after 48 h. **(E)** 231MFP cell proliferation. 231MFP cells were transfected with siControl or siPPP2R1A oligonucleotides for 48 h and then cells were seeded and treated with either DMSO or withaferin A (10 μM) for an additional 48 h and cell viability was assessed by Hoechst staining. **(F)** Gel-based ABPP analysis of IAyne labeling of pure PPP2R1A. Purified proteins were pre-treated with DMSO or covalent ligands (100 μM) (positive control DKM 2-90 and negative control DKM 2-93 and DKM 2-94) for 30 min at 37 °C before IAyne labeling (10 μM) for 30 min at room temperature. Probe labeled proteins were subsequently appended to rhodamine-azide by CuAAC and analyzed by SDS/PAGE and in-gel fluorescence. **(G)** IsoTOP-ABPP analysis of DKM 2-90 treatment in 231MFP cells. 231MFP cells were treated with DMSO or DKM 2-90 (100 μM) for 4 h. Proteomes were subsequently labeled *ex situ* with IAyne for 1 h and subjected to the isoTOP-ABPP method. Light to heavy ratios of probe-modified peptides are shown. **(H)** 231MFP cell proliferation. 231MFP cells were transfected with siControl or siPPP2R1A oligonucleotides for 48 h and then cells were seeded and treated with either DMSO or DKM 2-90 (100 μM) for an additional 48 h and cell viability was assessed by Hoechst staining. Data in **(A, D, E,** and **G)** is presented as mean ± sem, n=3-5/group. Significance in **(D, E,** and **G)** is expressed as *$p<0.05$ compared to vehicle-treated siControl cells and #$p<0.05$ compared to withaferin A or DKM 2-90-treated siControl cells.

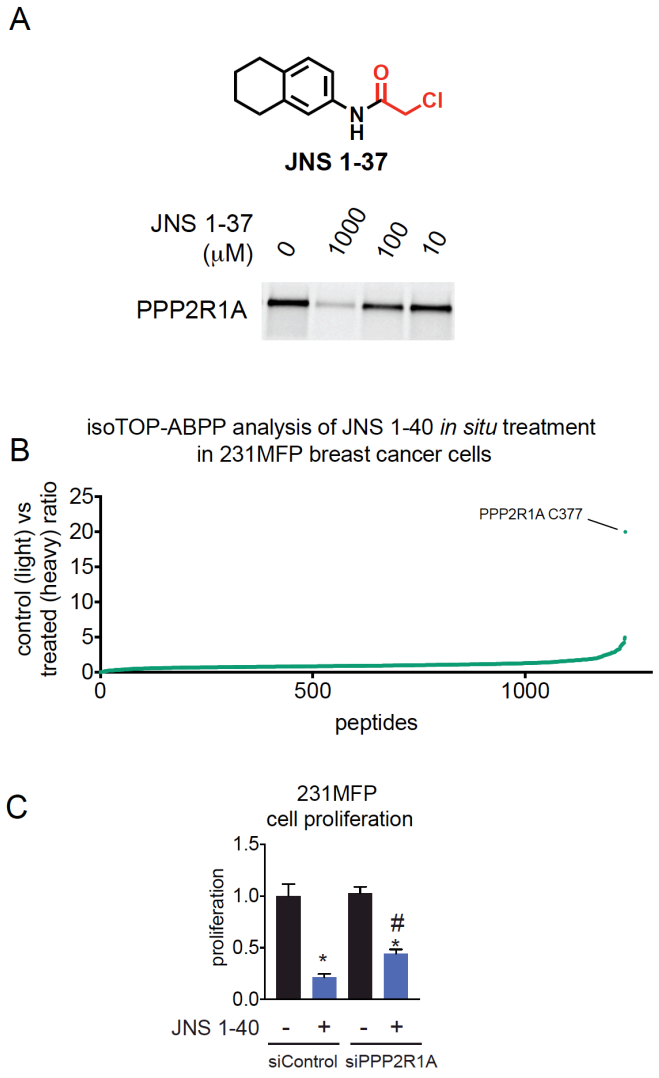

Supplementary Figure 4.3.2. Characterization of DKM 2-90 analogs JNS 1-37 and JNS 1-40.

Related to Figure 4.3.5. (A) Structure of JNS 1-37 and gel-based ABPP analysis of its potency against PPP2R1A. Reactive chloroacetamide is shown in red. Pure human PPP2R1A was pre-treated with DMSO or JNS 1-37 for 30 min at 37 °C prior to IAyne labeling for 30 min at room temperature. Probe-labeled proteins were appended to rhodamine-azide by CuAAC and analyzed by SDS/PAGE and in-gel fluorescence. **(B)** IsoTOP-ABPP analysis of JNS 1-40 treatment in 231MFP cells. 231MFP cells were treated with DMSO or JNS 1-40 (100 μM) for 4 h. Proteomes were subsequently labeled *ex situ* with IAyne for 1 h and subjected to the isoTOP-ABPP method. Light to heavy ratios of probe-modified peptides are shown. **(C)** 231MFP cell proliferation. 231MFP cells were transfected with siControl or siPPP2R1A oligonucleotides for 48 h and then cells were seeded and treated with either DMSO or JNS 1-40 (100 μM) for an additional 48 h and cell viability was assessed by Hoechst staining. Data in **(C)** is presented as mean ± sem,

n=5/group. Significance in **(C)** is expressed as *p<0.05 compared to vehicle-treated siControl cells and #p<0.05 compared to JNS 1-40-treated siControl cells.

Synthetic Methods and Characterization

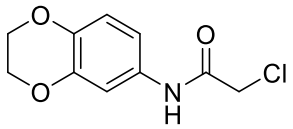

2-Chloro-N-(2,3-dihydrobenzo[b][1,4]dioxin-6-yl)acetamide (DKM 2-90)
Following **General Procedure B** starting from 1,4-benzodioxan-6-amine (1.51 g, 10 mmol) product was obtained after silica gel chromatography (40% ethyl acetate in hexanes) in 70% yield as an off-white solid (1.59 g).

^{1}H NMR (400MHz, $CDCl_3$): δ 8.11 (s, 1H), 7.18 (d, *J* = 2.4 Hz, 1H), 6.92 (dd, *J* = 2.4, 8.7 Hz, 1H), 6.83 (d, *J* = 8.7 Hz, 1H), 4.25 (s, 4H), 4.17 (s, 2H).

^{13}C NMR (100MHz, $CDCl_3$): δ 163.8, 143.7, 141.3, 130.4, 117.5, 114.0, 110.2, 64.5, 64.4, 43.0.

HRMS (+ESI): Calculated: 228.0422 ($C_{10}H_{11}ClNO_3$). Observed: 228.0421.

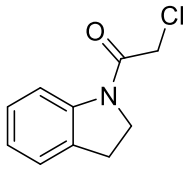

2-chloro-1-(indolin-1-yl)ethan-1-one (DKM 2-79)
Following **General Procedure B** starting from indoline (331 mg, 2.8 mmol) product was obtained after silica gel chromatography (0% to 20% ethyl acetate in hexanes) in 51% yield as a pale brown solid (278 mg).

^{1}H NMR (400MHz, $CDCl_3$): δ 8.17 (d, *J* = 8.0 Hz, 1H), 7.20-7.16 (m, 2H), 7.04 (t, *J* = 7.4 Hz, 1H), 4.09 (s, 2H), 4.05 (t, *J* = 8.4 Hz, 2H), 3.17 (t, *J* = 8.4 Hz, 2H).

^{13}C NMR (100MHz, $CDCl_3$): δ 164.0, 142.4, 131.3, 127.6, 124.7, 124.5, 117.1, 47.7, 43.02, 28.1.

HRMS (+ESI): Calculated: 196.0524 ($C_{10}H_{11}ClNO$). Observed: 196.0523.

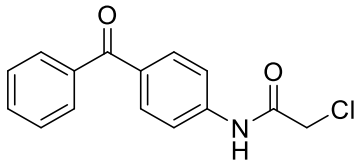

***N*-(4-Benzoylphenyl)-2-chloroacetamide (DKM 3-22)**

Following **General Procedure B** starting from 4-aminobenzophenone (590 mg, 3.0 mmol) product was obtained after silica gel chromatography (30% to 50% ethyl acetate in hexanes) in 83% yield as a light brown solid (679 mg).

^{1}H NMR (400MHz, $CDCl_3$): δ 8.48 (s, 1H), 7.85-7.83 (m, 2H), 7.78-7.76 (m, 2H), 7.71-7.68 (m, 2H), 7.61-7.57 (m, 1H), 7.50-7.46 (m, 2H), 4.22 (s, 2H).

^{13}C NMR (100MHz, $CDCl_3$): δ 195.7, 164.2, 140., 137.7, 134.1, 132.5, 131.7, 130.0, 128.5, 119.3, 43.0.

HRMS (-ESI): Calculated: 272.0484 ($C_{15}H_{11}NO_2Cl$). Observed: 272.0482.

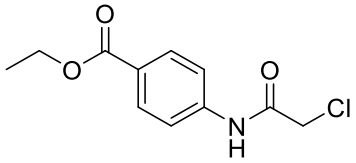

Ethyl 4-(2-chloroacetamido)benzoate (TRH 1-17)
Following **General Procedure B** starting from benzocaine (498 mg, 3.0 mmol) product was obtained after silica gel chromatography (2% to 20% ethyl acetate in hexanes) in 68% yield as a white solid (494 mg).

^{1}H NMR (400MHz, $CDCl_3$): δ 8.67 (s, 1H), 7.98 (d, *J* = 8.0 Hz, 2H), 7.62 (d, *J* = 8.0 Hz, 2H), 4.33 (q, *J* = 8.0 Hz, 2H), 4.15 (s, 2H), 1.34 (t, *J* = 6.0 Hz, 3H).

^{13}C NMR (100MHz, $CDCl_3$): δ 166.1, 164.5, 141.0, 130.7, 126.7, 119.3, 61.1, 43.0, 14.3.

HRMS (-ESI): Calculated: 240.0433 ($C_{11}H_{11}NO_3Cl$). Observed: 240.0430.

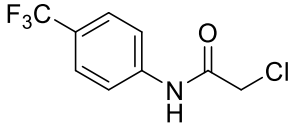

2-Chloro-*N*-(4-(trifluoromethyl)phenyl)acetamide (TRH 1-51)
Following **General Procedure B** starting from 4-(trifluoromethyl)aniline (346 mg, 2.0 mmol) product was obtained after silica gel chromatography (10% to 30% ethyl acetate in hexanes) in 61% yield as a white solid (309 mg).

^{1}H NMR (400 MHz, MeOD): δ 7.77 (d, *J* = 8.3 Hz, 2H), 7.61 (d, *J* = 8.3 Hz, 2H), 4.20 (s, 2H).

^{13}C NMR (100 MHz, MeOD): δ 167.7, 162.4, 142.9, 127.14, 127.10, 127.06, 127.02, 124.3, 120.9, 44.0.

HRMS (-ESI): Calculated: 236.0095 ($C_9H_6NOClF_3$). Observed: 236.0094.

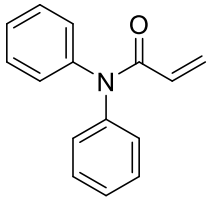

N,N-diphenylacrylamide (DKM 3-70)
A solution of diphenylamine (347 mg, 2.1 mmol) in DCM (10 mL) was cooled to 0 °C. To the solution was added acryloyl chloride (222 mg, 2.5 mmol) followed by triethylamine (279 mg, 2.8 mmol). The solution was allowed to warm to room temperature and stirred overnight. The solution was washed with brine and citric acid and the crude product was purified via silica gel chromatography (20% to 60% ethyl acetate in hexanes) to afford the product in 24% yield as a dark yellow oil (112 mg).

^{1}H NMR (400MHz, $CDCl_3$): δ 7.43-7.28 (m, 10H), 6.52 (dd, *J* = 2.0, 16.8 Hz, 1H), 6.25 (dd, *J* = 10.2, 16.8 Hz, 1H), 5.67 (dd, *J* = 1.8, 10.2 Hz, 1H).

^{13}C NMR (100MHz, $CDCl_3$): δ 165.8, 142.6, 129.7, 129.3, 128.5, 127.0.

HRMS (+ESI): Calculated: 246.0889 ($C_{15}H_{13}NONa$). Observed: 246.0887.

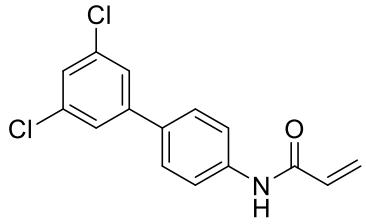

N-(3',5'-dichloro-[1,1'-biphenyl]-4-yl)acrylamide (DKM 3-3)
Following **General Procedure A** starting from 4-amino-3,5-dichlorobiphenyl (717 mg, 3.0 mmol), product was obtained after silica gel chromatography (20% to 45% ethyl acetate in hexanes) and recrystallization from toluene in 23% yield as a white solid (203 mg).

^{1}H NMR (600MHz, MeOD): δ 7.77 (d, *J* = 8.6 Hz, 2H), 7.59 (d, *J* = 8.6 Hz, 2H), 7.56 (d, *J* = 1.7 Hz, 2H), 7.37 (t, *J* = 1.7 Hz, 1H), 6.46 (dd, *J* = 9.9, 17.0 Hz, 1H), 6.39 (dd, *J* = 1.7, 17.0 Hz, 1H), 5.80 (dd, *J* = 1.7, 9.9 Hz, 1H).

^{13}C NMR (150MHz, MeOD): δ 166.2, 145.2, 140.4, 136.5, 135.2, 132.4, 128.5, 128.0, 127.7, 126.2, 121.7.

HRMS (-ESI): Calculated: 290.0145 ($C_{15}H_{110}NOCl_2$). Observed: 290.0143.

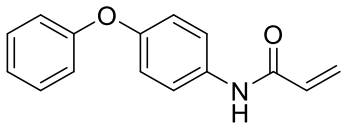

N-(4-phenoxyphenyl)acrylamide (DKM 2-119)
Following **General Procedure A** starting from 4-phenoxyaniline (571 mg, 3.1 mmol), product was obtained after silica gel chromatography (10% to 30% ethyl acetate in hexanes) in 69% yield as a white solid (512 mg).

^{1}H NMR (400MHz, $CDCl_3$): δ 8.17 (s, 1H), 7.55 (d, *J* = 8.9 Hz, 2H), 7.33-7.29 (m, 2H), 7.08 (t, *J* = 7.4 Hz, 1H), 6.98-6.94 (m, 4H), 6.42 (dd, *J* = 1.4, 16.9 Hz, 1H), 6.31 (dd, *J* = 10.0, 16.9 Hz, 1H), 5.73 (dd, *J* = 1.4, 10.0 Hz, 1H).

^{13}C NMR (100MHz, $CDCl_3$): δ 16.0, 157.5, 153.8, 13.4, 131.2, 129., 12.8, 123.3, 122.1, 119.6, 118.6.

HRMS (+ESI): Calculated: 240.1019 ($C_{15}H_{14}NO_2$). Observed: 240.1015.

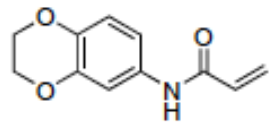

N-(2,3-dihydrobenzo[b][1,4]dioxin-6-yl)acrylamide (DKM 2-87)
Following **General Procedure A** starting from 1,4-benzodioxan-6-amine (462 mg, 3.1 mmol), product was obtained after silica gel chromatography (40% ethyl acetate in hexanes) in 38% yield as a light yellow solid (239 mg).

^{1}H NMR (400MHz, $(CD_3)_2SO$): δ 9.97 (s, 1H), 7.33 (d, *J* = 2.4 Hz, 1H), 7.03 (dd, *J* = 2.4, 8.7 Hz, 1H), 6.79 (d, *J* = 8.7 Hz, 1H), 6.38 (dd, *J* = 10.0, 17.0, 1H), 6.22 (dd, *J* = 2.1, 17.0 Hz, 1H), 5.71 (dd, *J* = 2.1, 10.0 Hz, 1H), 4.23-4.18 (m, 4H).

^{13}C NMR (100MHz, $(CD_3)_2SO$): δ 162.7, 142.9, 139.5, 132.7, 131.9, 126.4, 116.8, 112.5, 108.4, 64.2, 63.9.

HRMS (+ESI): Calculated: 206.0812 ($C_{11}H_{12}NO_3$). Observed: 206.0807.

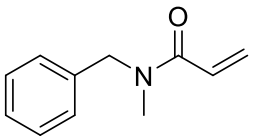

N-((tetrahydrofuran-2-yl)methyl)acrylamide (DKM 3-15)

Following **General Procedure A** starting from tetrahydrofurfurylamine (294 mg, 2.9 mmol), product was obtained after silica gel chromatography (20% to 70% ethyl acetate in hexanes) in 55% yield as a pale yellow oil (246 mg).

^{1}H NMR (400MHz, $CDCl_3$): 6.48 (s, 1H), 6.20 (dd, *J* = 1.7, 17.0 Hz, 1H), 6.07 (dd, *J* = 10.1, 17.0 Hz, 1H), 5.54 (dd, *J* = 1.7, 10.1 Hz, 1H), 3.96-3.90 (m, 1H), 3.80-3.75 (m, 1H), 3.70-3.64 (m, 1H), 3.58-3.52 (m, 1H), 3.17-3.11 (m, 1H), 1.95-1.87 (m, 1H), 1.86-1.78 (m, 2H), 1.53-1.44 (m, 1H).

^{13}C NMR (100MHz, $CDCl_3$): δ 165.7, 130.8, 126.3, 77.7, 68.0, 43.2, 28.7, 25.7.

HRMS (+ESI): Calculated: 156.1019 ($C_8H_{14}NO_2$). Observed: 156.1017.

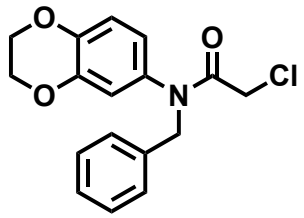

***N*-benzyl-2-chloro-*N*-(2,3-dihydrobenzo[*b*][1,4]dioxin-6-yl)acetamide (JNS 1-40)**
A solution of DKM 2-90 (1 g, 4.39 mmol) and sodium hydride (0.7 g 60% dispersion in mineral oil, 17.56 mmol, 4 eq.) in THF (50 mL) was allowed to stir at 0 °C for 15 min, after which benzyl bromide (2.1 mL, 17.56 mmol, 4 eq.) was added. After 3 hr at 0 °C, the reaction was quenched with $NaHCO_3$ and diluted with EtOAc for extraction. The organic layer was subsequently washed with brine and dried over $MgSO_4$. The crude product was purified by silica gel chromatography (30% ethyl acetate in hexanes) to obtain the desired product in 55% yield as an off-white solid (770 mg).

^{1}H NMR (400MHz, $CDCl_3$): δ 7.26 (m, 5H), 6.79 (d, *J* =8.6 Hz, 1H), 6.56 (d, 2.5 Hz, 1H), 6.45 (dd, *J* =8.5 Hz, 2.5 Hz, 1H), 4.84 (s, 2H), 4.25 (s, 4H), 3.90 (s, 2H).

^{13}C NMR (100MHz, $CDCl_3$): δ 166.4, 144.0, 143.9, 136.7, 134.0, 129.0, 128.5, 127.7, 121.31, 118.0, 117.1, 64.3, 53.8, 42,2.

HRMS (+ESI): Calculated: 318.0891 ($C_{17}H_{17}ClNO_3$). Observed: 318.0898.

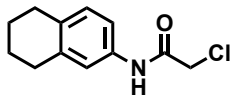

2-Chloro-N-(5,6,7,8-tetrahydronaphthalen-2-yl)acetamide (JNS 1-37)
Following **General Procedure B** starting from 5,6,7,8-Tetrahydro-2-napthylamine (1.472 g, 10.0 mmol) product was obtained after silica gel chromatography (30% ethyl acetate in hexanes) in 98% yield as an off-white solid (2.2 g).

^{1}H NMR (400MHz, $CDCl_3$): δ 8.17 (s, 1H), 7.23 (m, 2H), 7.03 (d, *J* = 8.1 Hz, 1H), 4.12 (s, 2H), 4.55 (s, 4H), 1.78 (s, 4H).

^{13}C NMR (100MHz, $CDCl_3$): δ 170.9, 163.8, 137.8, 134.3, 134.0, 129.4, 120.6, 117.6, 60.2, 53.4, 42.9, 30.7, 29.4, 28.8, 23.0, 20.8, 14.1.

HRMS (+ESI): Calculated: 224.0837($C_{12}H_{15}ClNO$). Observed: 224.0835.

Supplementary Tables
The following supplementary tables have been deposited online with the submission of this dissertation.

Supplementary Table 1. Structures of covalent ligands screened against RNF114

Supplementary Table 2. Structures of covalent ligands screened in 231 MFP cells.

Supplementary Datasets
The following supplementary datasets have been deposited online with the submission of this dissertation.

Supplementary Dataset 1. IsoTOP-ABPP analysis of nimbolide treatment *in situ* in 231MFP breast cancer cells.
IsoTOP-ABPP analysis of nimbolide treatment *in situ* (10 μM). 231MFP breast cancer cells were treated with DMSO or nimbolide (10 μM, 1.5 h *in situ*), after which cells were harvested and proteomes were labeled *ex situ* with IA-alkyne (100 μM, 1 h), followed by appendage of isotopically light (for DMSO-treated) or heavy (for nimbolide-treated) TEV protease cleavable biotin-azide tags by copper-catalyzed azide-alkyne cycloaddition (CuAAC). Control and treated proteomes were subsequently combined in a 1:1 ratio, probe-labeled proteins were avidin-enriched, digested with trypsin, and probe-modified tryptic peptides were eluted by TEV protease, analyzed by LC-MS/MS, and light to heavy probe-modified peptide ratios were quantified. Shown are data from n=3 biological replicates/group.
Tab 1. Total isoTOP-ABPP proteomic dataset
Tab 2. Analyzed isoTOP-ABPP dataset. For those probe-modified peptides that showed ratios >2, we only interpreted those targets that were present across all three biological replicates, were statistically significant, and showed good quality MS1 peak shapes across all biological replicates. Light versus heavy isotopic probe-modified peptide ratios are calculated by taking the mean of the ratios of each replicate paired light vs. heavy precursor abundance for all peptide spectral matches (PSM) associated with a peptide. The paired abundances were also used to calculate a paired sample t-test p-value in an effort to estimate constancy within paired abundances and significance in change between treatment and control. P-values were corrected using the Benjamini/Hochberg method.

Supplementary Dataset 2. TMT-based quantitative proteomic analysis of proteins enriched by nimbolide-alkyne probe *in situ* treatment in 231MFP breast cancer cells.
231MFP breast cancer cells were treated with DMSO vehicle or the nimbolide-alkyne probe (50 μM) for 1.5 h. Probe-labeled proteins were conjugated to biotin-azide by CuAAC and subsequently avidin-enriched from 231MFP proteomes and tryptic digests

from enriched proteins were analyzed by TMT-based quantitative proteomics. Shown are the proteins from this experiment that showed at least 2 unique peptides, as well as TMT ratios of no-probe versus probe. The data shown are from n=3 biological replicates/group.

Supplementary Dataset 3. TMT-based quantitative proteomic profiling of XH2-treatment in 231MFP breast cancer cells.
Tandem mass tag (TMT)-based quantitative proteomic profiling of 231MFP breast cancer cells treated with DMSO vehicle or nimbolide (100 nM) **(Tab 1)** or XH2 (100 nM) **(Tab 2)** for 12 h. Shown are the data for proteins identified that showed at least 2 unique peptides from n=3 biological replicates/group.

Supplementary Dataset 4. IsoTOP-ABPP analysis of EN219 in 231MFP breast cancer cells. IsoTOP-ABPP analysis of EN219 in 231MFP breast cancer cells. 231MFP cells were treated *in situ* with DMSO vehicle or EN219 (1 μM) for 90 min. Control and treated cell lysates were labeled with IA-alkyne (100 μM) for 1 h, after which isotopically light (control) or heavy (EN219-treated) biotin-azide bearing a TEV tag was appended by CuAAC. Proteomes were mixed in a 1:1 ratio, probe-labeled proteins were enriched with avidin and digested with trypsin, and probe-modified peptides were eluted by TEV protease and analyzed by LC-MS/MS.

Supplementary Dataset 5. TMT-based proteomic analysis of EN219-alkyne pulldown competed by EN219. 231MFP cells were treated with DMSO vehicle or EN219 (20 μM) 30 min prior to treating cells with DMSO or EN219-alkyne probe (2 μM) for 90 min. Resulting cell lysates were subjected to CuAAC with biotin-azide to append a biotin enrichment handle onto EN219-alkyne labeled proteins *ex situ*. EN219-alkyne labeled proteins were subsequently avidin-enriched, digested with trypsin, and resulting tryptic peptides from each treatment group were labeled with TMT reagents and combined and fractionated for LC-MS/MS analysis.

Supplementary Dataset 6. TMT-based proteomic analysis of ML 2-14-mediated protein level changes in 231MFP cells. TMT-based quantitative proteomic data showing ML 2-14-mediated protein level changes in 231MFP cells. 231MFP cells were treated with DMSO vehicle or ML 2-14 for 8 h.

Supplementary Dataset 7. IsoTOP-ABPP Analysis of Withaferin A and DKM 2-90 Targets in 231MFP Breast Cancer Proteomes. We mapped the cysteine reactivity of withaferin A and DKM 2-90 by pre-incubating withaferin A (10 μM) or DKM 2-90 (100 μM) for 30 min in 231MFP breast cancer cell proteomes, prior to labeling with the cysteine-reactive iodoacetamide-alkyne (IAyne) probe (100 μM, 30 min). Probe-labeled proteins were then tagged with an isotopically light (for control) or heavy (for withaferin A- or DKM 2-90-treated) biotin-azide tag bearing a TEV protease recognition site by copper-catalyzed azide-alkyne cycloaddition. Control and treated proteomes were then mixed in a 1:1 ratio, probe-labeled proteins were avidin-enriched and tryptically digested, probe-labeled tryptic peptides were avidin-enriched again, released by TEV protease and analyzed by quantitative proteomic methods, and light to heavy peptide ratios were

quantified. Competitive isoTOP-ABPP analysis of withaferin A and DKM 2-90 cysteine reactivity in 231MFP breast cancer cell proteomes. Light to heavy ratios of ~1 indicate peptides that were labeled by IAyne, but not bound by withaferin A or DKM 2-90. We designate light to heavy ratios of >10 as targets that were bound by withaferin A or DKM 2-90. Tabs 1 and 3 show average light versus heavy ratios from those probe-modified peptides found in at least 2 out of 3 biological replicates. Tabs 1–7. IsoTOP-ABPP analysis of withaferin A (10 μM), DKM 2-90 (100 μM), JNS 1-40 (100 μM) treatment *in vitro* in 231MFP proteomes or *in situ* in 231MFP cells, or 231MFP tumors from JNS 1-40 daily *in vivo* treatment in mice. For *in vitro*experiments, DMSO or compounds were pre-treated for 30 min prior to labeling with IAyne. For *in situ* experiments, cells were treated with DMSO or compounds for 4 hr and cell proteomes were subsequently labeled with IAyne. For *in vivo* study in Tab 7, tumors were taken from the study shown in Figure 4.3.5G**.** Tabs 8–14. All peptides identified in isoTOP-ABPP experiments from Tabs 1–7.